VRIJE UNIVERSITEIT BRUSSEL

FACULTY OF ENGINEERING
Department of Hydrology
and Hydraulic Engineering

Thesis submitted in fulfilment of the requirements for the award of the degree of Doctor of Engineering Sciences (Doctor in de Ingenieurswetenschappen)

Changing storage:
A global perspective on reservoirs in a changing climate

Promotors:
Prof. Dr. Wim Thiery
Prof. Dr. Nicole P. M. van Lipzig
Prof. Dr. Ir. Ann van Griensven

Inne Vanderkelen

June 2022

CHANGING STORAGE:
A GLOBAL PERSPECTIVE ON RESERVOIRS IN A CHANGING CLIMATE

Inne Vanderkelen

Thesis submitted in fulfilment of the requirements for the award of the degree of Doctor of Engineering Sciences (Doctor in de Ingenieurswetenschappen)

DEPARTMENT OF HYDROLOGY AND HYDRAULIC ENGINEERING
VRIJE UNIVERSITEIT BRUSSEL

June 2022

Printed by
Crazy Copy Center Productions
VUB Pleinlaan 2, 1050 Brussel
Tel: +32 2 629 33 44
crazycopy@vub.be
www.crazycopy.be

ISBN: 9789464443301
NUR CODE: 934
THEMA: RBPC

PhD Jury Composition

Prof. Dr. Wim Thiery	*Promotor* Department of Hydrology and Hydraulic Engineering Vrije Universiteit Brussel (VUB), Belgium
Prof. Dr. Nicole van Lipzig	*Co-promotor* Department of Earth and Environmental Sciences KU Leuven, Belgium
Prof. Dr. Ir. Ann van Griensven	*Co-promotor and Secretary* Department of Hydrology and Hydraulic Engineering Vrije Universiteit Brussel (VUB), Belgium
Prof. Dr. Benoît Smets	*Chair* Department of Geography Vrije Universiteit Brussel (VUB), Belgium
Prof. Dr. Ir. Iris de Graeve	*Vice-Chair* Department of Electrochemical and Surface Engineering Vrije Universiteit Brussel (VUB), Belgium
Dr. Peter Greve	*External Examiner* Water Security Group International Institute for Applied Systems Analysis (IIASA), Austria
Prof. Dr. Sonali McDermid	*External Examiner* Department of Environmental Studies New York Univeristy (NYU), United States of America

Acknowledgements

A PhD thesis does not write itself, nor does its author operate from a deserted island (or isolated home office, for that matter). As such, I would like to acknowledge the many individuals that contributed to the realization of this work in, what will most likely be, one of the most read sections of this thesis. This work would not have been possible without the support, collaboration and friendship of my family, friends and colleagues during the past 5 years. To that end, I attempted to thank all of them in the following paragraphs.

First and foremost, words cannot express my gratitude and appreciation for professor Wim Thiery, my promotor and mentor. You initiated and guided me through me through the wondrous world of science, at every step giving me that extra push to believe in myself. I'm grateful for the entire journey; from meeting you for the first time in the Geo-Institute at KU Leuven about my prospective master thesis topic, writing the PhD proposal together, getting it funded after the second try, setting up the new BCLIMATE research group at VUB, guiding numerous master students and colleague PhD candidates, to today, almost holding my PhD degree. Your excellence, level of ambition, endless stream of ideas, but also your kind personality and ability to see and create opportunities for people in your vicinity to grow were invaluable and will serve as an inspiration for the rest of my life. It was fantastic to have worked with you, and I am confident the BCLIMATE future looks very bright. Wim, bedankt voor alles. Ik had mij geen betere promotor kunnen wensen.

Then I would like to thank professor Nicole van Lipzig, my co-promotor, for her enthusiasm that sparked my excitement for climate science since my bachelor studies in geography at KULeuven. I particularly valued your generous knowledge and expertise, problem-solving mindset and welcoming atmosphere in the RCS research group at KU Leuven. Dankjewel Nicole, je bent en blijft een belangrijk rolmodel voor mij.

I am also grateful to have professor Ann van Griensven as my co-promotor. Especially in the last chapter, your critical views and thoughtful advice kept me and our science sharp. But more importantly, I would like to thank you for the joy, encouragement and continuous support during my time at VUB. I will miss your (sometimes loud) laughter resounding through the corridor of building T's first floor. You showed me the importance of being open-minded, positive and not being afraid to face difficult challenges. Bedankt voor de goeie sfeer, vele luch- en koffiepauzes en fijne momenten gedurende mijn tijd bij HYDR.

I would like to acknowledge the members of my examination committee, prof. Benoît Smets, dr. Peter Greve, prof. Sonali McDermid and prof. Iris De Graeve, for the thoughtful questions during the private defense, which sparked discussions I really enjoyed. Special thanks to prof. Steven Eisenreich for being in my advisory commission, your encouragements along the way were invaluable.

Without the generous support from the Fonds voor Wetenschappelijk Onderzoek (FWO), this research would not have been possible. I am also grateful to have received the Prize Ernest Dubois from the King Baudouin Foundation.

This endeavour would never have been possible without the very open and collaborative international research communities I had the opportunity to be part of. As communities are made of individuals, there are several international collaborators who I need to mention as they provided key contributions to this thesis.

There is nothing more inspirational for a starting climate researcher than visiting the National Center for Atmospheric Research (NCAR) in Boulder, Colorado. I am extremely grateful to dr. Dave Lawrence from NCAR. Without your support, commitment and guidance, I would probably not even have started the source code developments. Thank you for inviting me to the tutorials, working group meetings and research stay at NCAR, and the ski and cabin weekend in the Colorado Rocky Mountains. Recently, I discovered we have the *Bananagrams* game in Dutch as well and I'm pretty confident I will do better in that version. Thank you, dr. Bill Sacks, with your tedious help on the source code developments, and thank you Erik Kluzek for your valuable technical support and insights when working on the software. Dr. Naoki Mizukami and prof. Martyn Clark, without you there would be no global mizuRoute version, and I am grateful for the opportunity to contribute my bit on the reservoirs with your help and support. Dr. Shervan Gharari, without you I would likely still be suffering on the FORTRAN implementation of the algorithm. I hope we eventually get to meet each other in person, without a global pandemic hindering international travel to Canada.

Many thanks to prof. Yadu Pokhrel, his expertise and valuable insights strengthened many of my studies. Special thanks should also go to prof. Naota Hanasaki, for his overall support of my research notably on the proposal and the final paper. I sincerely look forward to meeting you in person one day.

Throughout my PhD I became more and more involved in the ISIMIP project, especially within the lake and global water sectors. My gratitude goes to the sector coordinators for their community work, the modellers for running their lake and hydrological models and the scientists working at PIK for their hard work to make the simulations available to the community.

As a climate modellers we are often working in worlds of bits and bytes. It was therefore really cool to contribute to the actually tangible UHasselt Ecotron experiment, knowing that the sprinklers in the units are raining based on the data we provided. Thank you prof. Francois Rineau and collaborators for the opportunity to join this exciting project.

Being the first PhD student in our group using the High Performance Computing systems to install, run, and teach CESM has been a bumpy ride. Without the indispensable help from the HPC staff at VUB, we would still be stuck on installing CESM on our cluster Hydra. Thank you Alex, Ward, and Samuel for answering my many, many tickets.

During my five years at VUB, I was privileged to see the BCLIMATE group grow from just Wim and me to a group of nine brilliant researchers, all fantastic colleagues. Sebastian, when starting our PhDs together, you didn't always make it easy for me to be next to you and your outstanding achievements, but I quickly figured to see it as an exceptional opportunity to learn from your professionalism. Bedankt voor je fijne kantoorbezoekjes met stroopwafels en ander lekkers! Luke, witnessing you grow scientifically, as my master student and colleague, was one of the most rewarding experiences during my PhD. I'm so grateful for all the glorious moments we had in our office. Yi, thanks man for the moral support and great talks and jokes, they really kept me going when things were harder. Steven, jouw zelfvertrouwen en vermogen tot het behouden van je 'cool' zal altijd een na te streven doel voor mij blijven. Seppe, bedankt voor je immer goed humeur en frisse kijk op de zaken. And guess what, you and James are hereby officially *rickrolled* in my acknowledgements! Finally, Axel and Sabin, thank you for the great atmosphere you bring to the group. I really, really enjoyed my attempts of being a 'big sister' for you all.

One of the main reasons I arrived (almost) everyday with a big smile to work in building T are the fabulous colleagues of the Hydrology department, many of who became good friends. My office mates over the years, Ting, Syed, Yannick, Cas, Mónica, Inti, Alexis, Afnan, Luke, Yi and Annika made our PhD room a better place, which I missed a lot during periods of mandatory remote work. Thanks to the esteemed members of our HYDR Green Team, Charlotte, Imeshi, Gert, Dimitri, Steven and Yi, we increased the sustainability of our department while having good fun. (And, in my humble opinion, the fact we got most colleagues joining the (night)train to the EGU conference demonstrated that we did have an impact!) The VUB colleagues, James, Boud, Marijke, Albert, Elga, Joanna, Veronica, Margret, Zainab, Ihab, Estifanos, Helen, Douglas, Matheusz, Anna, Sarah, Solomon, Nahad, Jiri, Analy, Annabel, Lorenzo, Kaoutar, Buruk, Leyla and others, coming from literally all parts of the world, gave me an incredible international experience while being only $\sim$ 15 km away from the town where I grew up. I feel very blessed to have spent time with all of you, ranging from many afterwork drinks in Pilar and beyond, numerous coffee breaks, lunches, dinners and BBQs, conferences, train rides, Kubb games, and endless werewolf nights at team buildings. All of you contributed to the exceptional warm and cosy atmosphere at our department and I cherished every minute.

Thank you Hilde, for guiding us through the maze that the VUB administration can be sometimes.

I had the pleasure to supervise great master students for their theses. Daniela, Luke, Faluku, Seppe, Ann and Rosa, working with you was inspiring and I feel very lucky to have been part of your first steps in scientific research.

My regular trips to the colleagues of the RCS group at KU Leuven to present my work were very important to me, especially during the first years of my PhD. Special thanks go to Jonas, for numerous chats about research, methods and technical set-ups.

I met a lot of great scientists and fantastic people along the way, and would like to thank them all for the fruitful exchanges and fun. In particular, thank you Caroline for being such a nice roommate to hang out at the Swiss Climate Summerschool in 2018, I believe we made a good Belgian delegation. Many thanks Florentine, for the nice talks on the glacier hike at the Swiss Climate Summerschool, as well as bumping into each other at EGU and beyond. Kayla, you were a good roommate with your encouraging words at the CTSM tutorial. Thanks Peter for our weekend trips in Colorado including cross-country skiing and the climbing movie. Thibault, thanks again for the scientific discussion and practising my French while drinking beers and eating nachos after the LAKES workshop in Toulouse. I hope we meet again sometime!

Thank you Jan, Lineke and Nora for hosting me during my two week research visit at NCAR. Jullie zorgden voor een vertrouwde en warme omgeving tijdens een de moeilijkere periode waarin ik mijn modelontwikkelingen startte.

You would most likely not be holding this book in your hands in its current form if it wasn't for Liesa. We, rather unsurprisingly, embarked on the PhD adventure together, albeit at different institutions, just like many other things during our geography studies. Dankje om zo'n goeie vriendin te zijn, om te luisteren, te delen en te zeveren. Bram, Hans, Basaltje, Ann, Arno en Tine, bedankt voor de vele kampeertripjes in zomer en winter, die waren uiterst efficiënt voor het opladen van de batterijen! Naar 't schijnt kan je in Zwitserland ook op elanden jagen...

Bedankt Lennert en Sara, voor de fijne avonden in de Grensstraat in Saint-Josse, ons leven was zo Anders toen. Younes, bringer of light and joy tijdens je vele tripjes naar Brussel, ook in Bern zal er altijd een slaapbank voor je klaarstaan. Dankje Niels en Marthe, praten met jullie heeft mij door de iets moeilijkere momenten heengesleurd. Bedankt aan mijn (geografen)vrienden uit alle (veelal Belgische) windrichtingen. De vakanties, weekendjes, grensfietstochten en andere avonturen brachten de nodige afleiding. Ik hoop dat er toch een aantal tradities in ere worden gehouden, ook nu de volgende levensfases zich aandienen met (ver)huizen, schoonfamilies en kleine spruitjes.

Ik besef dat ik mezelf heel gelukkig mag prijzen met zo'n uitgebreide en warme familie. Dankjewel oma Rachel, opa Michel, Marie-Louise, tantes, nonkels, neven en nichten voor de aanmoedigingen en het aandachtig luisteren wanneer ik weer een klimaatveranderingsverhaal afstak op familiefeest. In het bijzonder bedankt aan de familie Verdoodt dat ik mijn presentatie over klimaatverandering mocht brengen op het familieweekend.

Een dikke dankjewel aan Hilde, Daniel, Evi, Pieter. Jullie onvoorwaardelijke steun als schone familie was onontbeerlijk. Lieve kleine Oscar en Maurice, jullie herinneren mij eraan wat echt telt in het leven.

En dan, grootse dank aan An, Johan en Jana, mijn ouders en zus. Zonder jullie steun, trots, enthousaisme en liefde door de jaren heen zou ik hier niet gestaan hebben.

Finally, last but not least, Dries. Words cannot describe how thankful I am to had you on my side during the PhD roller coaster, with large ups and deep downs. Thank you for comforting me when I felt discouraged and self conscious, for cheering my big and small victories, for providing me with my basic needs, for staying calm when I again forgot or lost something, and for just unconditionally being there for me. You are my all-time sparring partner and soulmate, thank you for everything. Ik zie je graag.

Inne

June 2022

Abstract

Humans are an integral component of the terrestrial water cycle. Global water resources are fundamentally altered by anthropogenic climate change and direct human management. Dams and reservoirs are a key example, as they regulate the river flow and store freshwater. Worldwide, more than 45,000 reservoirs are built since the start of the 20th century. The creation of these new open-water surfaces impacts the interactions with the atmosphere. At the same time, anthropogenic climate change causes changes in the hydrological cycle and affects global freshwater resources. To assess the role of reservoirs within the Earth system and under a changing climate, they need to be represented in integrated modelling frameworks, like Earth system models. This thesis aims both to implement the role of reservoirs in the state-of-the-art Community Earth System Model (CESM) framework and advance our understanding of reservoirs in the Earth system across different spatial and temporal scales.

To start, we estimate the potential consequences of climate change and dam management for future water level fluctuations of Lake Victoria, located in East-Africa. Lake Victoria is the second largest freshwater lake in the world and controlled by two dams for hydropower. Using a water balance model forced with lake precipitation, evaporation and inflow projections based on simulations from the Coordinated Regional Climate Downscaling Experiment ensemble, lake level projections are conducted under various climate change and idealized dam management scenarios. The results reveal that the operating strategies at the dam are the main controlling factors of future lake levels, and that regional climate simulations used in the projections encompass large uncertainties. This case study therefore highlights the importance of dam operations and reservoir management when modelling future river flow and water resources.

In the following study, we zoom out to the global scale to provide the first estimate of the global heat uptake by inland waters. Mapping the different components of the heat inventory is key to understand the Earth system response to anthropogenic greenhouse gas forcing. By employing a combination of global lake models, global hydrological models and Earth system models, we quantify the energy stored in lakes, reservoirs and rivers from 1900 to 2020. The total heat uptake amounts up to $2.6 \cdot 10^{20}$ J, corresponding to 3.6% of the continental heat uptake. Most energy is used to warm natural lakes (111.7%), followed by reservoirs (2.3%). Rivers contribute negatively (-14%) mainly due to decreasing water

volumes. Further, dam construction and subsequent reservoir creation leads to a redistribution of heat contained in the water, and thereby increases the potential of inland water heat uptake by warming of reservoir waters, due to the high heat capacity of water.

Then, global reservoir expansion is implemented in the Community Land Model (CLM5), the land model of CESM, as dynamically changing lake area to account for the large increase in open-water area following reservoir construction. Land-only simulations covering 20th century highlight that reservoir expansion increases in terrestrial water storage and decreases the surface albedo, matching the increase in open water area. In addition, atmosphere-land coupled CESM simulations indicate that globally, reservoirs dampen the diurnal temperature range and mute temperature extremes in the present-day climate. The responses scale with reservoir extent and can be substantial locally, but the influence on global climate is limited.

Finally, we implement and evaluate a widely-used dam parametrisation of Hanasaki et al. (2006) in the global routing model mizuRoute to be coupled to CESM. As this dam parametrisation requires irrigation water demand to determine releases of irrigation reservoirs, we develop a new irrigation topology to integrate the irrigation demands of the vector-based catchments to specific reservoirs. Using a local model setup with observations from individual reservoirs as a benchmark, the reservoir parametrisation outperforms the natural lake scheme, highlighting a clear added value of our model development for river flow modelling. In the global application, using a vector-based river network and simulated runoff from CLM5, the reservoir parametrisation outperforms simulations without lakes for river flow, but shows a similar performance compared to the natural lake scheme. This could be attributed to biases in inflow seasonality and amount, originating from the CLM5 runoff and detail of the river network.

Overall, this thesis advances the current understanding on the role of reservoirs in the changing climate and provides important steps towards better representing human water management in Earth system models. Globally, the effects of reservoir expansion on the global climate are small, but locally the influence can be substantial. Future work may build on this research by coupling the routing model mizuRoute into the CESM framework, and thereby represent a two-way coupling between land surface processes and surface water transport. Finally, this study is a direct contribution towards the next generation of Earth system models that fully integrate human management and climate change scenarios to investigate potential mitigation and adaptation strategies.

Samenvatting

Mensen spelen een belangrijke rol in de wereldwijde waterhuishouding. Dammen en de stuwmeren die gevormd worden door het afdammen van rivieren en meren zijn hier een belangrijk voorbeeld van. Wereldwijd werden in de afgelopen decennia meer dan 45 000 grote dammen gebouwd voor irrigatie, wateropslag, het controleren van overstromingen en het opwekken van elektriciteit. De stuwmeren hebben een grote invloed op de waterkringloop omdat ze de waterbeschikbaarheid en de regionale weersomstandigheden wijzigen. Tot op heden is er echter maar weinig geweten over de rol van stuwmeren in het klimaat. Bovendien houdt de huidige generatie klimaatmodellen geen rekening met de specifieke rol van stuwmeren. Deze doctoraatsthesis beoogt de interacties tussen stuwmeren en het aardsysteem en de klimaatverandering te ontrafelen op lokale, regionale en wereldwijde schaal. Door zowel de bouw van stuwmeren en de daaropvolgende toename in wateroppervlak, en de stroomregulatie door dammen te implementeren in het globaal klimaatmodel *Community Earth System Model (CESM)*, verbeteren we de simulatie van de hedendaagse watercyclus en kwantificeren we de effecten op het hedendaags klimaat.

Ten eerste kwantificeren we de mogelijke gevolgen van klimaatsverandering en dambeheer voor de toekomstige evolutie van het niveau van het Victoriameer in Oost-Afrika. Het Victoriameer is het tweede grootste zoetwatermeer op aarde en de bron van de Witte Nijl, die gecontroleerd wordt door een dammencomplex. Sommige regionale klimaatmodellen voorspellen een afname in neerslag boven het meer, terwijl de verdamping toeneemt. Door een waterbalansmodel te voeden met regionale klimaatsimulaties uit het *Coordinated Regional Climate Downscaling Experiment*, wordt de evolutie van het waterniveau voorspeld met verschillende emissie- en dambeheerscenario's. De resultaten tonen aan dat de waterregulatie aan de dam de belangrijkste factor is om het meerniveau op pijl te houden, ondanks de grote onzekerheden in klimaatprojecties voor neerslag, verdamping en instroom in het meer. Deze lokale studie dient daarom als een voorbeeld om het belang van dambeheer voor rivierdebieten en waterhuishouding te benadrukken.

In het volgende hoofdstuk zoomen we uit naar de wereldwijde schaal, waarbij we de eerste schatting maken van de wereldwijde hitte-opslag van binnenwateren. Het kwantificeren van de verschillende componenten van de warmte-inventaris is belangrijk om de reactie van het aardsysteem op de antropogene broeikasgasforcering te begrijpen. We kwantificeren daarom de hoeveelheid energie die sinds 1900 opgeslagen werd in natuurlijke meren,

stuwmeren en rivieren op basis van globale meer-, hydrologische- en klimaatmodellen. In totaal is er in deze periode $2.6 \cdot 10^{20}$ J opgenomen door binnenwateren, wat overeenkomt met 3.6% van de totale continentale hitte-opslag. De meeste energie wordt gebruikt om natuurlijke meren op te warmen (111.7%), gevolgd door stuwmeren (2.3%). Rivieren kennen een negatieve hitte-opslag, voornamelijk door afnemende watervolumes. Verder tonen de resultaten aan dat door de bouw van stuwmeren er een herverdeling van warmte van de oceaan naar het land heeft plaatsgevonden. Daarbij is er een groot bijkomend potentieel voor hitteopslag op land gecreëerd, mede door de hoge warmtecapaciteit van water.

Vervolgens implementeren we de bouw van dammen en de daaropvolgende creatie van open water oppervlakken sinds 1900 in het *Community Land Model (CLM5)*, het land model van CESM. Globale simulaties met CLM5 voor de 20ste eeuw tonen aan dat de bouw van stuwmeren de water opslag op land doet toenemen en het albedo van het aardoppervlak doet afnemen, consistent met de toename in wateroppervlak. Bovendien blijkt uit gekoppelde atmosfeer-land simulaties met CESM voor het huidige klimaat dat wereldwijd stuwmeren zowel de dagelijkse en seizoensgebonden temperatuurscyclus afvlakken als de temperatuurextremen dempen. De impact daarvan is afhankelijk van de omvang van de reservoirs en kan plaatselijk aanzienlijk zijn, maar de invloed op het mondiale klimaat is beperkt.

Ten slotte implementeren en evalueren we een veelgebruikte damparametrisatie in het globale riviermodel mizuRoute, dat aan CESM zal worden gekoppeld. Daarbij ontwikkelen we een nieuwe irrigatie-topologie, die bepaalt welke deelbekkens in rekening worden gebracht bij het berekenen van de vraag naar irrigatiewater aan individuele stuwmeren. In een modeltoepassing waarin we het model aandrijven met waarnemingen van individuele stuwmeren, toont de damparametrisatie een beter resultaat in vergelijking met een parametrisatie voor natuurlijke meren. In de mondiale setting, gebruikmakende van een vector-gebaseerd riviernetwerk en aangedreven door de gesimuleerde afvloeiing van CLM5, is de toegevoegde waarde van de damparametrisatie ten opzichte van de simulatie van natuurlijke meren niet langer aanwezig. Dit kan worden toegeschreven aan fouten in de seizoensvariaties en de hoeveelheid van de stuwmeerinstroom, die terug te leiden zijn tot de afvloeing simulaties van CLM5 en het detailniveau van het gevectoriseerde riviernetwerk.

Dit proefschrift verdiept het wetenschappelijk inzicht inzake de rol van stuwmeren in het aardsysteem en in een veranderend klimaat. Daarbij levert het ook een belangrijke bijdrage aan een betere weergave van de menselijke factor inzake waterbeheer in aardsysteemmodellen. Wereldwijd zijn de effecten van stuwmeren op het klimaat klein, maar lokaal kan de invloed substantieel zijn. Toekomstige studies kunnen verder bouwen op deze ontwikkelingen door het riviermodel mizuRoute te koppelen met CESM, in het bijzonder voor de tweezijdige koppeling tussen landschapsprocessen en watertransport. Tot slot effent deze studie de weg naar de volgende generatie aardsysteemmodellen die menselijke beheers- en klimaatveranderingsscenario's volledig integreren om daarmee beter potentiële mitigatie- en aanpassingsstrategieën te onderzoeken.

List of abbreviations

ALBM	Arctic Lake Biogeochemistry Model
AMIP	Atmospheric Model Intercomparison Project
CAM	Community Atmosphere Model
CDF	Cumulative Density Function
CESM	Community Earth System Model
CIME	Common Infrastructure for Modeling the Earth
CISM	Community Ice Sheet Model
CLM	Community Land Model
CMIP5	Coupled Model Intercomparison Project Phase 5
CN	Curve Number
CORDEX	Coordinated Reginal Climate Downscaling Experiment
COSMO-CLM^2	Consortium for Small-Scale Modelling in climate mode
CTSM	Community Terrestrial Systems Model
DAHITI	Database ffor Hydrological Time Series of Inland Waters
DTR	Diurnal Temperature Range
ECMWF	European Center for Medium-Range Weather Forecasts
ESM	Earth System Model
ETCCDI	Expert Team of Climate Change Detection and Indices
GCM	Global Circulation Model
GHM	Global Hydrological Model
GLC 2000	Global Land Cover 2000 dataset
GLDB	Global Lake Database
GOODD	Global Georeferenced Database of Dams
GRACE	Gravity Recovery and Climate Experiment
GRanD	Global Reservoir and Dam dataset
GSIM	Global Streamflow Indices and Metadata
GSWP3	Global Soil and Wetness Project
HDMA	Hydrologic Derivatives for Modeling and Applications
HPP	Hydropower production
HRU	Hydrologic Response Unit
ILAMB	International Land Model Benchmarking software
IPCC	International Panel on Climate Change
IRF	Impulse Response Function
ISIMIP	Inter-Sectoral Model Intercomparison Project

KGE	Kling-Gupta Efficiency
KWT	Kinematic Wave Tracking
LHF	Latent Heat Flux
LSM	Land Surface Model
LUH2	Land Use Harmonization project
LVB	Lake Victoria Basin
LW_{net}	Net longwave radiation at the surface
MATSIRO	Minimal Advanced Treatments of Surface Interaction and Runoff model
MERIT	Multi Error Removed Improved Terrain
MOSART	Model for Scale Adeptive River Transport
NCAR	National Center for Atmospheric Research
NLDAS	North American Land Data Assimilation System
PBIAS	Absolute percent bias
PERSIANN-CDR	Precipitation Estimation Remotely Sensed Information using Artificial Neural Networks
POP	Parallel Ocean Program
RCM	Regional Climate Model
RCP	Representative Concentration Pathway
SD	Standard Deviation
SHF	Sensible Heat Flux
SW_{net}	Net shortwave radiation at the surface
SWOT	Surface Water and Ocean Topography
TNn	Monthly minimum temperature
TWS	Terrestrial Water Storage
TXx	Monthly maximum temperature
VIC	Variable Infiltration Capacity Model
WACCM	Whole Atmosphere Community Climate Model
WB	Water Balance
WBM	Water Balance Model
WMO	World Meteorological Organisation

Contents

List of Figures

List of Tables

Chapter 1

Introduction

1.1 General Background

1.1.1 Reservoirs in the hydrological cycle

The terrestrial water cycle is vital for the functioning of the Earth System and directly supports the fundamental needs of human life. Every year, humans appropriate about 24,000 km^3 of water, which is equivalent to half of the annual global river discharge (Abbott et al., 2019; Rockström et al., 2009). Humans need freshwater for drinking and sanitation purposes, and even higher quantities are used for irrigation, industry, hydroelectricity generation and cooling of thermoelectric power plants (Schewe et al., 2014). Thereby, water systems are altered by human activities like urbanisation, industrialisation and land cover changes, and impacted by the effects from anthropogenic climate change (Vörösmarty et al., 2010). Humans interfere directly with the hydrological cycle through altering freshwater flows and storage by groundwater pumping, water abstraction and diversions for irrigation and constructing dams and reservoirs (Fig. 1.1; Oki and Kanae, 2006; Wada et al., 2014). In some regions, the impacts from human disturbances on mean annual runoff are similar or exceeding impacts from anthropogenic climate change (global warming of +2 K; Haddeland et al., 2014), even though the climate signal dominates river flow changes at the global scale (Gudmundsson et al., 2021). It therefore is important to depict and represent the hydrological cycle with human interactions included, in order to highlight the active role humans play in water scarcity and governance (Abbott et al., 2019).

The construction of dams, and the reservoirs thereby created, are one of the key components of human interference in the terrestrial water cycle. Since the start of the 20^{th} century, humans have built more than 50,000 large dams worldwide (with dam height >15 m; Lehner et al., 2011). During the 20^{th} century, dam construction steadily rose, with a rapid increase from the 1950s to 1980s (Fig. 1.2). These large water management infrastructures are build for hydropower production, irrigation, flood control, water supply, navigation and recreational purposes.

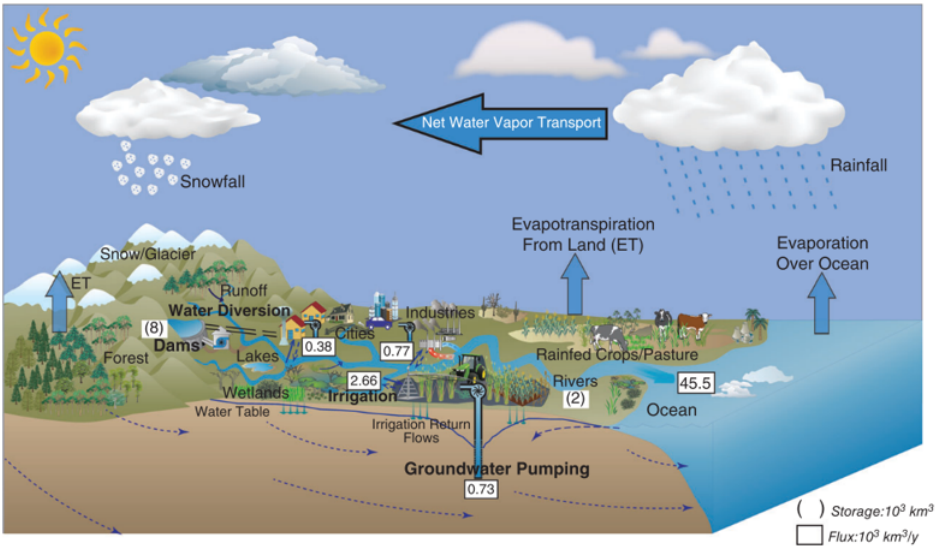

Figure 1.1: **The global water cycle with the main natural processes and human water management practises.** Figure from Pokhrel et al. (2016).

All together, they cover more than 305,000 km^2 of open water (Lehner et al., 2011), corresponding to more than 7% of Earth's terrestrial freshwater surface and 0.2% of global land area (Messager et al., 2016; Mulligan et al., 2020). In total, reservoirs impound between 7,000 and 8,300 km^3 of water (Chao et al., 2008), which is about one sixth of the annual continental discharge to the oceans (Oki and Kanae, 2006). The filling of these reservoirs slowed down global sea level rise, notably during the boom of reservoir construction and concurrent filling in the 1970s (inset Fig. 1.2; Frederikse et al., 2020). The overall reduction in global sea level rise by reservoir water storage is estimated to be around 30 mm (Chao et al., 2008).

Human-controlled reservoirs are therefore an important category of inland water bodies, next to natural lakes, rivers and wetlands. Level and storage fluctuations of natural lakes are governed by both variability and long-term change in climatic drivers like precipitation and evaporation, and by basin characteristics determining the basin runoff, inflow and lake outflow. In contrast, the storage dynamics of newly constructed reservoirs and dammed natural lakes are not only controlled by climate and inflow variability and change, but also by human decisions following downstream demand pressures (Nazemi and Wheater, 2015b). This leads to large impacts on downstream flow characteristics.

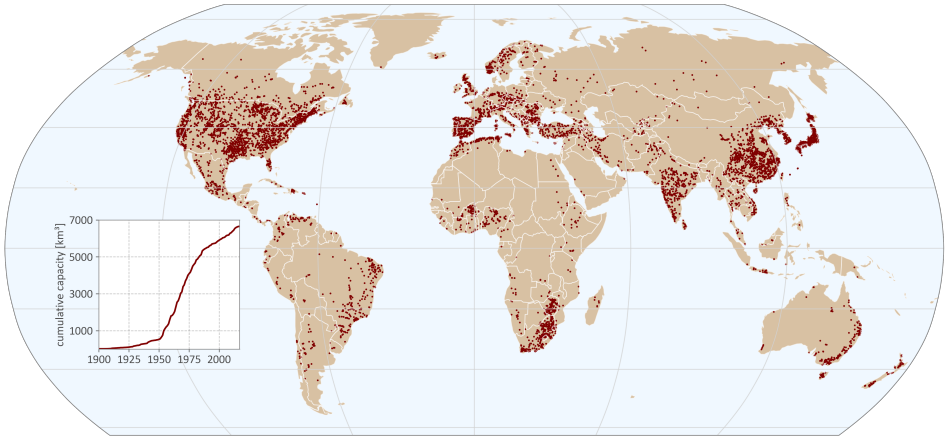

Figure 1.2: **Global distribution of large reservoirs** (maximum capacity > 0.1 km^3) based on GRanD (Lehner et al., 2011). Inset figure shows the cumulative reservoir capacity from 1900 to 2017.

By regulating the flow through dam operations, reservoirs have a large impact on the timing, peak and amount of natural discharge (Döll et al., 2009). Depending on their purpose, they alter the water availability in their immediate surroundings and further downstream (Veldkamp et al., 2017). For example, irrigation reservoirs are operated to accumulate water in the high-flow seasons that can be used to sustain the irrigation-fed agriculture during the remainder of the year (Biemans et al., 2011). Today, 57% of the variability in terrestrial surface water storage is controlled by human-managed reservoirs (Cooley et al., 2021). This reservoir-induced seasonal storage variation corresponds to 700 km^3, or 10% of the total water stored in reservoirs worldwide (Zhou et al., 2016). Next to their influence on seasonal fluctuations, reservoirs alter the interannual storage variability by storing water during wet years, making it available during dry years (Hanasaki et al., 2006). Their impact on flow amplitude affect flow extremes, leading to a reduced flood exposure (Boulange et al., 2021). In addition, reservoirs could reduce drought impacts, by their capacity to store water during wet seasons. Together with water use, their influence on droughts can be substantial, but with large regional and seasonal variations (Wanders et al., 2019). Finally, dam construction has led to the regulation and fragmentation of large river systems (Nilsson et al., 2005). Today, 63% of rivers worldwide longer than 1000 km are flowing into the ocean with human imprints due to interruption or regulation (Grill et al., 2019).

Next to the clear benefits related to irrigation water supply, flood protection and hydropower production, reservoirs also have important detrimental impacts on environmental flows, greenhouse gas emissions, ecosystems and enhanced erosion downstream (Johnson et al., 2021; Gillespie et al., 2015; Kondolf et al., 2014). Moreover, human decisions related to dam management could lead to various feedbacks and could result in adverse effects, like

increased dependency on reservoir water supply or increased vulnerabilities in response to different hydrological extremes (Di Baldassarre et al., 2018, 2017). Still, driving factors like population growth, economic development and the need for renewable energy sources led to initiatives on expanding current hydropower capacity (Zarfl et al., 2014; Sterl et al., 2020, 2021b). Likewise, the construction of more than hundreds of reservoirs are planned worldwide (Winemiller et al., 2016; Pokhrel et al., 2018; Zarfl et al., 2014). These developments and their potential impacts are important to account for, particularly in the light of anthropogenic climate change.

1.1.2 Reservoirs in a changing climate

Anthropogenic greenhouse gas emissions cause a radiative imbalance at the top of the atmosphere. This results in a net energy gain for the whole Earth system, which is taken up by different components. More than 90 % of excess heat is taken up by oceans, leading to increasing water temperatures and rising sea levels through thermal expansion (Rhein et al., 2013; Trenberth, 2009). The remainder is used to warm up the continents, melt sea and land ice, and to increase atmospheric temperatures and water evaporation (Von Schuckmann et al., 2020; Beltrami, 2002). However, the amount of heat taken up by inland waters such as lakes, reservoirs and rivers, remains unknown. Next to the process of heat uptake, the radiative imbalance is directly driving global climate change, leading to the alteration of precipitation patterns and the intensification of the global hydrological cycle (Masson-Delmotte et al., 2021).

Climate change will have a large influence on global freshwater resources, ranging from increases in extreme precipitation and floods to prolonged periods of drought, affecting water availability and scarcity (Greve et al., 2014; Haddeland et al., 2014; Schewe et al., 2014; Pokhrel et al., 2021). Already today, observed trends in mean and maximum river flow are attributed to anthropogenic forcing (Gudmundsson et al., 2021) and rising lake temperatures and shortening of lake ice cover duration can only be explained by climate change (Grant et al., 2021). Climate change is also directly impacting reservoirs and their water supply. For example, reservoir evaporation represent a substantial loss of available water, which is enhanced by the creation of more open water surfaces due to dam construction (Friedrich et al., 2018). As lake evaporation is projected to increase globally in a warmer climate (Zhou et al., 2021), the interplay and relative importance of this type of processes are important to assess future water availability and hydropower potential of reservoirs. Moreover, reservoir inflows are influenced by climate change through alteration of precipitation patterns, leading to deficits in water supply, which also impacts reservoir dynamics (Wanders et al., 2019).

Next to the impacts of the overlying atmospheric processes and climate change on reservoirs, the presence of the reservoirs themselves could also influence the surrounding climate. Dam construction and subsequent reservoir filling changes the preexisting land cover to an open water surface, thereby altering surface properties like albedo, surface roughness

and atmospheric heat exchange through turbulent surface fluxes (Sterling et al., 2013). Together with concurrent land use changes in the vicinity of the reservoirs (e.g. deforestation for cropland expansion following irrigation water availability, urban expansion due to availability of water), such changes could alter the local climate. A small body of observation-based studies exists, which suggest that large reservoirs could increase the convective available potential energy as well as specific humidity (Degu et al., 2011), and thereby influence extreme precipitation (Hossain et al., 2010, 2012). The physical mechanisms behind these impacts are, however, not known (Woldemichael et al., 2012). Additionally, the global-scale impact of reservoir expansion on the present-day climate remains unknown due to the limited spatial scope of previous studies.

1.1.3 Studying reservoirs in the Earth system: need of integrated frameworks

Given the importance of reservoirs in the global terrestrial water cycle, it is key to adequately understand their functioning in the Earth system, as well as to quantify their impacts on the climate system at a global scale. Addressing these research questions, calls for the use of holistic modeling frameworks in which all relevant processes are represented, including components of the terrestrial hydrological cycle, human water management, atmospheric processes and climate change drivers, in a globally integrated way (Nazemi and Wheater, 2015a; Pokhrel et al., 2016). In such coupled frameworks, interactions and feedbacks between the land surface and climate are directly modelled, and land cover and management change are represented under different scenarios and for different time periods, which allow to investigate both the physical mechanisms and spatial and temporal extents of impacts. To date, Earth System Models (ESMs) provide this type of integrated framework, but do generally not include accurate representations of reservoirs. They are, however, the ideal tools to investigate the global climate impacts of reservoir expansion and the corresponding increase in open water area, as well as the impacts of dam regulation on streamflow characteristics, for the historical and present-day periods, and for scenarios of future climate change. Such model-based assessments can aid future mitigation and adaptation strategies linked to reservoir construction and operation to assess future water scarcity and ensure future water availability in a changing climate.

1.2 Modeling reservoirs in the Earth system

Different approaches exists to model reservoirs in the Earth system. Below, we outline the major global-scale modelling frameworks. First, we provide a general description of ESMs with a specific focus on the Community Earth System Model (CESM) and its components, as this is the model used in this thesis. Then, we present an overview of impact models, focused on global hydrological models and their reservoir representations.

1.2.1 Earth System Models

ESMs are key tools to study past and future evolution of Earth processes by simulating and integrating physical, chemical and biological processes and feedbacks of the atmosphere, ocean, land, ice, and biosphere. At their core, ESMs represent the climate by simulating atmospheric and ocean processes using mathematical equations based on physics. They advance their predecessors, the General Circulation Models (GCMs), by representing the global carbon cycle, atmospheric and ocean biochemistry, dynamic vegetation and continental ice sheets in a single, consistent modeling framework (Bonan and Doney, 2018). Therefore, ESMs are able to better simulate human influence on the climate, by interlinking all components defining Earths climate. Due to their global extent and large computational cost, ESMs mostly use coarser resolutions of typically $\sim$100 km. To provide more details on regional and meso-scale processes, they can be dynamically downscaled with Regional Climate Models (RCMs, Giorgi et al., 2009).

The terrestrial water cycle is represented by the land component of ESMs, the Land Surface Models (LSMs). These models simulate water and energy exchanges between the surface and atmosphere, and represent the energy, water, carbon and nitrogen cycles (Fig. 1.3). Originally developed to provide the boundary condition for atmospheric processes of GCMs, land models are now advanced tools with detailed representations of vegetation and soil processes including two-way feedbacks with the atmosphere, like plant responses to changes in temperature, precipitation and CO_2 concentration. While natural components of the hydrological cycle, like snow dynamics, evaporation and soil hydrology are generally well represented in land models, the inclusion of human interventions in the water cycle remains limited (Pokhrel et al., 2016). Past efforts aimed to address this limitation by advancing implementations of irrigation practises, crop growth, groundwater abstractions and human water use (e.g. De Vrese et al., 2016; Sacks et al., 2008; Thiery et al., 2017; Lombardozzi et al., 2020; Pokhrel et al., 2015; Zhou et al., 2020; Yokohata et al., 2020; Felfelani et al., 2020). Very recently, water management modules have been coupled to the E3SM and MIROC ESMs (Zhou et al., 2020; Yokohata et al., 2020).

In this thesis, we use the Community Earth System Model version 2 (CESM2; Danabasoglu et al., 2020). CESM2 is a fully-coupled, state-of-the art ESM, which contributed simulations to the Coupled Model Intercomparison Project phase 6 (CMIP6; Eyring et al., 2016). It simulates the Earth system using ocean, atmosphere, land, sea-ice, land-ice, river and wave models, of which continuously communicate states and fluxes to each other

through a coupler. CESM2 is an open-source community model hosted at the National Center for Atmospheric Research (NCAR) and is actively developed by a large international research community including universities and research institutions (Danabasoglu et al., 2020). CESM2 includes two atmosphere models, the Community Atmosphere Model Version 6 (CAM6), with 'low-top' atmosphere, and the Whole Atmosphere Community Climate Model Version 6 (WACCM6), with better stratosphere representation and advanced atmospheric chemistry ('high-top' atmosphere).

The ocean is solved by the Parallel Ocean Program Version 2 (POP2) and sea ice using CICE, while land ice is modelled with the Community Ice Sheet Model Version 2.1 (CISM2.1). State and flux exchanges between the components are controlled by the Common Infrastructure for Modeling the Earth (CIME), which serves both as the coupler and as the infrastructure to build and run the model (Danabasoglu et al., 2020).

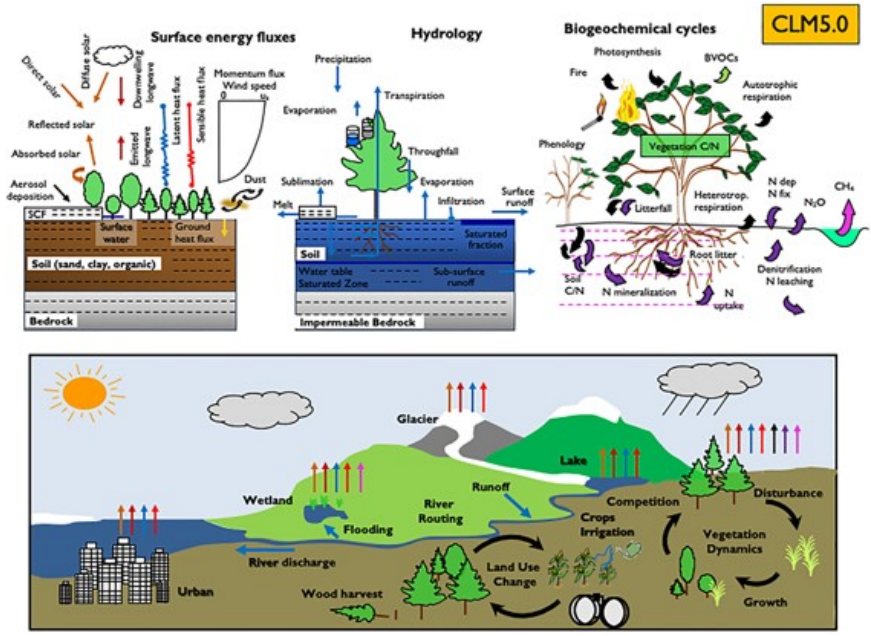

Figure 1.3: **Terrestrial processes simulated by CLM5.** Figure from Lawrence et al. (2019a).

In CESM, land processes are solved by the Community Land Model version 5 (CLM5; Lawrence et al., 2019a), an advanced LSM representing the physical, chemical and biological processes related to terrestrial ecosystems and climate in a variety of spatial and temporal scales (Fig. 1.3). Surface heterogeneity is accounted for by a nested tile approach, in which each grid cell is subdivided in different land units, representing natural vegetation, crops, lakes, glaciers and urban areas (Fig. 1.4). The default version of CLM5 has the functionality of modeling land use and land management change through altering grid cell fractions of different land units, with the possibility of accounting for transitions between natural vegetation, crop and glacier land units, while conserving total grid cell mass and energy. In the standard configuration, land cover and land use data are prescribed to CLM5 based on past and future land use available from the Land Use Harmonization 2 dataset (LUH2; Hurtt et al., 2020).

River routing, the process of over-land water transport to the ocean through rivers, is modeled as a separate component in the coupled CESM framework, but is linked to CLM as it directly receives surface runoff from CLM as input. The default river routing component in the release version of CESM2 is the Model for Scale Adaptive River Transport (MOSART; Li et al., 2013). Within a grid cell, MOSART first routes overland flow along hillslopes before entering it in the tributary stream network, where it confluences with the unrouted subsurface runoff. Within each grid cell, all tributaries are treated together. The flow from the tributary stream enters the main channel, which receives water from the upstream cell(s) and discharges it to the downstream grid cell or to the ocean.

In the upcoming release of CLM and CESM, however, MOSART will be replaced by the vector-based routing model mizuRoute, of which the name refers to *mizu*, which is Japanese for water, and the first part of the main developers' surname (Mizukami et al., 2016). MizuRoute is a stand-alone routing tool to estimate spatially distributed river flow along the stream network based on spatially distributed runoff provided by hydrological or land models. To this end, the model first routes the basin runoff from the hillslopes with a gamma distribution shaped unit-hydrograph. In a second step, mizuRoute routes the water downstream along the river network, either with an impulse response function (IRF) or a kinematic wave tracking routing technique (Mizukami et al., 2016). The runoff of the land surface or hydrological model is remapped from its original spatial unit (e.g. grid cells) using areal weighted averages. In its global configuration, the model has the ability use parallel computing units, due to a hierarchical spatial decomposition subdividing the stream network into hydrologically independent subbasins (Mizukami et al., 2021). Lakes in mizuRoute are modeled as integral parts of the stream network (Gharari et al., 2022).

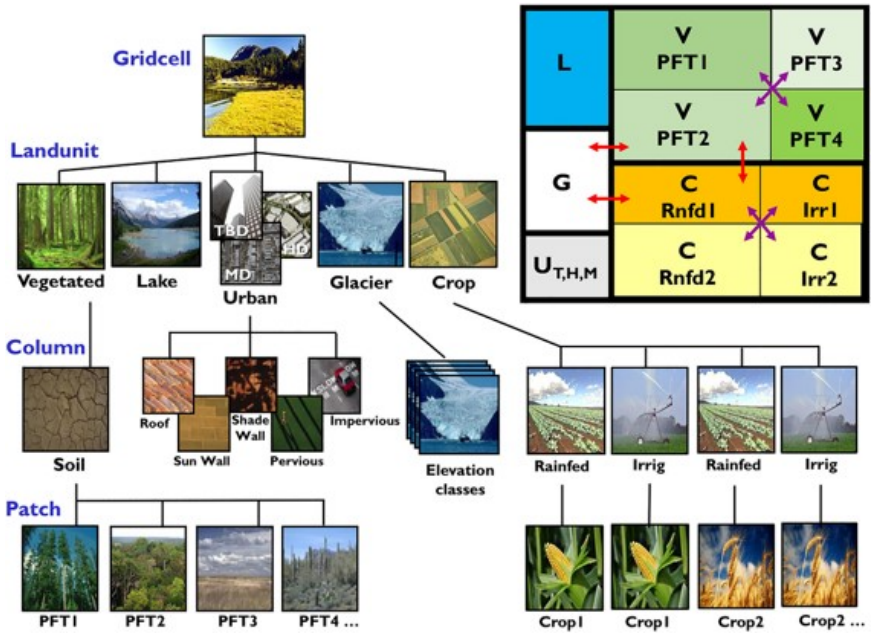

Figure 1.4: **The CLM5 subgrid hierarchy.** The upper right box shows an example subgrid distribution in landunits: lake (L), glacier (G), urban (U) different vegetation (V) plant functional types (PFTs) and crop (C) with rainfed (Rnfd) and irrigated crops (Irr). Figure from Lawrence et al. (2019a).

In CLM5, many efforts are directed towards improving the hydrological processes of the natural water cycle (Clark et al., 2015). This resulted in a better representation of groundwater schemes (Swenson and Lawrence, 2015), updates in soil hydrology (Swenson and Lawrence, 2012), more realistic snow due to a fresh snow density parametrisation (Lawrence et al., 2019a), the explicit modeling of plant hydraulics through leaves, stems and roots (Kennedy et al., 2019) and an updated lake model including snow and ice physics and improved parametrisation of lake surface properties (Subin et al., 2012c). In contrast, less attention has been given to incorporating human activities in the water cycle. Recent efforts implemented irrigation (Sacks et al., 2008; Thiery et al., 2015; Yao et al., 2022) and groundwater abstractions (Felfelani et al., 2020), but representations of reservoirs and their effect on river flow, as well as and human water withdrawal for domestic and industrial use, are currently not included in CLM5 and MOSART (Pokhrel et al., 2015; Nazemi and Wheater, 2015a).

1.2.2 Impact Models

Next to ESMs with their land and river components, which are designed to represent the Earth system in a holistic framework accounting for feedbacks and interdependencies between the different components, there is another modelling approach targeted to modeling specific impacts or sectors. These impact models are typically highly specialized, process-based models. In hydrology for example, large-scale water resource assessments are conducted using models with different complexities, ranging from simple water balance models, catchment-scale hydrological models, water management models to global hydrological models representing the global terrestrial water cycle (Sood and Smakhtin, 2015; Telteu et al., 2021).

The different ranges of complexity, types of impacts modeled, model set-up and forcing make it difficult to combine and compare individual impact models across different sectors. To overcome this hurdle, the Inter-Sectoral Impact Model Intercomparison Project (ISIMIP) provides a simulation protocol to harmonize impact modeling efforts across different models and sectors (i.e. Frieler et al., 2017). The protocol includes socio-economic and bias-corrected meteorological forcing consisting of reanalysis, historical simulations and future climate change projections and prescribes the resolution and simulation periods (Frieler et al., 2017). This set-up allows for model comparison, as well as aggregation of cross-sectoral impacts (Lange et al., 2020; Thiery et al., 2021). For example, in the ISIMIP lake sector simulations with six different lake impact models are available to estimate climate change impacts on lake temperature, ice cover and shifts in lake stratification (Grant et al., 2021; Woolway et al., 2020). From a simulation protocol perspective, these simulations are consistent with other sectors, like the simulations with global hydrological models from the global water sector.

In contrast to the land models used in ESMs, global hydrological models typically incorporate human water management, as their main aims is to assess global freshwater availability (Wada et al., 2017; Bierkens, 2015; Veldkamp et al., 2017; Wada et al., 2014; Droppers et al., 2020; van Vliet et al., 2016; Döll et al., 2003; Hanasaki et al., 2008). Examples of global hydrological models are H08 (Hanasaki et al., 2008), PCR-GLOBWB (Van Beek et al., 2011; Wada et al., 2014), CWatM (Burek et al., 2020), WaterGAP2 (Döll et al., 2003) and LPJmL (Biemans et al., 2011). Seen the impact of dam operations on global streamflow, reservoir management is well represented in large-scale hydrological models (Telteu et al., 2021). These models serve as the main tool in various impact studies related to reservoirs, like the assessment of their impact on river flow variability (Döll et al., 2009), their role in reducing flood exposure (Boulange et al., 2021), their impact of water use and reservoirs on projected droughts (Wanders and Wada, 2015), the potential of global hydropower and cooling water discharge (van Vliet et al., 2016) and to formally attribute observed changes in streamflow to climate change rather than human water management (Gudmundsson et al., 2021).

Due to the large variations on operation rules and limited knowledge on dam operations worldwide, large-scale hydrological models typically employ generic schemes to represent reservoir regulation in relatively simple, wide-applicable procedures designed to simulate reservoir storage and release (Pokhrel et al., 2015). Currently, a wide range of different approaches exists (Gutenson et al., 2020; Yassin et al., 2019). According to Nazemi and Wheater (2015a), they can broadly be categorized in three groups: optimization-based, simulation-based and data-driven approaches.

The optimization-based approaches, mostly based on the parametrisation of Haddeland et al. (2006), search for the optimal release for all individual reservoirs based on several functional rules and using optimization algorithms. These approaches require prior knowledge of inflows in the coming year to optimize the outflows, which is less favourable in coupled frameworks (Haddeland et al., 2006; Van Beek et al., 2011). The second, simulation-based approaches contain simplified methods like described in Wisser et al. (2010), where release is estimated based on mean annual inflow and empirical coefficients. The most prominent scheme in this category, however, is the parametrisation of Hanasaki et al. (2006), where reservoir release is determined based on inflow seasonality and water demand, particularly accounting for irrigation reservoirs. Many subsequent studies implemented, adjusted and further improved this parametrisation (Döll et al., 2009; Hanasaki et al., 2008; Biemans et al., 2011; Pokhrel et al., 2012; Voisin et al., 2013a; Droppers et al., 2020).

The third, data-driven category covers many different approaches, which use observed historical reservoir releases and storages to calibrate the parameters of release functions. One approach is to determine reservoir releases based on targeted reservoir storage levels divided in different 'zones' (e.g. dead, conservation, flood control and emergency storage) and piece-wise linear release functions (Burek et al., 2013; Yassin et al., 2019). Observed reservoir releases and corresponding storages are used to calibrate the boundaries of these zones. More recently, machine learning methods like neural networks and fuzzy logic are employed to derive reservoir release curves (Coerver et al., 2018; Ehsani et al., 2016). Another option is to employ decision tables in which reservoirs are operated following user-specified conditions (Chawanda et al., 2020). Ultimately, the choice of reservoir scheme highly depends on various elements, including the scientific questions asked, intended purpose, domain, spatial and temporal resolutions (Turner et al., 2020). While many data-driven approaches are essential to provide detailed information on for example release forecasts at seasonal scales, global models with lower resolution and used for simulations at longer timescales could benefit more from more simple, 'one-size-fits-all' generic dam parametrisations (Pokhrel et al., 2016).

The potential to use large-scale hydrological models to study the interactions between reservoirs and their surrounding climate is limited. Generally, global hydrological models are process-based models in which vegetation and soil processes are solved in more conceptual ways and omit the land surface energy balance (Nazemi and Wheater, 2015b). In addition, their goal is to provide accurate river flows. To this end, model parameters are often cali-

brated to match simulated river flow with observations. Moreover, as reservoirs are often included in the river routing components, their interactions with soil and atmosphere are not modeled (Pokhrel et al., 2016). Nonetheless, global hydrological models and their well-tested reservoir representations are the ideal candidate to serve as an inspiration for implementing human water management in the land components of ESMs.

As such, bridging between impact models and Earth System models provides unique opportunities to improve the human water management representations in ESMs. In this thesis, we aim to use both impact model simulations from the ISIMIP initiative, and a single Earth system model, CESM to study the role of reservoirs in the Earth system. We also aim to advance the representation of reservoirs in a single Earth System Model, CESM, using state-of-the art reservoir data sets and leveraging from the way reservoirs are represented in global hydrological models. This advancement is twofold. First we aim to extend the functionality of CLM5 to account for changes in lake cover in order to represent the rapid reservoir expansion of the 20^{th} century, which allows to quantify the land-atmosphere interactions resulting from these land cover changes. Second, we aim to include human regulation in reservoir release and storage dynamics in the upcoming routing module of CLM5, mizuRoute. Summarized, the main objective of this thesis is to provide a solid baseline for incorporating reservoirs in CESM2 and thereby improve the representation of the terrestrial water cycle in fully-coupled climate models. These developments will eventually allow to better understand the interplay between climate change and human water management, and the consequences for future water availability.

Before conducting global analyses however, we focus on a local case study with a single reservoir: Lake Victoria, a natural lake controlled by two dams. Studying the interplay between dam management, climate variability and future climate change in determining the lake's water level with a simple water balance model, provides a stepping stone to explore the role of reservoirs in a global perspective. Therefore, in the following section, the case study on Lake Victoria is introduced by providing an overview of historical lake level variations, a description of the local water balance model and the role of different water balance terms in determining the lake level.

1.3 Case study: Modeling the water balance of Lake Victoria[1]

1.3.1 Lake Victoria's water level

Lake Victoria is the largest lake in Africa and one of the two major sources of the Nile River, directly sustaining the 30 million people living in its Basin and the 200 000 fishermen operating from its shores (Semazzi, 2011) and supporting natural resources impacting the livelihood of over 300 million people living in the Nile Basin (Semazzi, 2011). Fluctuations in the water level of the lake are therefore of major importance, as a drop in lake level may have massive implications for the ability of local communities to access water, to collect food via fishing and to transport goods (Semazzi, 2011). Moreover, a decreased outflow due to declining lake levels may have major consequences downstream, as the Nile river is already under immense pressure of various competitive uses and social, political and legislative conditions (Taye et al., 2011). In addition, lake level fluctuations also influence the amount of outflow released by the dam and by consequence the amount of hydropower generated and energy available in the region.

Lake level fluctuations are determined by the Water Balance (WB) of the lake. Precipitation on the lake surface provides the largest part of the water input to Lake Victoria. The rainfall in the African Great Lake region is mainly controlled by the annual migration of the Inter-Tropical Convergence Zone (ICTZ; Nicholson, 1996), with two rainy seasons: the long rains during March, April and May and the short rains during September, October and November (Yang et al., 2015; Williams et al., 2015). Approximately 25 major rivers flow from the basin into Lake Victoria, contributing to the inflow in the lake.

Water is lost by evaporation from the lake surface, which is often assumed to be constant (Kite, 1981; Piper et al., 1986; Sene and Plinston, 1994; Tate et al., 2004; Smith and Semazzi, 2014). Finally, the lake outflow is since 1951 controlled by the Nalubaale dam complex for hydropower located at Jinja, Uganda. The outflow amounts are regulated by the Agreed Curve, a rating curve relating lake level and outflow in natural conditions. This dam operating rule was closely followed until 2000, when increasing power demands in Uganda led to the construction of a second dam (called Kiira), parallel with the Nalubaale dam (Kull, 2006). The combination of the two dams facilitated deviation from the Agreed Curve by releasing more water (Awange et al., 2007b; Kull, 2006; Sutcliffe and Petersen, 2007).

The level of Lake Victoria fluctuated up to 3 meters over the last 65 years (Fig. 1.5). The rapid rise in the years 1961-1964 could not be attributed to the construction of the dam in 1951, but is linked to unusual heavy precipitation in East Africa as a similar rise is observed in the levels of other African Great Lakes (Lake Albert, Malawi and Tanganyika) in the early 60s (Kite, 1981).

[1] This section is based on the MSc thesis of the author, published as Vanderkelen et al. (2018a).

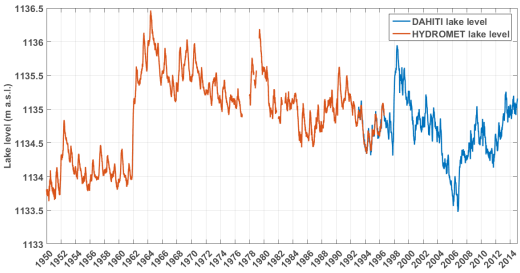

Figure 1.5: Lake Victoria water levels from in situ measurements from the HYDROMET survey (WMO, 1981) and Database for Hydrological Time Series of Inland Waters (DAHITI) satellite altimetry measurements (Schwatke et al., 2015).

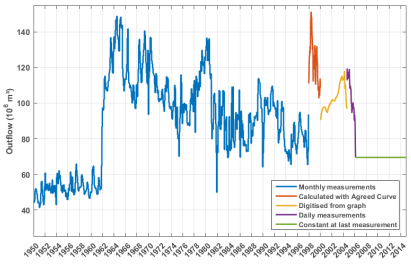

Figure 1.6: Daily outflow time series compiled from different data sources: monthly measurements, digitzed values from Lake Victoria Basin Commission (2006), daily measurements and constant outflow at 2006-value.

Given the high societal importance, several studies have attempted to reconstruct historical variations in the water levels of Lake Victoria based on observations (Kite, 1981; Piper et al., 1986; Sene and Plinston, 1994; Yin and Nicholson, 1998; Tate et al., 2004; Awange et al., 2007a; Swenson and Wahr, 2009; Hassan and Jin, 2014). However, due to scarcity of in-situ observations, many estimates of individual water balance terms are characterised by substantial uncertainties, which makes that the water balance is often not closed independently. Vanderkelen et al. (2018a) presents a water balance model for Lake Victoria, using state-of-the-art remote sensing observations, high resolution reanalysis downscaling and outflow values recorded at the dam. Below we provide a summary of the Vanderkelen et al. (2018a) study, focusing on the WBM and the role of human dam management in the recent lake level evolution. Further details on the data and methods, and an elaborated discussion and comparison to WB terms to values found in literature can be found in the paper.

1.3.2 The water balance model

The most general way to represent the water balance of Lake Victoria is given by:

$$\frac{dL}{dt} = P - E + \frac{Q_{in} - Q_{out}}{A} \tag{1.1}$$

Looping over all days in the model period, each day dt the difference in lake level dL (m) is calculated based on the daily mean precipitation on the lake P (m day^{-1}), daily mean evaporation of the lake E (m day^{-1}) , inflow Q_{in} (m^3 day^{-1}) and outflow Q_{out} (m^3 day^{-1}) on that specific day. This difference in lake level is added to the lake level of the previous day. In this way, a lake level time series is modelled.

The inflow and outflow are divided by the surface area of Lake Victoria ($6.83 \cdot 10^{10}$ m^2) to convert their values from discharge (m^3 day^{-1}) to lake level changes (m day^{-1}). In this WBM, the baseflow is assumed to be negligible.

We use daily precipitation observations from the Precipitation Estimation from Remotely Sensed Information using Artificial Neural Networks - Climate Data Record (PERSIANN-CDR), which provides daily precipitation for the period 1983-2015 at a 0.25° by 0.25° spatial resolution based on multi-satellite records (Ashouri et al., 2015). Lake evaporation is assessed by using the Latent Heat Flux (LHF) output of the regional climate model COSMO-CLM^2 (Davin and Seneviratne, 2012), of which the high resolution downscaling ($\sim$7 km) with the ERA-Interim reanalysis provides an adequate representation of the climate over and around the African Great Lakes (Thiery et al., 2015, 2016, 2017; Docquier et al., 2016). The annual evaporation climatology is estimated from daily LHF of the COSMO-CLM^2 model output for 1996-2008 and applied to each year of the observational water balance analysis period. Inflow by tributary rivers is calculated using the Soil Conservation Service-Curve Number method (NEH4, 2004), relating daily precipitation to daily runoff through the Curve Number (CN), obtained based on an empirical model with parameters associated to land use, hydrological soil types and antecedent hydrological conditions (see Vanderkelen et al. (2018a) for the methodological details). Finally, daily outflow time series is complied from different data sources (Kull, 2006; Lake Victoria Basin Commission, 2006, Fig. 1.3), as a complete time series is not publicly available and could not be obtained. All spatial variables are remapped to a predefined model grid, containing Lake Victoria and it's basin at a resolution of 0.065° by 0.065° (about 7 by 7 km). The WB model integration is performed using observational data for the period 1993-2014, a 21-year period for which all observational products are available.

1.3.3 Modelling the level of Lake Victoria

Precipitation over the lake and evaporation from the lake are the largest terms in the water balance (Fig. 1.7). On monthly time scales, the variation in precipitation is much larger than the variation in evaporation (7.44 mm day^{-1} versus 1.8 mm day^{-1}). As a consequence, monthly variations in precipitation have a much larger influence on lake levels both by lake precipitation and inflow than monthly variations in evaporation. However, the assumption of a constant annual evaporation (e.g. Piper et al., 1986; Sene and Plinston, 1994; Tate et al., 2004; Smith and Semazzi, 2014) is not completely justified, because evaporation does have a seasonal cycle. Inflow and outflow have the same mean magnitude, but a different seasonal cycle (Fig. 1.7). Since inflow is directly related to precipitation, it is not surprising that this term follows a similar seasonal variability as precipitation. The outflow is controlled by dam operations and is nearly constant throughout the year. The outflow, however, does change up to 266 % on inter-annual time scales (Fig. 1.6). The annual cycle of the WB residual reflects bimodal variation of the precipitation and inflow term with positive values during the two rainy seasons (Fig. 1.7).

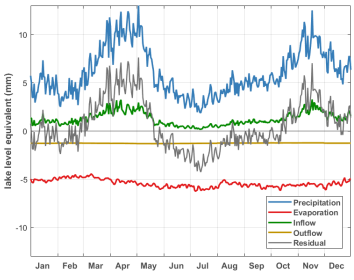

Figure 1.7: Seasonal cycle of the water balance terms and residual (1993-2014)

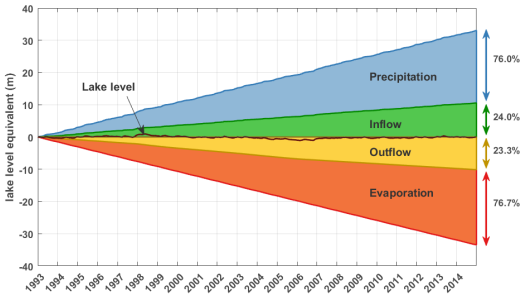

Figure 1.8: Time series of the cumulative water balance terms and resulting lake level

The annual mean values of precipitation and evaporation on the one hand, and inflow and outflow on the other, are similar in magnitude, which is reflected in an almost perfect symmetry when the cumulative terms are plotted for the observational period (Fig. 1.8). Accumulated over the 1993-2014 period, lake precipitation represents 76 % and lake inflow represents 24 % of the total input. This is more or less in line with Awange et al. (2007a) who stated that inflow accounts for 20 % of the lake refill. The total output accumulated over 1993 to 2014 consists for 77 % of lake evaporation and 23 % of lake outflow. The difference of the input and output terms results in lake level variations around the zero line. By adding the initial lake level, the variations in the absolute lake levels are reflected (Fig. 1.9).

The modelled lake level follows the observed lake level very well, notably representing the fluctuations up in 1998 and the severe drop in 2006-2007 (Fig. 1.9). From 2006, the modelled lake level slightly underestimates the lake level. This is likely due to the outflow values, which are not known from 2007 on, and which are set to the last known outflow measurement. Considering the magnitude of the net input and output terms of the water balance (Fig. 1.8), a small bias in one of these terms could lead to large variations in the lake level. Moreover, no tuning is performed to match the WBM outcome to the observed lake levels. Taking these elements into account, the close correspondence of the observed and modelled lake levels is remarkable.

The severe decline in lake levels from 2004 until the end of 2005, can be attributed to a drought combined with an enhanced dam outflow. During 2004 and 2005, the annual precipitation amount decreases with 13% compared to the mean precipitation during the whole study period. This decrease was part of a drought occurring in the entire region, leading to a decline in both lake levels as well as total water storage measured with Gravity Recovery and Climate Experiment (GRACE) in three of the African Great Lakes (Lake Victoria, Tanganyika and Malawi) (Hassan and Jin, 2014). When the outflow follows the Agreed Curve, dam releases are adjusted based on the current climatological conditions. If the Agreed Curve scenario would have been followed from 2004 until 2005, the outflow would have

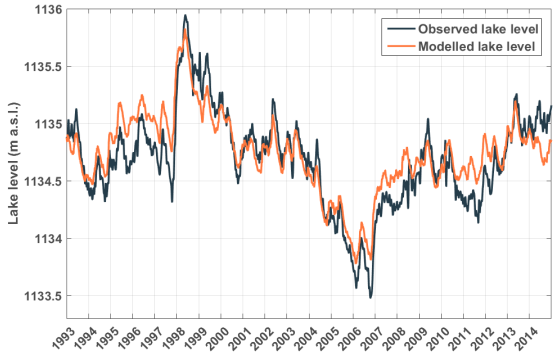

Figure 1.9: Modelled and observed lake levels from DAHITI satellite altimetry measurements.

been 59 km^3, instead of the observed 78 km^3. Consequently, the lake level would have declined by only 0.35 m rather than the recorded 0.69 m. Accordingly, 52 % of the decline can be attributed to a drought over Lake Victoria and its basin. The remaining 48 % of lake level decline can be attributed to an enhanced dam outflow compared to the Agreed Curve protocol, as it is the only WB term that can be altered by human management. Kull (2006) did a similar analysis and found an average contribution of 55% of increased dam outflow to the lake level changes in 2004 and 2005. Also Sutcliffe and Petersen (2007) concluded that the measured lake level fall during the years 2000 to 2006 is about half due to over abstraction of lake outflow.

Water level fluctuations of Lake Victoria are controlled by both climatic conditions and human dam management, which makes the lake a hydropower reservoir. Variability in precipitation over the lake and basin is the main cause of seasonal and inter-annual lake level fluctuations, and these natural fluctuations are accounted for in the human-controlled outflow through the Agreed Curve. Still, the lake level evolution shows to be very sensitive to man-made decisions at the dam, as shown by the 2004-2005 lake level drop.

Here, the WB of Lake Victoria is modelled based on spatio-temporal data and independently from lake level observations. A major advantage of this approach is that it is now possible to force the WBM with climate simulations for the future, which show a decrease in annual precipitation amounts over Lake Victoria (Souverijns et al., 2016). Currently, there is no information on future projections of Lake Victoria's water level. Such projections are, however, relevant given the high societal importance of the future behaviour of the water levels. Changes in the water levels can have far reaching consequences for the people living in the basin, water availability downstream in the Nile Basin and for estimating the future potential for hydropower generation.

1.4 Research aims

This thesis aims to advance our understanding of reservoirs in the climate system both from a climate impact as well as from a coupled Earth system perspective. To better understand impacts on the global scale, we first focus on Lake Victoria, a single reservoir in a local case study. In addition to assessing climate impacts on reservoirs, this thesis aims to advance the representation of reservoirs in CESM2 by including reservoir construction and flow regulation in CLM and mizuRoute, CESM's land and river components, respectively. These overarching research objectives are translated into four separate research goals:

1. **Project the future levels of Lake Victoria under different emission and dam management scenarios.** The combination of the water balance model specifically designed for Lake Victoria (section 1.3) and future projections from the CORDEX-Africa ensemble allow to assess the future evolution of the lake level [Chapter 2].

2. **Quantify the global heat uptake by inland waters.** Thanks to consistent global lake and hydrological model ensembles, made available through the ISIMIP framework, it is now possible to quantify the hereto unknown amount of energy gained by natural lakes, reservoirs and rivers [Chapter 3].

3. **Assess the impact of 20th century global reservoir expansion on the present-day climate.** Recent advancements on global linked global datasets of lakes and reservoirs now enable to prescribe reservoir expansion in CLM as growing lakes. We implement dynamically changing lakes in CLM accounting for mass and energy conservation. This added model functionality allows to conduct land-only and coupled simulations, to estimate the effects of the newly created open water surfaces on the climate [Chapter 4].

4. **Implement and evaluate reservoir regulation in the river routing model mizuRoute.** To represent reservoir regulation in the coupled CESM framework, we integrate an existing reservoir parametrisation in CESM's new river routing model mizuRoute and evaluate its performance both in a local and global configuration [Chapter 5].

1.5 Outline of the thesis

This doctoral thesis is organized based on a series of international peer-reviewed journal articles, which are all published (see page 223 for an overview). The thesis is structured as follows:

In chapter 2, we investigate the impact of climate change and human dam management on the future water level of Lake Victoria. The chapter thereby elaborates the case study on Lake Victoria's water levels by using the water balance model described in section 1.3. Using regional climate model simulations from the CORDEX ensemble, future lake levels are projected along three emission scenarios and four idealized management scenarios.

In chapter 3, simulations from the ISIMIP initiative are used to quantify – for the first time – the amount of energy taken up by inland waters. To this end, lake temperature simulations from three global lake models forced with climatic information from 4 ESMs are linked with global lake and reservoir distributions to quantify the heat uptake due to warming waters, as well as the heat redistribution due to reservoir construction and associated water trapping on land. In addition, two simulations from global hydrological models are combined with a river temperature parametrisation to quantify global river heat uptake.

In chapter 4, the impact of historical global reservoir expansion on the present-day climate is assessed. Reservoir construction is implemented in CLM by allowing for dynamically changing lake area, while conserving water and heat, and prescribing expanding lake area by a combining a global-scale lake and reservoir dataset that incorporates the reservoir construction years. Subsequently, transient land-only simulations with and without reservoir expansion are conducted for the 20^{th} century to uncover the effect on terrestrial water storage and albedo. In addition, coupled atmosphere-land simulations with and without reservoirs are conducted to investigate the impacts of reservoirs on the present-day climate.

Chapter 5 describes the implementation of a widely used reservoir parametrisation scheme in the global routing model mizuRoute to represent reservoir operations. The reservoir scheme is evaluated both in a local set-up for individual reservoirs, using observed reservoir inflows as input, and in a global set-up in which the water is routed over the river network using simulated runoff from CLM. Next to the evaluation based on inflow, outflow and storage of individual reservoirs, the global reservoir simulation is compared to a simulation without lakes for their skill in representing streamflow indices worldwide.

The key findings of this doctoral research are summarized in chapter 6, as well as potential avenues for future research. During the doctoral studies, the author conducted an additional study on deriving meteorological forcing for ecosystem experiments. This paper is not part of the main doctoral thesis, but is included in the appendix.

Chapter 2

Projecting the future levels of Lake Victoria

Lake Victoria, the second largest freshwater lake in the world, is one of the major sources of the Nile River. The outlet to the Nile is controlled by two hydropower dams of which the allowed discharge is dictated by the Agreed Curve, an equation relating outflow to lake level. Some regional climate models project a decrease of precipitation and an increase of evaporation over Lake Victoria, with potential important implications for its water balance and resulting level. Yet, little is known about the potential consequences of climate change for the water balance of Lake Victoria. In this chapter, we feed a new water balance model for Lake Victoria presented in section 1.3 (Vanderkelen et al., 2018a) with climate simulations available through the Coordinated Regional Climate Downscaling Experiment (CORDEX) Africa framework. Our results reveal that most regional climate models are not capable of giving a realistic representation of the water balance of Lake Victoria and therefore require bias correction. For two emission scenarios (RCP 4.5 and 8.5), the decrease in precipitation over the lake and an increase in evaporation are compensated by an increase in basin precipitation leading to more inflow. The future lake level projections show that the dam management scenario and not the emission scenario is the main controlling factor of the future water level evolution. Moreover, inter-model uncertainties are larger than emission scenario uncertainties. The comparison of four idealized future management scenarios pursuing certain policy objectives (electricity generation, navigation reliability and environmental conservation) uncovers that the only sustainable management scenario is mimicking natural lake level fluctuations by regulating outflow according to the Agreed Curve. The associated outflow encompasses however ranges from 14 m^3 day^{-1} (-85%) to 200 m^3 day^{-1} (+100%) within this ensemble, highlighting that future hydropower generation and downstream water availability may strongly change in the next decades even if dam management adheres to he Agreed Curve. Our results overall underline that managing the dam according to the Agreed Curve is a key prerequisite for sustainable future lake levels, but that under this management scenario, climate change might potentially induce profound changes in lake level and outflow volume.

This chapter is published as: Vanderkelen I., van Lipzig N.P.M., Thiery W. (2018) Modelling the water balance of Lake Victoria (East Africa), part 2: future projections. Hydrology and Earth System Sciences, 22, 5527-2249.

2.1 Introduction

Lake Victoria is directly sustaining 30 million people living in its basin and 200 000 fishermen operating from its shores. Therefore, the water level fluctuations of the lake are of major importance. Declining water levels may affect the local communities by their ability to access water, to fish and to transport goods (Semazzi, 2011). Further downstream, the livelihood of about 300 million people in the Nile Basin is supported by the natural resources of Lake Victoria, as it is one of the two major sources of the Nile (Semazzi, 2011). Originating from Lake Victoria, the White Nile provides a more constant flow during the year, providing 70 to 90% of the total Nile discharge during the dry season in the Ethiopian highlands, where the second major source is located (Di Baldassarre et al., 2011). A drop in the water level could imply a decreasing outflow, which may have major implications downstream in the Nile Basin. The countries of the Nile Basin require sufficient water resources for their future development and welbeing, considering the population growth and economic development (Deconinck, 2009; Taye et al., 2011). Consequently, there are a lot of tensions between countries in the Nile Basin. The outflow of the lake is controlled by the Nalubaale and Kiira dams for hydropower generation, located in Jinja (Fig. 2.1). Human strategies towards regulating the outflow might therefore play a crucial role in the downstream Nile Basin water resources and associated political tensions. This will be even more relevant in the light of climate change, where water will become an even more important resource, both around the lake and downstream in the Nile Basin (Taye et al., 2011). While the released outflow affects the lake level, climate-driven lake level fluctuations also influence the outflow volume released by the dam. The hydropower potential, and thus energy availability in the region therefore strongly depends on the interplay between outflow and lake levels. Information on the future evolution of the levels and outflow volumes of Lake Victoria is thus vital for future generations living along its coasts.

The water levels of Lake Victoria are determined by the Water Balance (WB) of the lake, consisting of precipitation on the lake, lake evaporation, inflow by tributary rivers and dam outflow. Since the construction of the dam complex in 1954, a rating curve called the "Agreed Curve" was established relating the lake level and outflow in natural conditions (Sene, 2000):

$$Q_{out} = 66.3(L - 7.96)^{2.01} \tag{2.1}$$

In this equation, the dam outflow Q_{out} (m^3 day^{-1}) is calculated based on the lake level, L (m), as directly measured at the dam. The Agreed Curve can be used to calculate outflow volumes based on lake levels which lie in the historical observed range going from 10 to 13.5 measured at the dam (Sutcliffe and Parks, 1999).

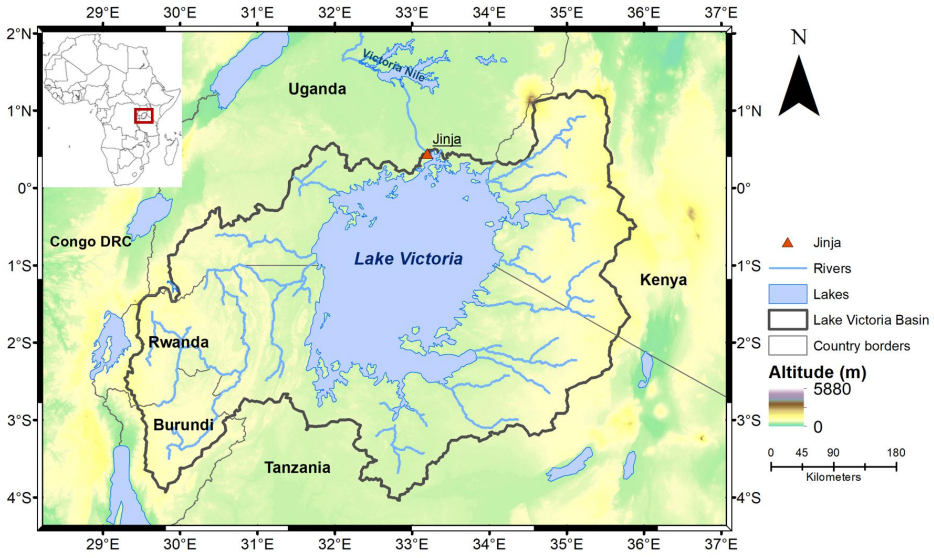

Figure 2.1: Map of Lake Victoria and its basin with surface heights from the Shuttle Radar Topography Mission (SRTM).

The climate in East Africa experiences large interannual variability in precipitation (Nicholson, 2017). The region is a hotspot for climate change, as it is very likely that climate change will have a major influence on precipitation (Nicholson, 2017; Kent et al., 2015; Otieno and Anyah, 2013; Souverijns et al., 2016). Precipitation over the Lake Victoria Basin (LVB) experiences a seasonal cycle with two main rainfall seasons: the long rains in March, April and May and the short rains in September, October and November (Williams et al., 2015). In the last decades, the long rain seasons in East Africa have experienced a series of dry anomalies (Lyon and Dewitt, 2012; Rowell et al., 2015; Souverijns et al., 2016; Nicholson, 2016, 2017; Thiery et al., 2016), while there was no trend observed for the short rains due to a large year-to-year variability (Rowell et al., 2015). This drying trend of the long rains is in contrast with climate model projections for the upcoming decades, projecting an increase in precipitation over East Africa (Otieno and Anyah, 2013; Kent et al., 2015). This apparent contradiction has been called the East African climate paradox of which the causes remain unclear (Rowell et al., 2015). To find explanations Rowell et al. (2015) stated that more research is needed on the reliability of climate projections over East Africa, to the attribution of changing anthropogenic aerosol emissions and to the role of natural variability in recent droughts. However, Philip et al. (2017) found that the severe drought in northern and central Ethiopia in 2015 is attributable to natural variability and therefore conclude that there is no paradox for this type of events.

Future climate simulations with Regional Climate Models (RCMs) project a decreasing mean precipitation and an increasing evaporation over Lake Victoria (Thiery et al., 2016; Souverijns et al., 2016). Compared to Global Climate Models (GCMs), RCMs have a high spatial resolution and are therefore able to represent regional and local scale forcings (Kim et al., 2014; Giorgi et al., 2009). In East-Africa, accounting for local variations in topography, vegetation, lakes, soils and coastlines is of major importance, as these variations have a significant effect on the regional climate. Over the LVB, models with sufficiently high resolution are needed to reproduce key circulation features such as the lake-land breeze system (Williams et al., 2015). High resolution ($\sim$7km grid spacing) coupled lake-land-atmosphere climate simulations for the African Great Lakes region with the Consortium for Small-Scale Modelling in climate mode (COSMO-CLM²) regional climate model were therefore performed by Thiery et al. (2015). These simulations outperform state-of-the-art regional climate simulations for Africa conducted at $\sim$50km grid spacing, because of the coupling to land surface and lake models and enhanced model resolution, which allows a better representation of the fine-scale circulation and precipitation patterns (Thiery et al., 2015, 2016).

At the moment, almost no research is dedicated to the potential consequences of climate change for the WB of Lake Victoria. This is remarkable, since the evolution of the future levels of lake Victoria is vital information for the future generations living on its coasts. Tate et al. (2004) used simulations with one fully coupled GCM to model future fluctuations of the lake level. Model disparities were however very high over East-Africa and the GCM was not capable to sufficiently model precipitation over the African Great Lakes (Tate et al., 2004). Therefore, the results from Tate et al. (2004) serve as an illustration of the sensitivity of lake levels and outflows to climate change scenarios, rather than as an actual lake level projection. Recently, high resolution ensemble climate projections became available for Africa through the Coordinated Regional Climate Downscaling Experiment (CORDEX; Nikulin et al., 2012). Operating at 0.44° ($\sim$50 km) horizontal resolution, these models attempt to resolve the lake and its mesoscale circulation. When these simulations are used as input for a water balance model (WBM) for Lake Victoria, future lake level projections can be generated. The ensemble approach ensures that the model spread incorporates uncertainties associated with individual model deficiencies, concentration pathways and natural variability.

Here, we use the WBM constructed in (Vanderkelen et al., 2018a) (see section 1.3) and drive it with climate simulations from the CORDEX over the Africa domain from 1950 to 2100. First, we assess the ability of regional climate models from the CORDEX ensemble to reproduce the historical lake level of Lake Victoria. Based on this analysis it appears that it is not possible to use a subset of models for which the WB closes. Therefore, a bias correction based on observations is applied on these simulations. Last, the future evolution of the water level of Lake Victoria under various climate change scenarios is investigated, together with the role of different human management strategies at the outflow dams based on three policy objectives (electricity generation, navigation reliability and environmental conservation).

2.2 Data and methods

2.2.1 CORDEX ensemble

In recent years, RCM downscalings of the Coupled Model Intercomparison Project Phase 5 (CMIP5) GCMs have become available through the CORDEX framework. The CORDEX-Africa project provides simulations over the Africa domain, which includes the whole African continent with a spatial resolution of 0.44° by 0.44° and a daily output frequency (Nikulin et al., 2012). In CORDEX-Africa, there are currently simulations with six RCMs available (*CCLM4-8-17, CRCM5, HIRHAM5, RACMO22T, RCA4* and *REMO2009*) for the historical (1950-2005) and future period (2006-2100) under Representative Concentration Pathways (RCPs) 2.6, 4.5 and 8.5. In the *CRCM5* and *RCA4* model, lakes are represented by a one dimensional lake model FLake (Samuelsson et al., 2013; Hernández-Díaz et al., 2012; Martynov et al., 2012), while the other RCMs have no lake model embedded. By using different GCMs as initial and lateral boundary conditions, there are in total 25 historical model simulations, 11 simulations for RCP 2.6, 21 simulations for RCP 4.5 and 20 simulations for RCP 8.5 (see supplementary table 2.1). The use of model ensembles is essential, because separate simulations show larger biases than ensemble means when they are compared to the observed climate (Nikulin et al., 2012; Endris et al., 2013; Kim et al., 2014; Davin et al., 2016). Next to the historical and RCP simulations, the CORDEX framework also provides an evaluation simulation for each RCM, driven by the European Centre for Medium-Range Weather Forecasts (ECMWF) ERA-Interim reanalysis as initial and lateral boundary conditions for the period 1990-2008. Here we use these reanalysis downscaling simulations to evaluate the skill of the RCMs by comparing them with observations.

2.2.2 Water balance model

For a detailed description of the WBM used in this chapter, we refer to Vanderkelen et al. (2018a) and section 1.3. In summary, the WB is modelled following Eq. 2.2 in which the change in lake level per day dL/dt (m day^{-1}) is calculated based on the precipitation on the lake P (m day^{-1}), the evaporation from the lake E (m day^{-1}), the inflow from tributary rivers Q_{in} (m^3 day^{-1}) and the dam outflow Q_{out} (m^3 day^{-1}) divided by the lake surface area A ($6.83 \cdot 10^{10}$ m^2).

$$\frac{dL}{dt} = P - E + \frac{Q_{in} - Q_{out}}{A} \tag{2.2}$$

First, relevant spatial variables provided by the CORDEX simulations are regridded using a nearest neighbour remapping to the WBM grid with a resolution of 0.065°by 0.065°(about 7 by 7 km) containing Lake Victoria and its basin. P is computed by taking the daily mean over the lake cells of the regridded CORDEX precipitation. Basin and lake cells are defined by using masks based on lake and basin shapefiles. E is calculated from the latent heat flux (W m^{-2}) simulated by the CORDEX models, using the latent heat of vaporization, which is assumed to be constant at $2.5 \cdot 10^6$ J kg^{-1}. This term is aggregated in the same way as the

precipitation term. The inflow term is calculated from the daily gridded basin precipitation with the Curve Number method as described in Vanderkelen et al. (2018a) using daily basin precipitation retrieved from the CORDEX precipitation simulations. The same land cover classes based on the Global Land Cover 2000 data set (GLC 2000; Mayaux et al., 2003) and the hydrological soil groups are applied to all CORDEX simulations. Note that this approach does not account for potential influences of future land use changes on runoff. However, the Curve Number does change based on the antecedent moisture condition for a particular day, derived from the preceding 5-day precipitation.

First, a set of WBM integrations is conducted by driving the WBM with the six CORDEX evaluation simulations. As these evaluation simulations are driven by 'ideal' boundary conditions, this WBM simulation allows to examine the ability of the RCMs to represent precipitation, lake evaporation, inflow and the resulting lake levels during the period when observations for these terms are available (1990-2008). Therefore, the outflow is given by observations too. Second, the WBM is driven by the 25 historical CORDEX simulations for the period 1951-2005. Finally, future WBM runs are conducted following the RCP 2.6, 4.5 and 8.5 scenarios. One GCM-RCM combination is excluded from the analysis because of inconsistencies between the historical and future simulations (see section 2.6). To be comparable, the input terms to the transient WBM need to adhere to the same calendar. Therefore, the number of days are adjusted in a number of historical and future CORDEX simulations, as described in section 2.6. Finally, the WBM requires an initial lake level. The evaluation simulations start with the observed lake level in 1990 (1135 m a.s.l.) and the historical simulations with the observed lake level in 1950 (1133.7 m a.s.l.). For the future simulations, the last lake level calculated by the corresponding historical simulation is used.

2.2.3 Dam management scenarios

The evaluation WBM simulations use recorded outflow values. In the historical WBM simulations, the outflow is calculated based on the Agreed Curve. While observed outflow volumes are available for the historical period, these cannot be used in the WBM as RCMs driven by GCMs represent the general climatology and do not account for the actual observed weather, reflected in the recorded outflow volumes. Considering the known deviations of water release from the Agreed Curve during the period 2000-2006 (Kull, 2006; Vanderkelen et al., 2018a), future outflow is subject to uncertainty. Therefore, we start from three main policy objectives concerning the environmental conservation, navigation reliability and constant electricity generation to determine future dam management scenarios. These policy objectives lead to four idealized dam management scenarios: (i) managing outflow following the Agreed Curve, reflecting natural conditions by mimicking natural outflow, (ii) managing outflow so that the lake level remains constant, to keep the lake accessible for fishing boats from the harbors in shallow bays, and (iii) managing outflow to provide a constant supply of hydropower from the dams: one scenario prescribing the historical mean production of hydropower and the other an elevated hydropower production, reflecting the supply needed to meet the rising power demand in Uganda (Adeyemi and

Asere, 2014). These scenarios are highly simplified and reflect very different management; they were chosen to investigate the effect of extreme dam management scenarios on the lake level fluctuations of Lake Victoria. Each scenario will thereby be applied with lake levels constrained to their physical boundaries.

A first assumption is that future outflow starts following the Agreed Curve again. In this *Agreed Curve scenario*, daily outflow is calculated following Eq. 2.1 based on the lake level of the previous day. Lake level fluctuations are restricted to fluctuate within the historical observed range (10 m to 13.5 m measured at the dam, corresponding to 1130 m to 1136.5 m a.s.l), as this is the range for which the Agreed Curve is known. If the lake level of the previous day drops below the lower limit, the outflow is set to 0 m^3 day^{-1} and if the lake level rises above the upper limit, all additional water is discharged.

Another possibility is to manage future outflow in such a way that the lake level remains constant and the water balance is closed. In this *constant lake level scenario*, daily outflow is calculated as residual of the water balance, with the lake level kept constant at the last known lake level, ranging between 1134.5 and 1135.2 m for the different simulations. If the water balance is negative, there is no outflow, but the lake level is allowed to decrease. When the water balance is positive again, the lake level is first restored to its predefined constant height. The possible remainder from the positive water balance results then in outflow for that day. By consequence, the lake level in this scenario is constant apart from short negative excursions.

In the last defined scenarios, future outflow is regulated in order to provide a constant hydropower production without interruptions while lake levels fluctuate in their physical range. In the study of Koch et al. (2013), hydropower production of a reservoir is quantified as

$$P_{el} = Q_{out} \times h \times k \tag{2.3}$$

with Q_{out} the outflow of the reservoir in m^3 day^{-1}, P_{el} the electricity produced (kW), h the water head (m) and k the efficiency factor (kN/m^3). After rearranging this equation and adding a constraint to maximum outflow, the outflow needed to produce a firm amount of electricity is given by

$$Q_{out} = MIN(\frac{P_{el}}{h \times k}, Cap_{hpp}) \tag{2.4}$$

with Cap_{hpp} the maximum turbine flow capacity (m^3/s). Lake Victoria is controlled by both the Nalubaale and Kiira dams. As these dams operate parallel of each other, we simplified the analysis by assuming only one dam regulating the outflow, with the combined hydropower capacity of both real dams. This results in a Cap_{hpp} of 1150 m^3/s (the average of 1200 m^3/s for Nalubaale and 1100 m^3/s for Kiira; Kizza and Mugume, 2006). h is assumed to be equal to the relative lake level, as measured at the dam. For the efficiency factor k a value of 13.77 kN/m^3 is used, calculated from eq. 2 using the values for maximum turbine flow Cap_{hpp}, maximum water head (h_{max} = 24 m) and the sum of maximum

electricity production, 380 MW (180 MW for Nalubaale and 200 MW for the Kiira dam; Kull, 2006). Based on this, two management scenarios providing a constant hydropower production (HPP) are defined. The *historical HPP management scenario* prescribes a daily HPP equal to the mean historical HPP (P_el = 168 MW), which is calculated using eq. 2.3 with the historical observed mean outflow ($88 \cdot 10^6$ m^3/day) and the mean relative lake level (11,9 m). Second, in the *high HPP management scenario*, HPP is set equal to the electricity produced in the year in which the outflow was maximum (P_{el} = 247 MW, in 1964 with an outflow of $138 \cdot 10^6$ m^3 day^{-1}).

In both the constant lake level scenario and the HPP management scenarios, we impose physical constraints to the lake level fluctuations: the lake level should fluctuate between 0 m and 26 m as measured at the dam, 1122.9 m and 1146.9 m a.s.l. (the height of the dam is 31 m with a safety level of 7 m). Similar to the limits of the Agreed Curve, the outflow is set to 0 m^3 day^{-1} whenever the lake level drops below 1122.9 m a.s.l. and all additional water is discharged by the sluice gates if the lake level rises above 1146.9 m a.s.l. These are merely theoretical limits. In extreme cases, lake levels could drop under the lower limit if there is more water evaporating than precipitating and flowing in the lake.

2.2.4 Bias correction method

In this chapter, we applied a bias correction on the three WB terms derived from the CORDEX simulations (daily mean lake precipitation, lake evaporation and inflow). For every historical simulation from the CORDEX ensemble, a transformation function is calculated based on the WB terms from the observational WBM presented in Vanderkelen et al. (2018a) and section 1.3. This is done for the overlapping period of 22 years ranging from 1983 until 2005. Next, the transformation functions specific to each simulation are applied on the full historical simulation and on the available corresponding future simulations for all three RCPs. Finally, the resulting lake levels are calculated by forcing the WBM with the bias corrected WB terms. The main assumption of bias correction is that the bias in the RCM simulations is stationary for all scenarios (historical, RCP 2.6, 4.5 and 8.5).

WB closure is adhered with two of the 7 tested bias correction methods of the *qmap* package, provided in the R language by Gudmundsson et al. (2012). The first method uses a linear parametric transformation to model the quantile-quantile relation between the observed and modelled data according to

$$\hat{P_o} = a + bP_m \tag{2.5}$$

with $\hat{P_o}$ the best estimate of P_o, the distribution of the observed values, P_m the modelled values and a, b calibration parameters. An overview of the a and b parameters generated per WB term for the different simulations can be found in supplementary table 5.1. The second method is the non-parametric quantile mapping method and is described in section 2.6.

2.3 Results

2.3.1 Evaluation water balance simulations

Results of the evaluation WBM runs are compared directly to the terms used in the observational WBM (Vanderkelen et al., 2018a) and section 1.3. Precipitation observations are retrieved from the Precipitation Estimation Remotely Sensed Information using Artificial Neural Networks - Climate Data Record (PERSIANN-CDR; Ashouri et al., 2015). Evaporation is estimated from the latent heat flux output of the high resolution reanalysis downscaling of the COSMO-CLM^2 regional climate model (Thiery et al., 2015).

The modelled annual precipitation over the study area during the evaluation period (1990 - 2008) shows different spatial distributions (Fig. 2.2). Compared to the observed precipitation, the majority of the models (CCLM4-8-17, RACMO22T, RCA4 and REMO2009) underestimates the amount of lake precipitation up to -79% compared to the reference. Only HIRHAM5 gives a large overestimation of precipitation over the lake of +78% compared to the reference. The mean annual lake evaporation varies a lot among the models as well (Fig. 2.3). The evaporation amount is underestimated by CCLM4-8-17, RACMO22T and REMO2009 up to -71% compared to the reference and overestimated by HIRHAM5 and RCA4 up to +39 %. Similar conclusions can be drawn from the comparison of the histograms of observed and simulated lake precipitation (Fig. 2.4). The difference between the distributions is also found for inflow and the resulting lake levels. The seasonal cycles of the water balance terms, lake precipitation, evaporation and inflow (Fig. 2.5b, c and d) show the same over- and underestimations compared to the observed values. This indicates that even RCMs downscaling reanalysis data still entail important precipitation and evaporation biases. In most cases, the biases in precipitation and evaporation result in drifting lake levels (Fig. 2.5a). The overestimation of HIRHAM5 in the precipitation term is too large to be compensated by its overestimated evaporation term. The modelled HIRHAM5 lake levels shows therefore an unrealistic increase. The lake levels modelled with CCLM4-8-17, RACMO22T, RCA4 and REMO2009 show a large, unrealistic drop up to 13.3 m, which is mainly due to the underestimation of lake precipitation and inflow. Overall, only CRCM5 is able to represent the lake level within an acceptable range.

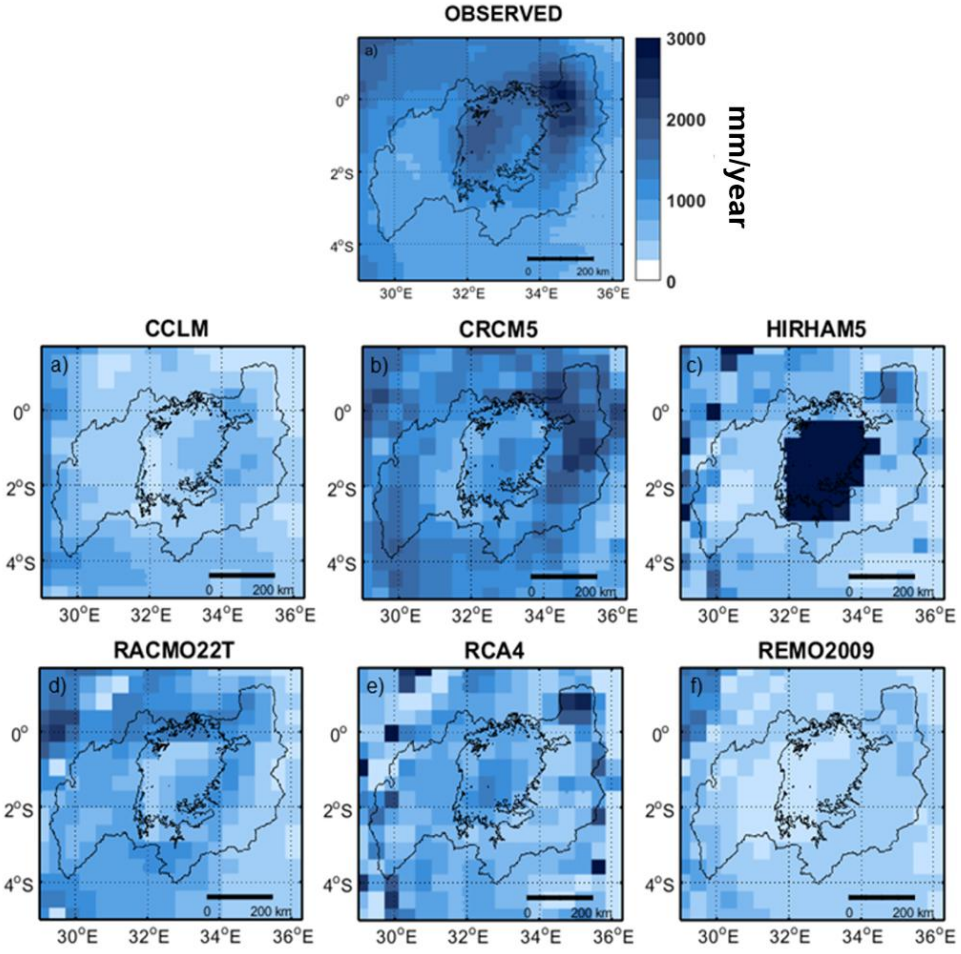

Figure 2.2: Annual accumulated precipitation during the period 1993-2008 as derived from PERSIANN-CDR (a) the CORDEX evaluation simulations (b-g).

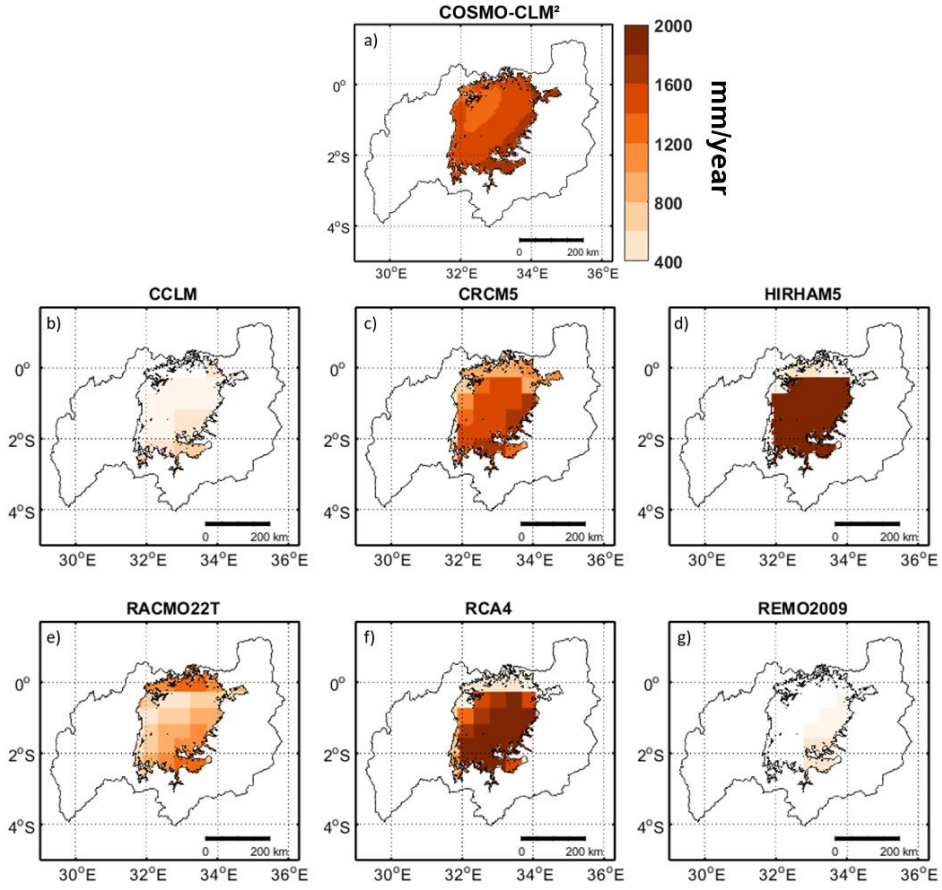

Figure 2.3: Annual accumulated evaporation during the period 1993-2008 as derived from COSMO-CLM^2 (a) the CORDEX evaluation simulations (b-g).

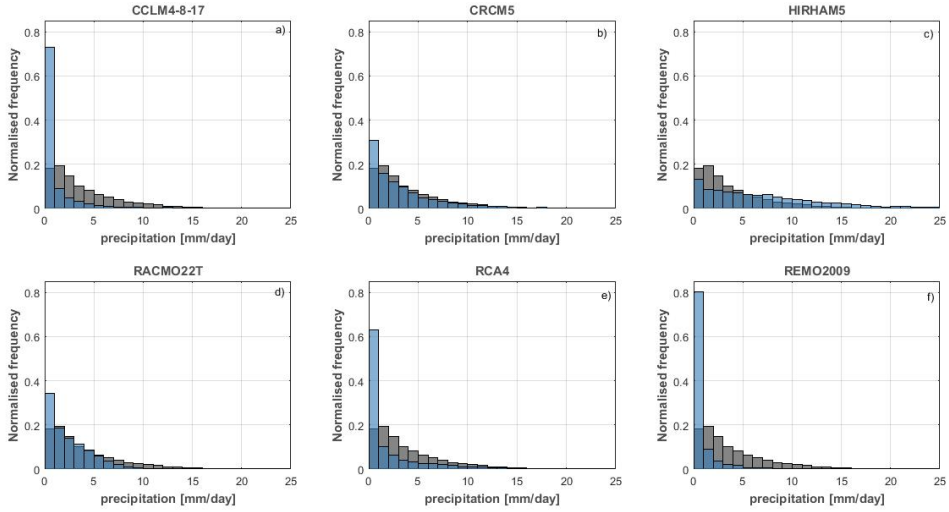

Figure 2.4: Histograms of lake precipitation derived from the CORDEX evaluation simulations for the period 1993-2008 (observated distributions, derived from PERSIANN-CDR are indicated in grey).

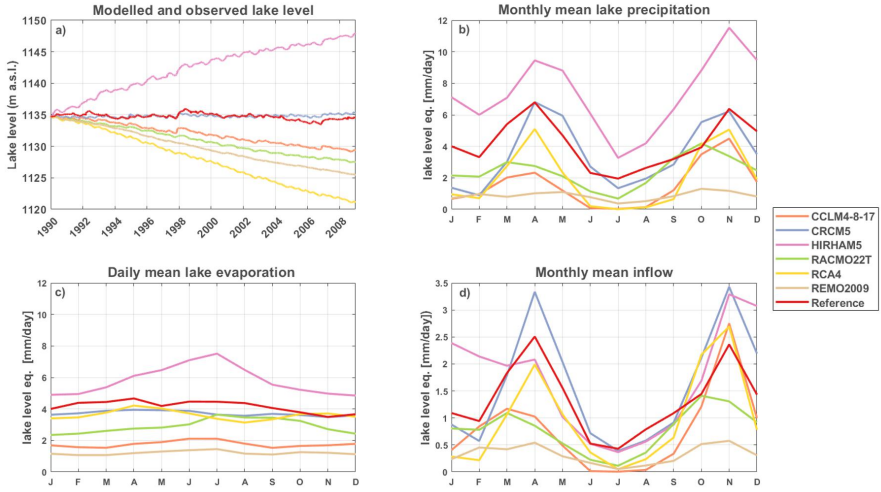

Figure 2.5: Modelled lake levels (a), seasonal precipitation (b), evaporation (c) and inflow (d) according to the CORDEX evaluation simulations without bias correction. Note the different y-axis scales.

2.3.2 Simulations with bias corrected water balance terms

As only CRCM5 is able to close the WB and there are only two simulations following RCP 4.5 with this RCM available, it is not possible to base the analysis of lake level projections on an observationally-contrained RCM ensemble. Therefore, we applied two bias correction methods to be able to use all CORDEX simulations. After applying the linear parametric transformation on the CORDEX evaluation simulations, the seasonal cycle of the lake precipitation, lake evaporation and inflow term approximates the observations (Fig. 2.6). Consequently, the resulting lake levels lie within the range of observed lake levels. As the linear parametric bias correction method provides a closed WB for all six RCMs, it is applied on the WB terms of the historical and future CORDEX simulations. Using the second bias correction method, with empirical quantiles, also leads to WB closure. Applying this bias correction method on the historical and future CORDEX simulations yields similar results as the linear parametric transformation. Therefore, only results from the linear parametric transformation are shown hereafter. Results with the empirical quantile bias correction method are presented in the supplementary material section.

After applying the linear parametric bias correction, we quantified the future change of the three WB terms according to the three RCP scenarios for all simulations. This is achieved by computing the difference between the future (mean of the period 2071-2100) and the historical (mean of the period 1971-2000) simulations (Fig. 2.7). The climate change signal for lake precipitation differs between the simulations in every RCP scenario (Fig 2.7a, b, c). For some simulations, lake precipitation demonstrates a strong decrease (e.g. CCLM4-8-17 driven by EC-EARTH, CRCM5 driven by CanESM2 and REMO2009 driven by EC-EARTH) while other simulations show an increase (e.g. RACMO22T driven by HadGEM2-ES and REMO2009 driven by CM5A-LR). The model simulations with a smaller increase or decrease also vary in sign. In contrast to lake precipitation, the lake evaporation signal is more consistent for the different simulations, with generally an increasing trend (Fig. 2.7d, e and f). The future changes in the inflow term are generally consistent as well and show an increase of inflow under all three RCP scenarios. As lake inflow is directly related to precipitation, the increase in inflow can be attributed to the increase of precipitation over the LVB. For all three WB terms, the width of the 95% confidence intervals is larger for strong climate change signals.

The signs of the signals are broadly consistent with the signs of the original, non bias corrected WB terms (see supplementary Fig. 2.11). The amplitude of the signals, however generally decreases after applying the bias correction. This decrease is larger for the simulations with the more extreme signals, with important effects on the multi-model means.

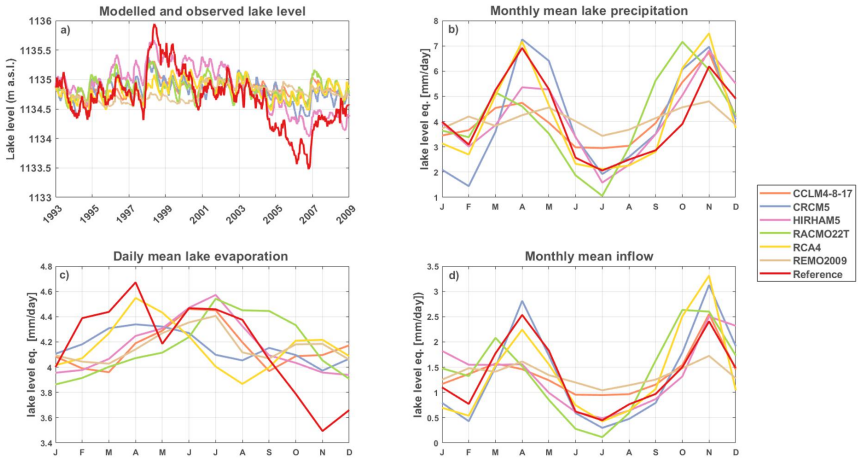

Figure 2.6: Modelled lake levels (a), seasonal precipitation (b), evaporation (c) and inflow (d) according to the CORDEX evaluation simulations, bias corrected using parametric linear transformations. Note the different y-axis scales.

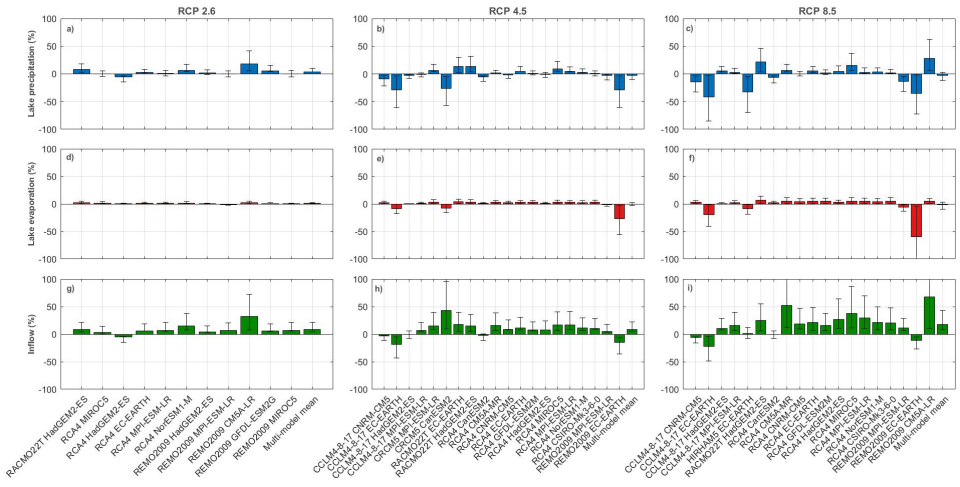

Figure 2.7: Barplots showing the relative projected climate change following RCP 2.6, 4.5 and 8.5 for lake precipitation (a-c), lake evaporation (d-f) and inflow (g-i) for the CORDEX simulations bias corrected with the linear parametric transformation. The climate change signal is defined as the mean difference between the future (2071-2100) and the historical (1971-2000) simulations. The whiskers indicate the 95% confidence interval of the change based on the 30-year annual difference.

2.3.3 Future lake level and outflow projections

Lake level projections following different dam management scenarios are computed from the CORDEX simulations, bias corrected with a linear parametric transformation (Fig. 2.8). Future lake levels according to the constant lake level scenario are not represented in this figure, as they are constant at their 2006 level per definition. Under the historical HPP scenario, the ensemble mean projects a lake level increase of 1.03 m for RCP 2.6, 2.2 m for RCP 8.5 and a decline of -0.36 m for RCP 4.5 in 2100, compared to the 2006 level (Fig. 2.8a). The ensemble mean lake levels projections thereby all stay within the observed range. The model uncertainty increases over time for three RCPs with an enveloped width ranging up to 24 m. The uncertainty range encompasses both rising and decreasing lake levels (e.g. up to +12 m and -12 m in 2100 under RCP 8.5). The different simulations tend to diverge with a more or less constant ensemble mean as a result, as is shown by their inter quartile range (supplementary Fig. 2.10). Overall, lake level projections thus encompass large uncertainties within this management scenario. In the high HPP scenario the ensemble mean projections of the three RCPs project a decrease in lake level (-3.9 m for RCP 2.6, -3.2 m for RCP 4.5 and -1.5 m for RCP 8.5; Fig. 2.8b). The model uncertainty again increases with time for the three RCPs, consistent with the rising spread in the historical HPP management scenario.

In the Agreed Curve scenario, the outflow is adjusted every day based on the lake level of the previous day. In this scenario, the modelled lake levels stay within the range of the historical fluctuations and show no clear trend (Fig. 2.8c). The seasonal cycles in lake level are clearly visible in the ensemble mean. In 2100, the uncertainty has increased to 1.1 m for RCP 2.6, 3.1 m for RCP 4.5 and 3.9 m for RCP 8.5. It is not surprising that the lake level modelled with this scenario stays within the historical range, as the approximated WB equilibrium is maintained by adjusting the outflow based on the lake level on a daily basis. Moreover, the Agreed Curve relation between lake level and outflow is originally made to mimic natural outflow, accounting for the natural climate variability (Sene, 2000).

The outflow projections following the Agreed Curve scenario fluctuate around the historical observed outflow volume for RCP 2.6 and 4.5. For RCP 8.5 the model projects a slight increase towards the end of the century, resulting in an averaged outflow volume being $6.7 \cdot 10^6$ m^3 day^{-1} (+7.6 %) higher than the historical observed outflow. This increase in outflow results from outflow volumes for some simulations that are larger than prescribed by the Agreed Curve, as the lake level for these simulations reaches the prescribed maximum lake level and all additional water is discharged. The uncertainty of the projections is therefore very large, ranging from $14 \cdot 10^6$ m^3 day^{-1} to $209 \cdot 10^6$ m^3 day^{-1} for RCP 8.5, whereby the latter constitutes more than double the historical observed outflow ($88 \cdot 10^6$ m^3 day^{-1}).

In the constant lake level scenario, the outflow volume varies following a spiky pattern (fig. 2.9b). Since the outflow is altered each day to maintain a constant lake level given the precipitation, inflow and evaporation terms of that day, the outflow volume greatly varies

on daily time scales with an average standard deviation of $172 \cdot 10^6$ m^3 day^{-1}. Fig. 2.9b therefore shows annually averaged daily outflow values. The three RCPs show no clear trend, but uncertainties range up to $253 \cdot 10^6$ m^3 day^{-1}. Fluctuating around a multi-model mean of $88.9 \cdot 10^6$ m^3 for RCP 2.6, $90.3 \cdot 10^6$ m^3 for RCP 4.5 and $95.5 \cdot 10^6$ m^3 for RCP 8.5, annual average outflow volumes are higher than historical outflow, with an average outflow volume of $88 \cdot 10^6$ m^3 day^{-1}, measured from 1950 until 2006.

Finally, outflow volumes following the historical HPP scenario decrease slightly until roughly 2055, whereas outflow volumes following the high HPP scenario remain constant until 2055 (fig. 2.9c and d). Afterwards, the ensemble mean outflow projections start to diverge and uncertainties strongly increases. From this moment, most lake level projections reach the imposed minimum or maximum levels (Sect. A.2). No outflow is released for projections which drop to the minimum level, while all additional water is discharged for lake levels which reach the maximum level. Consequently, with outflow volumes reaching these extremes, it is not possible to maintain a constant hydropower supply, despite the management scenario being designed for this aim.

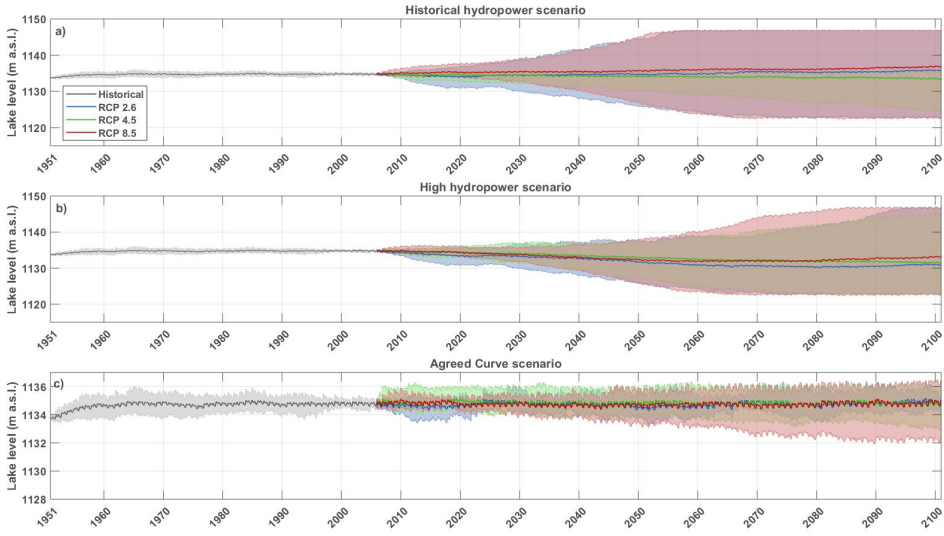

Figure 2.8: Lake level projections for the *historical HPP management scenario* (P_el is 168 MW) (a), the *high HPP management scenario* (P_{el} is 247 MW) (b) and the *Agreed Curve scenario* (c). The full line shows the ensemble means and the envelope the 5th - 95th percentile of the CORDEX ensemble simulations, bias corrected using the parametric linear transformation method. Note the different y-axis scale for panel c.

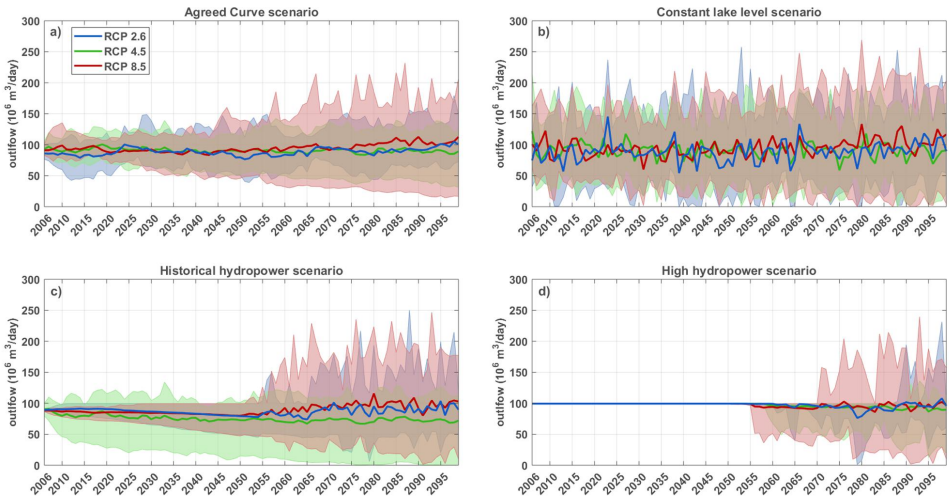

Figure 2.9: Outflow projections (annual averaged) for the *Agreed Curve scenario* (a), the *constant lake level scenario* (b), the *historical HPP management scenario* (c) and the *high HPP management scenario* (d). The full line shows the ensemble means and the envelope the 5th - 95th percentile of the CORDEX ensemble simulations, bias corrected using the parametric linear transformation method.

2.4 Discussion

2.4.1 Model quality and projected changes

None of the RCMs, except for CRCM5, are able to provide reliable estimations of the water balance terms in the LVB (Figs 2.4 and 2.5). Endris et al. (2013) found that most RCMs simulate the main precipitation features reasonably well in East-Africa. Over the whole CORDEX-Africa domain, all RCMs capture the main elements of the seasonal mean precipitation distribution and its cycle, but also inhibit significant biases are present in individual models depending on season and region (Nikulin et al., 2012; Kim et al., 2014). Here, a specific region is investigated wherein lakes act as main driving features of the regional climate (Thiery et al., 2015, 2016, 2017; Docquier et al., 2016). Therefore, model performance is primarily determined by how lakes are resolved in the models. A correct representation of lake surface temperatures in the models is crucial to account for the lake-climate interactions and associated mesoscale circulations (Stepanenko et al., 2013; Thiery et al., 2014a,b). The good performance of CRCM5 can be attributed to the presence of the lake model FLake, ensuring a realistic representation of lake surface temperatures, while the other models have no lake model embedded. The fact that RCA4, which also uses FLake as lake model, gives no accurate representation of the water balance terms in the LVB, is most likely due to other model biases apart from the lake model.

Thiery et al. (2016) performed high resolution simulations (∼7km grid spacing) with the coupled land-lake-atmosphere model COSMO-CLM² under RCP 8.5 over the LVB. In these simulations, the precipitation shows a decrease of -7.5% towards the end of the century over the lake surfaces of the African Great Lake region, which is a higher decrease than found in this study (-2.3%). The increase in lake evaporation following RCP 8.5 according to Thiery et al. (2016) (+ 142 mm year^{-1}) confirms the sign of the evaporation signal of most CORDEX simulations of this study (Fig. 2.11f). However, the effect is not visible in the bias-corrected multimodel mean (-0.07 mm year^{-1}) which results from the negative signal of three CORDEX simulations (Fig. 2.11f). While COSMO-CLM² generally outperforms CORDEX-Africa simulations, these simulations are only available in time slices and could therefore not be used to drive the WBM.

The decrease in lake precipitation for RCP 4.5 and 8.5 (respectively -2.5% and -2.3% is not visible in the lake level projections following the Agreed Curve or the HPP scenarios. This is due to the fact that the decrease in lake precipitation is largely compensated in the total WB by the increase in lake inflow, which is determined by the increase in precipitation over the LVB. In the bias corrected simulations using the linear parametric transformation, the deficit in lake precipitation is compensated for 184 % (RCP 4.5) and 450 % (RCP 8.5) by an increase in inflow. In RCP 2.6, this effect is not present.

2.4.2 Water management and climate change

The analysis reveals that the management scenario has an important influence on the future lake levels and outflow volumes. The physical lake level constraint makes that the effect of unsustainable management scenarios is reflected in the outflow volumes, which become highly variable once the lake level limit is reached. In both constant HPP scenarios, various simulations reach these limits, leading to very high or almost no outflow anymore, and a hydropower production which does not meet the goal for which it was designed. The multi-model mean lake level projections following these management scenarios appear sustainable, but are the result of averaging two branches of drifting lake levels, as illustrated by the interquartile range being large compared to the Agreed Curve (see supplementary fig. 2.10). Lake levels diverge towards their limits, leading to extreme situations where the lake extent is altered substantially, causing various impacts along the shoreline, such as reduced accessibility of fishing grounds and harbours located in shallow bays. Therefore, the dam management scenarios aiming at constant hydropower production are not sustainable. Furthermore, to meet the goal of a constant lake level, the outflow volumes have to be highly variable, which is not realistic if hydropower generation is pursued. Therefore also the constant lake level scenario can be qualified as unsustainable.

If the released dam outflow follows the Agreed Curve, the lake level will reflect the climatic conditions and it will fluctuate within its natural range. Moreover, the corresponding outflow following the multi-model mean stays also within the observed range. However,

the uncertainties of the outflow simulations reach up to 229% of the projected multi-model mean, highlighting that future lake level trajectories may strongly differ even under a single climate change realisation. This has important implications for the potential hydropower generation and water availability downstream: while the lowest projected outflow volumes close to zero inhibit hydropower potential and exacerbate hydrological drought in the White Nile, increased outflow volumes could lead to more flooding downstream. Hence, strong changes in downstream water availability may occur in the next decades even if dam managers adhere to the Agreed Curve. Nevertheless, considering the multi-model mean, the Agreed Curve scenario can be denoted as a sustainable management scenario. However, violations against the prescribed outflow can have important consequences for the lake levels, as shown by the observed drop in lake level in 2004-2005, which was for 48% attributable to an enhanced dam outflow (Vanderkelen et al., 2018a) and section 1.3. In Uganda, hydropower provides up to 90% of the electricity generated (Adeyemi and Asere, 2014). There is a rapidly growing gap between electricity supply and a rising demand, as the electricity consumption per capita in Uganda is among the lowest in the world. The Kiira and Nalubaale hydropower stations, managing Lake Victoria's outflow, are the largest power generators in the country (Adeyemi and Asere, 2014). The third largest capacity is provided by the new Bujagali hydropower dam located 8 km downstream of Lake Victoria. Therefore, operations at those dams will become even more important in the future. If there are again violations against the Agreed Curve because of the increasing hydropower demand, this may have substantial consequences for the future evolution of the lake level. A relative stable lake level is however necessary for local water availability providing resources to the 30 million people living in its basin and to the 200 000 fisherman operating from its shores (Semazzi, 2011).

Within each management scenarios, the climate model uncertainty appears to be larger than the uncertainty related to the emission scenario. This could be seen by the large spread around the multi-model mean and the coinciding RCP curves and spread (Fig. 2.8 and 2.9). The spread according to the RCP 2.6 scenario is the smallest. This scenario contains only 11 simulations, while there are 19 simulations following RCP 4.5 and 17 simulations following RCP 8.5. The future projections provide no clear differentiation between the three RCP scenarios, indicating that uncertainties associated with the model deficiencies and initial conditions play a more important role. Therefore, to further refine lake level projections presented in this study, it is of vital importance to account for model deficiencies and natural variability.

Apart from the large climate model uncertainties, this approach using the WB model has some other shortcomings. First, we do not account for future land cover changes in the inflow calculations, as a static land cover map for the year 2000 is used (Vanderkelen et al., 2018a). Changes in land cover are however very important in future simulations, as they affect the Curve Number and therefore the amount of runoff (Ryken et al., 2014). Moreover, future changes in land use could induce changes in precipitation in tropical regions (Akkermans et al., 2014; Lejeune et al., 2015). Second, the employed management scenarios are based on three simple assumptions. The management scenario exerts a major influence on

future lake level fluctuations and future lake levels appeared to be sustainable only if the Agreed Curve is followed. As the importance of dam management in response to rising hydropower demand increases, more sophisticated management scenarios accounting for the rising hydropower demand could be developed and examined for their ability to preserve historical lake level fluctuations.

2.5 Conclusions

In this chapter, a water balance model developed for Lake Victoria is forced with climate projections from the Coordinated Regional Climate Downscaling Experiment (CORDEX) ensemble following three Representative Concentration Pathways (RCPs 2.6, 4.5 and 8.5). Lake level fluctuations are projected up to 2100 using four different dam management scenarios, which emerge from three policy objectives.

This study identified the following key messages: (i) regional climate models incorporated in the CORDEX ensemble are typically not able to reproduce Lake Victoria's water balance, and therefore require bias correction. Applying the bias correction closes the water balance and results in realistic simulated lake levels. (ii) The projected decrease in lake precipitation under RCP 4.5 and RCP 8.5 is compensated by an increase in lake inflow, which is directly determined by precipitation over the Lake Victoria Basin. (iii) The choice of management strategy will determine whether the lake level evolution remains sustainable or not. Idealized dam management pursuing a constant hydropower production (electricity policy objective) leads to unsustainable lake levels and outflow fluctuations. The management scenario in which the lake level is kept constant, targeting a reliable navigation policy, leads to highly variable outflow volumes, which is not realistic in terms of hydropower production. (iv) When outflow is managed following the Agreed Curve, mimicking natural outflow pursuing environmental policy targets, the evolution of lake level and outflow remains sustainable for most realizations. (v) The outflow projections following the Agreed Curve however encompass large uncertainties, ranging from $14 \cdot 10^6$ m^3 day^{-1} to $209 \cdot 10^6$ m^3 day^{-1} (up to 229% of the historical observed outflow). Although the multi-model mean projected lake levels demonstrate no clear trend, these large uncertainties show that even if the Agreed Curve is followed, future lake levels and outflow volumes could potentially rise or drop drastically, with profound potential implications for local hydropower potential and downstream water availability. (vi) Next to the management scenario, we found that climate model uncertainty (RCM-GCM combination) is larger than the uncertainty related to the emission scenario.

Here, we provide the first indications of potential consequences of climate change for the water level of Lake Victoria. The large biases and uncertainties present in the projections stress the need for an adequate representation of lakes in RCMs to be able to make reliable climate impact studies in the African Great Lakes region. Finally, the evolution of future lake levels of Lake Victoria are primarily determined by the decisions made at the dam.

Therefore, the dam management of Lake Victoria is of major concern to ensure the future of the people living in the basin, the future hydropower generation and water availability downstream.

Data and code availability

Data from the Coordinated Regional Climate Downscaling Experiment (CORDEX) Africa framework is available at `http://cordex.org/data-access/esgf/`. The Water Balance Model code is publicly available at `https://github.com/VUB-HYDR/2018_Vanderkelen_etal_HESS_ab`. The qmap R-package is available on the Comprehensive R Archive Network (`https://cran.r-project.org/`).

Acknowledgements

We acknowledge the CLM-community (clm-community.eu) for developing COSMO CLM^2 and making the model code available. Computational resources and services used for the COSMO-CLM^2 simulations were provided by the VSC (Flemish Supercomputer Center), funded by the Hercules Foundation and the Flemish Government department EWI. In addition, we are grateful to the World Climate Research Programme (WRCP) for initiating and coordinating the CORDEX-Africa initiative, to the modelling centres for making their downscaling results publicly available through ESGF. Wim Thiery was supported by an ETH Zurich postdoctoral fellowship (Fel-45 15-1). The Uniscientia Foundation and the ETH Zurich Foundation are thanked for their support to this research.

2.6 Supplementary material

Details on used CORDEX simulations

The CORDEX ensemble simulations used in this study are listed in table 2.1. From all available simulations, the simulation of HIRHAM5 driven by EC-EARTH following RCP 4.5 is not used because it exhibits discrepancies between its historical and future simulation. These discrepancies are nonphysical and inhibit the application of a bias correction.

Table 2.1: Overview of the different CORDEX simulations and their availability. (* data not used because of discrepancy between historical and future simulation).

RCM	Driving GCM	RCP 2.6	RCP 4.5	RCP 8.5
CCLM4-8-17	EC-EARTH	N	Y	Y
CCLM4-8-17	HasGEM2-ES	N	Y	Y
CCLM4-8-17	MPI-ESM-LR	N	Y	Y
CCLM4-8-17	CNRM-CM5	N	Y	Y
CRCM5	MPI-ESM-LR	N	Y	N
CRCM5	CanESM2	N	Y	N
HIRHAM5	EC-EARTH	N	Y*	Y
RACMO22T	EC-EARTH	N	Y	Y
RACMO22T	HadGEM2-ES	Y	Y	Y
RCA4	CanESM2	N	Y	Y
RCA4	EC-EARTH	Y	Y	Y
RCA4	MIROC5	Y	Y	Y
RCA4	HadGEM2-ES	Y	Y	Y
RCA4	NorESM1-M	Y	Y	Y
RCA4	GFDL-ESM2M	N	Y	Y
RCA4	CM5A-MR	N	Y	Y
RCA4	CNRM-CM5	N	Y	Y
RCA4	MPI-ESM-LR	Y	Y	Y
RCA4	CSIRO-Mk3-6-0	N	Y	Y
REMO2009	MIROC5	Y	N	N
REMO2009	GFDL-ESM2G	Y	N	N
REMO2009	CM5A-LR	Y	N	Y
REMO2009	HadGEM2-ES	Y	N	N
REMO2009	EC-EARTH	N	Y	Y
REMO2009	MPI-ESM-LR	Y	Y	Y

Correction of CORDEX ensemble members for number of days

Not all simulations from the CORDEX ensemble have the same number of days. As a fixed number of days is a necessary condition to compare the WBM simulations, a correction was applied on the daily WB terms of some simulations.

First, simulations driven by HadGEM2-ES (CCLM4-8-17, RACMO22T, RCA4, REMO2009), have 30 day-months and only go until 2099. To account for the missing days, 5 extra days are added for every 72 days in the year, starting after the 36th day. The index of these 5 extra days within each year are given in table 2.2. The added days are the average of the respective WB terms during the previous and next day. In addition, we accounted for the fact that these model simulations do not include the year 2100, by repeating the year 2099. The simulations with HadGEM2-ES for RCP 4.5 have no december month in the year 2099. This is also the case for the HadGEM2-ES CCLM4-8-17 simulation for RCP 8.5. In both cases, December 2099 is added by repeating the month November of the same year.

Table 2.2: Indices where extra days are added per year

Original index	36	108	180	252	324
Index of added day	37	110	183	256	329

Finally, in all simulations that do not account for leap years (RCMs driven by CanESM2, NorESM1-M, MIROC5, GFDL-ESM2M, CM5A-MR and CSIRO-Mk3-6-0), an extra day in the leap years is added by taking the average WB term value of the days corresponding to the 28th of February and the 1st of March. Overall, compared to the total number of days of the future projections (34698 days), we note that corrections on single days (up to 888 days depending on the simulations) have a little influence on the outcomes of this study.

Inter quartile ranges of lake level projections

The interquartile range of the lake level projections (fig. 2.10) compared with their 5th and 95th percentile envelope shows a large decrease in uncertainty range for outflow following the Agreed Curve, while the uncertainty following the HPP management scenarios knows a smaller decrease.

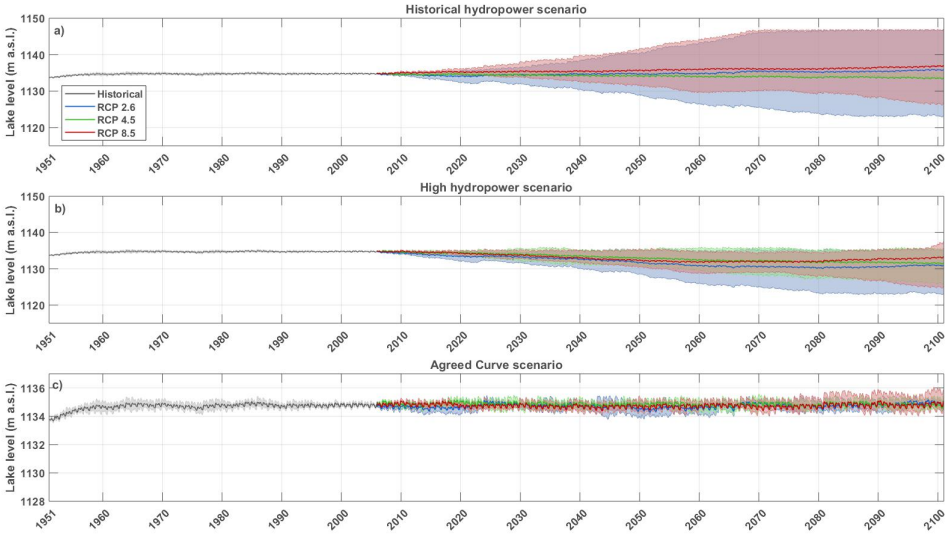

Figure 2.10: As in Fig. 2.8, but the envelope shows the inter quartile range of the CORDEX simulations.

Overview of the parameters used in the linear parametric transformation

Table 5.1 shows the *a* and *b* calibration parameters for the different CORDEX simulations used in the linear parametric transformation to bias correct the lake precipitation, evaporation and inflow terms of the WB.

Table 2.3: Parameters *a* and *b* of the linear parametric transformation of the WB terms for the different CORDEX simulations (Eq. 2.5).

		Lake precipitation		**Lake evaporation**		**Inflow**	
RCM	**Driving GCM**	a (10^{-3})	b	a (10^{-3})	b	a (10^{6})	b
CCLM4-8-17	CNRM-CM5	0.65	0.350	2.30	0.476	27.0	0.257
CCLM4-8-17	EC-EARTH	1.68	0.574	2.82	0.536	38.1	0.315
CCLM4-8-17	HadGEM2-ES	1.69	0.425	2.88	0.339	47.6	0.404
CCLM4-8-17	MPI-ESM-LR	1.20	0.342	2.05	0.556	36.6	0.261
CRCM5	MPI-ESM-LR	1.06	0.810	1.71	0.676	-16.5	0.705
CRCM5	CanESM2	-1.54	0.850	2.86	0.655	-15.0	0.647
RACMO22T	EC-EARTH	-0.01	0.528	1.95	0.206	-31.1	2.041
RACMO22T	HadGEM2-ES	0.43	1.823	2.98	0.944	-16.0	2.225
HIRHAM5	EC-EARTH	1.04	1.630	1.59	0.424	0.90	0.730
RCA4	CanESM2	1.78	0.926	1.78	0.658	16.0	0.759
RCA4	CM5A-MR	1.81	0.860	1.86	0.629	24.4	0.691
RCA4	CNRM-CM5	1.95	0.982	1.78	0.643	27.6	0.916
RCA4	EC-EARTH	1.64	0.794	1.66	0.706	19.0	0.657
RCA4	GFDL-ESM2M	2.04	0.878	1.73	0.699	36.8	0.652
RCA4	HadGEM2-ES	2.40	1.125	2.70	0.433	36.5	1.177
RCA4	MIROC5	1.73	0.885	2.00	0.593	23.9	0.767
RCA4	MPI-ESM-LR	1.79	0.889	1.76	0.657	21.8	0.812
RCA4	NorESM1-M	2.04	0.994	1.81	0.657	31.3	0.946
RCA4	CSIRO-Mk3-6-0	1.74	1.048	1.89	0.648	22.9	0.971
REMO2009	HadGEM2-ES	0.16	0.425	2.90	0.241	33.5	0.525
REMO2009	MPI-ESM-LR	1.23	0.639	2.50	0.519	42.2	0.814
REMO2009	EC-EARTH	1.76	0.923	2.59	0.703	40.7	1.013
REMO2009	CM5A-LR	0.73	0.414	2.81	0.271	19.7	0.453
REMO2009	GFDL-ESM2G	0.51	0.415	2.58	0.327	13.3	0.470
REMO2009	MIROC5	0.57	0.481	2.88	0.279	23.1	0.524

Simulations with empirical quantiles bias correction

Next to bias correction method using a linear parametric transformation (see section 2.2.4), WB closure was adhered with a second method which is the non-parametric quantile mapping method, a common approach for statistical transformation (e.g. Panofsky and Brier, 1968; Wood et al., 2004; Boé et al., 2007; Themeßl et al., 2011; Themeßl et al., 2012). Following Gudmundsson et al. (2012) and Boé et al. (2007), this method uses the Cumulative Density Function (CDF) based on the empirical quantiles from the observed variable to transform the modelled variable. First, the cumulative density functions of the three WB terms following each historical simulation in the overlapping period (the reference simulations) are matched with the cumulative density function of the WB terms from the observational WBM (observations). This generates a correction function, relating the quantiles of both distributions. Next, this correction function is used to unbias the WB term simulations for the whole simulation period quantile by quantile (Boé et al., 2007).

When a bias correction based on empirical quantiles is used, very similar results are found (compare Figs. 2.12, 2.13, 2.14 and 2.16). Based on this, we conclude that the bias correction methods has very little effect on the results presented.

In this study, applying a bias correction on the WB terms of the CORDEX simulations was necessary to be able to make lake level and outflow projections, as subsetting as not possible. RCMs are often bias corrected, as their simulations inhibit errors (Christensen et al., 2008; Teutschbein and Seibert, 2013; Maraun et al., 2010; Themeßl et al., 2012; Lange, 2018). Both linear parametric transformation and the quantile mapping bias correction methods are used. The advantage of the first is the simplicity and transparency of the method (Teutschbein and Seibert, 2013). The quantile mapping method on the other hand, is a non-parametric method and is able to correct for errors in variability as well (Themeßl et al., 2011). Yet, no substantial differences could be noted between the resulting projections of both methods, which supports that there is no single optimal way to correct for RCM biases (Themeßl et al., 2011). It is however important to consider the limitations concerning the bias correction methods. In both methods, each WB term is corrected independently, whereas biases may not be independent among the terms, which may be important in the context of climate change (Boé et al., 2007). The consistency between the variables could be preserved by using a more sophisticated method using a multivariate bias correction (Cannon, 2017; Vrac and Friederichs, 2015). However, Maraun et al. (2017) showed that bias correction could lead to improbable climate change signals and cannot overcome large model errors.

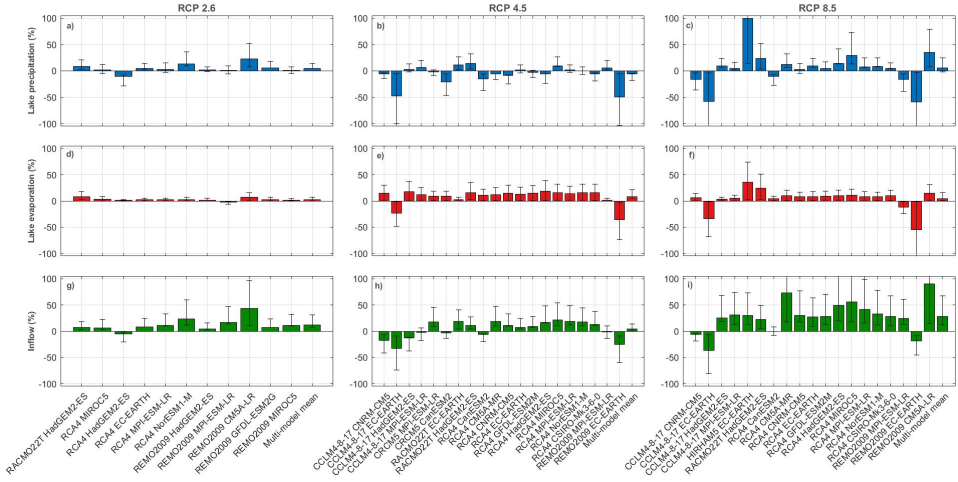

Figure 2.11: Barplots showing the relative projected climate change following RCP 2.6, 4.5 and 8.5 for lake precipitation (a-c), lake evaporation (d-f) and inflow (g-i) for the CORDEX simulations without bias correction. The climate change signal is defined as the difference between the future (2071-2100) and the historical (1971-2000) simulations. The whiskers indicate the 95% confidence interval of the change based on the 30-year annual difference.

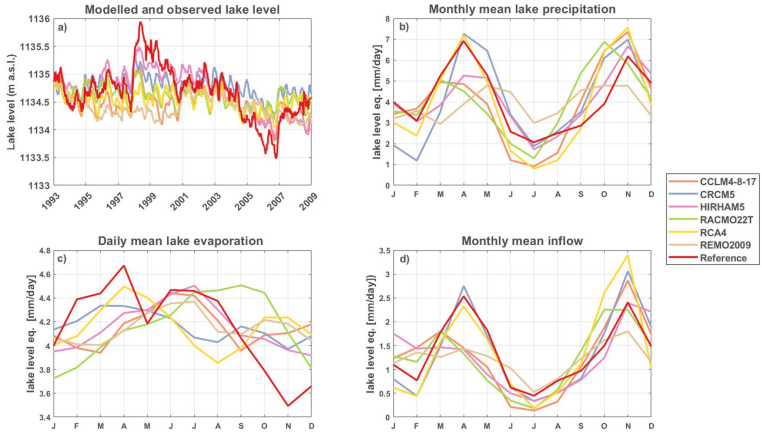

Figure 2.12: As in Fig. 2.6, but bias corrected using empirical quantiles.

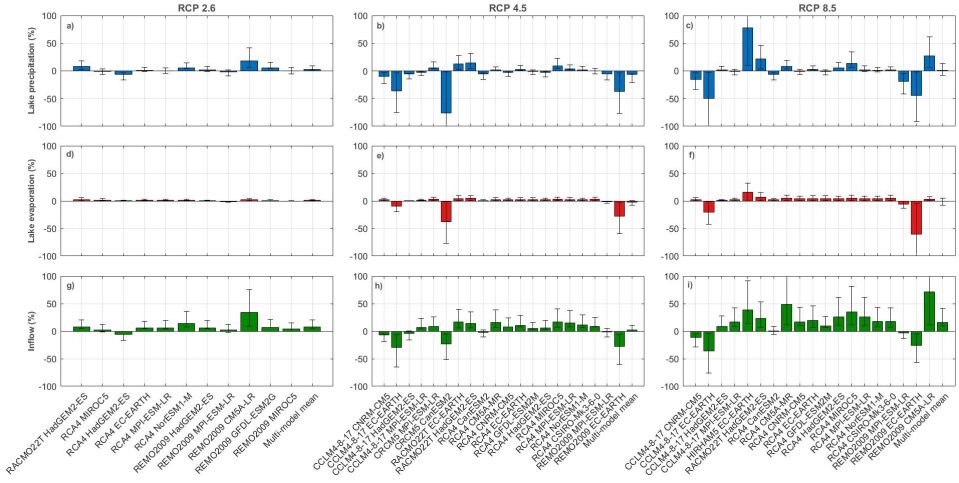

Figure 2.13: As in Fig. 2.7, but bias corrected using empirical quantiles.

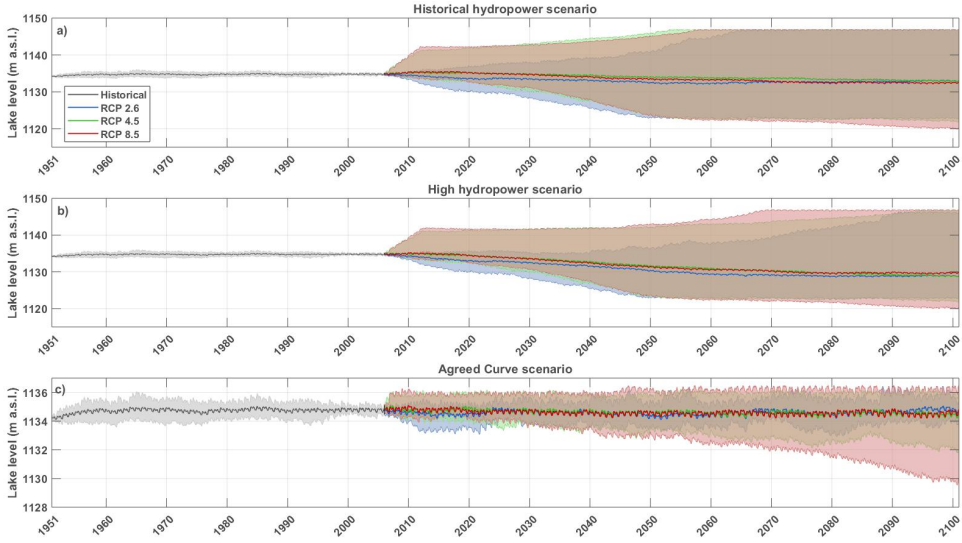

Figure 2.14: As in Fig. 2.8, but bias corrected using empirical quantiles.

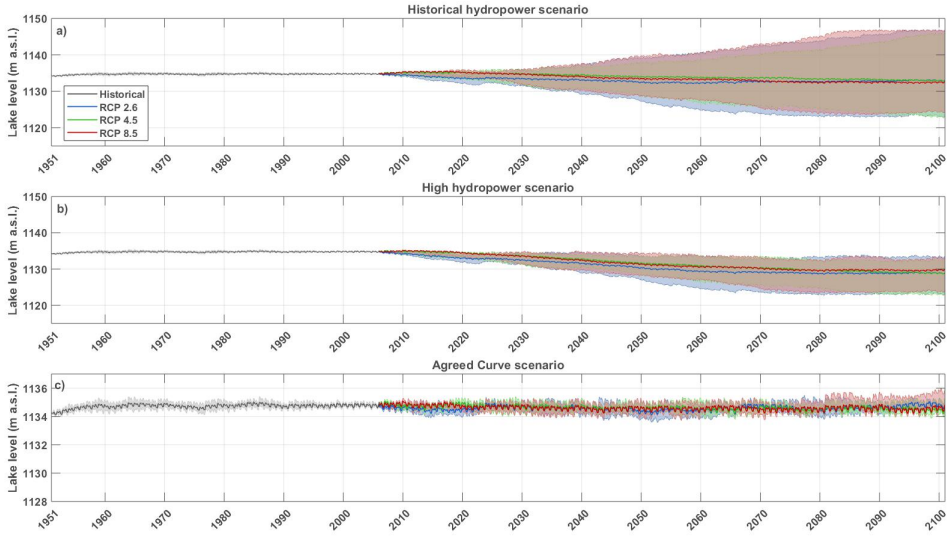

Figure 2.15: As in Fig. 2.10, but bias corrected using empirical quantiles.

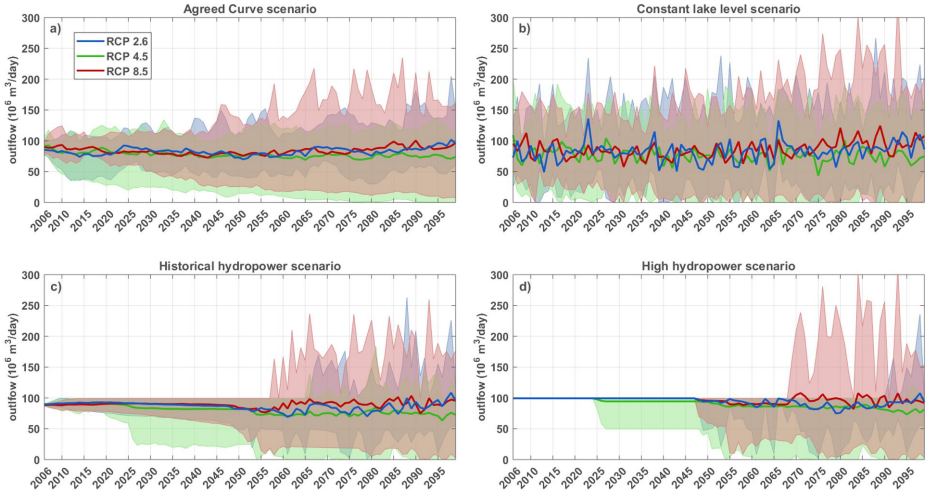

Figure 2.16: As in Fig. 2.9, but bias corrected using empirical quantiles.

Chapter 3

Global heat uptake by inland waters

Heat uptake is a key variable for understanding the Earth system response to greenhouse gas forcing. Despite the importance of this heat budget, heat uptake by inland waters has so far not been quantified. Here we use a unique combination of global-scale lake models, global hydrological models and Earth system models to quantify global heat uptake by natural lakes, reservoirs and rivers. The total net heat uptake by inland waters amounts to $2.6 \pm 3.2 \cdot 10^{20}$ *J over the period 1900-2020, corresponding to 3.6% of the energy stored on land. The overall uptake is dominated by natural lakes (111.7%), followed by reservoir warming (2.3%). Rivers contribute negatively (-14%) due to a decreasing water volume. The thermal energy of water stored in artificial reservoirs exceeds inland water heat uptake by a factor ∼10.4. This first quantification underlines that the heat uptake by inland waters is relatively small, but non-negligible.*

This chapter is published as: Vanderkelen I., van Lipzig N.P.M., Lawrence D. M., Droppers B., Gosling S. N., Janssen A. B. G., Marcé R., Müller-Schmied H., Perroud M., Pierson D., Pokhrel Y., Satoh Y., Schewe J., Seneviratne S. I., Stepanenko V. M., Tan Z., Woolway R. I., Thiery W. (2020) Global heat uptake by inland waters. Geographical Research Letters. 47(12), e2020GL087867.

3.1 Introduction

Increasing greenhouse gas concentrations in the atmosphere cause a net heat uptake in the Earth System. Over 90% of this extra thermal energy is stored in the oceans, causing ocean warming and global sea level rise through thermal expansion (Rhein et al., 2013). The most recent estimates of heat uptake are described in the Special Report on the Ocean and Cryosphere in a Changing Climate (SROCC) by the Intergovernmental Panel on Climate Change (IPCC). The report concludes that the ocean has taken up $4.35 \pm 0.8 \cdot 10^{21}$ J yt^{-1} in the upper-700 m of water and $2.25 \pm 0.64 \cdot 10^{21}$ J yt^{-1} between the depths of 700-2000 m, respectively (averages of 1998-2017 compared to 1971-1990), and attributes this increase to anthropogenic forcings (Bindoff et al., 2019). The remaining excess heat is taken up by melting sea and land ice, by specific heating and water evaporation in the atmosphere and by warming of the continents (Trenberth, 2009).

Despite the key role of heat uptake in driving Earth system response to greenhouse gas forcing, currently little is known about global-scale heat uptake by inland waters. Inland waters include natural lakes, man-made reservoirs, rivers and wetlands, with lakes covering 1.8% of the global land area (Messager et al., 2016) and rivers 0.58% of the global non-glaciated land area (Allen and Pavelsky, 2018). However, the abundance and total area covered by inland waters (natural and artificial) is continuously changing (Pekel et al., 2016a). For example, reservoir expansion following dam construction experienced a marked acceleration during the 1960s and 1970s, now covering 0.2% of the global land area (Lehner et al., 2011). Despite occupying <3% of the global land surface, inland waters play an important role in the climate system (e.g., Subin et al., 2012b; Vanderkelen et al., 2018a; Choulga et al., 2019) and are sentinels of climate change (e.g., Adrian et al., 2009; Schewe et al., 2014). Compared to other types of land surfaces, water (i) has a higher specific heat capacity, (ii) typically has a lower albedo, (iii) allows for radiation penetration below the surface, and (iv) seasonally mixes warmer surface masses to deeper layers. Consequently, inland waters are generally regarded as heat reservoirs compared to adjacent land. In addition, lake surface temperatures have been observed to have increased rapidly in recent decades, in some locations even faster than ambient air temperatures (O'Reilly et al., 2015; Schneider and Hook, 2010).

To quantify the heat uptake by inland waters, an estimation of both the water volumes and evolution of water temperature profiles is necessary. Water temperature observations of lakes, reservoirs, rivers and wetlands are however sparse and spatially limited. So far, studies of energy fluxes and heat storage have been limited to individual lakes (Heiskanen et al., 2015; Strachan et al., 2016). To overcome this, global models are developed for estimating water temperatures on local, regional and global scales.

In this chapter, we develop the first estimate of the global-scale heat uptake by inland waters over the period 1900-2020. To this end, we combine global lake and hydrological simulations from the Inter-Sectoral Model Intercomparison Project (ISIMIP) with a river temperature parameterisation and spatially-explicit data sets of lake abundance, reservoir

area expansion and lake depth. This enables us to quantify the heat uptake by natural lakes, reservoirs and rivers. We do not consider the contribution of wetlands and floodplains, given their highly disperse spatial and temporal character and limited data availability. Next, we also quantify the redistribution of heat from ocean to land due to increased inland water storage as a result of the construction of reservoirs.

3.2 Data and methods

3.2.1 Lake and reservoir heat content

The ISIMIP initiative is a recent effort to provide consistent climate impact simulations across different sectors which allows for the integration and comparison of global hydrological and lake model simulations (Frieler et al., 2017). For lake water temperatures, we used the global ISIMIP2b simulations from three one-dimensional lake models: the Community Land Model 4.5 (CLM4.5, Oleson et al., 2013) including the Lake, Ice, Snow and Sediment Simulator (LISSS, Subin et al., 2012b), SIMSTRAT-UoG, a physically sophisticated k-ε model (Goudsmit et al., 2002) and the Arctic Lake Biogeochemistry Model (ALBM), a process-based lake biogeochemistry model (Tan et al., 2015, see table 3.3). Following the ISIMIP2b protocol, simulations are performed at a 0.5° by 0.5° spatial resolution using bias-adjusted atmospheric forcing data from four Earth System Models (ESMs: GFDL-ESM2M, HadGEM2-ES, IPSL-CM5A-LR and MIROC5). SIMSTRAT-UoG does not represent human-influences, while CLM4.5 and ALBM assume that land use and human influences (irrigation extent, land use, population and GDP) are constant at the 2005 level. We use ESM simulations for the historical period with historical climate and greenhouse gas conditions, ranging from 1900 to 2005 and Representative Concentration Pathway 6.0 simulations for the period 2006-2020 (Frieler et al., 2017). The lake models simulate a representative lake with a constant depth in each grid cell, of which the extent is given by the lake area fraction of that grid cell. The albedo and light attenuation coefficient are given by the models (Table 3.3, Potes et al., 2012). Using the four climate forcings for each lake model results in a total of 12 simulations of spatially-explicit global-scale lake temperatures.

Global lake area distribution is given by the HydroLAKES dataset (Messager et al., 2016), containing 1.42 million individual polygons of natural lakes. This data set is linked to the Global Reservoir and Dam data set v. 1.3 (GRanD, Lehner et al., 2011). We convert both HydroLAKES and GRanD polygons to lake area fraction on a 0.5° by 0.5° grid to match the ISIMIP resolution. Reservoir construction is provided by GRanD, and changes in reservoir area are accounted for by creating annual lake area fraction maps, in which reservoir areas are added in their year of construction. Natural lakes which become controlled by a dam are categorized as 'natural lakes' based on information from GRanD. As GRanD provides construction years up to 2017, we assume a constant reservoir area from 2017 to 2020. Lake and reservoir depths are obtained from the Global Lake Database v.3 (GLDB,

Kourzeneva, 2010; Choulga et al., 2014, 2019), providing estimates of mean lake depth for every land grid cell. This data is remapped from its original 30" ($\sim$ 1 km grid) to the 0.5° by 0.5° resolution using bi-linear interpolation.

Annual lake heat content Q_{lake} [J], per grid cell is calculated as

$$Q_{lake} = c_{liq}\, A_{lake}\ \rho_{liq} \sum_{n=1}^{n=nlayers} T_n\, d_n$$

with c_{liq} (J kg^{-1} K^{-1}) the specific heat capacity of liquid water (here taken constant at 4188 J kg^{-1} K^{-1}), A_{lake} (m^2) the lake area, ρ_{liq} (kg m^{-3}) the density of liquid water (here taken at 1000 kg m^{-3}), and the sum of annual mean temperatures T_n (K) over all lake layers, where d_n (m) is the layer thickness. As the layering of each lake model is different, lake heat per layer is rescaled by calculating the weights of the model layer depths relative to the models' grid cell lake depth. These weights are then applied on the grid cell lake depth from GLDB. This allows for a consistent volume computation. To also ensure a consistent lake coverage across the different lake models, the water temperatures are spatially interpolated to the lake coverage map derived from HydroLAKES using nearest neighbour remapping. The Caspian Sea is included in the analysis, as this inland sea is often not accounted for in ocean heat content estimates (e.g. Cheng et al., 2017). We define the spatial extent of natural lakes by the lake extent in 1900. Lake ice, with a heat capacity of 2117 J kg^{-1} K^{-1}, is simulated by the lake models, but not included in the analysis due to constraints in model harmonisation. Inter-annual temperature changes of the liquid water below the ice cover is accounted for, but changes related to snow are not.

Heat content anomalies, hereafter denoted as heat uptake, are computed relative to the average lake heat content in 1900-1929, (hereafter referred to as pre-industrial period) and represent changes in lake and reservoir temperatures. Changes in the amount of water stored on land by the construction of reservoirs are also taken into account, thereby assuming the water temperature of the constructed reservoir is given by the grid cell lake temperature. We do not consider inter-annual variations in lake and reservoir volumes. Total annual global heat uptake is calculated by summing all grid cells.

As the lake models conserve energy, the heat related to freezing and melting of ice is included in the resulting water temperature given by the models. The relative contribution of this term in the total heat uptake can be determined separately by calculating Q_{phase} (J), the heat related to phase changes:

$$Q_{phase} = L_f\, \Delta d_{ice}\, \rho_{ice}\, A_{lake}$$

with L_f (J kg^{-1}), the heat of fusion ($3.337 \cdot 10^5$ J kg^{-1}) and Δd_{ice} (m) the ice thickness.

3.2.2 River heat content

River water mass is retrieved from the grid-scale monthly river storage (kg m^2) given by the two Global Hydrological Models from the ISIMIP 2b global water sector providing this variable: the Minimal Advanced Treatments of Surface Interaction and Runoff (MATSIRO, Pokhrel et al., 2015) and WaterGAP2 (Müller Schmied et al., 2016, see table 3.3), by multiplying with the grid cell area and taking the annual mean. Annual grid cell river water temperatures are estimated using the global non-linear regression model of Punzet et al. (2012) with the global coefficients and an efficiency fit of 0.87. This regression prescribes river temperatures based on monthly gridded air temperatures, which are given by the four different ESM forcings (GFDL-ESM2M, HadGEM2-ES, IPSL-CM5A-LR and MIROC5). River heat content, Q_{river} (J), is calculated as

$$Q_{river} = c_{liq}\, m_{river}\, T_{river}$$

with m_{river} (kg) the water storage in the grid cell rivers and T_{river} (K) the river temperature. As for lakes, river heat uptake is defined as the anomaly compared to the average river heat content in the reference period 1900-1929 and consists of the change in temperature and the change in water stored in the rivers. This approach uses a total of 8 ISIMIP simulations. The set-up of the models, dictated by the ISIMIP protocol, allows the direct comparison of the resulting lake, reservoir and river heat uptake.

3.3 Inland water heat uptake

Natural lakes have taken up $2.9 \pm 2.0 \cdot 10^{20}$ J ($\pm$ one standard deviation of the 12 simulations) averaged over the period 2011-2020, relative to pre-industrial times (1900-1929; Table 3.1), due to an increase of lake water temperatures integrated over the lake column. The dip in heat uptake in 1960-1978 originates from a decrease in surface temperature in the ESM forcings associated with global dimming (Frieler et al., 2017; Wild, 2009). From the 1980s onwards, lake heat uptake increased continuously, following the trend of increasing atmospheric temperatures (Figs. 3.1a, 3.5). In the last 30 years, the mean trend in global lake heat uptake of the model simulations is $10.2 \cdot 10^{18}$ J yt^{-1}. The heat uptake related to melting of the ice in 1900-2020 is negligible, as it contributes only 0.004% ($8.8 \pm 10.4 \cdot 10^{15}$ J) to the total heat uptake by natural lakes.

The construction of dams and the resulting artificial reservoirs have increased global lake volume by 3.2% (Messager et al., 2016, ; Fig. 3.4b). The steep increase in reservoir heat uptake from the 1980s onwards stems from the combination of accelerated reservoir construction, making more water on land available for warming, and regional emergence of warming signals due to climate change during this period (Fig. 3.1b). In total, reservoirs have taken up $5.9 \pm 2.7 \cdot 10^{18}$ J on average in the period 2011-2020, compared to pre-industrial times (Table 3.1).

Global heat uptake by rivers encompasses large uncertainties and no detectable trend. In the late 1960s the ensemble mean heat uptake shifts to overall negative heat uptake compared to pre-industrial values (Fig 3.1c). Global-scale stream temperatures show a clear positive trend, reflecting the increase in air temperatures (Fig. S3, a-d). However, global-scale river storage is marked by large inter-annual variability for both global hydrological models (Fig. S3, e-l), thereby effectively masking the positive temperature trend in the resulting river heat uptake. River storage evolution is dictated mainly by the ESM forcing, as differences in river storage between the four different ESM forcings are more pronounced than between the two global hydrological models (Fig. S3). Altogether, with a heat uptake of $-0.36 \pm 3.2 \cdot 10^{20}$ J averaged for 2011 to 2020, compared to pre-industrial times, rivers contribute negatively to the total heat uptake by inland waters, but their contribution is accompanied by a large variability, as well as uncertainty originating from the spread across climate forcings.

The total heat uptake in inland waters is thus dominated by the heat uptake of natural lakes, accounting for 111.7% of the average total net increase by 2020, while reservoir heating has taken up 2.3% and rivers contributed negatively with -14% in 2020, but the latter with a large uncertainty (Fig. 3.3a).

Table 3.1: Total heat uptake and trend for the different inland water components. Heat uptake is calculated as the average heat content of 2011-2020 relative to the reference period 1900-1929. Uncertainties are given by the ensemble standard deviation of the used simulations. Heat fluxes are calculated as the difference in heat uptake between 2020 and 1991, divided by the area (lake and reservoir area from HydroLAKES, and the river surface area from Allen and Pavelsky, 2018). Trends in heat content in 1991-2020 are calculated using a linear regression.

	Heat uptake	**Heat flux (1991-2020)**	**Trend (1991-2020)**
Natural lakes	$2.87 \pm 2.01 \cdot 10^{20}$ J	0.1 ± 0.04 W m^{-2}	$10.2 \cdot 10^{18}$ J yr^{-1}
Reservoirs	$0.06 \pm 0.03 \cdot 10^{20}$ J	0.02 ± 0.001 W m^{-2}	$0.2 \cdot 10^{18}$ J yr^{-1}
Rivers	$-0.36 \pm 1.20 \cdot 10^{20}$ J	0.05 ± 0.05 W m^{-2}	$2.7 \cdot 10^{18}$ J yr^{-1}
Total heat uptake	$2.57 \pm 3.23 \cdot 10^{20}$ J	0.09 ± 0.04 W m^{-2}	$13.1 \cdot 10^{18}$ J yr^{-1}
Redistribution by reservoir expansion	$26.76 \pm 2.13 \cdot 10^{20}$ J	0.52 ± 0.30 W m^{-2}	$15.2 \cdot 10^{18}$ J yr^{-1}

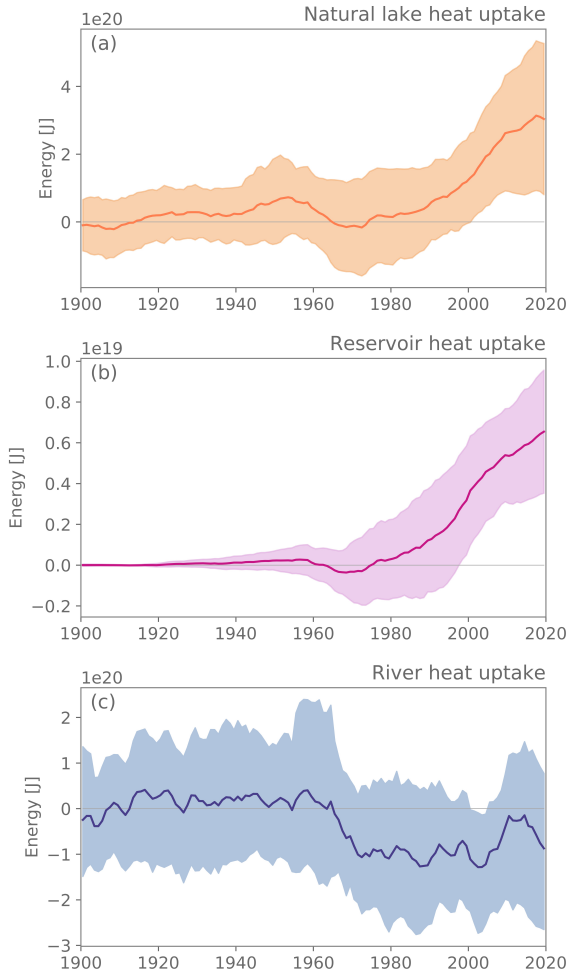

Figure 3.1: Heat uptake by natural lakes (a), reservoirs (b) and rivers (c). Shown are 10-year moving means relative to the 1900-1929 reference period. Note the different y-axis scales. Color shades represent uncertainty range shown as the standard deviation of the used simulations.

Most lake heat uptake is concentrated in the major lake regions of the world. The Laurentian Great Lakes, including Lakes Superior, Michigan, Huron, Erie and Ontario in central North America make up 12.4% of global lake volume (Messager et al., 2016). These lakes all demonstrate a steady increase in heat uptake from the 1980s onwards (Fig. 3.2b), resulting in a total uptake of $2.28 \pm 1.64 \cdot 10^{19}$ J (8.9% of global inland water heat uptake) compared to pre-industrial times, with a trend of $6.8 \cdot 10^{17}$ J yt^{-1} over the last 30 years. The spatial pattern of heat uptake is mainly dictated by the bathymetry and resulting lake volume: the deeper Lake Michigan and Lake Superior have taken up more heat compared to the other lakes, while the much shallower Lake Erie has the lowest heat uptake estimates (Fig. 3.2a).

The African Great Lakes region in East Africa, consisting of Lake Victoria, Tanganyika, Kivu, Kyoga, Albert and Edward (12.38% of global lake volume Messager et al., 2016), are known to affect the local weather and climate conditions (Thiery et al., 2014c, 2015, 2016, 2017; Vanderkelen et al., 2018b; Van de Walle et al., 2019) and their water temperatures are observed to be warming (Tierney et al., 2010). We find that the heat uptake is largest in Tanganyika, the lake with the highest volume in the region (Fig. 3.2c). Overall, the African Great Lakes show an increase in heat over the whole study period (Fig. 3.2d, a total heat uptake of $4.04 \pm 1.62 \cdot 10^{19}$ J, 15.7% of global inland water heat uptake). The Great European lakes, including Lake Ladoga and Onega show a smaller increase compared to other major lake regions, corresponding to the smaller volume of the lakes, but the lake heat content shows a sudden increase from the 1990s (Fig. 3.2e,f; total heat uptake of 2.31 $\pm 1.13 \cdot 10^{18}$ J, 0.9% of global inland water heat uptake). The Amazon, world's highest discharge river, depicts no temporal trend in river heat uptake, but the uncertainty is large, mainly owing to the diverging river mass estimations (Fig. 3.2h; heat uptake of $0.18 \pm 1.50 \cdot 10^{20}$ J, 7% of global inland water heat uptake). Heat uptake increases towards the river mouth, as the water volume increases (Fig. 3.2g). To summarize, the global picture of heat uptake is confirmed at the regional scale by all model combinations.

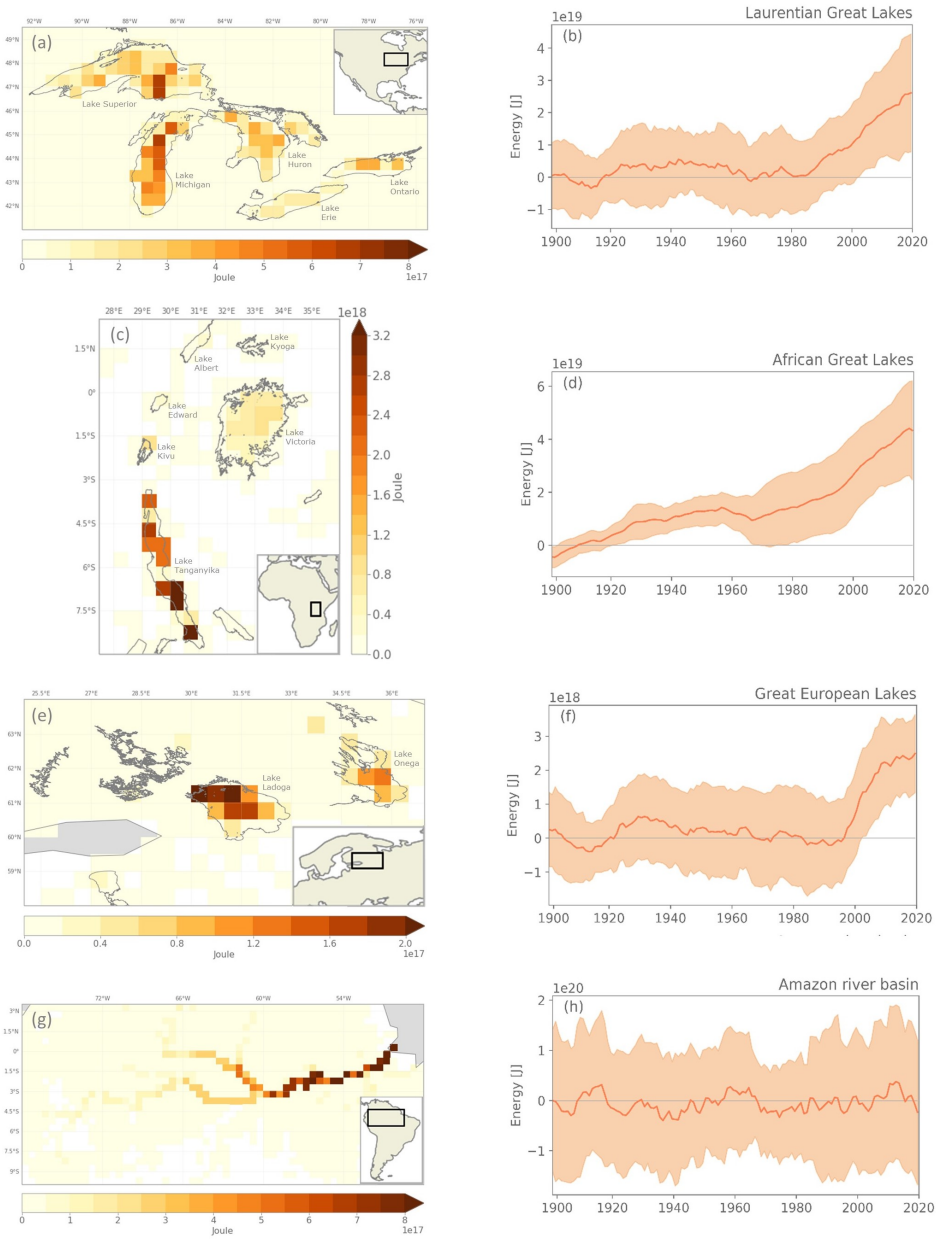

Figure 3.2: Heat uptake by the Laurentian Great lakes (a-b), the African Great Lakes (c-d), the Great European Lakes (e-f), and the Amazon River (g-h). The maps represent the average heat uptake during the 2001-2020 period with the grey colors indicating ocean grid cells, and white colors grid cells without water. The graphs show 10-year moving means, where the color shades represent uncertainty range shown as the standard deviation of the used simulations. The reference period is 1900-1929. Note the different y-axis scales.

3.4 Heat redistribution due to reservoir area expansion

In the second half of the 20^{th} century, reservoir capacity strongly increased, raising the water volume stored on land and offsetting sea level rise by 30 mm (Chao et al., 2008; Lehner et al., 2011; Pokhrel et al., 2012, Fig. 3.4b). This extra water stored on land does not only increase the potential of the land surface for taking up excess atmospheric heat (Sect. 2), but also carries energy in itself. By constructing reservoirs, humans are thus not only redistributing mass from the oceans to the land, but also the thermal energy carried within this water. This heat redistribution by reservoir expansion is growing over time, following the increasing number of reservoirs constructed (Fig. 3.3b). During the historical period, 26.8 $\pm$ 2.1 $\cdot 10^{20}$ J of heat was redistributed from ocean to land, exceeding inland water heat uptake from climate change by a factor of $\sim$10.4.

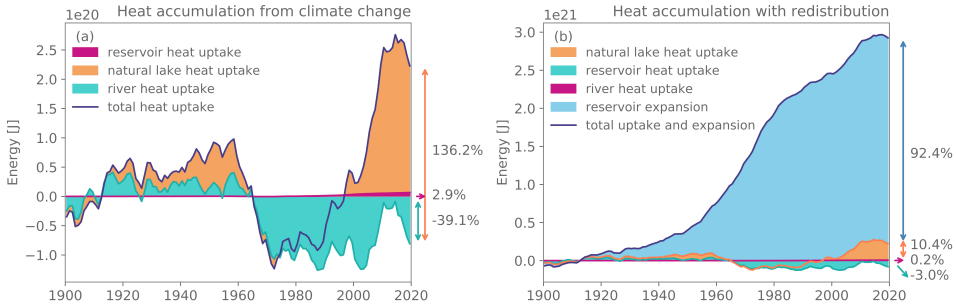

Figure 3.3: Inland water heat accumulation from climate change (a) and including redistribution by reservoir construction (b). Shown are 10-year moving ensemble means relative to the 1900-1929 reference period. Note the different y-axis scales.

3.5 Discussion and conclusions

Large lakes take up most heat, as they have the largest volume to warm up. The increase in lake heat content complies with recent observations of increasing lake surface temperatures and reported changes in mixing regimes (O'Reilly et al., 2015; Woolway and Merchant, 2019) and is robust for different lake regions. The difference between the three lake models (Fig. 3.5) could arise from differences in the structure of the models, like lake layers and internal physics.

River heat uptake is negative in most simulations during the second half of the 20^{th} century. This seemingly contradictory result stems from a decrease in river storage, which could be attributed to less precipitation or the construction of reservoirs, lowering water flow in rivers or to drying of rivers by increased land evaporation due to global warming or increased water use. These changes in river storage should, however, be taken with care,

as the uncertainties are very large. In addition, no conclusions can be made about global trends in observed streamflow, because changes in streamflow and the hydrological conditions causing it, are characterized by complex spatial patterns (Gudmundsson et al., 2019; Müller Schmied et al., 2016).

The quantification of heat uptake facilitates comparison of the effects of climate change on different components of the climate system. Globally, inland waters have taken up $\sim$0.08% of heat compared to oceans. The continental heat uptake occurs through a heat flux into the solid surface of the lithosphere and has been estimated between 9.1 and $10.4 \cdot 10^{21}$ J (Beltrami, 2002; Huang, 2006) for the period 1950-2000 based on borehole temperature observations. Estimates based on the Coupled Model Intercomparison Project Phase 5 (CMIP5) are consistently lower ($1 \pm 5 \cdot 10^{21}$ J), mainly due to the limited depth of the bottom boundary of the land surface schemes of the Earth system models (Cuesta-Valero et al., 2016). Relative to the geophysical estimate reported by Beltrami (2002), the share of inland waters is $\sim$3.6%, while inland waters cover about $\sim$2.58% of the global continental area. This comparison has to be taken with care, as the borehole-based estimations of heat uptake are only quantified until 2000 and surface air temperatures have risen at record rates since then (Rhein et al., 2013).

The redistribution of heat by reservoir construction, is equivalent to $\sim$38% of the land mass heat uptake. This is mainly a transfer of water mass with its associated internal energy. As it only increases the potential of storing extra heat on land, the redistribution has little influence on the potential heat uptake on a global scale. In particular, the warming of the water in the created reservoirs might cause local impacts such as masking surface temperature increase on diurnal and seasonal timescales by their buffering capacity. In addition, the extra continental water storage by reservoir expansion could have a dampening effect on local temperature extremes and could affect river temperatures downstream. It is therefore important to account for reservoir expansion and resulting heat redistribution in Earth System Models, to increase our understanding of how reservoirs affect the climate (Pokhrel et al., 2016; Wada et al., 2017). Capturing heat redistribution by reservoir expansion could also increase the quality of climate change projections on regional to global scales.

There are several opportunities to refine the heat uptake calculations presented in this chapter. First, the volume calculation does not account for lake hypsometry. By using average lake depths to multiply with lake area, the resulting total lake volumes are reasonable, as most lakes have a linear hypsometric relationship (Busker et al., 2019). This rectangular hypsometry assumption results in relatively higher weights for the deeper lake layers, which makes our heat uptake estimates more conservative. Second, apart from reservoir construction, the heat calculation does not account for variations in lake and reservoir volumes, while changes in river storage are included. This could have important effects, especially for lakes with a high inter-annual variability. Third, variations in heat capacity are not considered in our analysis, which could lead to a lower estimate of heat uptake as the specific capacity of ice is lower than that of water (2117 J kg^{-1} K^{-1} compared to 4188 J kg^{-1} K^{-1}, respectively). Next, variations in salinity of inland waters are not included.

Evaluating the modeled lake heat uptake with observations from individual lakes reveals substantial inconsistencies (see Supporting Information), which are partly due the result of model uncertainty, but also highlight the need for constraining parameter values such as water transparency, refining the ISIMIP simulation setup to include observed atmospheric forcing and increasing the collection of long-term lake temperature profiles. Furthermore, by using global lake and hydrological models driven by ESM forcings, an extra uncertainty related to climate sensitivity is added to the calculations. Despite these limitations, this chapter is the first step towards estimating heat uptake by inland waters.

In this chapter, we show that inland water heat uptake during the historical period is small compared to continental heat uptake, but in line with the surface area of inland waters relative to land. Furthermore, we highlight that by constructing reservoirs, humans have redistributed heat from the ocean to land as well as increased the potential of storing more heat on land, given the higher heat capacity of water compared to land. Compared to the other components of the Earth system, this is a small term, but locally the impacts might be large. By providing a first estimate of inland water heat uptake, this chapter provides new advances in the quantification of the global heat budget.

Data and code availability

All ISIMIP2b simulations used are publicly available through the Earth System Grid Federation (ESGF, `https://esgf-data.dkrz.de/`). The HydroLAKES dataset is available at `https://www.hydrosheds.org/page/hydrolakes`, GRanD at `http://globaldamwatch.org/`, GLDB at `http://www.lakemodel.net/` and observations from the North Temperate Lakes LTER at `https://lter.limnology.wisc.edu/about/lakes`. Scripts used are available at: `https://github.com/VUB-HYDR/2020_Vanderkelen_etal_GRL`.

Acknowledgements

This research is supported by the Research Foundation Flanders (FWOTM920). Wim Thiery acknowledges the Uniscientia Foundation and the ETH Zurich Foundation for their support. Zeli Tan is supported by the U.S. DOE's Earth System Modeling program through the Energy Exascale Earth System Model (E3SM) project. We are grateful to the Potsdam Institute for Climate Impact Research (PIK) for initiating and coordinating the ISIMIP initiative, and to the modelling centres for making their simulations available through ESGF. Computational resources and services were provided by the Shared ICT Services Centre funded by the Vrije Universiteit Brussel, the Flemish Supercomputer Center (VSC) and FWO.

3.6 Supplementary material

This supplementary material contains a section describing the evaluation of lake heat uptake, and 2 tables and 3 figures providing extra information on the data and model results. In section 2, the evaluation of lake heat uptake by individual lakes is described. Table 3.3 shows the used models from the Inter-Sectoral Impact Model Intercomparison Project phase 2b (ISIMIP2b). In Table , the observed and modelled heat uptake for the individual lakes is shown. Figure 3.4 shows maps of the input data used in the chapter: the area fraction for natural lakes (a), reservoirs (b) and the lake depth (c). Figure 3.5 illustrate the annual heat uptake by natural lakes for every individual simulation used in the analysis (per lake model and ESM forcing). Finally, figure 3.4 shows the terms used in the river heat uptake calculation and the resulting river heat uptake, all for both hydrological models and every ESM forcing.

Evaluation of natural lake heat uptake

The quantification of heat uptake by natural lakes is evaluated by comparing heat uptake calculated from observed temperature profiles of individual lakes to the modelled ensemble mean heat uptake of the corresponding grid cell. The observed lake temperature profiles are retrieved from the North Temperate Lakes US Long-Term Ecological Research Network and include 9 lakes located in Wisconsin, USA.
First, observed heat content is calculated for every individual lake based on their lake temperature profile, similar to the modeled heat content, using the following equation:

$$Q_{lake} = c_{liq}\,\rho_{liq} \sum_{n=1}^{n=nlayers} T_n\,d_n$$

with Q_{lake} ($J\ m^{-2}$) the heat content, c_{liq} ($J\ kg^{-1}K^{-1}$) the specific heat capacity of liquid water (here taken constant at 4188 $J\ kg^{-1}K^{-1}$), ρ_{liq} ($kg\ m^{-3}$) the density of liquid water (here taken at 1000 $kg\ m^{-3}$), and the sum of annual mean temperatures T_n (K) over all lake layers, where d_n (m) is the layer thickness. To eliminate the effect of different lake areas, the heat content is calculated per unit area. For each individual lake, heat uptake is calculated as the slope of the linear regression of the annual heat content over the longest time period available in the observational data. For each lake, the modelled lake heat uptake is derived by the heat content from the 0.5° by 0.5° grid cell in which the lake is located. The heat uptake is calculated in the same way using the corresponding observational period from the ensemble mean. The role of lake ice is not included in the evaluation.

For most lakes, there are considerable differences between observed and modelled heat uptake values (Table 3.2). These biases can be explained by different aspects. First, the global lake models (ALBM, CLM4.5 and SIMSTRAT-UoG) are uncalibrated, mainly due to a limited data availability on global scale. Second, lakes are not modeled as individual lakes, but as one representative lake per grid cell, with the mean depth and representative characteristics of all lakes in the grid cell. Third, the lake models are driven by a atmospheric forcing coming from ESMs. These ESMs provide climatologies, which do not

correspond to day-to-day observed atmospheric conditions due to natural variability, hindering a direct comparison. In addition, to correctly capture climatologies in observations, long observational periods are necessary. Fourth, the biases could be attributed to structural model deficiencies in the lake models. Finally, an additional source of uncertainty is the vertical resolution of the sampling profile of water temperature, which is different for all lakes. The biases are a combined effect of all these factors, and can thus not all be attributed solely to lake model uncertainty coming from model deficiencies.

Supplementary tables and figures

Table 3.2: Observed and modeled heat uptake per lake. Uncertainties are given by the ensemble standard deviation of the used simulations.

Lake name	**Period**	**Observed [Wm^{-2}]**	**Modeled [Wm^{-2}]**
Allequash Lake	1981-2014	0.003	0.003 ± 0.0002
Big Muskellunge Lake	1981-2008	0.039	0.001 ± 0.0002
Crystal Lake	1981-2007	-0.018	0.004 ± 0.0014
Lake Mendota	1995-2014	-0.096	0.001 ± 0.0007
Lake Monona	1995-2014	-0.156	0.001 ± 0.0007
Sparkling Lake	1981-2014	0.223	0.003 ± 0.0002
Toolik Lake	1998-2014	0.635	0.006 ± 0.0015
Trout Lake	1981-2014	0.136	0.003 ± 0.0002
Lake Wingra	2001-2014	-0.039	0.001 ± 0.0007

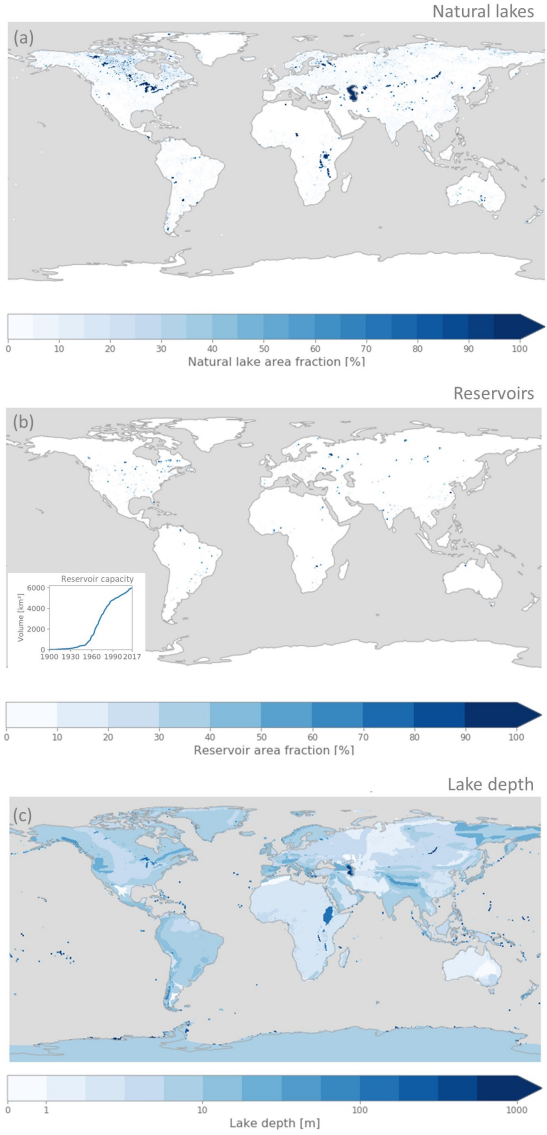

Figure 3.4: Lake data used in the lake heat assessment: lake area fraction, based on HydroLAKES (a; Messager et al., 2016), reservoir area fraction map representing the reservoir expansion in the period 1900-2017, based on GRanD coupled with HydroLAKES, inset: reservoir volume increase over time based on GRanD (b; Lehner et al., 2011; Messager et al., 2016) and (potential) lake depth adapted from GLDB v3 (c; Choulga et al., 2019).

Table 3.3: Overview of ISIMIP2b impact models used in this chapter.

Lake models	**# layers**	**Lake depth**	**Light extinction coefficient**	**Albedo**	**Reference**
CLM4.5	10	Constant at 50 m	Function of lake depth	Based on zenith angle	(Subin et al., 2012b)
SIMSTRAT-UoG	1 - 13	GLDBv1	Funtion of Particulate Organic Matter	Lambert-Beer Law	(Goudsmit et al., 2002)
ALBM	51	GLDBv1	Function of lake depth (Subin et al., 2012b)	Beer Law	(Tan et al., 2015)

Hydrological models	Human influences	**Reference**
MATSIRO	No human influences	Pokhrel et al. (2015)
WaterGAP2	Historical human influences	Müller Schmied et al. (2016)

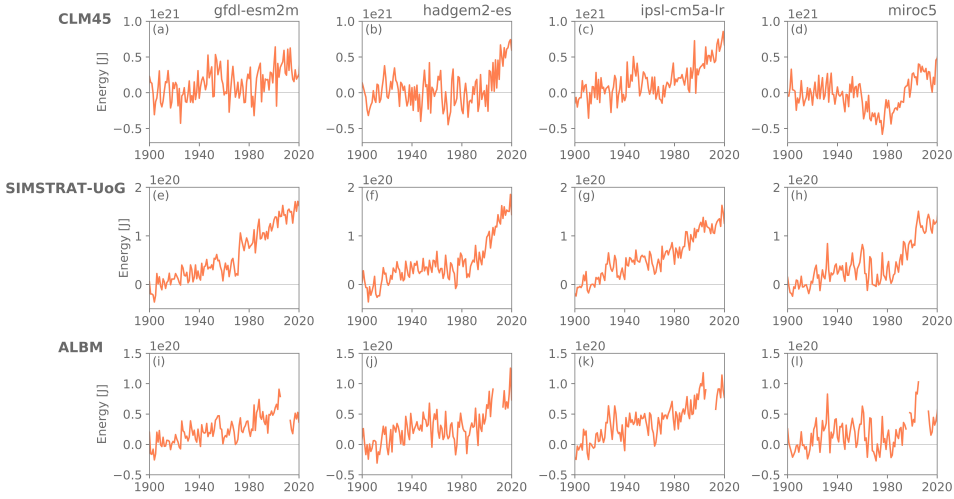

Figure 3.5: Annual heat uptake by natural lakes for the three different lake models (CLM45; a-d, SIMSTRAT-UoG; e-h, ALBM; i-l) and ESM forcings (GFDL-ESM2M, HadGEM2-ES, IPSL-CM5A-LR, MIROC5; columns). For all forcings, the years 2006-2012 of ALBM are excluded due to model spin up. For ALBM MIROC-5 the years 1996-1997 are additional exlcuded. Note the different y-axis scales.

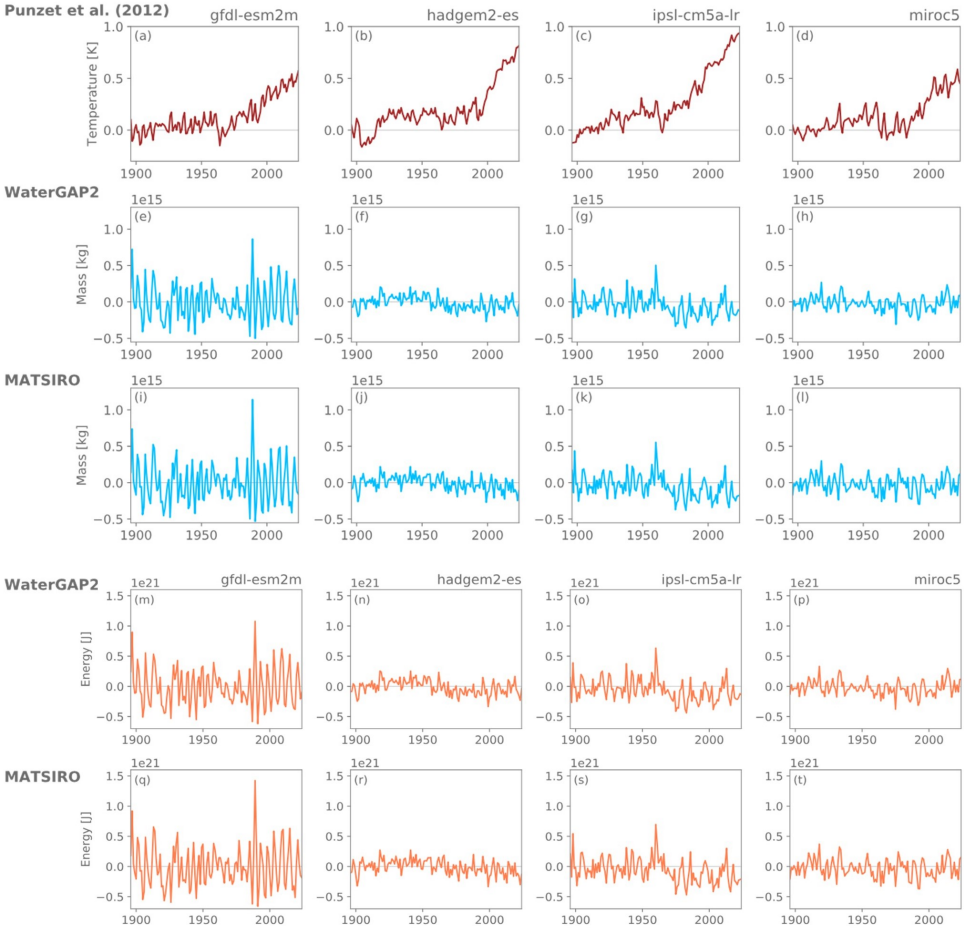

Figure 3.6: Global average river temperatures calculated with the parametrisation of (Punzet et al., 2012, ;a-d), global total river mass from WaterGAP2 (e-h) from MATSIRO (i-l) and resulting global river heat for WaterGAP2 (m-p) and MATSIRO (q-t), all per ESM forcing.

Chapter 4

Simulating the impact of global reservoir expansion on the present-day climate

Reservoir expansion over the last century has largely affected downstream flow characteristics. Yet very little is known about the impacts of reservoir expansion on the climate. Here we implement reservoir construction in the Community Land Model by enabling dynamical lake area changes, while conserving mass and energy. Transient global lake and reservoir extent are prescribed from the HydroLAKES and Global Reservoir and Dam databases. Land-only simulations covering the 20^{th} century with reservoir expansion enabled, highlight increases in terrestrial water storage and decreases in albedo matching the increase in open water area. Comparison of coupled simulations including and excluding reservoirs shows only limited influence of reservoirs on global temperatures and the surface energy balance, but demonstrates substantial responses locally, in particular where reservoirs make up a large fraction of the grid cell. In those locations, reservoirs dampen the diurnal temperature range by up to -1.5 K (for reservoirs covering $>$ 15 % of the grid cell), reduce temperature extremes and moderate the seasonal temperature cycle. This chapter provides a first step towards a coupled representation of reservoirs in Earth System Models.

This chapter is published as: Vanderkelen, I., Lipzig, N. P. M., Sacks, W. J., Lawrence, D. M., Clark, M. P., Mizukami, N., Pokhrel, Y., and Thiery, W. (2021). Simulating the Impact of Global Reservoir Expansion on the Present-Day Climate. Journal of Geophysical Research: Atmospheres, 126(16), e2020JD034485.

4.1 Introduction

Humans are fundamentally altering the terrestrial water cycle by changing freshwater storage and flows (Abbott et al., 2019; Rockström et al., 2009; Oki and Kanae, 2006). The most important human interventions in the natural hydrological cycle include the construction of large dams and the artificial reservoirs thereby created, groundwater pumping leading to aquifer depletion, diverging streamflow for irrigating crops and inter-basin water transfers (Pokhrel et al., 2016; Wada et al., 2017; Vörösmarty and Sahagian, 2000; Gleeson et al., 2020). Since the start of the 20th century, more than 50 000 large dams have been built (heights $>$ 15 m) with a remarkable acceleration in dam construction in the years 1950 to 1990 (Lehner et al., 2011; Mulligan et al., 2020). Altogether, these reservoirs impound at least 8300 km^3 of water (Chao et al., 2008), which is about one-sixth of the annual continental discharge (Oki and Kanae, 2006). Filling the reservoirs slowed down the sea level rise during the 1970s and overall reduced the global mean sea level by 30 mm (Frederikse et al., 2020; Chao et al., 2008). Reservoir operations alter downstream flow characteristics, like the timing and amount of streamflow (Döll et al., 2009; Vörösmarty and Sahagian, 2000; Wisser et al., 2010; Biemans et al., 2011; Shin et al., 2019), and lead to regulation and fragmentation of most large river systems (Grill et al., 2019; Nilsson et al., 2005). In addition, dam construction and resulting reservoir creation changes effectively converts land to open water, thereby affecting surface properties and evaporation rates (Grubert, 2016; Sterling et al., 2013). Moreover, with more than hundreds of reservoirs under construction or planned around the world, the impacts of reservoirs will likely increase in the future (Sterl et al., 2020; Zarfl et al., 2014; Winemiller et al., 2016; Pokhrel et al., 2018).

Despite these large influences in the terrestrial water balance, the impacts of reservoirs on the climate remain largely unknown (Pokhrel et al., 2016; Nazemi and Wheater, 2015b; Hossain et al., 2012). Some studies suggest that reservoirs can impact the local energy balance and influence extreme precipitation in the vicinity of the reservoir (Degu et al., 2011; Hossain et al., 2010, 2012). Investigating these reservoir-atmosphere interactions and feedbacks at the global scale requires an integrated framework, like Earth System Models (ESMs), in which land surface models (LSMs) are coupled to other Earth system component models (Pokhrel et al., 2016; Nazemi and Wheater, 2015b).

The current generation of ESMs mostly consider a natural water cycle, without, or only partly accounting for human water management like reservoirs, irrigation, industrial and domestic water use and groundwater extractions. Within ESMs, terrestrial systems are represented by land surface models (LSMs), which include process-based representations of the energy, water, and biogeochemical cycles and which require strict conservation of these properties to avoid unphysical climate drift. Recently, advances in incorporating human water management like irrigation and groundwater abstraction in LSMs have been made (Sacks et al., 2008; Thiery et al., 2017; Pokhrel et al.; Leng et al., 2015; Zhou et al., 2020; de Vrese et al., 2018; Felfelani et al., 2020). However, to our knowledge, currently none of the LSMs embedded in state-of-the-art ESMs represent the temporal dynamics of reservoir expansion in their water and energy cycles of their land component.

In contrast, global hydrological models and water management models include relatively advanced representation of human water management including reservoir operation (Van Beek et al., 2011; Hanasaki et al., 2008; Döll et al., 2009; Wisser et al., 2010) and are mainly focused on water resource assessments (Bierkens, 2015; Sood and Smakhtin, 2015; Wada et al., 2017). In these models, reservoirs are commonly integrated in the river network and their operation is simulated through schemes in which release is determined by operation rules based on the reservoir purpose (Hanasaki et al., 2006; Haddeland et al., 2006). The use of these outflow schemes in global hydrological models allows for estimation of large-scale impacts of reservoirs on the hydrological cycle, under prescribed meteorological forcing (Biemans et al., 2011; Voisin et al., 2013b; Döll et al., 2009; Wisser et al., 2010; Van Beek et al., 2011; Hanasaki et al., 2008; Droppers et al., 2020; Masaki et al., 2017; Shin et al., 2020). Recent efforts have adapted and/or coupled these schemes to simulate the effects of reservoir operation on river discharge in LSMs (Nazemi and Wheater, 2015b; Pokhrel et al., 2016). For example, Zhou et al. (2020) coupled a water management model, a river routing model and a LSM within the Energy Exascale Earth System model (E3SM). Furthermore, Yokohata et al. (2020) recently incorporated water regulation modules (Pokhrel et al.; Hanasaki et al., 2008), together with land use modules, into the integrated land surface model MIROC-INTEG-LAND. While both reservoir-accounting LSMs can be coupled with their respective ESMs, their frameworks do not allow to assess the climate impact of reservoirs in terms of land use change, as reservoirs are only represented within the river components and not in the land components.

The goal of this chapter is to incorporate reservoirs into ESMs by accounting for the land cover change induced by reservoir expansion and to examine the impact of reservoirs on the climate system. Since 1900, reservoir area has increased by about 272,000 km^2, which is about 10% of the global lake area (Lehner et al., 2011; Messager et al., 2016). The impounded water also increased the capacity of land to take up heat from the atmosphere by warming the reservoir waters (Vanderkelen et al., 2020a). Moreover, the largest human-induced increases in evaporation are attributed to reservoir construction (Sterling et al., 2013). The associated formation of open water bodies alter surface properties like albedo, surface roughness and impact fluxes of energy, moisture and momentum to the atmosphere (Strachan et al., 2016; Hossain et al., 2012). Hence, capturing these reservoir-atmosphere interactions is important to realistically represent the reservoir water and energy balance and related processes like evaporation, ice formation and water mixing (Friedrich et al., 2018; Thiery et al., 2014c).

Here, we implement reservoir construction in the Community Land Model as lake area expansion prescribed by the HydroLAKES and Global Reservoir and Dam databases. To this end, we developed an approach using correction fluxes and baselines to account for energy and mass conservation. We conduct land-only experiments for the period 1900-2014 with transient reservoir expansion enabled as well as coupled land-atmosphere simulations with the Community Earth System Model (CESM) with snapshots of the preindustrial and present-day reservoir extent. Using the latter ensembles, we investigate the effects of reser-

voirs on average and extreme temperatures and the energy balance. Finally, we investigate the influence of changes in individual energy flux terms on the surface temperature by applying a surface energy balance decomposition technique.

4.2 Data and methods

In this section, we first describe the release version of the model and data sets used. Next, we outline the data preparation and model developments conducted for this chapter. Finally, we describe the experimental set-up and the methodologies used in analyzing the results.

4.2.1 Model description

To investigate the impact of reservoir expansion on the global climate, we use the Community Earth System Model (CESM) version 2.1.3 (Danabasoglu et al., 2020), a state-of-the-art ESM. Within CESM, atmospheric processes are solved with the Community Atmosphere Model (CAM6) and land processes are represented by the Community Land Model version 5 (CLM5; Lawrence et al., 2019a), with advanced biogeophysical and biogeochemical parametrisations. CLM5 accounts for surface heterogeneity by using a nested subgrid hierarchy. Individual land grid cells are subdivided in different land units representing the vegetated, lake, urban, glacier and crop fraction of the grid cell.

In CLM5, lakes are simulated using the Lake, Ice, Snow and Sediment Simulator (LISSS), described more in detail by (Subin et al., 2012c). The lake model resolves the whole lake column, consisting of the lake water body, the soil and bedrock below, and potential ice and snow on top of the lake. In the lake body, water temperature and ice fractions are modeled in 10 layers. Except for overlying snow and underlying soil, the lake column has a constant water mass, which is determined by the lake depth and density. The water budget is balanced with a runoff term, which can be negative when evaporation exceeds precipitation. Consequently, lake water does not participate in the grid cell water balance, but its state and temperature are modeled. The soil layers below the lake are always saturated. For every grid cell containing lakes, one representative lake is modeled, with prescribed lake area and mean lake depth, which are constant in time.

The release version of CLM5 allows for land use and land cover change, by including changes in weights of vegetated, crop and glacier land units within a grid cell (Lawrence et al., 2019a). Glacier areas can change in a prognostic way when coupled to an evolving ice sheet model, while vegetated and crop land units are adjusted dynamically during the simulation, dictated by the Land Use Harmonization data set (LUH2, Hurtt et al., 2020). The transition between crop and vegetated units for a certain year are applied on the first day of that model year. To conserve mass and energy when transitioning, the model accounts for changes in water and heat by applying small correction fluxes to the river and atmosphere. The difference in the total water and heat content of the grid cell, before and after the transition, is calculated on the first day of the year. In the rest of the year, the amount of

imbalance is dribbled out in small correction fluxes - for water as liquid or ice runoff to the river and for heat as a sensible heat flux to the atmosphere. These correction fluxes can be either positive or negative. In this way, the total mass and energy content of the grid cell is conserved for all land unit transitions during the simulation.

4.2.2 Lake and reservoir data

Global lake distribution is given by the HydroLAKES dataset, providing individual polygons of 1.4 million natural lakes with a surface area of at least 0.1 km^2 (Messager et al., 2016). The Global Reservoir and Dam Database v.1.3 (GRanD) provides the global geographical distribution and characteristics of 7320 reservoirs, larger than 0.1 km^2 (Lehner et al., 2011). The reservoir polygons from GRanD are directly linked to the lake polygons in the HydroLAKES data set. According to these data sets, natural lakes make up a surface area of 2.67×10^6 km^2, (1.8% of global land area), while reservoirs cover 0.26×10^6 km^2 (0.2% of global land area).

4.2.3 Implementation of reservoirs as dynamical lakes

We represent global reservoir expansion in CLM5 by allowing the grid cell lake area to change dynamically (Fig. 4.1). First, we replace the static lake cover by annual maps including reservoir expansion (section 4.2.3). Second, we modify the CLM5 source code to perform the necessary mass and energy balance accounting, while minimizing the artificial mass and energy fluxes (section 4.2.3).

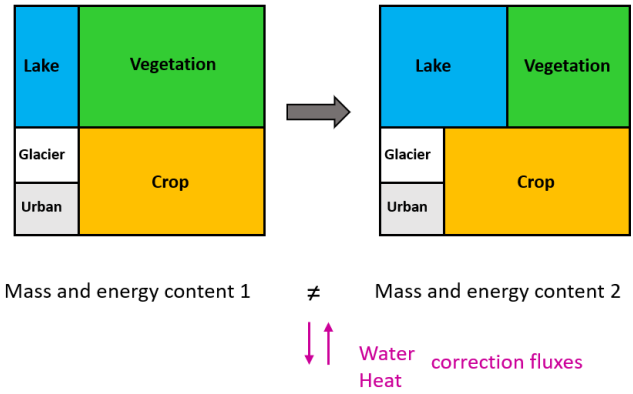

Figure 4.1: Reservoir expansion is represented by increasing the lake area fraction in the grid cell. Due to increase in lake fraction, the grid cell total water and energy content is altered, which is accounted for using correction fluxes for water (liquid and ice runoff to/from river) and heat (sensible heat flux to/from atmosphere).

Input data preparation

The HydroLAKES and GRanD polygons are rasterized to a 0.05° by 0.05° grid, where each grid cell represents the lake and reservoir area fraction. First, the natural lake area map is created based on HydroLAKES, and includes all natural lakes controlled by a dam (a GRanD attribute) and reservoirs with a construction year before 1900 (81 and 124 polygons, respectively). Then, we generate annual maps for the period 1900-2015, where the reservoir area fraction is added to the natural lake fraction in the construction year of the reservoirs (as given in GRanD). We assume that reservoirs are filled on the first day of the year they come into existence. The static lake depth map is created by calculating the area-weighted average lake depth per grid cell based on the lake depth attribute from the HydroLAKES and GRanD polygons. The lake cover and depth maps replace the original CLM5 lake cover and depth from the Global Lake Depth Database (GLDB, Kourzeneva, 2010; Subin et al., 2012c). To serve as input data for CLM5, the raw input maps are subsequently regridded to 0.9° by 1.25°, our simulation resolution. This is done consistently with the other land units to ensure that for each grid cell, the weights add up to 100%, whereby natural vegetation is used to fill up the grid cell.

Correction fluxes and baseline approach

Similar to the approach for other dynamical land units, the increased lake area fraction is applied on the first day of the model year. The added lake fraction adopts the state variables of the lake column already present in the grid cell. When a lake newly appears in a grid cell that previously had no lake area, it receives the state variables of a virtually spun up lake in that grid cell.

In CLM5, lake water is excluded in the grid-scale total water and heat content, as the amount of lake water is held constant and is considered effectively as 'virtual' water (section 4.2.1). Therefore, to apply the methodology used for transitioning between crop and natural vegetation for expanding lakes, the mass and energy of the lake body first needs to be included in the grid cell total water and heat content. Otherwise, the correction fluxes would only account for the difference in water and heat between the vegetated land unit on the one hand, and the saturated soil beneath the lake and potential snow cover on the other hand. By including the water and heat content of the lake water itself, mass and energy are conserved after applying the correction fluxes, as the heat content of lake water can be very different from a vegetated land unit (see supplementary material). For lake water mass, there is no difference, because the lake water content is tracked on a per-area basis and does not participate in the water balance, i.e. remains constant throughout a simulation. By incorporating lake water in the total grid cell water content, it is now also included in the terrestrial water storage (TWS) output variable.

Locally, the correction fluxes can become large compared to the physical fluxes (supplementary material table S1). To minimise these artificial fluxes, we implement a baseline approach, where at the start of the simulation, the reference states ('baselines') are saved.

These are spun up states of the heat and water content of the lake unit for every grid cell. During the simulation, the baseline states are subtracted from the heat and water content of the lake unit. In this way, only deviations from these baseline states are considered, when calculating the difference in total grid cell heat and water content. This minimizes the magnitude of the required correction fluxes (see supplementary material for a conceptual and simulation example demonstrating this). CLM5 uses a similar approach implemented for area changes of glaciated land units (Leguy et al., 2018). The developments presented in this chapter are incorporated in the CLM5 source code.

Including reservoirs and transient reservoir construction did not improve nor deteriorated the model skill, when tested within the International Land Model Benchmarking (ILAMB) software (Collier et al., 2018) for a range of variables related to the hydrology, radiation and energy cycle (see supplementary material). A possible reason for this is that the observational data sets used in the evaluation do not include the effects of expanding reservoir surfaces, as they do not cover these areas or they only exist for the satellite era, during which the increase in reservoir area is relatively limited.

4.2.4 Experimental design

Land-only simulations

We first conduct transient land-only simulations, using CLM5 (release-clm5.0.34 tag) with a prescribed atmosphere and vegetation phenology from MODIS (using the IHistClm50Sp component set). Meteorological forcing is prescribed from the Global Soil Wetness Project (GSWP3; `http://hydro.iis.u-tokyo.ac.jp/GSWP3/`; see also (Lawrence et al., 2019a), a global 0.5°, 3-hourly bias-adjusted reanalysis product, based on the dynamically downscaled 20th century reanalysis (version 2) of the NCEP model (Compo et al., 2011). Vegetation phenology is prescribed from satellite observations. Simulations are performed at a 0.9° by 1.25° grid spanning the period 1890-2015, using the first 10 years as spin up. Two simulations are performed: in the control simulation (hereafter referred to as CTL), transient land use is enabled, but lake area is kept constant at the 1900 level, i.e. no reservoirs are constructed. In the second simulation (hereafter referred to as transRES), lake area is allowed to change alongside the other land use categories, i.e. reservoirs are constructed throughout the simulation. Investigating the differences between transRES and CTL simulations allows us to quantify the transient land surface response on reservoir construction.

AMIP-style simulations

In addition to the land-only simulations with transient reservoir expansion, two climate ensembles are generated using CESM, one with present-day lake extent including reservoirs and the second with pre-industrial lake extent, without reservoirs. We prescribe sea surface temperatures and sea ice fraction from observations (FHISTclimo compset, Hurrell et al., 2008) to concentrate on land-atmosphere interactions, thereby omitting the potential role of atmosphere-ocean interactions in modulating the climate response to reservoirs. Likewise, transient greenhouse gas concentrations are prescribed from measurements. The simulation setup closely follows the framework of the Atmospheric Model Intercomparison Project (AMIP), except for the use of static land cover which represents the year 2000. The first 5-member ensemble (denoted RES) is conducted including reservoirs and uses the present-day open water cover. The second 5-member ensemble (denoted NORES) only contains natural lakes and employs the year-1900 lake cover map. In both RES and NORES ensembles the no-lake land cover fractions are given by the constant land cover map of the year 2000. The simulations span the period 1979-2014 (35 years, including 6 years of spin up) and have a horizontal resolution of 0.9° by 1.25°. Within each ensemble, five members are generated by randomly perturbing the atmospheric initial conditions by 10^{-14} K. In this way, each simulation is a unique realisation in terms of natural variability (Perkins and Fischer, 2013) while adhering to the same model physics and parameter values. Comparing the two ensembles allows to investigate the maximum signal of reservoir construction in the present-day climate.

4.2.5 Analysis

We use monthly and daily output from CESM, averaged over the ensemble members, to analyse the effect of reservoirs on global temperature, diurnal temperature range (DTR; the difference between daily maximum and minimum temperature), and the surface energy balance. For the temperature extremes, we use the definitions from the Expert Team of Climate Change Detection and Indices (ETCCDI; Zhang et al., 2011) with TXx, the monthly maximum value of daily maximum temperature and TNn, the monthly minimum value of daily minimum temperature. In the maps, we only show statistically significant responses by performing a two-sided Wilcoxon signed rank test of the lumped ensemble members on a 0.05 significance level. In addition, the shown responses are also tested for field significance using the false discovery rate to account for correlation in space (Lorenz et al., 2016; Wilks, 2006). For the seasonal cycles, we only look at the grid cells with reservoirs. Here we distinguish between reservoir sizes, ranging from more than 0% to 15% coverage of the total grid cell (table 4.1). The number of grid cells decreases with increasing reservoir area. As the water volume of reservoirs is constant by design, seasonal variations in reservoir area, storage and depth are not included in the seasonal cycles.

The impact on precipitation and precipitation extremes is not included in the analysis, as the uncertainty related to natural variability exceeds the forced signal for these variables (section 4.4.1; Fischer et al., 2014).

To investigate the changes in surface temperature T_s (K) induced by reservoirs, we apply the surface energy balance decomposition technique. Many previous studies have applied this method on simulations with CLM (Akkermans et al., 2014; Luyssaert et al., 2014; Thiery et al., 2015, 2017; Hirsch et al., 2017, 2018; Hauser et al., 2019). Here, the energy balance at the land-atmosphere interface is given by:

$$\varepsilon\sigma T_s^4 = (1-\alpha)\Delta SW_{in} + LW_{in} - LHF - SHF - R \tag{4.1}$$

with ε, the surface emissivity, σ the Stefan-Boltzmann constant ($5.67 \times 10^{-8}\ Wm^{-2}K^{-4}$), α the surface albedo, SW_{in} the incoming shortwave radiation LW_{in} the incoming longwave radiation, LHF the latent heat flux, SHF the sensible heat flux and R, a residual term including subsurface heat flux and storage.

When applying this energy balance reconstruction during the postprocessing, there is only a small imbalance of on average 0.05 W m^{-2} for reservoir grid cells. This highlights that the energy balance, which is closed per definition at the model time step level, can be reconstructed using the model output fields.

The change in surface temperature (ΔT_s) is subsequently obtained by taking the total derivative of Eq. 4.1 regarding to T_s and solving for ΔT_s:

$$\Delta T_s = \frac{1}{4\sigma T_s^3}(-SWin\Delta\alpha + (1-\alpha)\Delta SW_{in} + \Delta LW_{in} - \Delta LHF - \Delta SHF - \Delta R) \tag{4.2}$$

Here, ε is assumed to be constant at 1 and T_s is taken as the radiative surface temperature based on the outgoing longwave radiation (emitting radiation to the atmosphere) of the reference simulation (RES). All terms are calculated based on the difference of the RES and NORES ensembles.

Table 4.1: Number of reservoir grid cells with increasing reservoir area fraction

Reservoir threshold	**Number of grid cells**	**% of land grid cells**
>0%	1175	6.10%
>1%	450	2.34%
>2%	249	1.29%
>5%	91	0.47%
>10%	42	0.22%
>15%	15	0.08%

4.3 Results

4.3.1 Transient land impacts of reservoir expansion

The global reservoir distribution reveals certain areas with large reservoir area fractions, indicating the presence of large reservoirs, especially in northeastern Canada, western Russia and Siberia (Fig. 4.2a). Other regions, like India and China, have many grid cells with smaller reservoir area fractions per grid cell. In Africa, most grid cells with high reservoir fraction correspond to individual reservoirs: in the northeast, Lake Nasser controlled by the Aswan dam, in the west, Lake Volta controlled by the Akosombo dam and Lake Kariba in the south, on the border of Zambia and Zimbabwe. Globally, the total reservoir area sharply increases from the 1950s onwards, reflecting the reported increase in reservoir capacity (Fig. 4.2b; Lehner et al., 2011; Chao et al., 2008).

Using our land-only simulations, we can quantify the time-evolving impact of reservoir expansion on albedo, TWS and the turbulent surface fluxes, i.e. the latent and sensible heat flux (LHF and SHF; Fig. 4.3). In land-only simulations, the effects of reservoirs are by definition limited to reservoir grid cells. For all variables, the magnitude of the response increases consistently with increasing reservoir area fraction. The trajectory of the reservoir grid cell responses is similar to the reservoir area expansion (Fig. 4.2b), with a steep increase from the 1950s to the 1980s followed by a more modest increase from 1980s on wards.

The water retained trough reservoir construction is directly modeled through the increase in grid cell TWS (Fig. 4.3a). The ΔTWS encompasses the differences in water content between the original vegetated land fraction and the new lake fraction, which not only includes the lake water itself, but also the water content of the saturated soil below the lake and of the potential snow on top. In the largest reservoir grid cells ($>$ 15% becomes covered by reservoirs), the construction of reservoirs adds up to 2.5 m of water to the entire grid cell. According to our simulations, a total of 30 013 km^3 water is added through artificial reservoir construction, of which 26 148 km^3 is reservoir water. This part, the water added to the lake itself, is virtually added to the model and does not participate in the water cycle. The remaining part, coming from the soil in the lake unit, is taken from the grid cell runoff through the correction fluxes (section 4.2.3 and supplementary material). Reservoir expansion has only a small effect on snow depth (-3.4% averaged for grid cells with $>$15% reservoir area fraction). This decrease in snow has a very small (-4 km^3) contribution to ΔTWS. Our simulated total reservoir volume is largely overestimated compared to the reported volume estimates (7000-8300 km^3; Lehner et al., 2011; Chao et al., 2008). This difference can likely be attributed to differences between reservoir and lake bathymetry, and the fact that both lake and reservoir volumes are calculated using the grid cell average lake and reservoir depth, thereby most likely overestimating the average depth of the reservoir portion. As this water contained in the reservoir is static, this overestimation does not influence the other variables modeled.

This will however become important as the model is developed further to more directly couple the water balance of the lakes and reservoirs to the river network (section 4.4.2) and eventually coupling to the ocean with impacts on sea level rise and ocean salinity trends.

In addition to changes in TWS, reservoirs locally decrease grid cell albedo by expanding the darker lake area surface while submerging land with brighter vegetation. The sudden decrease in 1970-1971 is caused by the emergence of large individual reservoirs (changes in grid cell average albedo go up to -0.015). Reservoir expansion gradually increases LHF in reservoir grid cells, up to 0.6 W m^{-2} for all reservoir cells (5.2 W m^{-2} for cells with $>$ 15% reservoirs). The decrease in SHF follows a similar pattern, but does not fully compensate the increase in LHF (-0.4 W m^{-2} for reservoir grid cells and -2.7 for $>$ 15% cells). An in-depth analysis of the surface energy balance is provided in section 4.3.3.

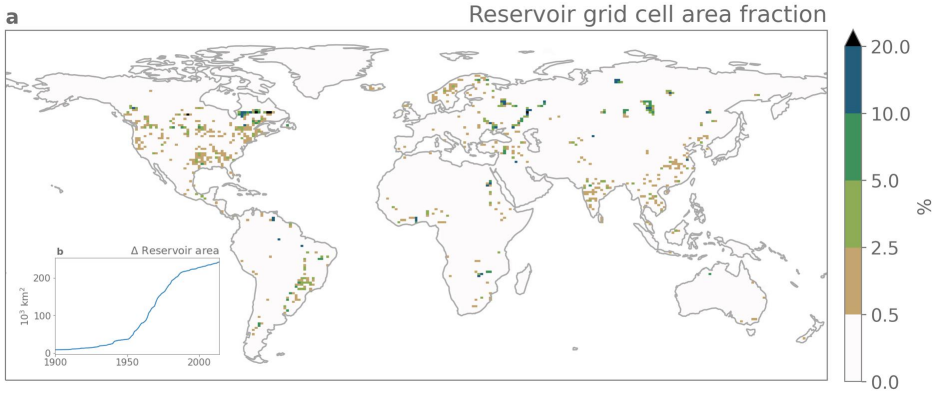

Figure 4.2: (a) Reservoir area fraction per grid cell (%, note the non-linear scale), (b) Global evolution of total reservoir area. The original data from GRanD is shown here after being implemented in CLM5.

4.3.2 Climate impacts of reservoirs

Impact of reservoirs on the mean climate

Our coupled simulations show a limited impact of reservoirs on 2 m air temperature (globally average of +0.1 K; Fig. 4.4a). Most responses can be directly related to the locations of individual reservoirs, except for the positive anomaly in the Gran Chaco plains in South America. The statistically significant response of turbulent surface fluxes are localised to and particularly pronounced in the grid cells with large reservoirs (Fig. 4.4b and c). In reservoir grid cells, the mean increase in LHF (1.7 W m^{-2}) is compensated by the mean decrease in SHF (-1.7 W m^{-2}). The influence of the turbulent fluxes on surface temperature

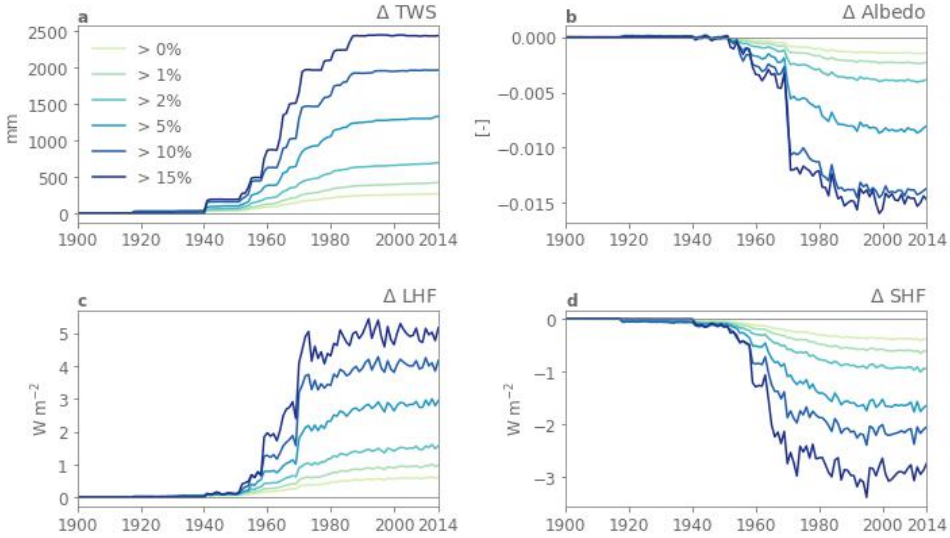

Figure 4.3: Impact of transient reservoir construction (transRES-CTL) during the period 1900-2014 on global mean (a) land surface albedo, (b) terrestrial water storage, TWS (c) latent heat flux, LHF and (d) sensible heat flux, all calculated over reservoir grid cells ($>$ 0% reservoir area fraction) and grid cells with increasing reservoir area fraction ($>$ 1%, $>$ 2%, $>$ 5%, $>$ 10%, and $>$ 15%, respectively).

is investigated in more detail in section 4.3.3. Overall, reservoir effects on mean climate are small compared to other water management activities like irrigation (Thiery et al., 2017, 2020; Pokhrel et al., 2017; Mishra et al., 2020)

Other than 2 m air temperature, reservoirs have a observable negative effect on DTR. The presence of reservoirs decreases the DTR with -0.3 K averaged over reservoir grid cells (Fig. 4.5a). This signal is more pronounced with higher reservoir area fractions, and is highest in July, August and September, up to -1.5 K for grid cells with a reservoir coverage of more than 15% (Fig. 4.5b). This could be explained by the increased daytime cooling from July to September, while nighttime warming extends until the end of the year. The effect on the seasonal cycle of DTR itself is very small.

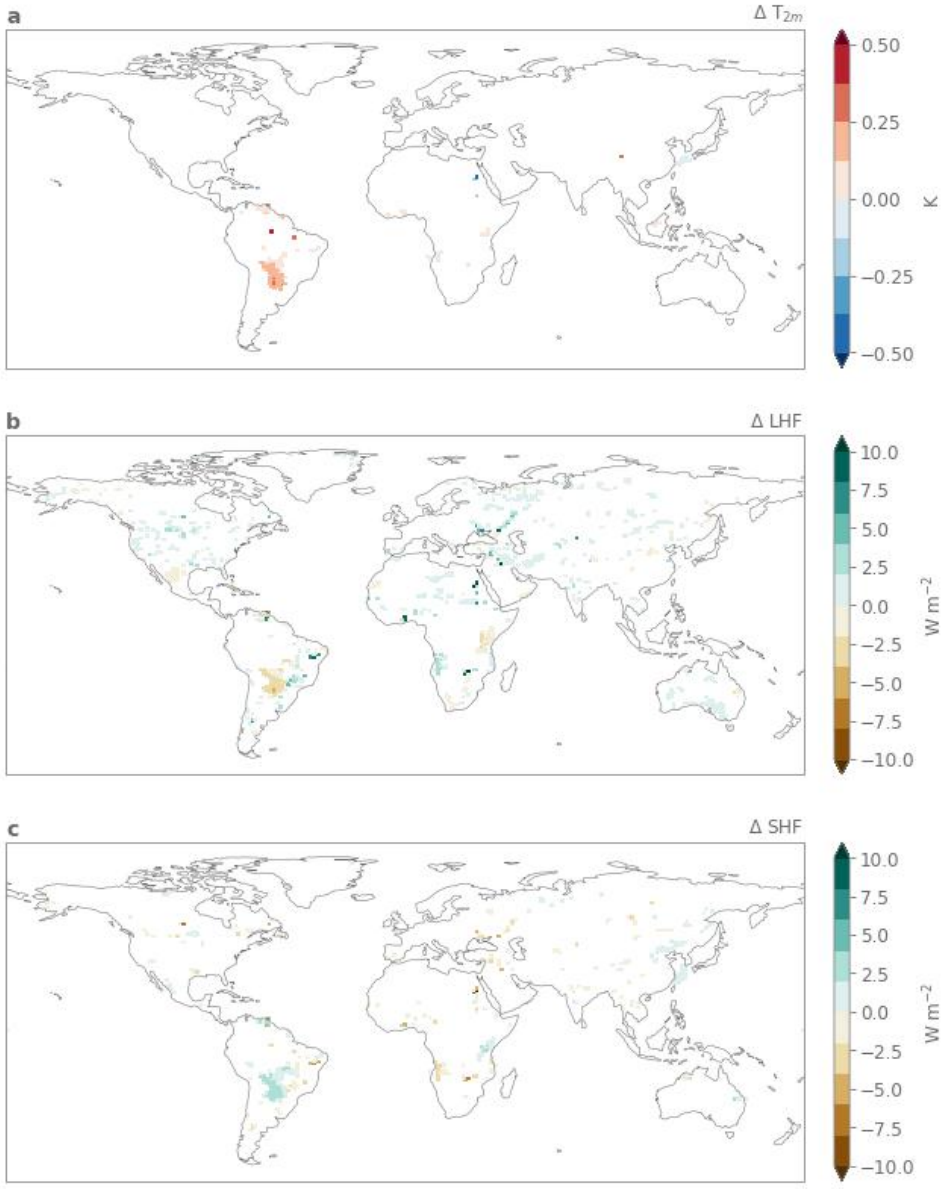

Figure 4.4: Impact of reservoirs (RES-NORES) on ensemble mean (a) 2 m air temperature, T_{2m} (b) Latent Heat Flux (LHF) and (c) Sensible Heat Flux (SHF). Only statistically significant changes are shown (0.05 significance level, two-sided Wilcoxon signed rank test of lumped ensemble members and field significance using the false discovery rate test).

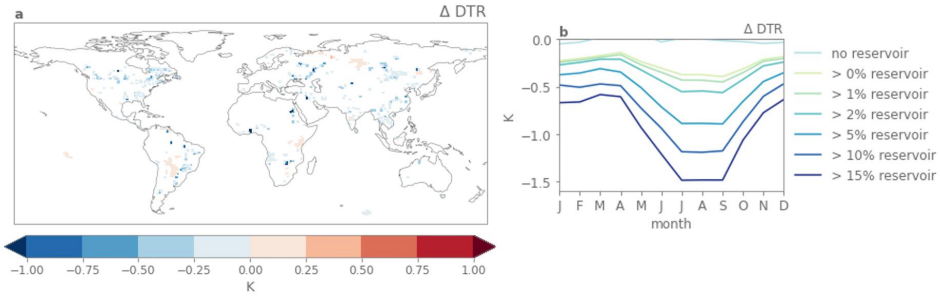

Figure 4.5: Impact of reservoirs (RES-NORES) on (a) mean Diurnal Temperature Range (DTR) and (b) the seasonal cycle of DTR for grid cells with increasing reservoir area fractions ('no reservoir' includes all grid cells with <1% reservoir coverage). Only statistically significant changes are shown (0.05 significance level, two-sided Wilcoxon signed rank test of lumped ensemble members and field significance using the false discovery rate test).

Impacts of reservoirs on extremes

Our results show that reservoirs dampen temperature extremes by decreasing TXx and increasing TNn. The spatial patterns in the TXx and TNn responses correspond to the reservoir distribution (Fig. 4.6a and c), with the largest responses in grid cells with the largest reservoir area coverage. The widespread increase in TNn north of the Caspian Sea could be related to the chain of reservoir grid cells impacting the surrounding region, but to robustly establish this signal, likely more ensemble members are needed (see section 4.4.1). Averaged over reservoir grid cells, reservoirs cool the hot extremes by -0.2 K and warm the cold extremes by +0.3 K, but locally, these values reach up to -1.6 K cooling of hot extremes and +1.3 K warming of cold extremes. Compared to other forms of land management, like conservation agriculture and irrigation, the impact of reservoirs on temperature extremes is smaller and highly localised (Thiery et al., 2017, 2020; Hirsch et al., 2018). On seasonal time scales, the response magnitude of both extremes increases with growing reservoir size (Fig. 4.6b and d). While the response of TXx is lowest from November to January, the response of TNn is lowest during the spring months March and April. These seasonal cycles could be related to the formation and melting of ice in the reservoirs located in the northern hemisphere, which prevent the dampening effect of open water in DJF. The shift in the TXx and TNn cycles could be due to the seasonality of heat uptake by the lake water (Fig. 4.7c), where the release of heat from September until December has most effect on the minimum nighttime temperatures.

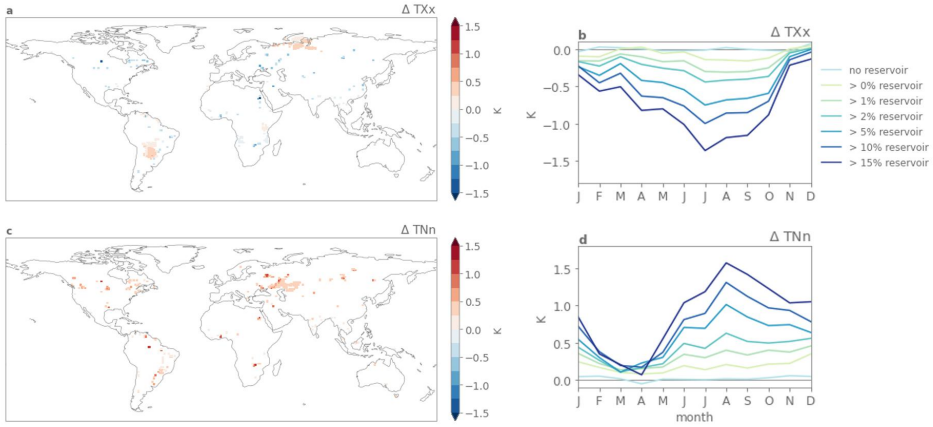

Figure 4.6: Impact of reservoirs (RES-NORES) on monthly temperature extremes: (a) monthly maximum of daily maximum temperature, TXx (b) seasonal cycle for different reservoir area fractions, (c) monthly minimum of daily minimum temperature, TNn (c) seasonal cycle for different reservoir area fractions ('no reservoir' includes all grid cells with <1% reservoir area fraction). The maps show values at 0.05 significance level using a two-sided Wilcoxon signed rank test of lumped ensemble members and the false discovery rate test for field significance.

4.3.3 Effect of reservoirs on the surface energy balance

To disentangle the global effects of reservoirs on surface temperature changes in detail, we first examine the seasonal cycles of the surface energy balance components and thereafter the response of surface temperature to changes in these terms. It is important to note that in the simulations reservoir area is constant throughout the year, as CLM5 does not account for seasonal changes in reservoir area, storage or depth. Reservoirs have a clear altering effect on the seasonal cycle, of which the magnitude increases with reservoir area fraction (Fig. 4.7).

Subsurface heat absorption, including light transmission in the lake water, increases from December to July, resulting in a maximum heat uptake of 10.4 W m^{-2} for the largest reservoirs (Fig. 4.7c). From July to November, heat is released to the atmosphere (up to +12.5 W m^{-2}). Annually averaged, the change in subsurface heat flux is only -0.02 W m^{-2}. The thermal inertia from large intra-annual differences in subsurface heat flux is compensated by the alteration of the LHF and SHF seasonal cycles. LHF, and likewise evaporation, is enhanced due to the presence of a larger open-water surface, which makes water permanently available to evaporate. The increase in LHF from September to December (up to +12.1 W m^{-2}) corresponds to the period of heat release by the lake water (Fig. 4.7a and c). The energy released by the lake is used to evaporate water from the reservoir surface. The period with lowest LHF change, March to July, corresponds to the period in which the reservoir

water takes up the most heat. The decrease in SHF is manifested throughout the year, except for November and December, with the largest decrease arising from June to August (up to -7.9 W m^{-2}; Fig. 4.7b). Next to the decrease in energy availability due to water heat uptake, this SHF decrease could be explained by the lower roughness length of water surfaces compared to vegetated land, which increases the aerodynamic resistance and therefore suppresses the heat transfer to the atmosphere due to reduced turbulence (Subin et al., 2012c; Thiery et al., 2015). These results are consistent with the climatic effects of natural lakes at mid and high latitudes (Subin et al., 2012a; Samuelsson et al., 2010; Dutra et al., 2010).

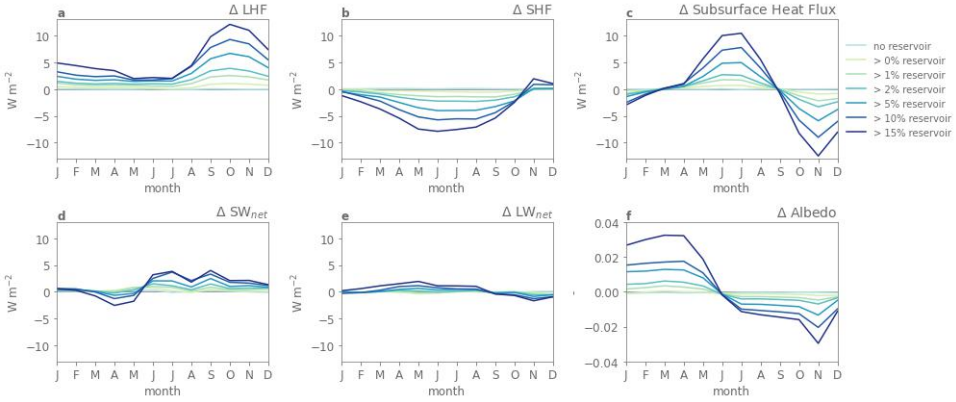

Figure 4.7: Impact of reservoirs (RES-NORES) on mean seasonal cycles of (a) latent heat flux, LHF, (b) sensible heat flux, SHF, (c) Subsurface heat flux (including light transmission through lake surface), (d) net shortwave radiation at the surface SW_{net}, (e) net long wave radiation at the surface, LW_{net}, (f) surface albedo, for all of grid cells with reservoir area fractions above a given threshold ('no reservoir' includes all grid cells with <1% reservoir area fraction). Note the different y-axis scale for panel f.

Compared to the surface fluxes, radiative fluxes experience smaller responses (Fig. 4.7d and e). Overall, reservoirs decrease global albedo by the creation of darker surfaces (-0.001 over reservoir grid cells). On a seasonal scale, this effect is dominant from June until December (Fig. 4.7f). In the first months of the year, however, reservoirs increase the albedo due to ice formation, which is brighter compared to the grid cell vegetation. This emerges in the course of the absorbed shortwave radiation (SW_{net}) together with cloud feedbacks, resulting in a net annual effect of +1.0 W m^{-2} in reservoir grid cells.

Overall, the seasonal patterns follow the seasonality of the northern hemisphere. This can be attributed to the reservoir distribution, with only few reservoir grid cells in the southern hemisphere (Fig. 4.2). In addition, our results do not show a substantial difference when rendered only for a mid-latitude band (30° to 60°) compared to the global domain, due to the limited number of reservoirs outside this region (Lehner et al., 2011).

The individual contributions of the surface energy balance terms to the change in net surface temperature (ΔT_s, eq. 4.2) are shown in figure 4.8. For reservoir grid cells, the annual net change in T_s (+0.05 K) is the result of a cooling (-0.09 K) owing to an increased LHF, which is partly balanced out by a warming from a decreased SHF (+0.05 K, whereby a decrease in SHF away from the surface leads to more heat available at the surface). Additional warming contributions come from a reduced albedo (+0.04 K), as well as enhanced incoming short- and longwave radiation (+0.017 K and +0.022 K, respectively), associated with atmospheric temperature and cloud feedbacks (Fig. 4.8a). The subsurface heat flux has a very small positive contribution (+0.004 K). For reservoir grid cells with $> 15\%$ reservoir fraction, the contribution to ΔTs of the turbulent fluxes are an order of magnitude larger (-1.1 K for LHF and 0.78 K for SHF) and dominate the other terms (Fig. 4.8c).

While the individual contributions to ΔTs are small on an annual basis, contributions on monthly scale are larger, with compensating effects on the resulting temperature (Fig. 4.8b and d). During boreal spring and summer months, the subsurface heat flux cools the surface temperature, as the reservoir water takes up the heat available at the surface to warm the water. This cooling is largely compensated by a warming effect of the decreased sensible heat flux. In the fall and winter months, the subsurface heat flux has a positive effect on ΔTs, as the warmer reservoir water releases heat to the surface. This temperature increase is partially offset by the cooling effect of the increased latent heat flux. Despite its large regulatory effect on the seasonal cycle, the subsurface heat flux does not influence annual ΔTs.

The other factors only play a minor role. Throughout the year, albedo has a warming influence on ΔTs. The indirect contributions from incoming short- and longwave radiation are the result of feedbacks from cloud cover and atmospheric temperature. The effect on Ts emerges mainly during fall and winter months (from October to February), when reservoirs warm the surface temperatures. This is a similar effect as natural lakes in mid and high latitudes, which can cause temperature anomalies of up to 1.5 K in fall and winter months (Samuelsson et al., 2010). For grid cells with $> 15\%$ reservoir coverage, the individual contributions are larger (Fig. 4.8d). Overall effects are similar, apart from albedo, which has a cooling influence during May, April and March, due to the presence of lake ice.

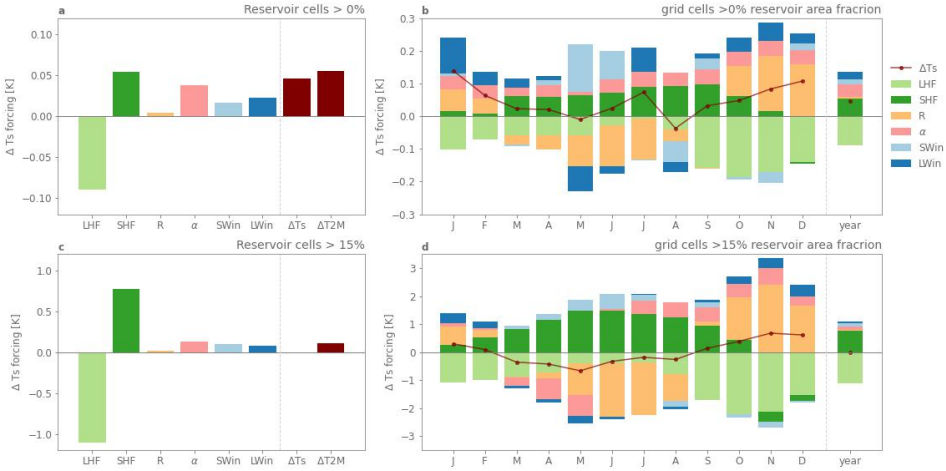

Figure 4.8: Changes in surface temperatures (T_s) induced by reservoirs. (a) Individual contributions of components (latent heat flux, LHF, sensible heat flux, SHF, subsurface heat flux, R, albedo, α, incoming shortwave and longwave radiation, SW_{in} and LW_{in}) and (b) seasonal cycle of individual components for all reservoir grid cells (reservoir area fraction > 0 %). (c,d) Similar results for grid cells with large reservoirs (reservoir area fraction $> 15\%$). The reservoir impact on T_{2m} is also shown for reference. Note the different y-axis scales.

4.4 Discussion

4.4.1 Role of natural variability

Our results indicate that reservoirs have a small but detectable climatic impact, mostly localised to reservoir grid cells. We find very limited remote effects of reservoir expansion, and the discerned remote effect could be an expression of internal climate variability rather than a remote response. At the subgrid scale, local impacts might be even larger, as we show cell averages of 0.9° by 1.25° grid cells with 1.9% average reservoir area coverage. To investigate the radius of reservoir influence on climate, and to disentangle local and non-local effects, a higher spatial resolution could be used, eventually within a regional climate model or using global simulations with static regional grid refinement, as has been done for lakes and irrigation (Thiery et al., 2015; Devanand et al., 2019). To maximise the climate signal, two extreme cases of reservoir extent (pre-industrial and present-day) are used in the AMIP-style simulations. Deploying coupled simulations at higher spatial resolutions will also allow to investigate the regional climate impacts of transient reservoir expansion. As CLM5 now accounts for reservoir expansion with dynamical lakes, these type of studies become possible.

Accounting for natural variability is of key importance, in particular when the responses are small compared to the natural climate variability (Lorenz et al., 2016). We reduced the role of natural variability in our ESM experiments by running five-member ensembles with perturbed initial conditions, adopting a similar approach as recent studies (Thiery et al., 2017, 2020; Hirsch et al., 2017, 2018; Hauser et al., 2019). To illustrate the importance of this approach, we calculated the average responses in reservoir grid cells of T2m, DTR, TXx and TNn in all possible combinations of the available RES and NORES simulations, thereby averaging across an increasing number of ensemble members (Fig. 4.9). Using only 1 ensemble member at a time, we obtain 25 possible combinations of RES and NORES simulations. When using 2 and 3 members there are 100 possibilities and for 4 members there are again 25 possibilities. Then, all combinations are plotted using a kernel density estimation per number of members used. For only 1 ensemble member, the possible responses of reservoirs on 2 meter temperature range between -0.05 and 0.21 K. While the average responses do not change, the range of possible responses remarkably decreases using more ensemble members, and in the case of 2 m air temperature and TXx removes the uncertainty regarding the sign of change. This decrease is most apparent for the temperature extremes.

In the analysis, we focus on the effects of reservoirs on temperature variables and the energy balance. We do not show precipitation and moisture related variables because the modeled responses did not emerge from the internal variability due to a low signal-to-noise ratio of these variables (Fischer et al., 2014; Deser et al., 2012). However, the increased evaporation from reservoir grid cells could increase atmospheric water vapour and thereby potentially induce changes in precipitation and precipitation extremes, as has been suggested by some regional- and local-scale observational studies (Strachan et al., 2016; Degu et al., 2011; Yigzaw, 2014; Hossain et al., 2010), but has not been confirmed by modeling studies so far.

4.4.2 Improving the representation of reservoirs in ESMs

While the current approach enables us to investigate the interactions at the reservoir-atmosphere interface and study the responses on the surface temperature and energy balance, it includes some limitations. These shortcomings can be highlighted as challenges for modeling reservoirs in any coupled Earth system framework. First, by design, reservoirs are part of the grid cell lake area fraction in CESM, and this lake fraction has a constant average depth (section 4.2.1). The bathymetry of artificial reservoirs, often V-shaped and enlarged water bodies emerging from rivers, can be however very different from natural lakes (Yigzaw et al., 2018). In addition, as reservoirs have a constant volume in the model, seasonal variations in storage, area and depth are not modeled. These could however be substantial and could impact the land-atmosphere interactions and seasonality of the surface energy balance terms (Zhou et al., 2016; Cooley et al., 2021). Third, when a reservoir comes into existence in our model, the additional lake area fraction takes over the temperature profile of the lake fraction. However, in reality the temperature of a new reservoir is mainly determined by the water temperature of the inflow (van Vliet et al., 2016). Runoff temperatures

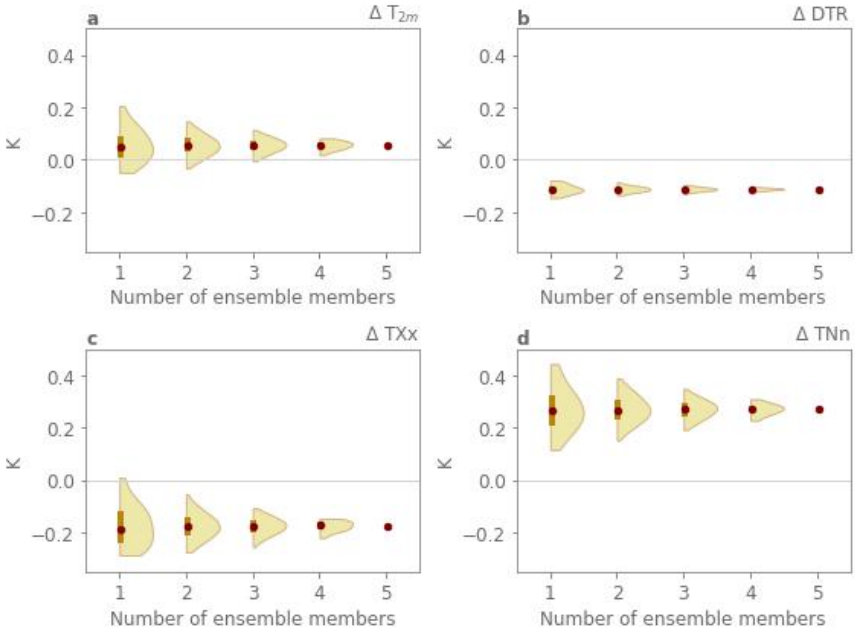

Figure 4.9: Role of ensemble size on impact on temperatures for reservoir grid cells: (a) mean 2m air temperature, T_{2m} (b) mean diurnal temperature range, DTR, (c) mean monthly maximum of daily maximum temperature, TXx, (c) mean monthly minimum of daily minimum temperature, TNn. Shown are the density kernels of the response of all possible combinations of different numbers of NORES and RES ensemble members. The bar represents the interquartile range, while the dot shows the median value.

are not explicitly modeled in CLM5, but the heat content of the lake water is adjusted for the heat that is carried away or supplied to the lake by the runoff term. Finally, we assume that reservoirs are instantly filled in their construction year, covering their total surface area, as given by GRanD. While this is true for small reservoirs, larger reservoirs might take a couple of years to fill (Hawley et al., 2020). These issues could have implications for the temperature profile, thermal stratification and resulting energy balance of reservoirs, of which the effects would become more important at higher spatial resolutions.

We only investigated the impact of reservoir expansion, i.e. the increase in lake area due to dam construction, and omitted the regulatory effect on discharge and connection to the river network. Reservoirs and dams have other large effects on terrestrial water resources by their flow regulation and altering of water availability in upstream and downstream basins (Biemans et al., 2011; Wisser et al., 2010; Wada et al., 2014; Di Baldassarre et al., 2018). Next steps in model development therefore include the integration of reservoirs and lakes on the river network and explicit modeling of the water balances of lakes and

reservoir (Shin et al., 2019, 2020). Thereby it is important to account for the relations between depth, area and storage of reservoirs (Yigzaw et al., 2018) to capture interannual dynamics in reservoir area (Gao et al., 2012; Pekel et al., 2016b). A key component of this water balance is modeling the reservoir outflow, which is highly regulated by human dam management (e.g. Vanderkelen et al., 2018a) and therefore very different from the release from natural lakes, which is mainly driven by climate variability (Nazemi and Wheater, 2015b). To this end, the existing dam parametrisations from global hydrological models can serve as inspiration (Hanasaki et al., 2006; Haddeland et al., 2006; Pokhrel et al.; Yassin et al., 2019; Zajac et al., 2017; Shin et al., 2019). Eventually, this will contribute to a more realistic representation of the water available for irrigation as well as floodplain dynamics (Shin et al., 2020; Biemans et al., 2011; Van Beek et al., 2011).

4.5 Conclusions

In this chapter, we implemented global reservoir expansion in the the Community Land Model (CLM) to assess the potential effects of reservoirs on the historic and present-day climate. The increase in open water surface through reservoir construction in the 20^{th} century is modeled by prescribing expanding lake area, based on the HydroLAKES and Global Reservoir and Dam Databases (GRanD). The implementation of correction fluxes ensures that energy and water are conserved within the grid cell. We performed land-only simulations for the period 1900-2014 with transient reservoir expansion enabled. In addition, two five-member ensemble AMIP-style simulations with the Community Earth System Model (CESM) for the period 1979-2014 with and without full reservoir extent are conducted.

Reservoir expansion during the 20^{th} century causes alterations with an increase in terrestrial water storage and a decrease in albedo with trajectories similar to reservoir area expansion. The responses scale with reservoir extent and are localized to reservoir grid cells. Our coupled climate simulations show that the climate impacts of reservoirs are overall small and localized to grid cells with reservoir expansion. Where reservoirs make up a large fraction of the grid cell, impacts can be substantial locally. Reservoirs dampen the diurnal temperature cycle up to -1.5 K for the largest reservoirs, and this dampening is strongest from July to September. In addition, the seasonal temperature cycle is moderated by the presence of open water. Decomposing the surface temperature impact highlights a large seasonal variation in heat uptake and release of the reservoir water, which is compensated by the turbulent surface fluxes. The remaining radiative fluxes play only a minor role. The presence of open water also reduces temperature extremes by increasing the monthly minimum nighttime temperatures and decreasing the monthly maximum daytime temperatures. Signals in precipitation and moisture related variables could not be differentiated from the natural variability within our ensembles.

We provide an important first step towards a fully coupled representation of reservoirs and human water management in an Earth System Model. Our results indicate that there is a small but detectable impact of reservoir expansion on the surface energy fluxes and on the

resulting diurnal and seasonal temperature cycles. However, a more prominent impact of reservoirs on the regulation of streamflow can be expected. A more complete integration of reservoir functionality in Earth System Models will therefore allow to quantify water availability and hydropower potential in future climate simulations, and to study the combined effects of reservoirs and other management activities like irrigation. In addition, the positive radiative forcing of reservoirs, due to the decrease in albedo, might be relevant to consider in climate impact studies (Wohlfahrt et al., 2021). With hundreds of new reservoirs being constructed or planned worldwide, these reservoir effects may even become more important in the future.

Data and code availability

The HydroLAKES dataset is available at `https://www.hydrosheds.org/page/hydrolakes`, GRanD at `http://globaldamwatch.org/`. The HydroLAKES and GRanD data are rasterised using `https://github.com/VUB-HYDR/polygon_to_cellareafraction`. CLM5.0 is publicly available through the Community Terrestrial System Model (CTSM) repository: `https://github.com/ESCOMP/CTSM/`. The developments presented in this study are available in the source code from tag *ctsm5.1.dev003* onwards. All scripts developed for this study are available at: `https://github.com/VUB-HYDR/2021_Vanderkelen_etal_JGR`, DOI: `10.5281/zenodo.5007504`. Finally, all simulations used in the analysis are available at `https://figshare.com/collections/Simulating_the_impact_of_global_reservoir_expansion_on_the_present-day_climate/5461275`.

Acknowledgments

We greatly thank Erik Kluzek for his support with the code development in CLM. This research is supported by the Research Foundation Flanders (FWOTM920). The CESM project is supported primarily by the National Science Foundation (NSF). This material is based upon work supported by the National Center for Atmospheric Research, which is a major facility sponsored by the NSF under Cooperative Agreement No. 1852977. Computing and data storage resources, including the Cheyenne cluster (doi:10.5065/D6RX99HX), were provided by the Computational and Information Systems Laboratory (CISL) at NCAR. We thank all the scientists, software engineers, and administrators who contributed to the development of CESM2. Other storage resources and services used in this work were provided by the VSC (Flemish Supercomputer Center), funded by the Research Foundation - Flanders (FWO) and the Flemish Government.

4.6 Supplementary material

Implementation of dynamical lakes: correction fluxes and baseline approach

Conceptual example

To illustrate the need and rationale behind the correction fluxes and baselines approach, we use a conceptual example (Fig. 4.10). We assume a grid cell existing of both vegetation and lake unit, both with their respective temperatures. In the example, the grid cell evolves by changing both the lake fraction and lake temperature to end up in exactly the same state as the reference state. As a consequence, energy needs to be conserved during this process. Without correction fluxes, the only land-atmosphere fluxes arise from warming and cooling of the lake fraction, which in this example violates energy conservation (Fig. 4.10a). Changing the lake area fraction changes the heat content of the total grid cell, as the added lake area fraction adopts the temperature of the existing lake fraction. Therefore, these changes in lake fraction need to be accompanied by correction fluxes to and from the atmosphere to conserve energy in the system (Fig. 4.10b). As these fluxes are artificial and thus not representing any physical process but only assuring conservation, we want to minimise them as much as possible. This is achieved using the baseline approach. The baseline state of each land unit is defined as the spun up state of that land unit at the start of the simulation. (As with other model state variables, these baselines are expressed on a per-area basis – for example, J m^{-2}.)

When calculating the correction fluxes, we consider the change in water or heat content of each model column relative to that column's baseline state, rather than relative to some arbitrary zero point. This results in energy conservation with smaller correction fluxes, as only their deviation from the baseline are taken in the calculation while still ensuring energy conservation (Fig. 4.10c).

This is of course a simplified, conceptual example for energy. The processes within a simulation are more complex, but the concept holds. We apply the same scheme for mass. As lake water does not participate in the water balance and therefore remains constant throughout the simulation, the correction fluxes do not account for changes in lake water content. Still, the correction flux for water is needed to correct for the difference in water content of the soil underneath the lake, and potential snow on top. As the soil beneath lakes is always saturated in the model (section 2.1), this correction flux can be important. But, as for the heat correction flux, the baseline approach minimizes its magnitude.

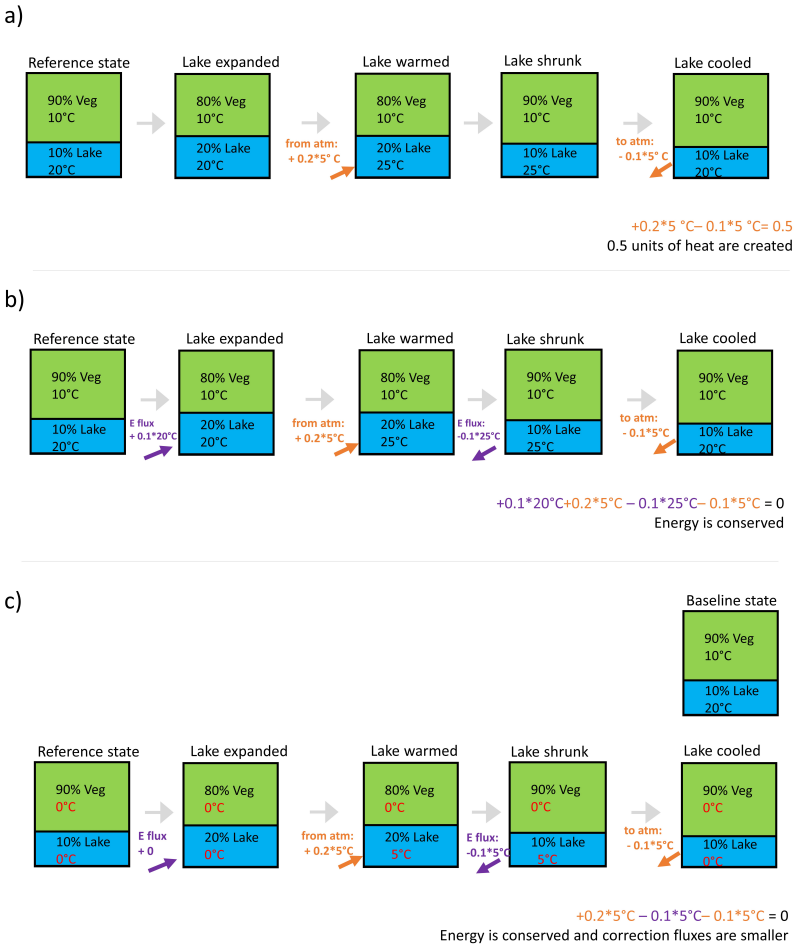

Figure 4.10: Conceptual example of energy conservation violation (a), the need for correction fluxes (b) and the need for using baselines (c). The example shows a grid cell consisting of a vegetated and lake fraction that evolves from its beginning state to the exact same end state, while interacting with the atmosphere. In the process, the lake expands, warms, shrinks and cools. The E flux represents an artificial sensible heat flux from or to the atmosphere to achieve conservation in the full land-atmosphere-ocean system.

Quantification of correction fluxes in CLM5 simulation

The correction fluxes used are artificial, and should be kept as small as possible. Table 4.2 shows the magnitude of the correction fluxes in the land-only simulations including reservoir expansion, described in section 2.4.1, but here simulated on a 1.9° by 2.5° resolution. We selected the year with the largest reservoir expansion (1970) and selected the two grid cells with the largest reservoirs. These correspond to the locations of Lake Nasser, controlled by the Aswan Dam located in Egypt, and the Khantayskoye Reservoir located in Siberia, Russia. Even for these two most extreme cases, the magnitude of the correction fluxes remains limited, highlighting that the correction fluxes will overall have negligible impact on the simulations.

Table 4.2: Correction fluxes for two grid cells in the year with the largest reservoir expansion (1970) in the land-only simulation with expanding reservoirs (1.9° by 2.5° resolution). The water correction flux is the sum of the liquid and ice fluxes. Sensible heat flux is abbreviated as SHF.

Lake Nasser (+5% lake area)

	Heat correction flux	Fraction of SHF	Water correction flux	Fraction of runoff
No baselines	-0.93 W m^{-2}	3%	0.67 m $year^{-1}$	670%
Baselines	0.48 W m^{-2}	1%	0.14 m $year^{-1}$	140%

Khantayskoye Reservoir (+6% lake area)

	Heat correction flux	Fraction of SHF	Water correction flux	Fraction of runoff
No baselines	0.78 W m^{-2}	5 %	0.66 m $year^{-1}$	244 %
Baselines	0.53 W m^{-2}	3 %	0.07 m $year^{-1}$	26 %

Model evaluation with ILAMB

We employed a thorough validation of our developments using the International Land Model Benchmarking (ILAMB) System (Collier et al., 2018). Within this framework, a suite of ten in situ, remote sensing and reanalysis data sets are used to assess the skill of various variables related to land surface modeling by combining statistical quantities related to the mean state and variability in monthly to decadal time scales. Per variable-observation combination, ILAMB calculates scores for the mean bias, root mean square error, phase shift of the annual cycle, inter-annual variability and the spatial distribution of the time averaged variable, and combines these to an overall score in a weighted sum. For more details on the equations and followed methodology, we refer to (Collier et al., 2018).

Table 4.3 gives an overview of the reference data products per variable.

Table 4.3: Datasets used for benchmarking in ILAMB, adapted from Collier et al. (2018).

Variable	Dataset	Reference
Evapotranspiration		
	GLEAM	Miralles et al. (2011)
	MODIS	De Kauwe et al. (2011)
Evaporative Fraction		
	GBAF	Jung et al. (2010)
Latent and sensible heat		
	Fluxnet	Lasslop et al. (2010)
	GBAF	Jung et al. (2010)
Runoff		
	Dai	Dai and Trenberth (2002)
	Fluxnet	
Terrestrial Water storage		
	GRACE	Swenson and Wahr (2006)
Albedo		
	CERES	Kato et al. (2013)
	GEWEX.SRB	Stackhouse et al. (2011)
	MODIS	De Kauwe et al. (2011)
Surface upward/net SW/LW radiation		
	CERES	Kato et al. (2013)
	GEWEX.SRB	Stackhouse et al. (2011)
	WRMC.BSRN	König-Langlo et al. (2013)
Surface net radiation		
	CERES	Kato et al. (2013)
	Fluxnet	Lasslop et al. (2010)
	GEWEX.SRB	Stackhouse et al. (2011)
	WRMC.BSRN	König-Langlo et al. (2013)

To fully assess the skill of our developments consisting of (i) a new lake mask based on Hydrolakes and GRanD and (ii) transient reservoir construction, we conducted the evaluation for the following simulations: CLM with its original constant lake mask derived from MODIS (orig_lakes), CLM with the new hydrolakes constant mask (hydrolakes_all), CLM with the new constant lake mask excluding artificial reservoirs (hydrolakes_nores) and CLM with the new lake mask and transient reservoir construction enabled (hydrolakes_transres). All simulations are conducted with GSWP3 forcing (IHist-CLM50Sp compset), and analysed for the period 1900-2015, with 10 years for spin up. We applied the ILAMB framework on the global scale, as well as for the IPCC AR6 reference regions (Iturbide et al., 2020).

At the global scale, there is no difference in skill scores between the different simulations across the variables considered. This is consistent for all the different variables and data products in ILAMB. At the regional scale, using the IPCC AR6 regions, there are small noticeable, but overall very small differences in skill for certain regions, but not consistent between regions and simulations (illustrated here for albedo scores for Eastern North-America (ENA) based on CERES for 2000-2012, panel b: latent heat scores for Eastern Europe (EEU), figure 4.12) Overall, the skill scores of the different simulations are very similar for all regions and variables, indicating very little change in skill.

The reasons that the analysis with the ILAMB framework did not capture substantial changes in model skill can be attributed to several reasons. First, the simulated changes in variables are small, and very localised to grid cells with reservoirs area fractions. To evaluate the skill of variables related to changes in lake extent, it is crucial that the reference products represent observations over lakes and resolve this lake extent. For example, the observations from Fluxnet originate from towers which are not localised near large reservoirs or lakes Lasslop2010 and the GLEAM product does not provide evaporation values over water surfaces like lakes Miralles2011. In addition, as most reference data sets are derived from satellite products, the period of with the largest reservoir construction (1950s to 1980s) is not covered by observations. For detailed evaluation at specific reservoir locations, targeted observations would be necessary. This is however out of scope of this chapter.

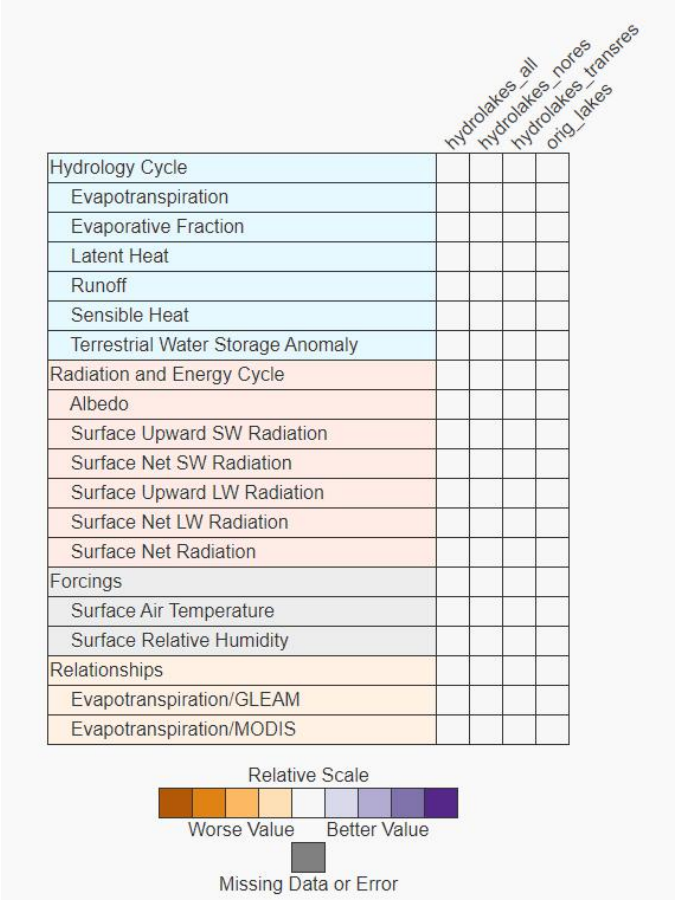

Figure 4.11: Relative scale for IlAMB for the different simulations on global scale. The white boxes indicate that there is no detectable change in skill between the simulations.

a) ENA scores for Albedo
(based on CERES for 2000-2012)

		Download Data Period Mean (original grids) [1]	Model Period Mean (intersection) [1]	Model Period Mean (complement) [1]	Benchmark Period Mean (intersection) [1]	Benchmark Period Mean (complement) [1]	Bias [1]	RMSE [1]	Phase Shift [months]	Bias Score [1]	RMSE Score [1]	Seasonal Cycle Score [1]	Spatial Distribution Score [1]	Interannual Variability Score [1]	Overall Score [1]
Benchmark	[-]	0.120													
hydrolakes_all	[-]	0.148	0.149		0.145	0.0582	0.00445	0.0578	1.87	0.558	0.376	0.718	0.857	0.631	0.586
hydrolakes_nores	[-]	0.149	0.149		0.145	0.0582	0.00458	0.0579	1.87	0.560	0.376	0.718	0.858	0.631	0.586
hydrolakes_transres	[-]	0.148	0.149		0.145	0.0582	0.00444	0.0579	1.87	0.558	0.376	0.718	0.858	0.631	0.586
orig_lakes	[-]	0.148	0.149		0.145	0.0582	0.00431	0.0580	1.88	0.555	0.375	0.718	0.860	0.630	0.585

b) EEU scores for Latent Heat
(based on GBAF for 1982-2008)

		Download Data Period Mean (original grids) [W/m2]	Model Period Mean (intersection) [W/m2]	Model Period Mean (complement) [W/m2]	Benchmark Period Mean (intersection) [W/m2]	Benchmark Period Mean (complement) [W/m2]	Bias [W/m2]	RMSE [W/m2]	Phase Shift [months]	Bias Score [1]	RMSE Score [1]	Seasonal Cycle Score [1]	Spatial Distribution Score [1]	Overall Score [1]
Benchmark	[-]	27.8												
hydrolakes_all	[-]	26.8	26.5	58.0	27.8		-1.28	11.3	0.366	0.882	0.690	0.978	0.952	0.838
hydrolakes_nores	[-]	26.7	26.3	58.0	27.8		-1.41	11.3	0.369	0.881	0.690	0.978	0.948	0.838
hydrolakes_transres	[-]	26.8	26.5	58.0	27.8		-1.28	11.3	0.366	0.882	0.690	0.978	0.952	0.838
orig_lakes	[-]	26.5	26.2	57.1	27.8		-1.59	11.0	0.343	0.881	0.691	0.980	0.963	0.841

c) AR6 regions

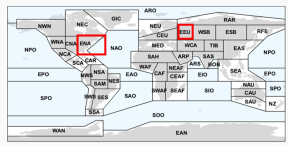

Figure 4.12: Example of ILAMB scores of the different simulations for 2 AR6 regions with large reservoir area fractions. Panel a: albedo scores for Eastern North-America (ENA) based on CERES for 2000-2012, panel b: latent heat scores for Eastern Europe (EEU) based on GBAF for 1981-2008 and panel c: IPCCAR6 regions (adapted from (Iturbide et al., 2020).

Supplementary figure

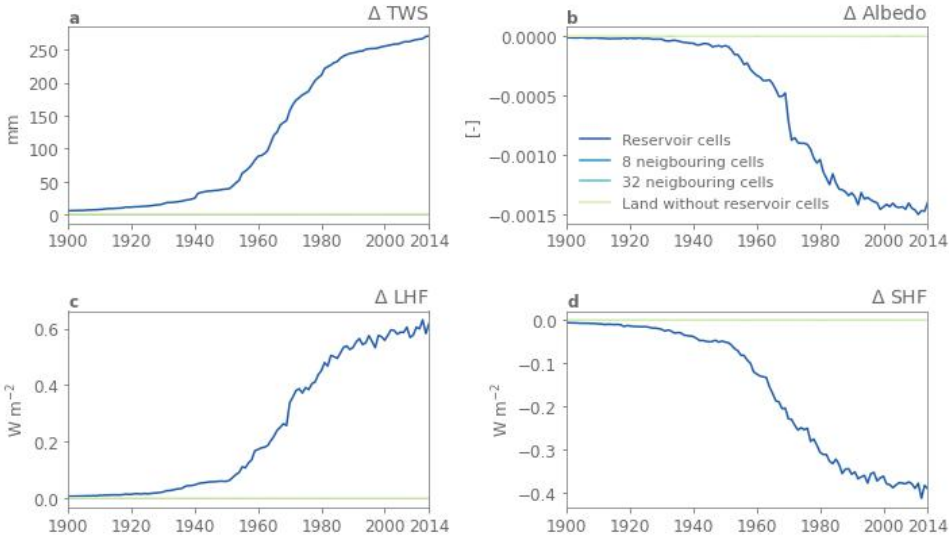

Figure 4.13: Impact of transient reservoir construction (transRES-CTL) on global mean (a) albedo, (b) terrestrial water storage, TWS (c) latent heat flux, LHF and (d) sensible heat flux, calculated for reservoir grid cells, the 8 grid cells surrounding the reservoir cell, the 32 grid cells surrounding the reservoir cell and all land cells. Note that the latter three curves are overlapping on the zero line, indicating the response is limited to the reservoir grid cells.

Chapter 5

Implementing and evaluating a reservoir parametrisation in a global routing model for Earth System Model coupling

Human-controlled reservoirs have a large influence on the global water cycle. While global hydrological models use generic parametrisations to model human dam operations, the representation of reservoir regulation is often still lacking in Earth System Models. Here we implement and evaluate a widely used reservoir parametrisation in the global river routing model mizuRoute, which operates on a vector-based river network resolving individual lakes and reservoirs. We develop an approach to determine the downstream area over which to aggregate irrigation water demand per reservoir. The implementation of reservoirs is evaluated by comparing to simulations ignoring inland waters, and with reservoirs represented as natural lakes, using (i) local simulations for 26 individual reservoirs driven by observed inflows, and (ii) global-scale simulations driven by runoff from the Community Land Model. The local simulations show a clear added value of the reservoir parametrisation. In the global-scale application, the implementation of reservoirs shows overall a similar performance compared to the natural lake parametrisation. This lack of impact could be attributed to biases in simulated river discharge, mainly originating from biases in simulated runoff from the Community Land Model. Finally, the comparison of modelled monthly streamflow indices against observations highlights that the inclusion of dam operations improves the streamflow simulation compared to ignoring lakes and reservoirs. This study overall underlines the need to further develop and test water management parametrisations, as well as to improve runoff simulations for advancing the representation of anthropogenic interference with the terrestrial water cycle in Earth System Models.

This chapter is published as: Vanderkelen, I., Gharari, S., Mizukami, N., Clark, M. P., Lawrence, D. M., Swenson, S., Pokhrel, Y., Hanasaki, N., van Griensven, A., and Thiery, W.: Evaluating a reservoir parametrisation in the vector-based global routing model mizuRoute (v2.0.1) for Earth System Model coupling. Geoscientific Model Development, 15, 4163-4192.

5.1 Introduction

The terrestrial global water cycle is fundamentally altered by human activities like groundwater pumping, river water abstraction for irrigation, and the construction of large dams (Oki and Kanae, 2006; Rockström et al., 2009; Wada et al., 2014). Worldwide, more than 45,000 large dams have been built to create reservoirs that provide hydropower, irrigation or drinking water supply or are used for flood control (Lehner et al., 2011; Sterl et al., 2020). Reservoir expansion since the 20^{th} century impounded at least 8,300 km^3 of water (Chao et al., 2008), counteracting global sea level rise by around 30 mm (Chao et al., 2008; Frederikse et al., 2020) and redistributing heat contained within the world's water resources and increasing anthropogenic heat uptake by inland waters (Vanderkelen et al., 2020a). By buffering seasonal river flow, reservoirs control more than half of the variability in global surface water storage (Cooley et al., 2021) and can substantially alter the timing and volume of natural streamflow (Döll et al., 2009). Today, more than 77% of global rivers are human-regulated or are interrupted by dams, reservoirs or other infrastructure (Grill et al., 2019). Therefore, accounting for reservoirs and dam operations is important when assessing the seasonality of global streamflow and water availability (Nazemi and Wheater, 2015a; Pokhrel et al., 2016).

Despite the clear human imprint on the terrestrial water cycle, Earth System Models generally do not yet account for human alterations to flow by dam operations in their component land models (Pokhrel et al., 2016). Yet, to adequately understand human alterations to flow, it is key to represent dam management in holistic modeling frameworks covering all Earth system components (Nazemi and Wheater, 2015b; Pokhrel et al., 2016). Recent efforts are beginning to address this limitation. For example, Zhou et al. (2020) coupled the MOSART-WM, a river routing and water management model including reservoir operation, to the land model of E3SM. Also in MIROC-INTEG-LAND, water management modules have recently been incorporated in the land component of the MIROC Earth System Model, together with crop production, land ecosystem and land use modules (Yokohata et al., 2020). Overall, these developments suggest that reservoir management could potentially be considered in upcoming rounds of the Coupled Model Intercomparison Project (CMIP; Eyring et al., 2016) or other multi-model assessments.

Due to their importance for water resource assessments, reservoir operations have long since been represented in large-scale hydrological models, including catchment models (e.g. Chawanda et al., 2020; Shin et al., 2019), water management models (e.g. Voisin et al., 2013b,a) and Global Hydrological Models (GHMs; see Sood and Smakhtin (2015) and Telteu et al. (2021) for a comprehensive overview). However, substantial variations in operating rules and the lack of operational knowledge of reservoirs worldwide, necessitate the use of generic parametrisations to describe reservoir operations (Pokhrel et al., 2016). Such generic schemes are typically not designed to reproduce the daily operations of individual reservoirs, but provide simple, yet widely applicable rules, mimicking human decisions in regulating dams, to the extent possible. A wide range of approaches exist, which can broadly be categorised into optimization-based methods (e.g. Haddeland et al., 2006),

methods based on target storage and release (e.g. Burek et al., 2013; Yassin et al., 2019) and inflow-and-demand-based methods (e.g. Wisser et al., 2010; Hanasaki et al., 2006). In addition to these approaches, which do not require prior information on historical reservoir operations, there are also a wide variety of reservoir models that use operational data for specific reservoirs to develop general operational rules (e.g. Coerver et al., 2018; Zhao et al., 2016; Ehsani et al., 2016), and extrapolate these empirical operating rules to data-scarce reservoirs with similar operating purposes and hydrologic conditions (Turner et al., 2021). For a comprehensive overview of the range of existing reservoir parametrisations, their characteristics, advantages and disadvantages, the reader is referred to Pokhrel et al. (2016); Yassin et al. (2019) and Gutenson et al. (2020).

Here, we evaluate the representation of reservoirs in the state-of-the art river routing model mizuRoute (Mizukami et al., 2016, 2021), in view of its anticipated coupling in the Community Land Model (CLM), the land component of the Community Earth System Model (CESM). The CLM modelling framework already accounts for historical reservoir construction by including lake area expansion (Vanderkelen et al., 2021), but an explicit representation of lake and reservoir water balance dynamics is currently lacking. We investigate the effect of dam operations on river flow when using the parametrisation of Hanasaki et al. (2006) in mizuRoute. Compared to other reservoir models, the Hanasaki parametrisation has low data requirements (it only needs information on irrigation water demand and instantaneous inflow), and it does not require prior knowledge (e.g. on future inflows, like the schemes derived from the Haddeland et al. (2006) parametrisation) and can thus be used instantaneously during a simulation. Moreover, due to its generic nature, the Hanasaki parameterization can be applied to every reservoir across the globe. Therefore, the Hanasaki parametrisation has been widely used as a basis in large scale hydrological modelling studies (e.g. Biemans et al., 2011; Voisin et al., 2013a; Droppers et al., 2020; Döll et al., 2009; Hanasaki et al., 2008; Pokhrel et al.; Shin et al., 2019).

In contrast to previous studies, we evaluate the implementation of the Hanasaki et al. (2006) parametrisation in a global river routing model that operates on a vector-based river network, mizuRoute. To provide seasonal irrigation demand per reservoir, we develop an irrigation topology, which defines the area over which the water demand is aggregated for an individual reservoir, based on the river network topology and catchments. We evaluate the added value of the Hanasaki et al. (2006) parametrisation for reservoir outflow and storage modelling in a stand-alone mizuRoute simulation that uses reservoir observations as input, and compare results to a simulation using the natural lake outflow parametrisation of Döll et al. (2003). Next, both parametrisations are evaluated using mizuRoute in a global routing-only application with runoff input from CLM to evaluate the capability to represent outflow and storage at individual reservoirs and to capture long-term trends in monthly streamflow indices. Our modelling framework enables us to identify biases in runoff from CLM by comparing previously not modelled variables (e.g. reservoir outflow and storage) to observations. Finally, we explore new avenues for future model development and towards coupling within CESM. This study provides an essential step towards incorporating human water management and reservoir dynamics in a coupled Earth System model,

which enables investigating complex interactions between climate change, human water management and natural systems in an integrated, holistic framework. In addition, including reservoir operations in CLM will allow to study the potential of water management strategies to mitigate climate change impacts on water resources.

5.2 Modelling framework

5.2.1 mizuRoute

The vector-based routing model mizuRoute is designed to use runoff provided by hydrological models or land models and simulate spatially distributed streamflow (Mizukami et al., 2016, 2021). The routing is performed in two steps: first, basin runoff is routed from the hillslopes to the river reach with a gamma distribution based unit-hydrograph. Then, the water is routed downstream through the river channel network, using either an impulse response function (IRF) or a kinematic wave tracking (KWT) routing scheme (Mizukami et al., 2016). In stand-alone applications, mizuRoute internally remaps the gridded runoff provided by the land model or hydrological model to the basin defined in the vector-based river network. In continental or global applications, mizuRoute provides a spatial decomposition of the river networks to allow for parallel routing computations (Mizukami et al., 2021). Natural lakes and reservoirs are integrated in the vector-based river network as hydrological features with additional parameters including information on the characteristics of the lake and/or reservoir, like maximum capacity (Gharari et al., 2022). This approach allows the lake and reservoir water balance to be modeled using data on precipitation and evaporation from the water surface, in combination with parametrisations providing information on the releases, including both natural outflow and regulated discharge. For this study, the IRF routing scheme was used for river channel routing that produces the discharge into lakes and reservoirs.

5.2.2 Lake and reservoir parametrisations

Gharari et al. (2022) introduces parametric lake and reservoir implementations in mizuRoute to simulate lake and reservoir outflow. Natural lakes are modelled as linear reservoirs using the parametrisation of Döll et al. (2003) (eq. 5.1) which resolves daily outflow (Q_{daily} in $m^3\ s^{-1}$), as a function of current active lake storage (S in m^3) with a release coefficient k_r (taken constant at 0.01 s^{-1}) and the maximal lake storage capacity (S_{max} in m^3). The exponent in the parametrisation is determined based on the theoretical value of outflow over a rectangular weir (Meigh et al., 1999).

$$Q_{daily} = k_r \cdot S \cdot \left(\frac{S}{S_{max}} \right)^{1.5} \tag{5.1}$$

In this study, we investigate the impact of implementing management of human-constructed reservoirs and dam-controlled lakes with the parametrisation described in Hanasaki et al. (2006). This algorithm minimizes intra- and inter-annual variability, while accounting for

irrigation and other water demands, making a distinction between reservoirs used for irrigation and other purposes such as hydropower, flood control, navigation or water supply. Irrigation reservoirs, which provide water for crops downstream, are characterised by a distinct seasonal variability guided by the downstream irrigation water needs. Since withdrawal periods do not necessarily coincide with high inflow periods, the parametrisation explicitly takes into account the downstream irrigation demand in the intra-annual outflow. The reservoirs with purposes other than irrigation are operated in the same way, aiming to reduce intra- and interannual flow variability. Furthermore, the parametrisation differentiates between "multi-year reservoirs" with high storage capacity compared to their annual inflow, and "within-a-year reservoirs", defined as reservoirs with annual inflow values that are more than half of the storage capacity. "Within-a-year reservoirs" carry the inflow seasonality in their outflow values to compensate for potential overflow and storage depletion, while "multi-year reservoirs" aim to maintain a constant outflow (Hanasaki et al., 2006).

Below, we outline the parametrisation as described in Hanasaki et al. (2006) and specify how it is implemented in mizuRoute. The parametrisation uses operational years, which are unique to every reservoir and different from the calendar year. The operational year starts on the first day of the month in which the multi-year monthly inflow drops below the annual inflow (Hanasaki et al., 2006; Haddeland et al., 2006). Then, at the start of the operational year, the monthly target release is determined based on the purpose of the reservoir. For non-irrigation reservoirs the monthly target release Q_{target} (m^3 s^{-1}) is taken as the annual mean inflow I_{mean} (m^3 s^{-1}; eq. 5.2).

$$Q_{target} = I_{mean} \tag{5.2}$$

For irrigation reservoirs, the target release is calculated by equation 5.3,

$$Q_{target} = \begin{cases} 0.1 \cdot I_m + 0.9 \cdot I_{mean} \cdot \frac{D_m}{D_{mean}} & \text{, if } D_{mean} \geq \beta \cdot I_{mean} \\ I_{mean} + D_m - D_{mean} & \text{, otherwise} \end{cases} \tag{5.3}$$

with I_m (m^3 s^{-1}) the mean monthly inflow for the corresponding month, I_{mean} (m^3 s^{-1}) the mean annual inflow, D_m (m^3 s^{-1}) the mean monthly irrigation water demand for the corresponding month, D_{mean} (m^3 s^{-1}) the mean annual irrigation demand and β, a coefficient representing the minimum release to meet environmental requirements (here β=0.9, leaving 10% of annual mean flow available to meet environmental requirements). Following the adjustments of Biemans et al. (2011) to the original Hanasaki et al. (2006) parametrisation, we only account for irrigation water withdrawal, while neglecting domestic and industrial water use. In addition, we also apply a minimum environmental flow requirement of 10% of mean annual inflow, instead of 50% used by Hanasaki et al. (2006) to ensure enough water is retained in the reservoirs during low-flow months to meet the irrigation demands (Biemans et al., 2011).

The actual release depends on how full the reservoir is at the start of the operational year, determined by the release coefficient (E_r, eq. 5.4), giving the ratio between the reservoir storage at the start of the operational year (S_{ini}, m^3) and the maximal storage capacity (S_{max},

m^3), scaled with α (set constant at 0.85). This coefficient quantifies the share of the total storage that is considered active storage, i.e. total storage excluding dead and emergency storage.

$$E_r = \frac{S_{ini}}{\alpha \cdot S_{max}} \tag{5.4}$$

The actual reservoir release (Q_{daily}, m^3 s^{-1}) depends on the reservoir type ("multi-year" or "within-a-year", defined by the capacity ratio c (given by S_{max}/I_{mean}), and is calculated by eq. 5.5.

$$Q_{daily} = \begin{cases} E_r \cdot Q_{target} & \text{, if } c \geq 0.5 \textit{ (multiyear reservoir)} \\ \left(\frac{c}{0.5}\right)^2 \cdot E_r \cdot Q_{target} + \left\{1 - \left(\frac{c}{0.5}\right)^2\right\} \cdot I_{daily} & \text{, if } c < 0.5 \textit{ (within-a-year reservoir)} \end{cases} \tag{5.5}$$

In this study, we prescribe the seasonal cycles for monthly mean inflow and demand based on naturalized simulations, but the implementation allows for transitioning from prescribed values to modelled mean inflows and demands over the last 5 years, similar to the approach of Biemans et al. (2011); Droppers et al. (2020). Using time-varying inflows and demands allows the model to respond to climatological changes when determining reservoir release, which is a capability that is particularly relevant in the context of climate change studies. When the reservoir storage drops below the dead storage level, defined as 10% of the maximal reservoir storage, no water is released. When the simulated storage exceeds the maximal reservoir capacity, the surplus is released as spillway overflow. Hence, the calculated reservoir release is required to be between these two constraints so as to keep reservoir storage within realistic limits.

5.2.3 Irrigation topology

The Hanasaki et al. (2006) parametrisation for irrigation reservoirs requires mean monthly irrigation water demand per reservoir as an input. Previous studies with grid-based river models defined the dependent area of a reservoir by number of cells downstream either to the next reservoir, the river mouth, a predefined maximum number of downstream cells (e.g. 5 cells at 0.5° or 10 cells at 1°, corresponding to the typical distance that river water travels within a month, Döll et al., 2009; Hanasaki et al., 2008), or grid cells which are located at a predefined threshold distance from the main river reach (e.g. 200 km or 2° Biemans et al., 2011; Voisin et al., 2013a). A vector-based river network, in contrast, needs a reservoir dependency database ('irrigation topology'), which provides for each reservoir the river segments and corresponding hydrological response units (HRUs) to which it supplies irrigation water.

When multiple reservoirs serve the same HRU, the irrigation topology should also include the share of the different reservoirs in meeting the water demand of the individual HRU. The total water demand of a reservoir is then calculated by taking the weighted sum of the irrigation demands of HRUs, which are dependent on that specific reservoir. The spatial

representation of rivers and reservoirs in a vector-based river network (lines and polygons) has a closer correspondence to reality than in grid-based river networks.

Here, we develop a global irrigation topology based on simple rules, in line with other large-scale hydrological models. Our approach utilizes the topological relation provided in the vector-based river network topology as well as the bottom elevation of each HRU. First, the reservoir for which the calculations will be done is selected and the corresponding segment on the river network is localised. Then, the downstream river segment for which the reservoir influence ends is determined based on a distance threshold along the main stem (here taken at 700 km). If the river mouth or another reservoir is located within this distance threshold, their corresponding segments are chosen as the ending segment. All HRUs corresponding to the segments along the main river stem and first order tributaries are added to the dependency data set. Third, the HRUs of all higher order tributaries below a threshold river length from the main stem (here taken at 100 km), are added. Finally, the HRUs with higher bottom elevation than the reservoir segment are excluded, to avoid cases where irrigation water would be transported uphill. This HRU selection procedure is showcased for the Island Park reservoir of the Snake river basin in Fig. 5.1a. The selection routine is repeated for every reservoir in the river network. For HRUs with two or more dependent reservoirs (Fig. 5.1b), the demand is distributed among the reservoirs along their ratio of the maximum storage capacity, following the approach of Haddeland et al. (2006) and Voisin et al. (2013a). Finally, the irrigation topology is used to derive the total irrigation demand for every reservoir based on the HRU irrigation water demands for every time step (Fig. 5.1c).

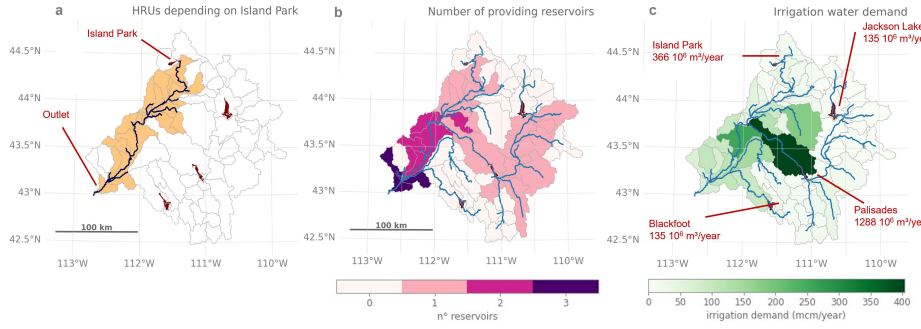

Figure 5.1: Illustration of the irrigation topology for the Snake River basin (with basin outlet taken at American Falls reservoir, ID, United States of America). Selection of river segments and corresponding downstream HRUs of the Island Park reservoir (panel a), number of reservoirs supplying water to each HRU (panel b), total irrigation water demand per HRU and reservoir, calculated using the irrigation topology (panel c). Reservoir locations from GRanD, river network from HDMA and irrigation demand remapped from a gridded CLM simulation (see section 5.3.2).

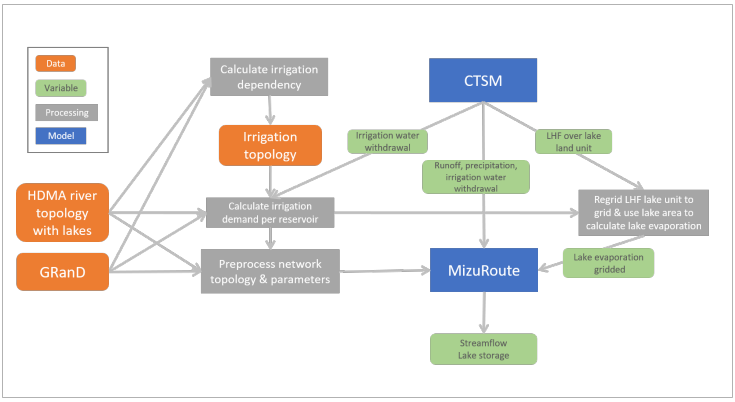

Figure 5.2: Schematic representation of the modelling workflow for the global-scale mizuRoute application, using input data and parameters based on Community Land Model (CLM) simulations. LHF refers to latent heat flux.

5.3 Simulation setup

The lake and reservoir parametrisations in mizuRoute are evaluated both in a local and global setting. By using observed streamflow values as forcing, the local mizuRoute application allows for direct evaluation of the implementation of the different outflow schemes. In the global-scale mizRoute application, outlined in Fig. 5.2, the reservoir schemes are embedded in global-scale routing simulations that receive forcing fields directly from the land model.

5.3.1 River network topology

The Hydrologic Derivatives for Modeling and Applications (HDMA; Verdin, 2017) is a vector-based river network based on HydroSHEDS, GMTED2010 and SRTM DEMs and entails 295,335 river reaches and HRUs, with a scale of 250 km^2 (the minimum upstream area to define the start of a river reach). Lakes are included on the HDMA river network by geo-referencing lake polygons of the HydroLAKES dataset (Messager et al., 2016) with a surface area larger than 10 km^2 to their corresponding river reaches (Gharari et al., 2022). The lake polygons from the HydroLAKES dataset are linked to the Global Reservoir and Dam dataset (GRanD; Lehner et al., 2011) which provides additional information about reservoirs including maximum reservoir capacity and reservoir purpose. Based on this information, a lake segment is classified as a reservoir if it is present in GRanD (including both man-made reservoirs and dam-controlled lakes). Of the 7250 reservoirs available in GRanD, 1773 are included in the river network, based on the corresponding polygon in HydroLAKES resolved on the river network, of which 484 are categorized as irrigation reservoirs. Likewise, every reservoir is resolved individually on the river network.

5.3.2 Land model forcing

We conducted a global land-only simulation with the Community Land Model (CLM; Lawrence et al., 2019b) that receives prescribed meteorological conditions from the Global Soil Wetness Project (GSWP3; `http://hydro.iis.u-tokyo.ac.jp/GSWP3/` see also Lawrence et al. (2019b)) and prescribed vegetation phenology from MODIS (IHist-Clm5SP component set). The simulation is run on a 0.5° by 0.5° grid, for the period 1961-2015 (including 5 years for spin up). The simulation is conducted with the updated lake and reservoir mask based on HydroLAKES and GRanD as described in Vanderkelen et al. (2021) and the default irrigation algorithm, without constraints on water availability. Therefore, simulated grid cell irrigation water withdrawal corresponds to the total irrigation water demand of the grid cell. The daily simulated gridded runoff is directly used as input to mizuRoute, and remapped to the river network catchments using the first-order conservative remapping method within mizuRoute. Furthermore, the precipitation and evaporation over lakes and reservoirs, necessary for their water balance, are also provided by CLM and remapped to the individual reservoir segments within mizuRoute. Precipitation is directly provided, while lake evaporation is calculated in an intermediate processing step, that is, by converting the latent heat flux at the lake 'land unit' level to evaporation using the latent heat of vaporization ($2.501 \cdot 10^6$ J kg^{-1}).

5.3.3 Parameters of the outflow parametrisations

All parameters required for the lake and reservoir schemes are provided through the network topology (Appendix Table 5.1). Maximum reservoir capacity and the reservoir purpose are both provided by the attributes from GRanD. Only the reservoirs for which GRanD assigns irrigation as the main purpose are categorized as irrigation reservoirs in mizuRoute. At the start of the simulation, the initial storage is set at the maximal storage capacity. In the local mizuRoute simulations, monthly mean inflow values are calculated based on observed inflows according to their availability (Appendix Table 5.1). For the global-scale mizuRoute simulations, monthly mean inflow values per reservoir are obtained from a mizuRoute simulation with only natural lakes using the Döll et al. (2003) parametrisation for the period 1979-2000. For both the local- and global-scale simulations, mean monthly irrigation water demands per reservoir are calculated based on the gridded CLM simulation for the same period. The gridded demands are first remapped to the HRUs of the vector-based river network, and subsequently the irrigation topology described in section 5.2.3 is applied, using dependency thresholds of 700 km (maximum downstream distance along the main river stem), and 100 km (maximum distance along tributaries from the main river stem).

5.3.4 mizuRoute simulations

First, local mizuRoute simulations are conducted for 26 individual reservoirs, using observed reservoir inflows as input forcing (section 5.4.1, appendix table 5.2). Reservoir outflow is either modelled as a natural lake with the Döll et al. (2003) parametrisation (hereafter denoted as NAT), as a human-operated reservoir with the Hanasaki et al. (2006) parametrisation (DAM) or as run-of-the river assuming there is no reservoir, using observed inflow as outflow (NOLAKES). To evaluate the use of the Hanasaki et al. (2006) parametrisation for irrigation reservoirs in particular, additional simulations are conducted with all reservoirs considered as non-irrigation reservoirs (DAM_NOIRR). Simulations are performed at daily time step, but compared to observations according to the observational time steps (daily for 18 reservoirs and monthly for 8 reservoirs).

Second, four global-scale mizuRoute simulations are conducted on a daily time step using the HDMA river network topology, gridded runoff from CLM and the IRF-UH routing method. Similar to the local simulations, four simulation types are performed. The first uses the Döll et al. (2003) parametrisation for all reservoirs and lakes on the river network (NAT). The second simulation (DAM) uses the parametrisation of Hanasaki et al. (2006) for reservoirs and dam-controlled lakes, in addition to Döll et al. (2003) for the natural lakes. Third, all lakes and reservoirs are treated as normal river segments (NOLAKES). Finally, an additional simulation is performed, similar to DAM but with all reservoirs considered as non-irrigation reservoirs (DAM_NOIRR). Comparing this simulation to the DAM simulation allows us to asses the added value of accounting for irrigation water demand using our irrigation topology. Every simulation is conducted for the period 1979-2000, of which the two first years are considered spin up and are excluded from the analysis.

5.4 Evaluation data sets and metrics

5.4.1 Local reservoir observations

Observations for reservoir inflow, outflow and storage are retrieved from the data set of Yassin et al. (2019), including information on 37 reservoirs worldwide assembled from different sources. We use a subset of 26 reservoirs from this dataset, corresponding to the reservoirs that could be located on the HDMA river network, and thus are modelled in our mizuRoute simulations (Table 5.2). Due to data availability, these reservoir observations are not evenly distributed over the globe (Fig. 5.6). The dataset provides daily inflow, storage and outflow observations for 18 reservoirs, and monthly observations for the remaining 6 reservoirs. To evaluate the global mizuRoute simulations, we complement the reservoir observations from Yassin et al. (2019), with the ResOpsUS historical reservoir data set for the contiguous United States (Steyaert et al., 2022). Of the 679 reservoirs in the dataset, we use a subset of 32 reservoirs for which both outflow and storage observations are available within the simulation period, and that are resolved on the employed HDMA river network.

5.4.2 Global streamflow indices: observations from GSIM

The Global Streamflow Indices and Metadata archive (GSIM) is a worldwide collection of indices derived from more than 35,000 daily streamflow time series (Do et al., 2018). The dataset provides quality controlled time series indices on yearly, seasonal and monthly resolution compiled from 12 databases with daily streamflow, including both research databases and national databases (Do et al., 2018; Gudmundsson et al., 2018). Here, we use the following indices, all on a monthly time scale: mean daily streamflow (MEAN; $m^3\ s^{-1}$), standard deviation of daily streamflow (SD; $m^3\ s^{-1}$) and the minimum and maximum daily streamflow (MIN and MAX, $m^3\ s^{-1}$). We only use stations that are located on the river network, based on the coordinates of the stations. First, the stations with suspect coordinates are excluded. Then, we select all stations with observation periods overlapping the simulations period (1981-2000) and within a 0.002° spatial error tolerance limit on the river network (10,233 stations). Finally, only stations less than 200 km downstream of a simulated reservoir are kept. This is results in 406 GSIM stations used in the analysis.

5.4.3 Global G-RUN runoff reconstructions

We evaluate CLM runoff using the global runoff reconstruction from the G-RUN ENSEMBLE (Ghiggi et al., 2019, 2021). G-RUN provides monthly runoff rates on a 0.5° grid for 1971-2010, based on upscaled river discharge using a machine learning algorithm (Ghiggi et al., 2019). The G-RUN ENSEMBLE extends the original G-RUN based on GSWP3 with 21 different atmospheric datasets (Ghiggi et al., 2021). In this study, we use the ensemble mean averaged for 1971-2000.

5.4.4 Evaluation metrics

Simulated time series are compared to observations for their corresponding periods using the Kling Gupta Efficiency (KGE; Gupta et al., 2009) and the absolute percent bias (PBIAS; eq. 5.6).

$$|PBIAS| = \frac{\sum_{i=1}^{n} |m_i - o_i|}{\sum_{i=1}^{n} o_i} \tag{5.6}$$

with n the number of observations m and o the simulated and observed series, respectively. To investigate the role of the different components, we use the KGE following eq. 5.7 (Gupta et al., 2009).

$$KGE = 1 - \sqrt{(r-1)^2 + \left(\frac{\sigma_{mod}}{\sigma_{obs}} - 1\right)^2 + \left(\frac{\mu_{mod}}{\mu_{obs}} - 1\right)^2} \tag{5.7}$$

with r the linear correlation between simulated and observed values, $\frac{\sigma_{mod}}{\sigma_{obs}}$, the ratio of modelled and observed standard deviation, representing the variability error, and $\frac{\mu_{mod}}{\mu_{obs}}$, the ratio of the modelled and observed means, representing the mean bias. Following Knoben et al. (2019), KGE values above -0.41 are considered better model performance compared to the mean flow benchmark.

5.5 Results

5.5.1 Local mizuRoute simulations

The local mizuRoute simulations with observed daily reservoir inflows enable directly comparing the different outflow parametrisations and run-of-the river conditions (Fig. 5.3). For outflow, the DAM simulation produces the highest KGE scores for 12 of 26 reservoirs (Fig. 5.3a), while the NAT simulation performs best for 8 reservoirs. The NOLAKES simulation typically yields good skill for reservoirs with a low capacity ratio, where outflows are strongly influenced by inflow seasonality as their storage capacity is small compared to the annual mean inflow (upper half of Fig. 5.3a, appendix Figs. 5.82 and 5.83). For all simulations, the performance of simulated outflow decreases with increasing reservoir capacity ratio, apart from a few exceptions.

For storage, the DAM simulation outperforms NAT for most reservoirs (18 out of 26; Fig. 5.3b, appendix Figs. 5.82 and 5.83), with a median KGE of 0.4 compared to 0.08. Especially for reservoirs with a high capacity ratio, DAM shows notably higher KGE values compared to NAT. This demonstrates the added value of the Hanasaki et al. (2006) parametrisation in minimizing the inter-annual outflow variability for reservoirs with a high capacity ratio. The individual time series of modelled storage show systematic over- and underestimation for the Glen Canyon, Amistad and Navajo reservoirs, with excessive outflow values indicating the reservoir reached its maximum capacity (appendix Fig. 5.82 and 5.83). In our modelling workflow, the maximum storage capacity is provided by GRanD for all reservoirs on the river network, and therefore these systematic storage biases may be caused by discrepancies between the real reservoir capacity and those reported in GRanD (e.g. for the Navajo reservoir, GRanD reports a maximum capacity of $1278 \cdot 10^6$ m^3, while the US Board of Reclamation reports a capacity of $2107 \cdot 10^6$ m^3, which better corresponds to the observations).

The comparison of the DAM with the DAM_NOIRR simulations for irrigation reservoirs reveals that accounting for irrigation only has a limited effect in the current implementation, except for Oldman, St-Mary, Nurek, Sirikit and Bhumibol reservoirs, where accounting for irrigation demands improves the outflow simulation (appendix Figs. 5.81 and 5.82). For example, Bhumibol and Sirikit are multi-year irrigation reservoirs with a clear irrigation signature in their observed outflow seasonality, as they buffer water during the high-flow season to release for irrigation during the low-flow season (Hanasaki et al., 2006). The simulated annual outflow cycle for the Sirikit reservoir shows slightly increased outflows during the low-flow season (February-May) for the original Hanasaki parametrisation compared to Hanasaki without irrigation demands (Fig. 5.82). The limited added value of accounting for irrigation demands for the 12 irrigation reservoirs suggests that reservoir irrigation demands are likely underestimated in this modelling framework (see section 5.6.2).

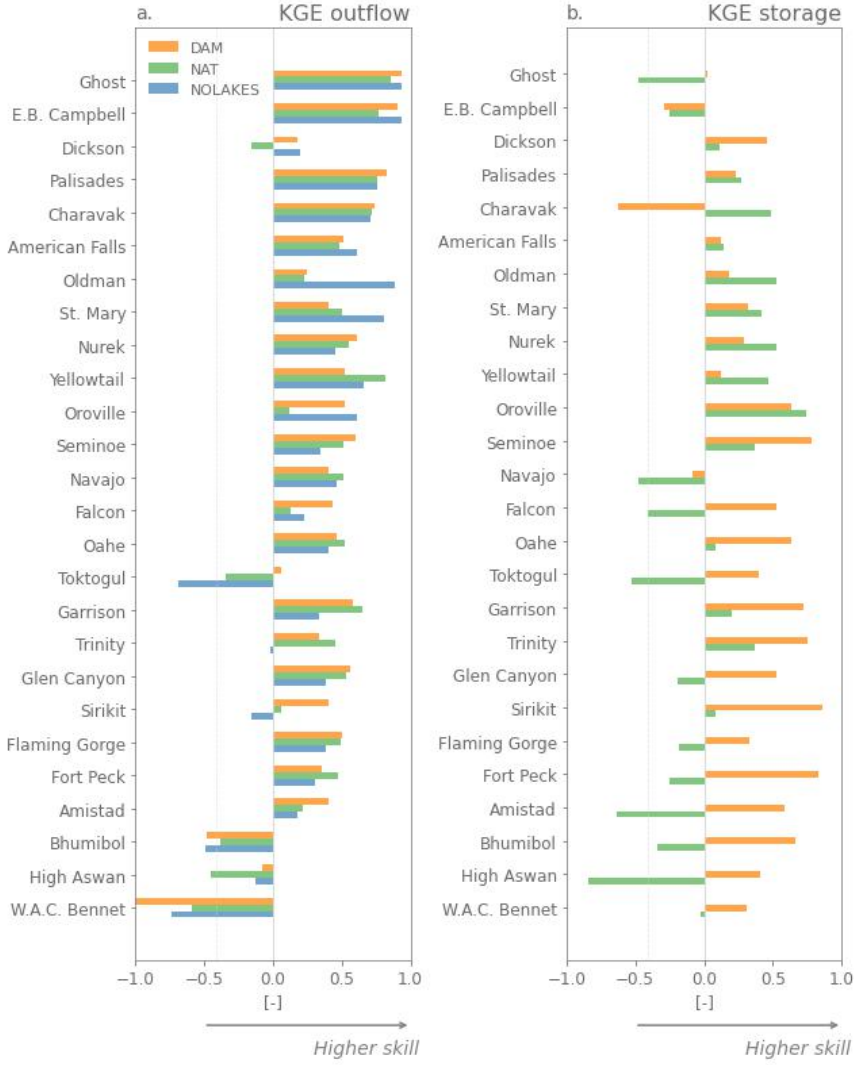

Figure 5.3: Evaluation using Kling-Gupta Efficiency (KGE) of the (Hanasaki et al., 2006, ; DAM) and (Döll et al., 2003, ; NAT) parametrisations with observed inflows, and using inflow as outflow (assuming there is no lake; NOLAKE) against observed outflow (panel a) and observed storage (panel b) using observations from Yassin et al. (2019). The reservoirs are ordered from low to high capacity ratio, defined as the ratio between the mean annual inflow and storage capacity (see Table 5.2).

5.5.2 Global-scale mizuRoute simulations: evaluation with reservoir observations

The evaluation using the Yassin et al. (2019) dataset shows that overall, the global-scale mizuRoute simulations are substantially worse than the simulations using observed inflows, with median KGE values for outflow of -0.29, -0.29 and -0.35 for the DAM, NAT and NO-LAKES simulations, respectively (Fig. 5.4b). Most reservoirs have negative KGE scores, and for four out of 26 reservoirs all simulations are outperformed by the mean annual flow benchmark. In terms of percent absolute bias for outflow, the difference between the DAM and NAT is very small or negligible for more than half of the reservoirs (Fig. 5.4a). This is also visible in the small differences between simulations in the bias term of KGE, in particular for DAM and NAT (Fig. 5.84b). For correlation, the NAT simulation has the best skill for 15 of 21 reservoirs, with highest correlations for reservoirs with low capacity ratios (Fig. 5.84c). The added value of using the Hanasaki et al. (2006) parametrisation for reservoir storage is less apparent in the global-domain mizuRoute simulation, as the DAM simulation outperforms the NAT simulation for 10 of the 21 reservoirs for absolute percent bias and KGE (Fig. 5.5). Consistent with the observation-driven local simulations, the global-domain DAM simulation performs systematically better for reservoirs with a high capacity ratio, and in most cases better than NAT. These findings are generally confirmed by the evaluation with the ResOpsUS reservoir observations, where the DAM outperforms the NAT simulation for 13 of the 32 reservoirs (Fig. 5.85).

While in the local mizuRoute application, the DAM simulation outperforms the NAT and NOLAKES simulations for most reservoirs, especially for storage, this is not the case in the global-domain mizuRoute simulations. The main cause for these discrepancies are biases in the simulated reservoir inflow, which could be originating from biases in the simulated runoff from CLM or from small reservoirs upstream and their dam operations which are not resolved in the HDMA river network, with the resultant streamflow alterations not included in the river flow. For 15 of the 21 reservoirs in the dataset, however, there is at least one upstream reservoir resolved in the HDMA river network, as only 6 reservoirs have no upstream reservoir resolved (Trinity, Navajo, Oldman, Seminoe, Sirikit and St-Mary). The same pattern is found when comparing simulated storage to the observed storage from the ResOpsUS dataset (Fig. 5.86). The next section therefore focuses on the biases in simulated inflow and runoff.

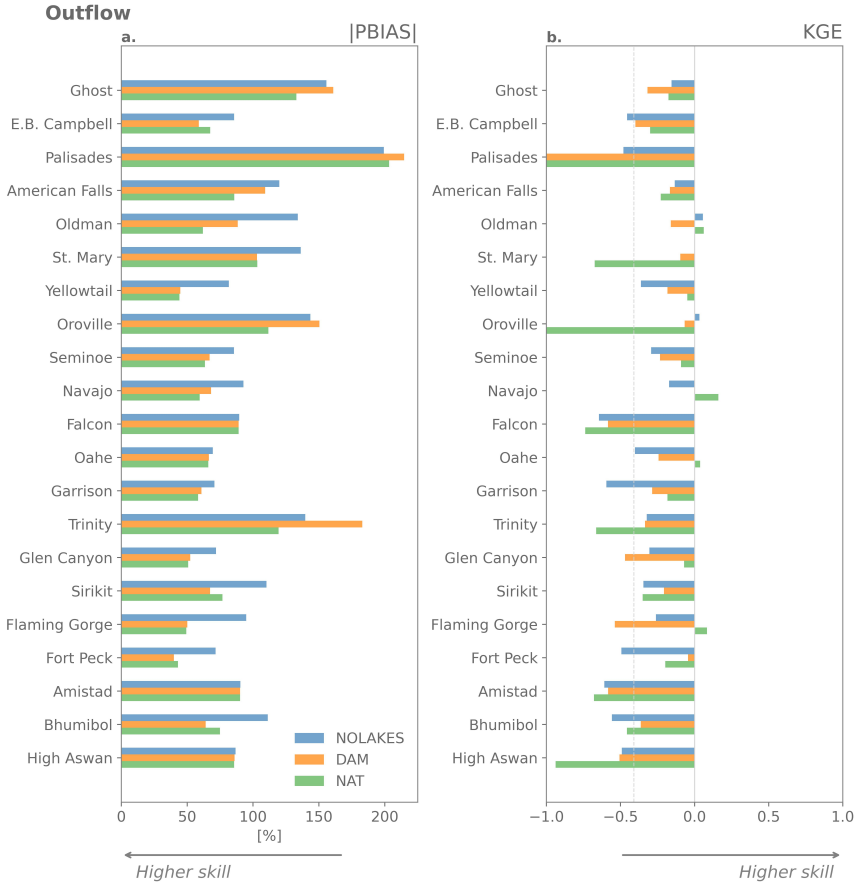

Figure 5.4: Performance of the global-domain mizuRoute simulations for outflow compared to reservoir observations using absolute percent bias (|PBIAS|; panel a) and Kling-Gupta Efficiency (KGE; panel b)

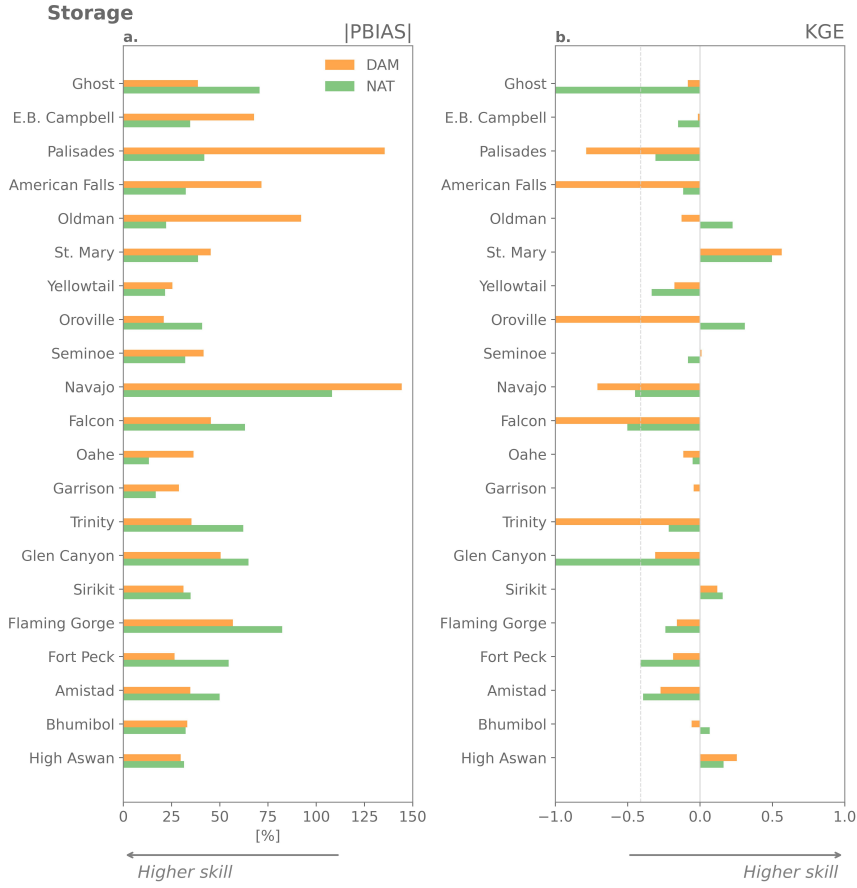

Figure 5.5: Performance of the global-scale mizuRoute simulations for storage compared to reservoir observations using the absolute percent bias (|PBIAS|; panel a) and Kling-Gupta Efficiency (KGE; panel b).

5.5.3 Inflow and runoff bias of CLM forcing

The comparison of simulated spatially distributed runoff from CLM with the global reconstructions of G-RUN reveals substantial biases (Fig. 5.6). The mean annual runoff bias is +0.077 mm day^{-1}, but regionally large differences exist: runoff is overestimated in the northwestern Amazon, West Africa, large parts of China, West India, Japan, and to a lesser extent in central US and the European mainland. CLM underestimates runoff in the tropical rainforest areas of central Amazonia and the Congo basin, and in mountain areas, like the Pakistani mountain ranges, the European Alps, the Rocky Mountains in the US and Canada, the northern part of the Andes and the Southern Alps in New Zealand.

As 20 reservoirs in the dataset are located in the Central and Western parts of the Contiguous United States and Canada, we focus on these regions to compare runoff and reservoir inflow seasonality to observations (Fig. 5.7). In the plains, runoff is generally slightly overestimated, while in the mountainous areas like the Rocky Mountains, Sierra Nevada and Cascade Range mean annual runoff is substantially underestimated (Fig. 5.7a). Via flow routing, these runoff biases translate into streamflow biases (Fig. 5.7b-s).

Overall, the simulated streamflow deviates from the observed seasonal cycles in terms of absolute bias, timing of the high flows and amplitude. The deviations can thereby roughly be grouped in four categories of reservoirs. First, for large reservoirs like Amistad and Falcon International on the Rio Grande, and Garrison and Oahe on the Missouri river (Fig. 5.7h-k), mizuRoute (forced with CLM output) largely overestimates the observed inflows (up to +1434 % for Falcon). For these reservoirs the upstream flows are highly regulated by dam operations and the positive inflow biases are therefore likely originating from unrepresented upstream dam operations (Shin et al., 2019) or from positive biases in simulated runoff (see discussion section 5.6.1). Other reservoirs have inflows highly controlled by snow melt, with their headwaters in the Rocky Mountains (Flaming Gorge, Navajo, Palisades, American Falls and Glen Canyon reservoir; Fig. 5.7n, l, r, q, m). For most of these reservoirs, the annual peak in inflow, likely coming from snow melt, is simulated 2-3 months too early (March-April-May) compared to the peak in observed inflows (June-July-August). This is also the case for the small within-a-year reservoirs in the Canadian Rocky Mountains (Oldman, Saint-Mary and Ghost reservoirs; Fig. 5.7b, c, s). These biases in runoff timing could potentially be related to unresolved topography in these coarse resolution simulations. For the mainly rain-fed Oroville and Trinity reservoirs (Fig. 5.7o, p), the release period is simulated too early in the year. Finally, some Canadian reservoirs, like E.B. Campbell show only little variation in storage, which could in part be explained by the linkages of these reservoirs with lake and swamp systems.

These inflow discrepancies point at deficiencies in the simulated runoff, as the comparison of spatially aggregated runoff from CLM versus G-RUN over the reservoir catchments show similar patterns (not shown). Moreover, local systematic biases in runoff are aggregated over the catchment and result in magnified inflow biases. Previous research showed that the runoff inputs are a more important bias source for river discharge in mizuRoute compared to the river network and routing scheme when analysed on monthly time steps (Mizukami et al., 2021). Also in other large-scale hydrological models, annual river discharge show broad range of values and large differences in runoff ratios among different models (Masaki et al., 2017; Haddeland et al., 2011).

The inflow biases are adversely affecting the skill of the reservoir parametrisation in the global-domain mizuRoute simulations compared to the local applications, especially for reservoir storage. We therefore anticipate that when the runoff simulations are improved within the driving land model, in this case CLM, improved results can be expected also in global-scale mizuRoute simulations. Therefore, we focus on comparing the DAM simulation to the NOLAKES simulation in the remainder of this paper.

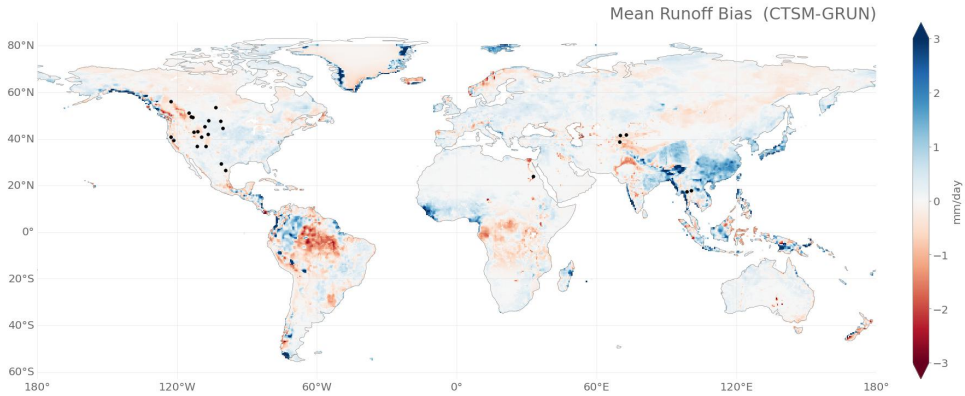

Figure 5.6: Mean runoff bias of CLM, compared to G-RUN for the period 1971-2000. Black circles indicate the reservoirs used from the Yassin et al. (2019) data set.

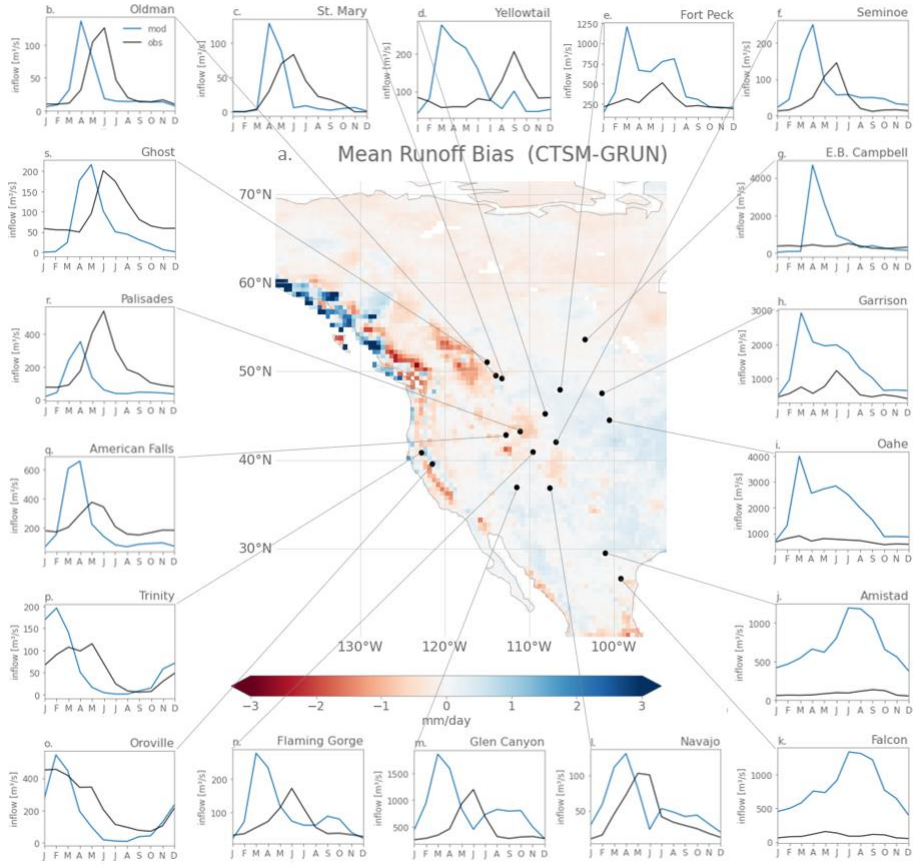

Figure 5.7: Mean runoff bias of CLM compared to G-RUN for CONUS and Canada with location of reservoirs (panel a). Simulated (blue line) and observed inflow (black line) seasonality per reservoir (panels b-s)

5.5.4 Global-scale mizuRoute simulations: evaluation for global streamflow indices

We evaluate the global impact of accounting for dam operations on long-term river discharge by comparing the skill of the DAM with the NOLAKES simulation for observed monthly streamflow indices from the GSIM archive (Fig. 5.8). In general, the DAM simulation shows improved skill compared to the NOLAKES simulation (Fig. 5.8e-h), with a median absolute percent bias for mean flows of 72 % compared to 81 %. The improvement is particularly strong for the standard deviation, with a mean absolute percent bias of 187 % for NOLAKES compared to 100 % for DAM, indicating an improvement of the total streamflow variability (Fig. 5.8c). This is not surprising, as reservoir operations typically minimize streamflow variability (Hanasaki et al., 2006). For high floods, the DAM simulation outperforms NOLAKES (79 % compared to 114 % mean absolute bias), with the best improvements in Canada, Western United States and Central Africa (Fig. 5.8e). Finally, for low floods, the overall improvement is smaller, with a mean absolute bias of 79 % for DAM compared to 91 % for NOLAKES, with the latter providing remarkably better results in India and southwestern USA.

Comparing the DAM and NAT simulations, it is remarkable that NAT shows the best skill for monthly standard deviation (Fig. 5.8f and appendix Fig. 5.88c), which could point at a better buffering of the biased river streamflow by the natural lake scheme of Döll et al. (2003). This corresponds to the findings of the global-scale mizuRoute evaluation to individual reservoirs observations (section 5.5.2). As the Hanasaki et al. (2006) parametrisation mainly depends on mean annual and monthly inflows, it suffers from the inflow biases, while the natural lake parametrisation of Döll et al. (2003) mainly attenuates the incoming inflow. In India and in southeastern US, daily low flows are better represented in the NOLAKES simulation (Fig. 5.8d). Overall, the difference between NAT and DAM is small compared to the difference between not representing lakes and representing lakes. On average, NAT is outperforming DAM for the mean, standard deviation and monthly maximum indices. For low flows however, DAM shows the best performance, with a median absolute percent bias of 90 % for the NAT simulation compared to 79 % for DAM (Fig. 5.8h). Especially in India and in southern Africa, the DAM simulation shows substantially higher skill in representing low flows (appendix Fig. 5.88).

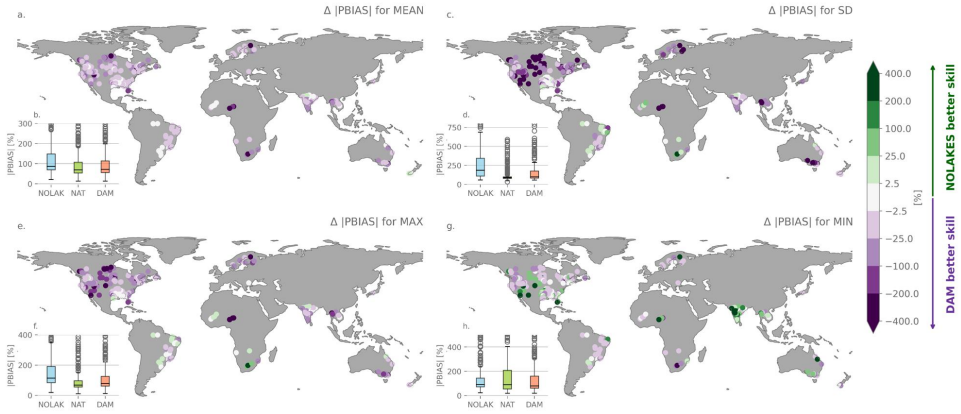

Figure 5.8: Performance of global-scale mizuRoute simulations for streamflow indices of GSIM. Added value in absolute percent bias of accounting for reservoirs (DAM) over simulations without lakes or reservoirs (NOLAKES) ($|PBIAS|_{DAM}$-$|PBIAS|_{NOLAKES}$) for monthly mean streamflow (MEAN; panel a), monthly streamflow standard deviation (SD; panel b), monthly maximum streamflow (MAX; panel c) and monthly minimum streamflow (MIN; panel d). Note the non-linear colorbar scale. Inset panels (e-h) show the |PBIAS| for the simulation without lakes (NOLAKE), with only natural lakes (NAT) and accounting for reservoirs (DAM). Only GSIM stations on the river network, maximum 200 km^2 downstream of a reservoir and with observations in the simulation period are included.

5.6 Discussion

5.6.1 Reservoir parametrisation and river network

The deterioration in skill of the Hanasaki et al. (2006) parametrisation relative to natural lakes when using simulated inflow, indicates a larger sensitivity of the Hanasaki et al. (2006) scheme to inflow magnitude and timing, which exacerbates the bias. The parametrisation of Hanasaki et al. (2006) is designed to provide generic operational rules, rather than observation-driven release rules for individual reservoirs (Turner et al., 2020). These generic rules likely exacerbates bias at some of the reservoirs. However, individual calibration could improve simulated releases of modelled reservoirs. Especially for highly regulated rivers with a series of cascading reservoirs, calibration schemes of upstream reservoir releases could improve the modelled river streamflow (Shin et al., 2019). However, prior to conducting such parameter calibration, it would be advisable to first reduce biases in the reservoir inflows as simulated by CLM (section 5.6.3).

The overestimated inflow for reservoirs with highly regulated upstream flows, like Amistad and Falcon International on the Rio Grande (Fig. 5.7j-k), is likely due to unresolved reservoirs upstream. For example, only 6 of the 23 dams and water diversions on the Rio Grande are resolved within the current river network, which could be attributed to the following reasons. First, cascade systems and run-of-river dam infrastructures (e.g. Leasburg and Isleta dams on the Rio Grande), which control the river flow but do not store water, are generally not included in GRanD and therefore are not in the river network. Second, several dams and associated reservoirs are not on the stream network due to the network resolution (e.g. the remote Platoro reservoir on the Conejos river). Third, reservoirs smaller than the area threshold of 10 km^2 are not included on the river network (e.g. Sumner reservoir).

These issues could be accommodated by the use of higher resolution stream networks on which more reservoirs would be resolved, like the Multi-Error-Removed-Improved-Terrain (MERIT) Hydro network which is derived from a global DEM at 3 arcsec resolution ($\sim$90 m; Yamazaki et al., 2019). An accurate high-resolution DEM is important to improve the reservoir representation and release, as has been shown by Shin et al. (2019). The choice of river network proves however to be less important compared to the runoff input from the land model for global-scale river flow simulations without lakes and reservoirs (Mizukami et al., 2021), so accounting for and reducing runoff biases remains an essential step. Finally, to account for run-of-river dams, the GRanD database could be updated or complemented by other data sources like the Global Georeferenced Database of Dams (GOODD; Mulligan et al., 2020).

The parametrisation of Hanasaki et al. (2006) is designed to provide generic operational rules, rather than observation-driven release rules for individual reservoirs (Yassin et al., 2019; Turner et al., 2020). In a recent study for CONUS and Canada, Turner et al. (2021) showed that empirically derived reservoir operating rules based on historical reservoir operations significantly improve release and storage simulations compared to the Hanasaki et al. (2006) scheme, even when extrapolated to similar reservoirs without historical records available. While such an approach provides promising results, it is only tested with observed reservoir inflows, and limited to regions where data-rich reservoirs can be representative for the operation rules and hydrological conditions of data-scarce reservoirs. In a coupled framework, the method would still propagate the inflow biases coming from the driving model, but might have improved storage representation due to the targeted operation range (Turner et al., 2021). In the context of ESMs and future projections however, generic methods allow to incorporate future climate changes and their impacts on the river flows and irrigation demands on a global scale.

5.6.2 Irrigation demand and topology

The local mizuRoute simulations showed only small differences in outflow values for the DAM and DAM_NOIRRIG simulations for irrigation reservoirs. Our results suggest that the total irrigation water demand per reservoir is underestimated, and that there are also potential biases in the irrigation seasonal cycle. These uncertainties are either originating

from the irrigation topology, defining the area to which the reservoir water is allocated, or from the gridded irrigation amounts simulated by CLM. Since applying the irrigation topology with different thresholds (1000 km instead of 700 km downstream along the main river stem and 200 km instead of 100 km along the tributaries) did not significantly improve the irrigation demands, disparities in simulated irrigation amounts likely play a major role.

The irrigation module in CLM is calibrated with one free parameter based on global observed irrigation water withdrawals from AQUASTAT (Thiery et al., 2017, 2020). It is however possible that these country-based irrigation amounts are under-reported by individual countries. In addition, while global crop calendar data exists to a limited extend (e.g. Sacks et al., 2010), there is almost no information on timing and amount of global irrigation water withdrawals to use for model evaluation. Yet, there are various possible pathways to improve the simulation of irrigation water withdrawal, like differentiating irrigation techniques applied in different regions around the world (Jägermeyr et al., 2015) and including crop rotation and other agricultural management practices (e.g. Hirsch et al., 2017, 2018). Furthermore, the use of remotely sensed soil moisture to estimate the amount and timing of irrigation demonstrates promising results (Brocca et al., 2018; Zaussinger et al., 2019; Massari et al., 2021; Lawston et al., 2017). Future improvements in the irrigation module of CLM will likely lead to improvements in the simulated reservoir storage and release.

Apart from the uncertainties in gridded irrigation demands from CLM, there are several opportunities to improve the irrigation topology routine. Here, we use the HDMA river network topology and determine the HRUs contributing to reservoir water demand, using simple rules based on distance and bottom elevation of river segments. However, more detailed river networks, like MERIT-Hydro (Yamazaki et al., 2019) enable refining the criteria. For example, MERIT-Hydro now includes more topological details such as the Height Above Nearest Drainage index (Nobre et al., 2011; Gharari et al., 2011). Future improvements of the irrigation topology could also account for water transfers, including water diversion for irrigation at weirs (Hanasaki et al., 2021).

5.6.3 Runoff biases in CLM

The inflow biases shown in section 5.5.3 for the reservoirs in contiguous United States and Canada, can be roughly subdivided into reservoirs where there is a bias in inflow timing, and reservoirs where the inflow is largely overestimated, with some exceptions. In our modelling framework, the biases in inflow timing for reservoirs with mountainous headwaters could originate from the lack of a representation of high elevation snow pack, and the associated timing of snow melt, in these relatively coarse resolution simulations. Another potential source of uncertainty is the sensitivity of runoff simulations to the meteorological forcing providing biased timing and amounts of precipitation, especially in high mountain catchments, which affect the runoff ratios. We tested these hypotheses by running mizuRoute over the North-American domain using a high resolution CLM simulation forced with North American Land Data Assimilation System NLDAS meteorological

forcing on a high resolution grid (0.125°; appendix Fig. 5.87). These simulations did not improve magnitude or timing of the inflow biases, so likely these uncertainties may be coming from CLM's representation of hydrological processes (e.g., the seasonal cycles of snow accumulation and melt). For the large reservoirs with headwaters in the plains like Falcon International and Amistad reservoir, a second reason for the large positive inflow biases next to unresolved upstream river regulation, is the suspected underestimation of the amount of irrigation water applied (section 5.6.2). In addition, CLM does not include water abstractions for domestic and industrial purposes (Telteu et al., 2021), which would explain the high bias in simulated streamflow.

There are several potential avenues for future model development that could potentially reduce the model runoff and streamflow errors, especially the timing errors. Natural processes related to snow accumulation and melt dynamics could be investigated and improved. Ongoing work with the new representative hillslope model within CLM, which now includes temperature and precipitation downscaling as well as the impacts of slope and aspect on hillslope to lateral flow, could potentially help resolve early runoff peak biases (Swenson et al., 2019). Felfelani et al. (2021) have also explored how explicit grid-to-grid lateral flow can improve high-resolution CLM simulations. Additionally, CLM parameters, which have previously been calibrated for evapotranspiration and gross primary production (Dagon et al., 2020), could be calibrated for runoff as well.

5.6.4 Future work on representing reservoirs in a coupled Earth System Model

The modelling framework in this study is an application of the routing scheme mizuRoute and the land model CLM, the land component of CESM, in which both models are employed in standalone mode. Prior to the simulation, mizuRoute remaps the gridded runoff, gridded precipitation and lake tile evaporation of CLM to the vector-based river network. In addition, the parameters needed for the Hanasaki scheme (table 5.1), like mean monthly reservoir inflow and the initial release coefficient, are calculated in an intermediate processing step before being used in the mizuRoute simulation. Finally, the mean monthly irrigation demand per reservoir is calculated using the irrigation topology prior to the mizuRoute simulation.

The coupling of mizuRoute to CLM and CESM will enable to directly route runoff from the land to the ocean with a network-based routing mode, thereby accounting for streamflow alteration through dam operations. Future work on coupling the vector-based model to the gridded land model will require an on-the-fly remapping step to communicate runoff from the land model to the vector-based river network. As the water balance of natural lakes and reservoirs is simulated within mizuRoute using precipitation and lake evaporation from CLM, the coupling would also enable more realistic lake and reservoir water balance dynamics to the Earth System Model, which were hereto not simulated (Gharari et al., 2022; Vanderkelen et al., 2021; Mizukami et al., 2021).

In addition to the water fluxes related to the lake and reservoir water balances, mizuRoute will need the gridded irrigation water demand from CLM, which can be aggregated to individual reservoirs using the irrigation topology. In a one-way coupling, mizuRoute will use this irrigation demand seasonality to determine the dam release for irrigation reservoirs. The two-way coupling of CLM and mizuRoute would ultimately allow for water to be extracted directly from the river for irrigation, thereby using runoff generated in upstream grid cells. In this way, the actual availability of water for irrigation would be better represented. To this end, the irrigation topology could serve as a blueprint for transporting irrigation water across grid cells. Eventually, the coupled system will enable more accurately modelling the human alteration of water resources globally in the present, and under different future emission and socioeconomic scenarios.

5.7 Conclusions

In this study, we evaluate a reservoir parametrisation (Hanasaki et al., 2006) that we integrated into the river routing model mizuRoute and assess how a simple treatment of human dam regulation affects global streamflow simulations. To this end, we develop an irrigation topology based on the vector-based river network that provides the area over which water demand is aggregated for each individual irrigation reservoir. Local mizuRoute simulations for 26 reservoirs using observed inflows demonstrate that the reservoir parametrisation has added value compared to the natural lake scheme of Döll et al. (2003) for the simulation of reservoir release and storage. The reservoir parametrisation shows high skill in simulating reservoir storage, particularly for reservoirs with a multi-year storage capacity. The benefits of accounting for irrigation demand seasonality appears to be limited in the existing modelling framework, but this could be either due to a spatial sampling bias of reservoirs with observations available or uncertainties in the simulated irrigation demand.

Biases in modelled river discharge, which can be attributed to runoff biases in CLM, prevent strict validation with observations of the impact from reservoir operations. However, monthly streamflow indices indicate that accounting for lakes and reservoir regulation does appear to improve the representation of mean and high flows as well as flow variability, even if the total amount and timing of runoff is biased.

Our results highlight the opportunities and challenges of global-scale reservoir and streamflow simulations, and provide an essential step for representing reservoirs in Earth System Models and for incorporating human dam operations in global assessments of water resources availability under present-day and future climates. This enables exploring the role of different reservoir management strategies and priorities in altering water availability under climate change. Moreover, modelling reservoirs in a coupled system will allow to more accurately evaluate water availability for human consumption, irrigation and ecosystems, while accounting for interactions between water management, atmospheric processes and climate change drivers.

Data and code availability

The reservoir dataset described in Yassin et al. (2019) is available at http://doi.org/10.5281/zenodo.1492043. The GSIM data can be found at https://doi.pangaea.de/10.1594/PANGAEA.887477, while the G-RUN ENSEMBLE reconstructions are available at https://doi.org/10.6084/m9.figshare.12794075. The HydroLAKES dataset is available at https://www.hydrosheds.org/page/hydrolakes, GRanD at http://globaldamwatch.org/ and the HDMA dataset at https://www.sciencebase.gov/catalog/item/5910def6e4b0e541a03ac98c. The source code of mizuRoute (tag cesm-coupling.n00_v2.0.1) is publicly available at https://github.com/ESCOMP/mizuRoute and CLM5.0 is available through the Community Land Model (CLM) repository: https://github.com/ESCOMP/CLM/. The scripts used in this study are available at: https://github.com/VUB-HYDR/2022_Vanderkelen_etal_GMD with the DOI: 10.5281/zenodo.6490979. Finally, all inputdata, ancillary data and settings used to conduct the mizuRoute simulations used in the analysis are available at https://doi.org/10.6084/m9.figshare.c.5965053.v1.

Acknowledgements

The authors would like to thank Erik Kluzek for his support on CLM. This research is supported by the Research Foundation Flanders (FWOTM920). The CESM project is supported primarily by the National Science Foundation (NSF). This material is based upon work supported by the National Center for Atmospheric Research, which is a major facility sponsored by the NSF under Cooperative Agreement No. 1852977. Computing and data storage resources, including the Cheyenne supercomputer (doi:10.5065/D6RX99HX), were provided by the Computational and Information Systems Laboratory (CISL) at NCAR. We thank all the scientists, software engineers, and administrators who contributed to the development of CESM2. Other storage resources and services used in this work were provided by the VSC (Flemish Supercomputer Center), funded by the Research Foundation - Flanders (FWO) and the Flemish Government. This study was supported by the LAMACLIMA project, part of AXIS, an ERA-NET initiated by JPI Climate, and funded by BELSPO (BE, Grant No. B2/181/P1) with co-funding by the European Union (Grant No. 776608).

5.8 Supplementary material

Table 5.1: Parameters for the Hanasaki et al. (2006) reservoir parametrisation in mizuRoute.

Parameter	Unit	Value	Description
S_{max}	m^3	from GRanD	Maximal reservoir storage
α	-	0.85	Fraction of active storage compared to total storage (value from Hanasaki et al., 2006)
β	-	0.9	Fraction of inflow that can be used to meet demand (value from Biemans et al., 2011)
S_{ini}	m^3	S_{max} from GRanD	Initial storage, used to calculate release coefficient before start of operational year
c_1	-	0.1	coefficient 1 of target release calculation (value from Hanasaki et al., 2006)
c_2	-	0.9	coefficient 2 of target release calculation (value from Hanasaki et al., 2006)
$exponent$	-	2	Exponent in actual release calculation (value from Hanasaki et al., 2006)
$denominator$	-	0.5	Denominator in actual release calculation (value from Hanasaki et al., 2006)
$c_{compare}$	-	0.5	Criterion to distinguish between "multi-year" and "within-a-year" reservoirs, compared against c (value from Hanasaki et al., 2006)
E_r	-	calculated based on GRanD	Release coefficient (provided with initial value and updated every start of operational year)
$I_{m,jan}$ - $I_{m,dec}$	$m^3 s^{-1}$	from CLM (preprocessed)	Mean monthly reservoir inflow
$D_{m,jan}$ - $D_{m,dec}$	$m^3 s^{-1}$	from CLM (preprocessed)	Mean monthly reservoir demand
$purpose$	-	from GRanD	Reservoir purpose (0 non-irrigation, 1 irrigation)

Table 5.2: Reservoirs of the Yassin et al. (2019) observational dataset used in this study. The asterisk in the observation period column indicates this reservoir has monthly instead of daily observations. Maximum capacity is derived from GRanD.

Dam name	**Country**	**Main purpose**	**Capacity (mcm)**	**Period**	**Capacity ratio**
American Falls	USA	irrigation	2061.5	1978-1995	0.30
Amistad	USA/Mexico	irrigation	6330	1977-2002	2.48
W. A. C. Bennett	Canada	hydropower	74300	2003-2011	3.27
Bhumibol	Thailand	irrigation	13462	1980-1996	2.62
Charavak	Uzbekistan	hydropower	2000	2001-2010*	0.28
Dickson	Canada	water supply	203	2005-2011	0.18
E.B. Campbell	Canada	hydropower	2200	2000-2011*	0.16
Falcon International	USA/Mexico	flood control	3920	1958-2001	1.20
Flaming Gorge	USA	water supply	4336.3	1971-2017*	2.27
Fort Peck	USA	flood control	23560	1970-1999*	2.43
Garrison	USA	flood control	30220	1970-1999	1.41
Ghost	Canada	hydropower	132	1990-2011	0.05
Glen Canyon	USA	hydropower	25070	1980-1996*	1.67
High Aswan	Egypt	irrigation	162000	1971-1997	2.79
Navajo	USA	irrigation	1278	1971-2011	1.07
Nurek	Tajikistan	irrigation	10500	2001-2010*	0.50
Oahe	USA	flood control	29110	1970-1999	1.22
Oldman	Canada	irrigation	490	1996-2011	0.44
Oroville	USA	flood control	4366.5	1995-2004*	0.72
Palisades	USA	irrigation	1480.2	1970-2000	0.24
Seminoe	USA	irrigation	1254.8	1951-2013	1.05
Sirikit	Thailand	irrigation	9510	1980-1996	1.82
St. Marry	Canada	irrigation	394.7	2000-2011	0.50
Toktogul	Kyrgyzstan	hydropower	19500	2001-2010*	1.39
Trinity	USA	irrigation	2633.5	1970-2000	1.51
Yellowtail	USA	irrigation	1760.6	1970-2000	0.57

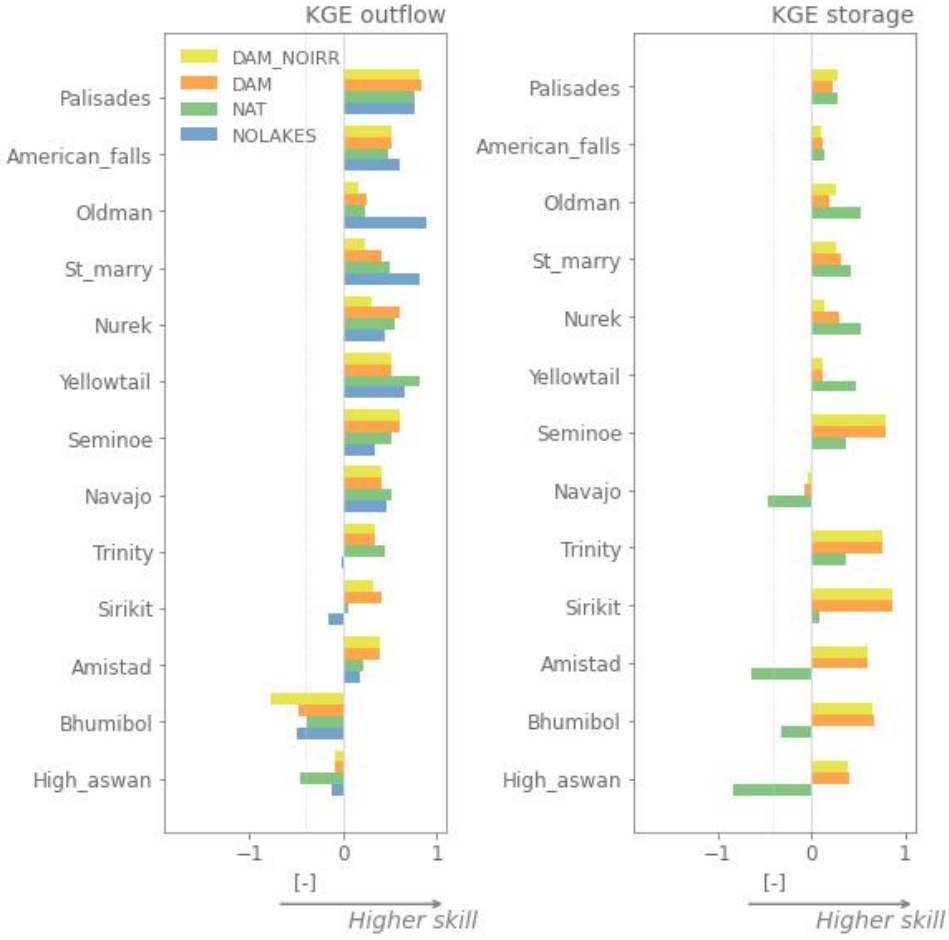

Figure 5.81: Evaluation with Kling-Gupta Efficiency (KGE) for irrigation reservoirs of the Hanasaki et al. (2006) (DAM) and (Döll et al., 2003) (NAT) parametrisations with observed inflows, and run-of-the river conditions (assuming there is no lake; NOLAKE) against observed outflow (panel a) and observed storage (panel b) using observations from Yassin et al. (2019). The reservoirs are ordered from low to high capacity ratio.

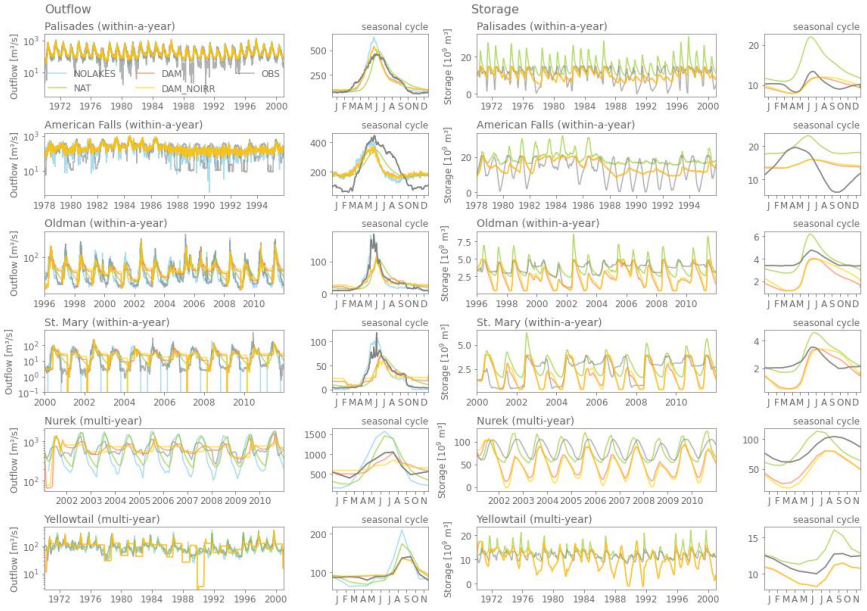

Figure 5.82: Time series and seasonal cycles of outflows and storage of observation driven simulations using the Hanasaki et al. (2006) parametrisation with and without accounting for irrigation (DAM and NO_DAM, respectively), the natural lakes Döll et al. (2003) parametrisation (NAT) and run-of-the river conditions (NOLAKES), all for irrigation reservoirs, compared to observations. Note the logarithmic axis for the outflow time series.

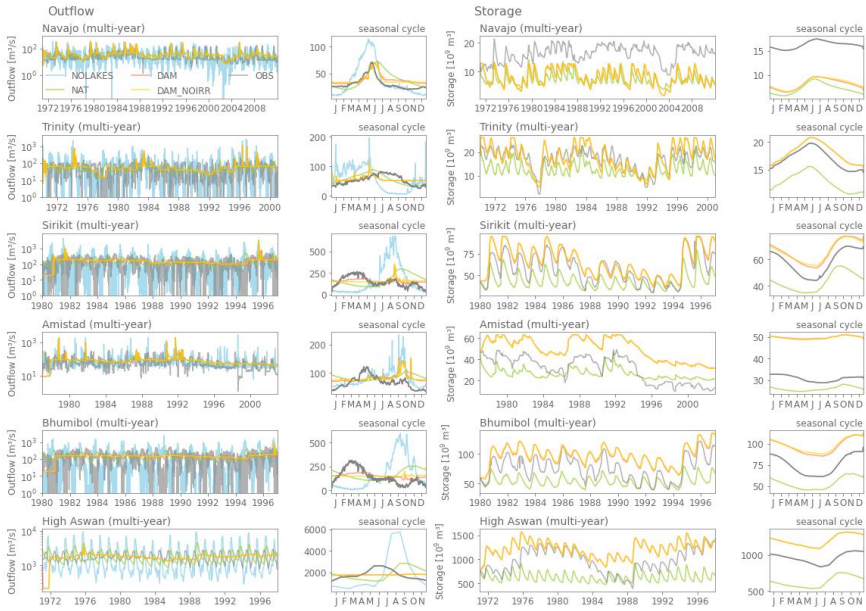

Figure 5.82: Continued.

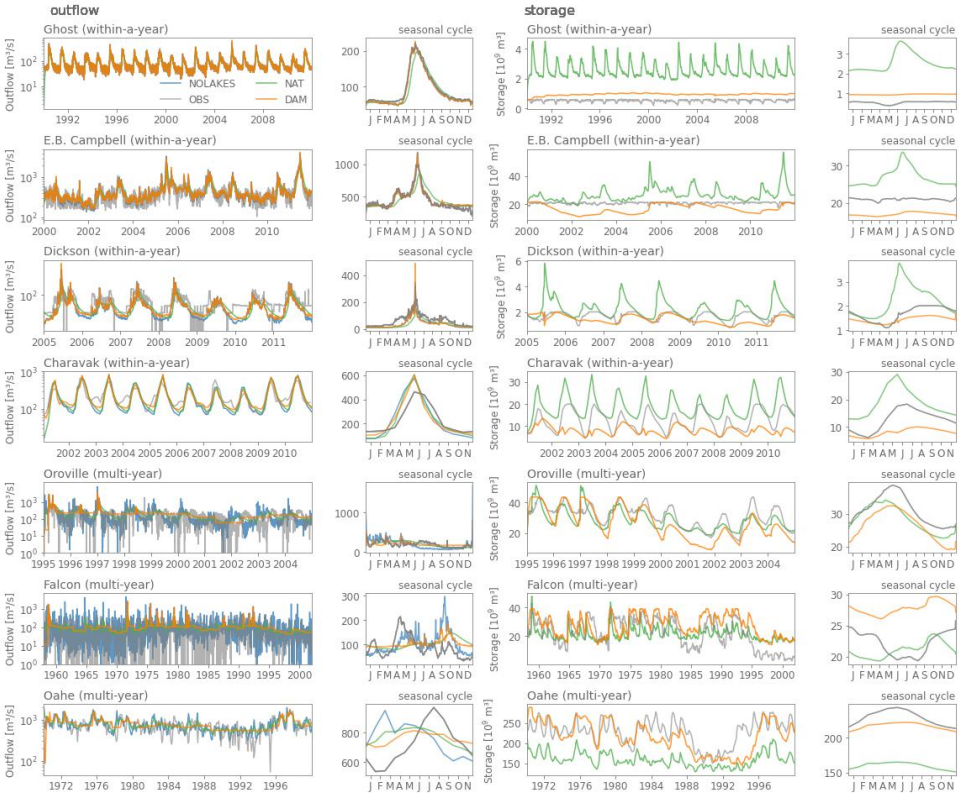

Figure 5.83: Same as Fig. 5.82, but for non-irrigation reservoirs.

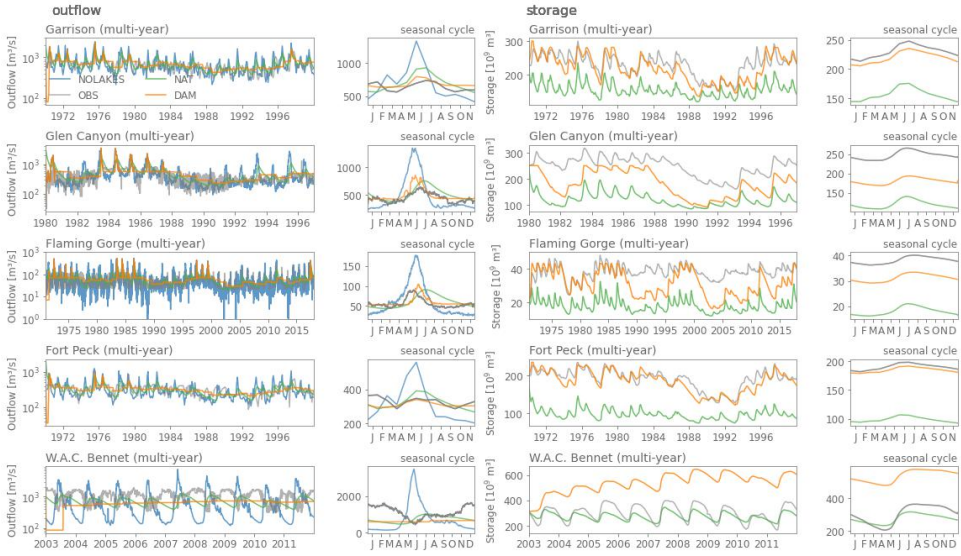

Figure 5.83: Continued.

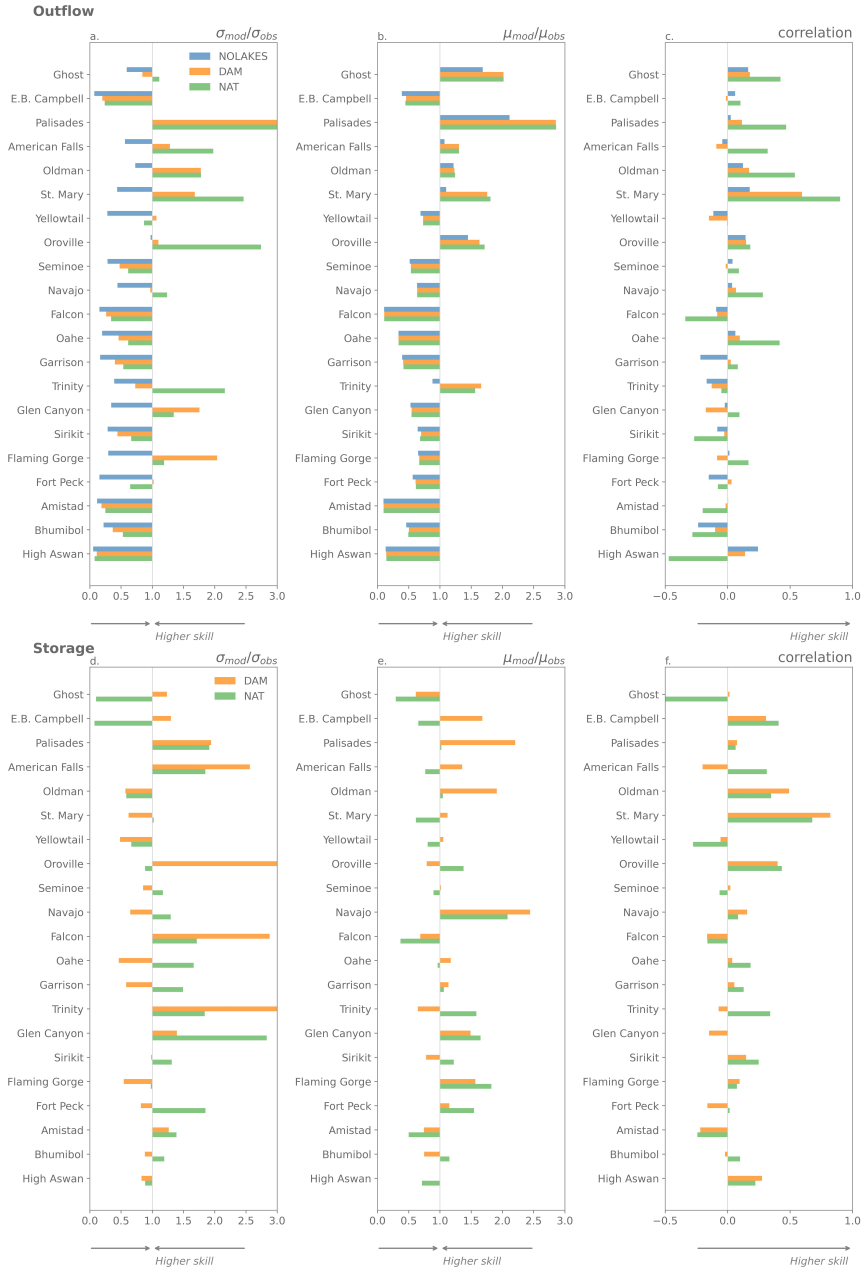

Figure 5.84: Performance for mizuRoute simulations for outflow (panel a-c) and storage (panel d-f) compared to reservoir observations using the KGE terms: variability error ($\frac{\sigma_{mod}}{\sigma_{obs}}$; panels a, c), mean bias ($\frac{\mu_{mod}}{\mu obs}$; panels b, e) and correlation (panels c, f).

Figure 5.85: Performance of the global-scale mizuRoute simulations for outflow compared to reservoir observations from the ResOpsUs dataset (Steyaert et al., 2022) using absolute percent bias (|PBIAS|; panel a) and Kling-Gupta Efficiency (KGE; panel b)

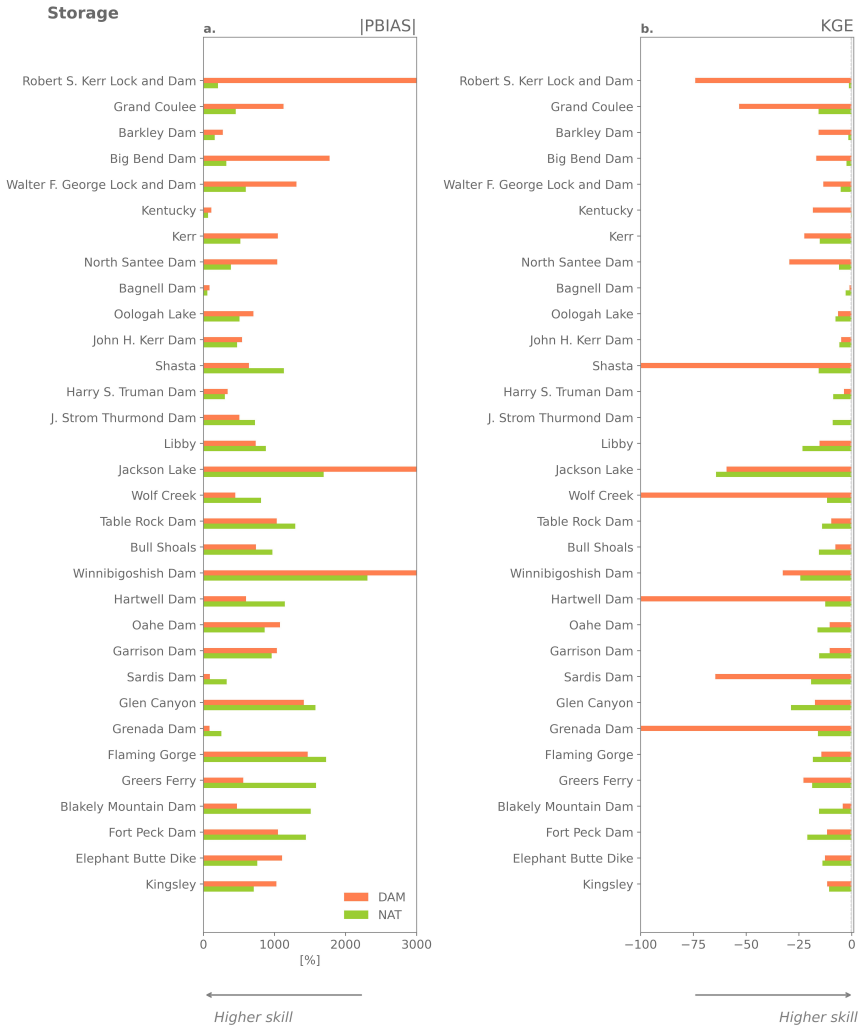

Figure 5.86: Performance of the global-scale mizuRoute simulations for storage compared to reservoir observations from the ResOpsUs dataset (Steyaert et al., 2022) using the absolute percent bias (|PBIAS|; panel a) and Kling-Gupta Efficiency (KGE; panel b).

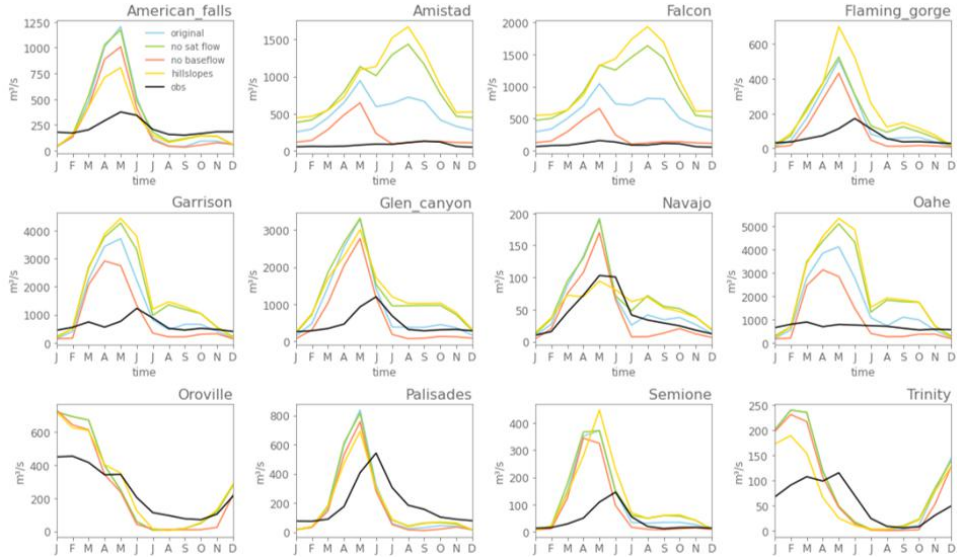

Figure 5.87: Simulated and observed inflow seasonality per reservoir with mizuRoute using runoff from different CLM simulations at 0.125° resolution with meteorological forcing from NLDAS. In the legend, 'original' refers to the simulation with the default CLM version used in the main analysis, 'no sat flow' refers to the simulation where surface saturation excess runoff is set to 0, 'no baseflow' refers to the simulation with a decreased baseflow parameter, 'hillslopes' refers to the simulation using the hillslope model described in Swenson et al. (2019), performed at 0.5° horizontal resolution, and 'obs' are the observed inflows from the Yassin et al. (2019) dataset.

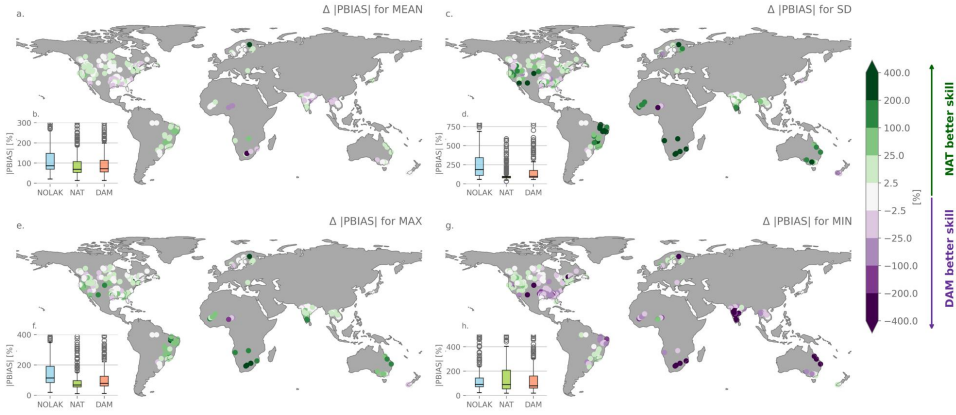

Figure 5.88: Same as Fig. 5.8 but for the absolute percent bias for natural lakes compared to reservoirs ($|\text{PBIAS}|_{\text{DAM}}$-$|\text{PBIAS}|_{\text{NAT}}$)

Chapter 6

Conclusion

6.1 Concluding summary

Humans are fundamentally altering the terrestrial water cycle. It is therefore key to account for human water management when investigating global-scale processes related to water. Dams and reservoirs are principal human interventions of the terrestrial water cycle, as they modify the timing, peak and magnitude of streamflow worldwide and influence the seasonal and inter-annual water availability. Moreover, dam construction and the subsequent creation of new water bodies transform the surface characteristics. At the same time, human-driven greenhouse gas emissions and land use changes cause a radiative imbalance and energy accumulation in the Earth system, leading to global warming. Anthropogenic climate change is fundamentally altering the hydrological cycle and has large impacts on global freshwater processes from global to local scales. An example reservoir is Lake Victoria, where historical lake levels and dam managements can be represented with a simple water balance model, but future lake levels in response to a range of climate change scenarios and different dam management strategies is unknown. Next to the one-way climate change impacts, reservoirs also directly influence the climate through the surface water interactions with the overlying atmosphere. The physical mechanisms behind these interactions remain, however, unexplored. To study reservoirs and their role in the global water cycle, coupled modelling frameworks are required that account for the two-way interactions between reservoirs and the climate. Such frameworks are provided by Earth System Models (ESMs). Yet, these models often lack a representation of human water management and reservoirs in their land and river components. Accounting for reservoirs is, however, key to improve the simulation of the terrestrial water cycle, and its effects on other components of the Earth system, particularly in a changing climate.

In this thesis, we aim to address the above-mentioned challenges to improve our understanding of reservoirs in the climate system both from a climate change impact and an Earth system perspective. The case study of the future water level projections for Lake Victoria (chapter 2) is a stepping stone to investigate interactions between human dam management

and climate change at a larger scales. Subsequently, we move to the global scale, to shed light on the potential of reservoirs and other inland water bodies to store abundant heat in a changing climate (chapter 3). In the last two contributions of this thesis, we advance the representation of reservoirs in the Community Earth System Model (CESM), by including historical lake expansion through reservoir construction (chapter 4) and accounting for dam operations in the river flow (chapter 5). These developments improve the representation of the terrestrial water cycle in ESMs by including a key component of human water management, and will eventually allow to study future changes in water availability for food, fiber and energy in fully coupled climate models. Below we summarize our key findings and provide avenues for future research directions.

The case study on Lake Victoria's future water levels demonstrates the interplay of climate change and idealised human dam management in projecting future impacts related to water availability (introduction section 1.3 and chapter 2). The effect of future climate change on lake level fluctuations is characterized by substantial uncertainties, originating from the simulations with Regional Climate Models (RCMs) forced by General Circulation Models (GCMs). For example, even after bias correction, individual RCM simulations do not agree on the sign of change in future over-lake precipitation, the water balance term responsible for most of the lake level variability. In a sustainable management scenario, these uncertainties range up to 3.9 m, corresponding to 299% of the projected multi-model mean. These results highlight the need for adequate representations of lakes and their exchanges with the atmosphere in RCMs, to provide reliable climate change projections for impact studies in the African Great Lakes region.

Regardless of the uncertainty associated to future climate change, we show that dam operation strategies are key for sustaining future lake levels within desirable limits. While the dam management strategies employed in the study are idealised scenarios, and are therefore likely not representative of realistic settings, they illustrate the strong influence of operation decisions on the future lake level evolution. Only the Agreed Curve scenario, which mimics natural outflow based on lake level governed by climate and inflow variability, treating Lake Victoria as a natural lake, could ensure sustainable future lake levels can be sustained. The controlling ability of human dam operations is further confirmed by severe lake level drop in 2004-2005, as it can only be explained by an enhanced outflow compared to the Agreed Curve (48 %) in addition to the prevailing drought conditions (52%). Overall, the Lake Victoria case study highlights the importance of human dam management for reservoir storage dynamics, water availability and the terrestrial water cycle as a whole. The results also underline the need to include reservoirs and their management in climate models, in order to study lake-climate interactions and climate change impacts on reservoirs.

The energy imbalance at the top of the atmosphere, caused by human-induced greenhouse gas emissions leads to net heat accumulation in the Earth System. Most of this excess energy is buffered by the oceans, and smaller amounts are used to melt the land and sea ice, and warm both atmosphere and continents. The fraction of heat taken up by lakes, reservoirs and rivers, however, is hereto unknown, despite the high heat capacity of wa-

ter. In chapter 3, we quantify this human-induced heat storage, using a suite of impact model simulations available from the Inter-Sectoral Impact Model Intercomparison Project (ISIMIP) phase 2b, including three global lake models (CLM4.5, SIMSTRAT-UoG and ALBM) and two global hydrological models (WaterGAP2 and MATSIRO), each forced by bias-adjusted atmospheric forcing from four ESMs (GFDL-ESM2M, HadGEM2-ES, IPSL-CM5A-LR and MIROC5). The total inland water heat uptake amounts up to $2.6 \pm 3.2 \cdot 10^{20}$ J. This corresponds to 3.6% of the continental heat uptake, which is proportional to the share of inland waters coverage of global continental area ($\sim$ 2.58 %).

While the amount of heat taken up by inland waters is small compared to the energy buffered by other components of the Earth system, local impacts of rising water temperatures can be large (Kraemer et al., 2021; Woolway et al., 2021). Furthermore, the quantification of inland water heat uptake term advances the Earth's heat inventory with a more complete quantification of the spatial distribution and amount of energy accumulation in different Earth System components (Von Schuckmann et al., 2020). As the targets set in the Paris Agreement require to halt the energy imbalance in order to stabilize the climate, it is key to map the Earth's heat inventory, including the inland water term. The quantification therefore directly featured in the Working Group I contribution to the 6$^{\text{th}}$ Assessment Report of the Intergovernmental Panel on Climate Change (IPCC), published in August 2021 (Forster et al., 2021).

The increase in water body heat storage is dominated by natural lakes (111.7%), while rivers are estimated to contribute negatively (-14%), but encompass large uncertainty ranges. The course of reservoir heat uptake (2.3%) reflects the evolution reservoir construction in the 20$^{\text{th}}$ century. The creation of new open water surfaces increases the potential of heat uptake through the high heat capacity of water. In addition, reservoir filling redistributes the thermal heat contained in the reservoir water from ocean to land, which is about 10.4 times larger compared to the total inland water heat uptake. To account for this buffering of atmospheric warming and the interactions of the water bodies with the climate system, reservoir expansion and heat redistribution needs to be included in ESMs. To this end, we implemented the rapid rise in 20$^{\text{th}}$ century reservoir construction in the CESM coupled modeling framework, as described in chapter 4.

Man-made reservoirs interact with the atmosphere in a similar way to natural lakes. Therefore, we implemented 20$^{\text{th}}$ century reservoir expansion in the Community Land Model version 5 (CLM5) as dynamically growing lakes, using lake and reservoir surface area and construction years from the state-of-the-art HydroLAKES and Global Reservoir and Dam (GRanD) datasets. In CLM5, sub-grid heterogeneity is represented through a nested tiling approach, with different land unit fractions per grid cell. Similar to transitions between the vegetated, cropland and glaciated grid cell fractions, we added the functionality of changing lake area fractions, while conserving the total mass and energy content of the grid cell through artificial correction fluxes. These correction fluxes, existing of sensible heat flux for heat and a runoff flux for water, are minimized using a baseline approach, in which only the deviations against a reference state are included in the resulting fluxes. The com-

parison of land-only simulations with CLM and prescribed meteorological forcing from the Global Soil Wetness Project (GSWP3) for 1900-2014, one with transient reservoir expansion enabled and the second with transient land use but constant lake area, show that reservoir expansion increased the terrestrial water storage and decreased the surface albedo. The course of these responses match the evolution in reservoir construction and scale with the grid cell reservoir fraction. The developments did not have a considerable influence on model skill when compared to available observational data. Nonetheless, the reservoir expansion through dynamically changing lake area improves the realism of the model by adding a hereto unaccounted process.

The impact of global reservoir expansion on the climate is investigated in chapter 4 through global CESM ensemble simulations for the period 1979-2014 with coupled land and atmosphere components. As the land-only simulations showed only limited spatial influence of reservoir expansion on the global climate, we conducted two five-member ensembles representing two snapshots, the first with only natural lakes, representing the preindustrial situation and the second including the full present-day reservoir extent. While the global mean climate responses of the human-induced open water surfaces are rather small (for example, global mean 2-meter air temperature rises with +0.1 K), the responses are substantial on local and seasonal scales. During boreal summer, reservoirs dampen the diurnal temperature range with -0.3 K over reservoirs grid cells, and up to -1.5 K for grid cells with a large reservoir coverage. Furthermore, reservoirs reduce temperature extremes like monthly maximum daytime and monthly minimum nighttime temperature, whereby the seasonality could be explained by ice formation and heat release. The main driver of the seasonal dampening is the heat uptake of the reservoir water from March to September and the following release from September to February. This buffering effect modulates the seasonal temperature cycle and the surface energy balance through compensating latent and sensible heat fluxes. The ensembles did not show statistically significant signals in precipitation and moisture related variables emerging above the natural variability.

Next to the creation of new open water surfaces upon their construction, reservoirs have a large influence on the timing and magnitude of river flow and water availability by managing outflow, which are accounted for in the river component of the model. As MOSART, the current river module in CLM5, will be replaced by the new vector-based river routing model mizuRoute, we use this model to implement river flow regulation through reservoirs in chapter 5. The vector-based river network on which mizuRoute operates resolves individual lakes and reservoirs based on the HydroLAKES and GRanD databases. We implement reservoir management through the generic, widely-used reservoir scheme of Hanasaki et al. (2006), which determines individual reservoir outflow based on generic rules using reservoir inflow, maximum capacity and current volume, with the overarching aim to minimize intra- and interannual outflow variability. The parametrisation differentiates between large reservoirs, with high storage capacities compared to annual inflows, and small reservoirs, where the resulting outflow is characterised by the inflow seasonality. In addition, for reservoirs that mainly serve irrigation purposes, the seasonality in downstream water demand is considered when determining the outflow. To derive this irrigation

water demand seasonality in the context of a vector-based river network, we developed an irrigation topology relating the spatially distributed irrigation water demands of catchments to individual reservoirs based on simple rules.

Before integrating new developments in the coupled framework, new schemes need to be rigorously tested in standalone mode. The new reservoir parametrisation is therefore evaluated both in a local setting for individual reservoirs, using observed inflows as forcing, and in a global-scale application using the vector-based river network forced with runoff simulations from CLM5. We assess the skill to represent reservoir outflow, storage and long term streamflow indices compared to simulations with natural lakes and ignoring inland waters.

The reservoir parametrisation shows improved skill compared to natural lakes when forced with observed inflows, in particular for reservoir storage and reservoirs with a large multi-year storage capacity. Accounting for seasonality in irrigation water demand entails only a limited influence, pointing at underestimations in irrigation water demands simulated by CLM5 and uncertainties related to the irrigation topology. The lack of reliable global datasets on irrigation water demand seasonality hampers separating the individual contributions to this overall uncertainty. In the global-scale simulations, using the Hydrologic Derivatives for Modeling and Applications (HDMA) stream network and runoff simulated by CLM5 as input, the added value of using the dam parametrisation compared to natural lakes is no longer present, mainly due to magnitude and timing biases in reservoir inflow. Likely, the main driver of these inflow biases is the simulated runoff from CLM5, which could be accommodated by improving the representation of hydrological processes in future research. These improvements may include high level snow pack and melting dynamics, and including other human factors like water abstraction for domestic and industrial use. Next to the simulated runoff, other reasons for biased inflows are the resolution of the river network used, and the level to which reservoirs within the network are included. Potential solutions include using higher resolution stream networks like the Multi-Error-Removed-Improved-Terrain (MERIT) Hydro network (Yamazaki et al., 2019) and complementing the data on reservoirs from GRanD with newly available datasets (section 6.2.4).

The model developments involving reservoir construction through lake area expansion in CLM5 (chapter 4) and flow regulation in mizuRoute (chapter 5) will be linked through reservoir volume dynamics in the coupling of CLM5 and mizuRoute, which is currently ongoing (see also section 6.2.2). In this way, the energy balance of water bodies will be solved in CLM5 and the water balance in mizuRoute. The energy and water balance are connected through the evaporation term. In particular for large lakes and reservoirs, the evaporation and precipitation terms can be substantial in the water balance, as shown in the Lake Victoria case study.

The case study also highlights that, next to changes in the other water balance terms driven by natural variability and climate change, dam regulation is key for sustaining future lake levels. In addition, the influence of individual decisions at the dam could have large im-

pacts on lake levels and reservoir dynamics. The parametrisation of Hanasaki et al. (2006) used in chapter 5, is not designed to capture these individual decisions due to its generic nature, and wide applicability. This is relevant in light of a current scientific debate on the use of data-driven reservoir schemes, which use site-specific information to derive release curves (Turner et al., 2020), and therewith constrain flow forecasts. These schemes have the potential to improve reservoir release simulations nurtured by specific observations on individual reservoirs Turner et al. (2020); Yassin et al. (2019), like the recently published inventory of dams and reservoirs in the Contiguous United States providing historical inflow, storage and outflow observations (Steyaert et al., 2022). However, the full potential of data-driven approaches for large scale hydrological models might not be reached, due to the large errors and biases inherently present in the simulated flows Turner et al. (2020), also encountered in chapter 5. MizuRoute is designed to be used at different spatial scales and has different reservoir schemes available, to be chosen by the user, and thus allows to integrate this type of outflow methods (Gharari et al., 2022). However, in the context of ESMs and future projections under various emission scenarios, data-driven methods do not incorporate future climate changes and their impacts on the river flows. Therefore, we argue that the choice of dam scheme depends on the intended purpose, and that generic parametrisations are best suited to simulate reservoir operations in an ESM context.

In conclusion, this dissertation provides essential steps to incorporate human water management and reservoir operations the CESM framework via the land and river routing components. These developments improve the representation of human influences in the terrestrial water cycle in these models. This allows for modelling the feedbacks and interactions with other components in the Earth system, like the atmosphere and ocean. In addition, the reservoir representation contributes to a more robust representation of climate change impacts using CLM5 as a standalone impact model, notably via its contributions to the ISIMIP initiative (Frieler et al., 2017; Telteu et al., 2021; Golub et al., 2022). Overall, this work paves the way towards better integrating human water management and climate change scenarios. Accounting for human activities in the water cycle will become even more important when assessing future adaptation and mitigation strategies to the changing climate, especially in a world where the human footprint is likely to increase due to growing demand for food, energy and water.

6.2 Ongoing work and recommendations

6.2.1 Update of inland water heat uptake estimates

The estimates presented in chapter 3 presented a first quantification of inland water heat uptake. Recent international efforts through the Global Climate Observing System (GCOS) aim to provide and monitor an inventory of the global energy budget (Von Schuckmann et al., 2020). In this context, the quantification of the land heat uptake component, existing continental heat storage, permafrost and inland water heat uptake will be improved. To this end, our estimates on lake, reservoir and river heat uptake will be updated and included in this community effort. The current estimates can be improved in various ways: in a first step, new estimate can be updated to include the years 2021-2022. Second, the ensemble of global lake models can be extended with new lake model simulations (LAKE, VIC-LAKE en GOTM) that became available in ISIMIP2b after the publication of the study. Further, the volume estimates used in the heat calculation can be refined by using more realistic assumption of lake shape, replacing the cylindrical shape by a the truncated cone, with a fixed relationship between mean and maximum depth or using bathymetric maps of the very recent GLOBathy data set (Khazaei et al., 2022). Challenges remain to reduce the uncertainties in the river temperature (section 6.2.2) and storage estimates. Here potential avenues are to estimate river volumes by combining simulated discharge from ISIMIP with river width databases (Allen and Pavelsky, 2018), or leveraging from recent progress in remote sensing products, like the upcoming Surface Water and Ocean Topography (SWOT) satellite mission (section 6.2.4).

6.2.2 Future pathways for model development

The coupling of mizuRoute and CLM5 is currently ongoing. Below we describe the next steps and discuss challenges and potential avenues for future model development.

Improve simulated runoff and irrigation water withdrawal in CLM5

To leverage from the dam parametrisation implemented in mizuRoute, future work should focus on improving the runoff in CLM5. Potential avenues to this end are discussed in chapter 5. A promising approach is to calibrate CLM5 parameters through a multi-objective approach for river flow metrics, which has been successfully applied in Alaskan catchments (Cheng et al., 2022). The methodology could be ported to individual catchments with human regulated reservoirs and limited impacts from other human water management. In addition, ongoing and future work should be dedicated to improving the representation of quantities and timing of irrigation water withdrawal and to including direct water withdrawals for different sectors, including households, industry and livestock.

In the current version of CLM5, water for irrigation is extracted from the river water storage in the grid cell. When the river storage cannot meet the irrigation demand, the deficient water amount is taken from the ocean model to conserve mass. There is a second option,

where the irrigation demand can be reduced to retain the river storage above a chosen threshold (Lawrence et al., 2019a). The incorporation of reservoir water storage and flow regulation can improve the timing and the amount of water available for irrigation. To transfer the water in rivers and reservoirs from the vector-based network of mizuRoute to the grid cell for irrigation water abstraction, the two-way coupling could utilize the irrigation topology in the remapping. To fully represent the irrigation water abstraction, groundwater abstractions should be explicitly accounted for, and this both from confined and unconfined aquifers.

Steps necessary for coupling and modeling of lake and reservoir water balances

In a first step, the coupling of CLM5 and mizuRoute will instantaneously communicate the CLM5 runoff for routing to mizuRoute. Communicating the fluxes from the gridded land model to the catchments of the vector-based river network will require an on-the-fly remapping step in the coupling module. These developments are currently ongoing. The one-way coupling will allow to model the water balance of individual reservoirs and lakes in mizuRoute. In the current release of CLM5, the lake water balance is not modeled and the lake column of the grid cell has a constant depth. The difference in the evaporation and precipitation over the lake column are compensated by a runoff term, which can be both positive and negative. As CLM5 solves the energy balance of the lake column, the resulting lake evaporation term should be communicated to mizuRoute. Lake precipitation can be retrieved from the grid cell precipitation rate, either coming from the prescribed atmospheric forcing or dynamically solved by the atmospheric component. The water balance of individual lakes and reservoirs will then be modeled in mizuRoute, using the internal calculated inflow and outflow, in combination with the lake precipitation and evaporation rates from CLM5. To obtain surface water area and levels, the resulting volume changes have to be converted using bathymetric relationships, like the reservoir storage-area-depth dataset of Yigzaw et al. (2018) and bathymetric maps of Khazaei et al. (2022).

In a second step, the two way coupling will allow to communicate changes in the individual water body volume, area and level back to CLM5, where this information can be used to dynamically adjust the grid cell mean lake depth and grid cell lake area. Challenges exist, however, to translate the changes of the individual water bodies to their corresponding grid cell column. Notwithstanding, this will allow to directly simulate the two-way land-atmosphere interactions and feedbacks between reservoir and lake storage, area and depth changes as a consequence of seasonal variations, changing climatic conditions or human water management. Furthermore, these developments will allow to model future impacts of various climate change scenarios and water management on lake and reservoir levels worldwide. In this way, projections of regional hydroclimatic trends can be translated to impacts on the water stored in lakes and reservoirs, with important consequences for local water availability (Zhou et al., 2021). To date, there are no global-scale assessments of storage changes in lake and reservoirs in response to climate change. The uncertainties related to future projections of the water balance terms may further complicate future projections (Woolway et al., 2020).

Explicit simulation of water temperatures

When reservoirs come into existence, the additional lake area adopts the temperature profile of the preexisting lake fraction in the grid cell. The correction fluxes are required to compensate for the difference in mass and energy to ensure conservation. In reality, however, the reservoir fills with river water and its associated temperature. To model this process more realistically, the temperature of water fluxes could be explicitly modeled, together with the reservoir and lake water balance. This would also obviate the corrections related to the heat carried away by the runoff. In large-scale hydrological models, approaches exist to calculate water temperatures and route this energy through a river network (Wanders et al., 2019). In addition to improving the processes, parametrisations and corrections related to the energy cycle, the explicit modelling of the river temperatures would allow to account for physical, chemical and ecological processes in rivers under changing climatic conditions, like the cooling water potential for power production (van Vliet et al., 2016), which becomes particularly relevant at higher resolutions. There are, however, various challenges related to implementing water temperatures within the CESM framework, notably to reconcile the river fluxes in water and energy, solved in either mizuRoute or CLM5.

6.2.3 High resolution simulations of climate impacts of dynamical lake areas

Our findings identified limited impacts of reservoir expansion on the global climate using global simulations of 0.9 by 1.25 °resolution. Moreover, the impacts of lake area changes at this resolution are mostly restricted to the grid cell in which they occurred. Other local climate responses to surface cover change might be masked by the climate variability within the $\sim$ 100 km by 100 km grid cell. Moreover, at these low resolutions, it is not possible to quantify to which extent reservoir expansion affects the surrounding climate. CLM5 can however be employed in different set-ups, like in the CESM2 Variable Resolution configuration (Gettelman et al., 2018; Devanand et al., 2020) and employed as land module for dynamically downscaled RCMs (Akkermans et al., 2014; Thiery et al., 2015, 2016). As the implementation of dynamical lakes described in chapter 4 is included in the model source code, this functionality can directly be used to study land cover changes related to open water bodies. Moreover, recent efforts at the National Center for Atmospheric Research (NCAR) are targeted to integrate land models from the Earth System (CLM5) and numerical weather predicting communities (Noah-MP and WRF-Hydro), unifying their community efforts into a single model framework, the Community Terrestrial System Model (CTSM). In particular, these developments facilitate the coupling of CLM5/CTSM to the Weather Research and Forecasting (WRF) model to conduct regional simulations at higher horizontal resolutions.

Simulating reservoir expansion with RCMs at high spatial resolutions will allow to investigate the impacts of reservoir expansion on local climate, mesoscale circulation, local temperatures as well as on moisture related variables, like extreme precipitation and the Convective Available Potential Energy (CAPE), as suggested by observation-based studies (Hossain et al., 2012; Degu et al., 2011). These type of responses are identified and well investigated for large lakes, such as the African Great Lakes, including Lake Victoria (Thiery et al., 2015) and European lakes (Samuelsson et al., 2010). Next to the land cover changes from land to open water, dam construction can also trigger other land use and land cover changes in the vicinity of the reservoir, like the conversion of natural vegetation into cropland and the development of urban areas due to increased water availability (Di Baldassarre et al., 2021). Furthermore, our developments allow to investigate the land-climate interactions related to changes in natural lake area, like the rapid increase in glacial lakes due to climate change and retreating glaciers (Shugar et al., 2020; Farinotti et al., 2019).

6.2.4 Improved information on reservoirs for model development and evaluation

The reservoir implementations presented in this thesis assumes a time-invariant presence and storage capacity of reservoirs (chapter 5) or the expansion of open water surface related to their creation in their construction year (chapter 3 and 4). Based on the GRanD dataset, this mainly includes large reservoirs with storage capacities > 0.1 km^3. However, today already more than hundreds of reservoirs are under construction or planned worldwide (Sterl et al., 2020, 2021a; Zarfl et al., 2014; Winemiller et al., 2016). At the same time, reservoirs cease to exists due to dam removal or are reduced in their maximal capacity as a result of sediment filling (O'Connor et al., 2015; Habel et al., 2020). International efforts, like the Global Dam Watch initiative (`http://globaldamwatch.org/`) aim to advance the development of a globally consistent and routinely updated database on dams, reservoirs and in-stream barriers for global assessments, by bringing existing global dam databases together (Mulligan et al., 2021). Next to GRanD, containing 7320 large reservoir polygons with featured metadata for every reservoirs, the initiative includes the Future Hydropower Reservoirs and Dams Database (FHReD; Zarfl et al., 2014) with 3700 records of planned hydropower dams, and Global Georeferenced Database of Dams (GOODD; Mulligan et al., 2020), providing the geo-referenced location of 38 667 dams, but without additional metadata. Beside these open-access datasets, the International Commission on Large Dams (ICOLD) provides extensive, but proprietary information on 60 000 dams worldwide. Finally, very recently, the best available information from these datasets is combined into the recently released Georeferenced global Dam and Reservoir (GeoDAR) dataset, encompassing more than 20000 reservoir polygons with extensive attribute information (Wang et al., 2021).

Complementary to the geo-spatial location and corresponding metadata of individual reservoirs, ongoing developments in remote sensing allow to monitor and document changes in reservoir surface area, level and discharge. This will aid future developments related to the implementation of lake and reservoir water balances, and the evaluation of their ability to represent these variables, supplementing frequently used benchmarking datasets like GRACE, providing observations on anomalies in terrestrial water storage. GRACE can, however, only capture changes for the very large reservoirs (Rodell et al., 2018) and is therefore less useful for model evaluation.

Water levels can be retrieved from satellite altimetry, like the recent analysis of Cooley et al. (2021) on water storage variability using the ICESat-2 mission, and can already be retrieved for various lakes and reservoirs through global open-data portals like the Global Reservoirs and Lakes Monitor (G-REALM; `https://ipad.fas.usda.gov/cropexplorer/global_reservoir/`), the HYDROWEB database (`https://hydroweb.theia-land.fr/`; (Crétaux et al., 2011), and the Database for Hydrological Time Series of Inland Waters, DAHITI; `https://dahiti.dgfi.tum.de/en/` Schwatke et al. (2015). In addition to altimetry, multispectral satellite missions, like Landsat, are used to map global surface water extent, like in the Global Surface Water (GSW) dataset (Pekel et al., 2016a), and to create dedicated reservoir surface area time series (Pekel et al., 2016b). The combination of information on water level and spatial extent, enables to analyse global lake and reservoir volumes (Busker et al., 2019) and high resolution reservoir bathymetry (Li et al., 2020). Finally, the long anticipated SWOT satellite mission, commissioned by NASA and expected to launch in 2022, will greatly improve current estimates of reservoir storage by producing high resolution observations on surface water levels and water areas. Altogether, the increasing availability and scientific advancements provide promising avenues to future model developments related to reservoirs.

6.2.5 Integrated climate and impact simulations

By including reservoir operations, we lay the ground for the next generation ESM and impact models, which fully integrate human management, climate change scenarios, mitigation and adaptation strategies. This type of research requires further improvements in present-day global human water management to use under different future emission and socioeconomic scenarios. Accounting for the two-way interactions between climate change impacts and human water management, provides future research pathways to not only better investigate climate change impacts on future water resources, but also to identify potential strategies to mitigate climate change impacts on water resources through management. Furthermore, incorporating additional feedbacks related to the social and human dimension of water management from the socio-hydrology field, like different dam operation strategies and memory effects after drought and flood conditions (Di Baldassarre et al., 2017, 2018) will open interesting opportunities to investigate climate, management and sociological responses and develop adaptation strategies. This is especially relevant in the context of water and food security in a changing climate, as well as related to extremes like floods and droughts.

The research in this thesis has both largely benefited from and contributed to the community work and open source science within the CESM and ISIMIP modelling communities. It serves therefore as a key example on how science and the training of scientists can be fostered by transparency, inclusivity and collaborative scientific processes within scientific communities. This is, to the author's opinion, indispensable to tackle the ongoing challenge of climate change.

Appendix

Appendix A

A novel method for assessing climate change impacts in ecotron experiments

Ecotron facilities allow accurate control of many environmental variables coupled with extensive monitoring of ecosystem processes. They therefore require multivariate perturbation of climate variables, close to what is observed in the field and projections for the future, preserving the co-variances between variables and the projected changes in variability. Here we present a new method for creating realistic climate forcing for manipulation experiments and apply it to the UHasselt Ecotron Experiment. The new methodology uses data derived from the best available regional climate model (RCM) projection and consists of generating climate forcing along a gradient representative of increasingly high global mean temperature anomalies. We first identified the best performing regional climate model (RCM) simulation for the ecotron site from the EURO-CORDEX ensemble based on two criteria: (i) highest skill of the simulations compared to observations from a nearby weather station and (ii) representativeness of the multi-model mean in future projections. Our results reveal that no single RCM simulation has the best score for all possible combinations of the four meteorological variables and evaluation metrics considered. Out of the six best performing simulations, we selected the simulation with the lowest bias for precipitation (CCLM4-8-17/EC-EARTH), as this variable is key to ecosystem functioning and model simulations deviated the most for this variable, with values ranging up to double the observed values. The time window is selected from the RCM projection for each unit based on the global mean temperature of the driving Global Climate Model. The units are forced with 3-hourly output from the RCM projections of the five-year period in which the global mean temperature crosses the predefined values. With the new approach, Ecotron facilities become able to assess ecosystem responses on changing climatic conditions. The presented methodology can also be applied to other manipulation experiments, aiming at investigating ecosystem responses to realistic future climate change.

This chapter is published as: Vanderkelen I. , Zscheischler J., Gudmundsson L. Keuler K., Rineau F., Beenaerts N., Vangronsveld J., Vicca S., Thiery W. (2020) A new method for assessing climate impacts in ecotron experiments. International Journal of Biometeorology, 64, 1709–1727.

A.1 Introduction

Ecosystem climate change experiments are one of the key instruments to study the response of ecosystems to a change in climate. There are primarily four different factors that are altered in such experiments: temperature, precipitation, CO_2 concentration, and nitrogen deposition (Curtis and Wang, 1998; Rustad et al., 2001; Lin et al., 2010; Wu et al., 2011; Knapp et al., 2018). More recently multi-factor experiments are starting to emerge. In those experiments, different combinations of the four main drivers are altered (Kardol et al., 2012; Yue et al., 2017). What is common in the majority of climate change experiments is that while the drivers of interest are being altered, all other variables are being held equal between the different treatment groups. Consequently, differences in the response can be related to the change in the main driving factor (or multiple driving factors).

Altering only one or a limited number of climate change drivers allows for a straightforward analysis of the observed responses and has provided a wealth of mechanistic insights in ecosystem responses to environmental changes (e.g. Hovenden et al., 2014; Karlowsky et al., 2018; Terrer et al., 2018). However, the resulting multivariate combination of climate variables may be physically unrealistic and may miss key aspects related to natural climate variability and the co-variance of multiple variables, linked to each other by synoptic conditions. This is particularly important for representing compound events, where a the combination of non extreme drivers can lead to extreme impacts (Rineau et al., 2019; Zscheischler and Seneviratne, 2017; Zscheischler et al., 2018). For example, droughts and heatwaves often co-occur (Zscheischler and Seneviratne, 2017) and, soil moisture conditions and precipitation occurrence are linked (Guillod et al., 2015; Moon et al., 2019). Incorporating the co-variability of key climate drivers is also important for the studied responses. For instance, heatwaves characterized by similar extreme air temperatures can lead to different plant responses depending on the atmospheric conditions: under different shortwave radiation, relative humidity and surface wind conditions, the leaf temperature and the potential for heat stress varies a lot (De Boeck et al., 2016).

Until recently, it was not possible to simulate realistic future climates in ecosystem climate change experiments (Korell et al., 2019), as these experiments require accurate manipulation of environmental variables to represent current and future climate conditions. Controlled environment facilities meet these requirements by providing systems to simultaneously manipulate as well as measure multiple parameters (e.g. Lawton, 1993, 1996; Griffin et al., 1996; Stewart et al., 2013; Clobert et al., 2018), especially in combination with an observation station in the field providing real time observations of most of those parameters (Rineau et al., 2019). This approach is powerful especially when combined with a measurement station in the field providing real time observations of most of these required parameters (Rineau et al., 2019). In such facilities, climate change experiments can be informed by meteorological forcing representing both present and future climatic conditions in a holistic manner. For instance this forcing can include both realistic changes of climate variability as well as important drivers of changes in the frequency, intensity and duration of meteorological extremes. This potential is especially interesting in gradient

experiments covering a range of global warming levels,, as this combination allows for the detection of non-linearities, thresholds and possible tipping points in ecosystem responses to increasing climate change forcing (Rineau et al., 2019; Kreyling et al., 2018).

Sampling realistic climate information in a climate change context is challenging, but can be achieved by using climate model output. Global Climate Models (GCMs) are generally used to assess the climate state and variability at global to continental scales with a resolution of 100 to 250 km. By dynamically downscaling GCMs, Regional Climate Models (RCMs) typically resolve the climate on a regional scale with higher spatial resolutions of 1 to 50 km. As such, RCMs allow a more realistic representation of meso-scale atmospheric processes and processes related to orography and surface heterogeneities. As climate models realistically simulate the atmospheric state under past, present and future climatic conditions with a high temporal resolution, they are suited to provide a holistic and physically consistent climate forcing for ecosystem climate change experiments. Generally, ensemble climate projections show a large spread for future climate conditions (Keuler et al., 2016), especially for variables relevant for ecosystem experiments such as extreme temperatures, droughts and intense precipitation (Sillmann et al., 2013; Orlowsky and Seneviratne, 2013; Greve et al., 2018; Rajczak and Schär, 2017). This spread is related to (i) different climate sensitivities of the GCMs, (ii) structural differences between the models and (iii) natural variability within the climate system. The Coordinated Regional Climate Downscaling Experiment in the European domain (EURO-CORDEX) provides an ensemble of high resolution dynamically downscaled RCMs (Kotlarski et al., 2014) and is therefore highly suitable to serve as a base for the selection of representative climate forcing for climate change experiments. With a suite of GCM/RCM combinations available, a well-informed choice on the most adequate RCM/GCM simulation can be made based on (i) the model skill in representing the observed climatology and (ii) the temperature sensitivity to future increases in greenhouse gas concentrations.

So far, statistically downscaled GCM output has only rarely been used as climate forcing in ecosystem experiments. Thompson et al. (2013) describe a process for generating temperature forcing for experiments in which they use daily temperature output from a GCM (MIROC) and a stochastic weather generator to generate hourly weather. They validated their method against statistical characteristics of temperature observations. Likewise, the Montpellier CNRS ecotron facility is driven by multivariate statistically downscaled GCM projections (using the ARPEGEv4 model; Roy et al. (2016). They force their experiment with climatic conditions of an average climatological year of the period 2040-2060. During the summer months, they artificially simulate an extreme event by including a drought and heatwave by reducing the irrigation amount to zero and increasing the air temperature artificially. However, by using a climatological year, possible extreme events are dampened by averaging. Both studies lack a thorough evaluation procedure for selecting the used climate model. Moreover, to the best of our knowledge, no study accounts for the co-variance between climate variables.

In this chapter, we present new method for creating realistic climate forcing for manipulation experiments. From an ensemble of dynamically downscaled climate model simulations, we select one simulation that well represents present-day climate conditions for four key variables in the region of interest and is representative of the multi-model mean of these variables in future projections. In this way, the new methodology accounts both for co-variance of climate parameters and for climate variability while naturally incorporating extreme events under present and future climate conditions. Furthermore, the method can be combined with a gradient approach. We apply the new methodology to generate climate forcing for the UHasselt Ecotron Experiment, an infrastructure consisting of 12 climate-controlled units, each equipped with a lysimeter containing a dry heathland soil monolith extracted from the National Park Hoge Kempen in Belgium (Rineau et al., 2019). In this experiment, six units are directly forced with regional climate model output along a Global Mean Temperature (GMT) gradient anomaly.

A.2 New methodology for generating climate forcing for ecosystem climate change experiments

In our methodology, variability and co-variance between variables is preserved by selecting the best performing RCM simulation and subsequently extract the required variables from the grid cell covering the location of the experiment. By extracting a single grid cell of a single RCM simulation, climate extremes are not smoothed and the climate variability inherent to the model is fully preserved. The units in the ecosystem climate change experiments follow a gradient of increasing Global Mean Temperature (GMT) anomalies. In this way, a given unit is forced with the climatic conditions consistent with e.g. a 2 °C warmer world, and the units represent conditions associated with increasingly warmer climates.

The methodology presented here is deployed in three steps. First, the best performing RCM projection needs to be selected based on two criteria: (i) the simulation should have high skill in reproducing mean and extreme present-day climatic conditions and (ii) the projected future temperature anomalies should be close to the multi-model mean, that is, the selected simulation should be representative of the future mean projection (Fig. A.21, step 1). To this end, the model performance is evaluated for four variables that are highly relevant for ecosystem climate change experiments: precipitation, temperature, relative humidity and surface wind speed. Precipitation is considered one of the most important variables, as water availability is likely to constrain plant growth the most.

Second, the time windows for the different units along the GMT anomaly gradient are defined based on the annual GMT projection of the driving GCM of the chosen RCM simulation (Fig. A.21, step 2). To span a large range of climate change scenarios, we use projections following the Representative Concentration Pathway (RCP) 8.5, a worst-case scenario following an unabated greenhouse gas emissions pathway (Riahi et al., 2011). The experiments are running for 5 years. We choose time windows corresponding to the

experimental period and centred around the year in which the climatological GMT anomaly (averaged with a 30-year period) crossed the pre-defined thresholds for the first time. In the third step, the values of all necessary variables are extracted from the chosen RCM projection based on the defined time windows for the grid cell covering the experiment location (Fig. A.21, step 3). These time series are then directly used to force the ecotron units, in the highest available temporal resolution.

A.3 Data and methods

A.3.1 The UHasselt Ecotron Experiment

The UHasselt Ecotron experiment is an ecotron infrastructure consisting of replicated experimental units in which ecosystems are confined in enclosures. By allowing the simultaneous control of environmental conditions and the on-line measurement of ecosystem processes, the ecotron units are suited for experiments with highly controlled climate change manipulation of large intact parts of the ecosystem. The infrastructure allows an intensive monitoring and control of key abiotic parameters on 12 large-scale ecosystem replicas, called “macrocosms”. These macrocosms had been extracted without disruption nor reconstitution of the soil structure from the same dry 6 to 8 years old heathland plot in the National Park Hoge Kempen (50°59’ 02.1" N, 5°37’ 40.0" E) in November 2016.

The infrastructure is a W-E oriented, 100 m by 10 m wide, and 6 m tall building (Fig. A.32a). Only 12 of the 14 units are used, excluding the outermost to avoid boundary effects. Each unit consists of three compartments in which the abiotic environmental variables are controlled: the dome, the macrocosm and the chamber. The dome is transparent for photosynthetic active radiation (PAR), UVa and UVb. Here, wind and precipitation are measured and generated, and CO_2 , N_2, CH_4, PAR and Net Radiation (NR; i.e. the difference in incoming and outgoing short-and longwave radiation) are measured. The second compartment, the macrocosm, contains the extracted soil column (the ecosystem) enclosed in a lysimeter. In this compartment, the soil water content, soil water tension, soil electrical conductivity and soil temperature are measured and controlled. The chamber, the third compartment, the air pressure, temperature, relative humidity, and CO_2 concentration are controlled (Rineau et al., 2019). The ecotron infrastructure is linked with an Integrated Carbon Observation System (ICOS) ecosystem station, which provides real-time information on local weather and soil conditions. These data are used to simulate the current weather conditions within the ecotron units with a frequency of at least once every 30 minutes (Rineau et al., 2019).

The aim of the UHasselt Ecotron experiment is to study the ecological and societal impacts of climate change, by manipulating climatic variables alone or in combination and, across a wide range of predicted values, while monitoring as many soil biota and processes as possible and to translate them into socio-economic values using heathland as a case study (Rineau et al., 2019). Examples of measured ecosystem processes are evapotranspiration,

net ecosystem exchange, CH4 or N2O emissions. The main research questions of this multi-disciplinary experiment are how climate change will affect the transitioning of the heathland ecosystem to alternative stable states like pine forest or acid grassland and what the consequences are for ecosystem services (Rineau et al., 2019). The experiment will run uninterrupted for a period of at least five years. Six units will be used to simulate a gradient of increasing variability in precipitation regime. They are driven by the ICOS station and a perturbed precipitation time series following a gradient of increasingly long periods with no precipitation (2, 6, 11, 23, 45 and 90 days; Rineau et al., 2019). In the remaining six units, atmospheric conditions along the GMT anomaly gradient will be simulated as described in section A.2. The 3-hourly RCM output is linearly interpolated to a 30-minute time resolution to force the ecotron units. For soil temperature and soil water tension however, the 30-min ICOS data is used. This is because leaving the lysimeter uncontrolled would lead to (i) an overestimation of soil temperature variability as the lysimeter is exposed to air temperatures in the chamber (despite being thermically insulated), and (ii) accumulation of water at the bottom of the lysimeter, hence considerably overestimating soil water level, as soil water movements are mimicked by suction from the bottom. Following the gradient design, each ecotron unit represents the local climate conditions of a globally 0 °C (historical), +1° C (present day), +1.5 °C (Paris Agreement), +2 °C, +3 °C and +4 °C warmer world. The climatology of the unit forced by +1° can thereby be directly compared to the unit driven by the ICOS station and thus representing the present-day observed conditions. In this regression design, there is no experiment replication. To minimize the noise in initial ecosystem responses, the units are allocated to the two gradient experiments based on a cluster analysis of the variance of the 14 variables measured during a test period of 11 months (Rineau et al., 2019).

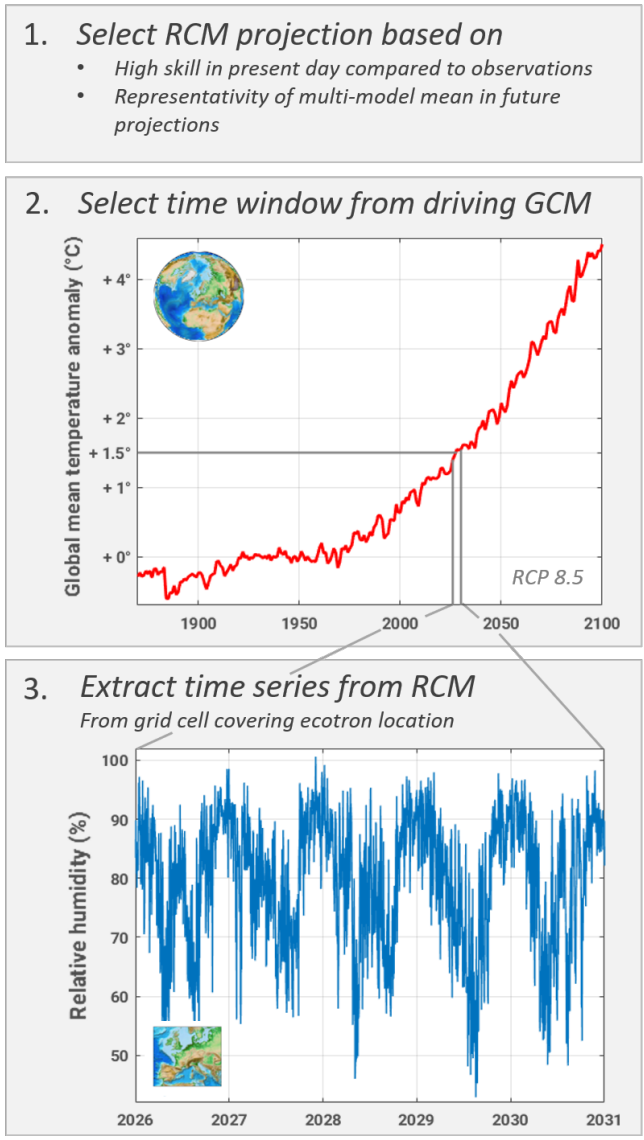

Figure A.21: Methodology for generating climate forcing along the GMT anomaly gradient.

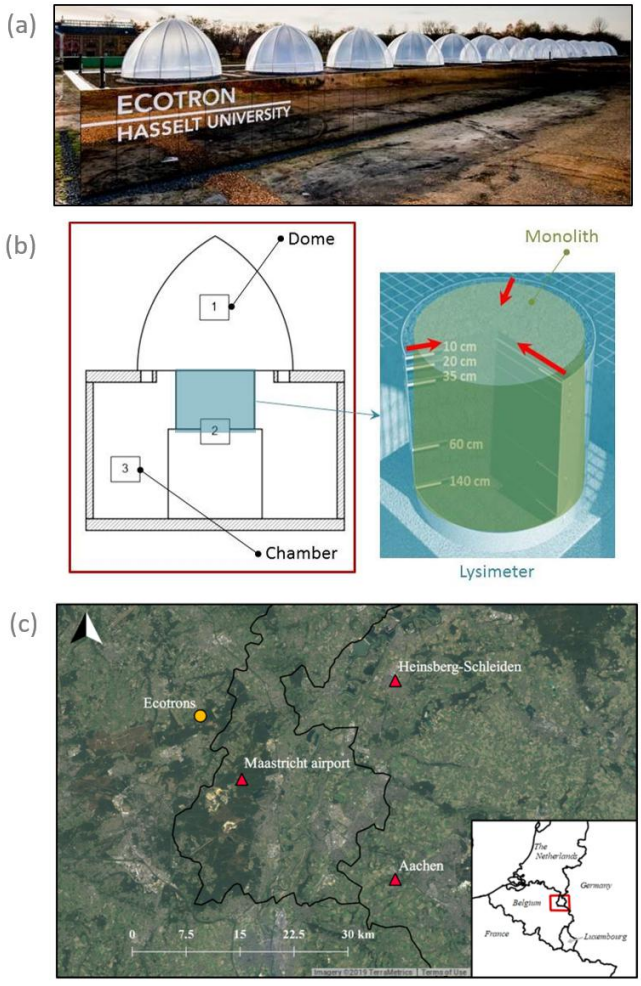

Figure A.32: **The UHasselt Ecotron experiment** (a; picture: Liesbeth Driessen), scheme of a unit with the three compartments and the lysimeter compartment in detail (b), and overview map with location of the infrastructure and reference weather observation stations (c).

A.3.2 Meteorological data

EURO-CORDEX

The best performing RCM simulation compared to observations is selected from the Coordinated Regional Climate Downscaling Experiment in the European Domain (EURO-CORDEX), an ensemble of high resolution dynamically downscaled simulations available at a horizontal resolution of 12 km (Kotlarski et al., 2014; Jacob et al., 2014). The simulations, hereafter referred to as GCM downscalings, cover the historical period (1951-2005) and the three RCP scenarios (RCP 2.6, 4.5 and 8.5, for the period 2006-2100) by using GCMs as initial and lateral boundary conditions. Additionally, for each RCM, a reanalysis downscaling is provided in which the RCM is driven by the European Centre for Medium-Range Weather Forecasts (ECMWF) ERA-Interim as initial and lateral boundary conditions for the period 1990-2008 (hereafter referred to as reanalysis downscalings). These reanalysis-driven simulations allow to evaluate the skill of the RCMs themselves by comparing them to observations (Kotlarski et al., 2014).

In this chapter, we use the variables for daily mean, minimum and maximum temperature, precipitation, mean surface wind and relative humidity of all available simulations (Table A.1). We consider the values of the 12 km by 12 km pixel covering the location of the reference station providing the observations. As relative humidity is not directly available for all simulations, we converted specific humidity to relative humidity using the mean temperature and surface pressure for every simulation. Comparing the applied conversion with the simulations for which relative humidity is available proves this conversion is applicable. Neither specific nor relative humidity are publicly available for the simulations with RegCM4-2 and ALARO-0 and the mean surface wind speed variable is not available for ALADIN53 and ALARO-0; therefore we do not analyse these variables for the respective simulations.

Once the EURO-CORDEX ensemble member is selected, the relevant variables (precipitation, mean temperature, surface pressure, surface up-welling latent heat flux and sensible heat flux, wind speed and relative humidity) are extracted from the 3 hourly RCP 8.5 simulation for the pixel covering the ecotron location for the time windows in which the GMT anomalies are crossed for each dome. These three-hourly values (except for surface up-welling latent heat flux and sensible heat flux) are then linearly interpolated to 30 minute resolution and used to drive the climate controllers in the ecotron units. For precipitation, one additional step was added where drizzle (precipitation of less than 1 mm) was postponed and accumulated until it reached 1 mm to start a rain event in the ecotron. The surface pressure is calculated from the mean sea level pressure using the altitude of the ecotron facility (43 m a.s.l.) and assuming hydrostatic equilibrium. The concentrations of the controllable greenhouse gases (CO_2, CH_4 and N_2O) are determined based on the annual values calculated by van Vuuren et al. (2011) according to RCP 8.5. These correspond to the prescribed concentrations of the RCM simulations.

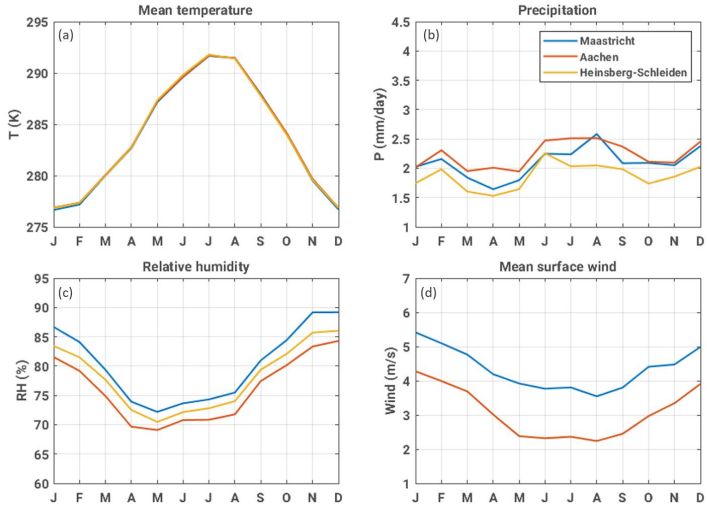

Figure A.33: Seasonal cycles of observed mean temperature (a), precipitation (b), relative humidity (c) and mean surface wind (d) in the weather stations of Maastricht Airport, Aachen and Heinsberg-Schleiden (monthly averages based on daily data from 1963 to 2018). For Heinsberg-Schleiden no surface wind observations are available. The curves for temperature are overlaying.

Weather station observations

Reference station data is obtained from the European Climate Assessment and Dataset (Klein Tank et al., 2002). The three operational weather stations closest to the UHasselt Ecotron experiment are Maastricht Airport (11km), Aachen (37km) and Heinsberg-Schleiden (29 km; Fig. A.32b). These weather stations provide daily observations from the end of the 19th century (Maastricht Airport and Aachen) or mid 20th century (Heinsberg-Schleiden) until the present-day, thereby covering both the EURO-CORDEX GCM and reanalysis downscaling periods. All stations record temperature [°C], precipitation [mm day^{-1}], relative humidity [%] and surface wind speed [m s^{-1}] at daily resolution, except for the Heinsberg-Schleiden station where there are no surface wind observations available.

The seasonal cycles of the observations for the different stations follow a similar annual course (Fig. A.33). For temperature, the curves overlay and for precipitation they are similar. Relative humidity has a small offset between the three stations, possibly owing to the differences in absolute height and local topography. The difference in surface wind speed between Maastricht-Airport and Aachen is considerable, but is plausible considering the large spatial variability in wind speed. Given that the model evaluation showed very little sensitivity to the choice of the reference station, we hereafter present the results with the reference station closest to the ecotron facility (Maastricht-Airport).

A.3.3 Metrics and diagnostics

The evaluation of the EURO-CORDEX ensemble members is performed using different metrics accounting for performance of representing the climatic means, distributions and extremes.

A ranking is made of the reanalysis downscalings, ranging from 1-best performing model to 9-worst. First, the bias is calculated as the difference between the averages of the daily modelled and observed variables. The second metric, the Perkins Skill Score (PSS), is a quantitative measure of how well each simulation resembles the observed probability density functions by measuring the common area between two probability density functions (Perkins et al., 2007). The mean absolute error (MAE) is calculated by taking the means of the absolute differences between the modelled and observed seasonal cycles, calculated based on the whole series. This is done for the whole series and to capture the potential errors in the extremes, also for the 1^{st}, 10^{th}, 90^{th} and 99^{th} percentiles which are calculated based on the daily time series of both observed and modelled time series. Next, the root mean square error (RMSE) is calculated by taking the root of the squared errors. The Spearman rank correlation (hereafter referred to as Spearman) coefficient shows the correlation of the observed and modelled series, calculated based on daily values. Finally, the Brier Skill Score (BSS) is calculated, which gives an indication of the improvement of the Brier Score (an index to validate probability forecasts) compared to a background climatology in which each event has an equal occurrence probability (Brier, 1950; Murphy, 1973). For the GCM downscalings, we use the same ranking method and scores, except for the RMSE, Spearman rank correlation and BSS because the internal variability, inherent to individual simulations with a coupled climate model, can not be predicted on multi-decal timescales, and can therefore not be compared to observations on a day-by-day basis (Fischer et al., 2014; Meehl et al., 2014).

In addition to the performance metrics computed on the actual time series, the RCM performance is also evaluated based on the bias in climatological diagnostics related to temperature and precipitation. To this extent, the average diurnal temperature range (DTR [K]; the difference between the daily maximum and minimum temperature) is calculated for the whole year, for the winter (December-January-February) and summer (June-July-August) season. Next, the number of wet days (defined as days during the year for which precipitation is larger than 0.1 mm or larger than 1 mm) and the number of frost days (days with a minimum temperature below 0 °C) are calculated. Furthermore, the monthly maximum 1-day precipitation (Rx1day [mm day^{-1}]) and the number of consecutive dry days (CDD [days]; the annual maximum number of days for which precipitation is below 1 mm) and consecutive wet days (CWD [days]; the annual maximum number of days for which precipitation is equal to or more than 1 mm) are included in the analysis. All indices are calculated for the simulated and observed time series, and consequently the ranking is established based on the difference between the model and observed diagnostic. Next, the correlation between the different variables is evaluated by comparing them to the observed correlation. This is done both on annual time scale and for the summer and winter seasonal

averages, as correlations are expected to differ in sign and magnitude between the two seasons (e.g. negative correlation between temperature and relative humidity in summer reflecting heatwave conditions, and a positive correlation between wind speed and precipitation in winter reflecting storm conditions).

After choosing the best performing simulation based on the evaluation of both the reanalysis and GCM downscalings, the climate change signals for this simulation are investigated by calculating changes in various climate change indices, based on the Expert Team on Climate Change Detection and Indices (ETCCDI; see `http://etccdi.pacificclimate.org/list_27_indices.shtml`) for the 5-year periods defined by the GMT anomalies relative to the reference period (1951-1955). These indices are widely used for analyzing changes in extremes (e.g. Zhang et al., 2009; Orlowsky and Seneviratne, 2013; Sillmann et al., 2013). The temperature indices are (i) ΔT [°C], the mean daily temperature change, (ii) ΔTXx [°C], the difference in annual maximum value of daily maximum temperature,(iii) ΔTNn [°C], the difference in annual minimum value of daily minimum temperature, (iv) Δ frost days, the difference in number of frost days (with a minimum temperature below 0°C), (v) Δ summer days, the difference in number of summer days (with the maximum temperature above 25°C), and finally (vi) ΔGSL [days], the difference in growing season length, defined as the annual count between the first span of at least 6 days with a daily mean temperature higher than 5 °C and the first span after July 1st of 6 days with a daily mean temperature lower than 5 °C. The precipitation indices are (i) $\Delta PRCPTOT$ [mm], the difference in annual accumulated precipitation (as simulated over the five-year period), (ii) $\Delta Rx1day$ [mm] the difference in monthly maximum 1-day precipitation, (iii) $\Delta R10mm$ [days] the difference in number of days per year with more than 10 mm precipitation, (iv) ΔCDD [days] the difference in the maximum length of a dry spell (measured as the maximum number of consecutive days with less than 1 mm precipitation) and finally, (v) ΔCWD [days] the maximum length of a wet spell (measured as the maximum number of consecutive days with more than 1 mm precipitation).

A.3.4 Applying the new methodology for the UHasselt Ecotron experiment

The best performing RCM simulation is identified by elimination based on expert judgment based on the performance of the two selection criteria. Next, we define the time windows for the different units along the gradient based on the 30-year averaged GMT anomaly of the driving GCM under RCP 8.5 relative to 1951-1955 (Section A.2, Fig. A.21, table A.2). Based on these time windows, we extract the three-hourly data for all necessary variables from the simulation for the 11 km by 11 km grid cell covering the location of the experiment.

A.4 Results

A.4.1 Identification of the best performing model simulation

First criterion: skill in present-day climate

Overall, model skill strongly varies across RCMs (Fig. A.44). While the annual temperature cycle is generally well represented by all RCMs, biases may reach up to 2 degrees in individual months for some RCMs. The biases in precipitation are generally positive (up to factor 2.4) and vary across RCMs. Only CCLM4-8-17 simulates precipitation in the same range as the observed climatology (nearly no bias (100.22%) on annual mean precipitation amounts), while the other RCMs overestimate the total precipitation amounts from 114% up to 182%. For relative humidity and surface wind speed, all RCMs generally succeed in representing the seasonal cycle, but exhibit deviations in amplitude and absolute values (e.g. amplitude biases of RCA4 (-37.8%), ALADIN53 (23.3%) and CCLM4-8-17 (+16.3%) for relative humidity, and annual mean biases for WRF331F (+15.6%) and HIRHAM5 (-9.1%) for surface wind speed). Overall, these seasonal cycles indicate that for all simulations, the relative bias in precipitation is large compared to biases in other variables.

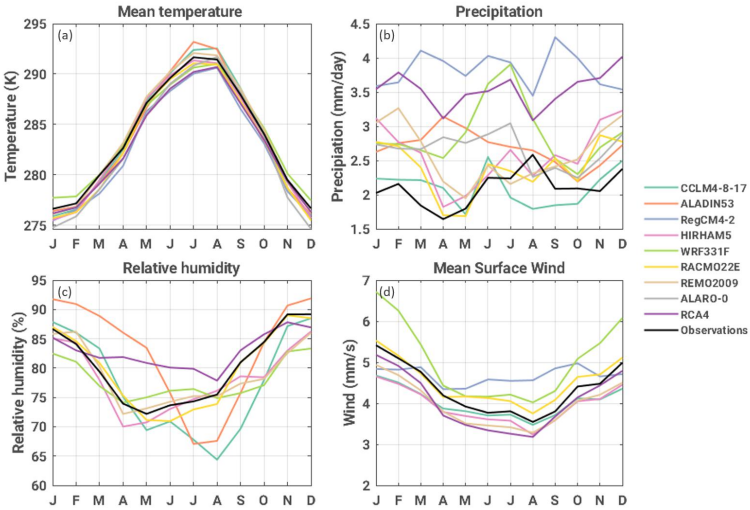

Figure A.44: **Seasonal cycle of the reanalysis downscalings** for mean temperature (a), precipitation (b), relative humidity (c) and mean surface wind speed (d). (The RegCM4-2 and ALARO-0 simulations are not available for relative humidity and the ALADIN53 and ALARO-0 simulations are not available for surface wind speed.)

The rankings of the reanalysis downscalings for the four variables (Fig. A.45) indicate that, overall, CCLM4-8-17, RACMO22E, REMO2009 and HIRHAM5 are performing best. CCLM4-8-17 and RACMO22E show the highest relative skill for precipitation, while REMO2009 and HIRHAM5 demonstrate high skill for temperature. CCLM4-8-17 is the best performing model based on the bias and total MAE metrics for temperature and precipitation, but is ranked in the mid range for the metrics related to the shape of its temperature distribution (PSS and percentile MAE). This can be attributed to an overestimation of the amplitude of the seasonal temperature cycle in this model (too cold in winters, too hot in summers; Fig. A.44a, (Kotlarski et al., 2014). For relative humidity and surface wind speed, RACMO22E generally demonstrates the highest skill. Considering the climatological diagnostics (Fig. A.47a), CCLM4-8-17 shows the highest relative skill for precipitation-related diagnostics (wet days, monthly maximum 1-day precipitation, length of dry and wet spells), while RACMO22E and RCA4 show higher relative skill for the annual, winter and summer diurnal temperature range. While RCA4 is highly ranked for temperature-related diagnostics, it is one of the models with the lowest relative skill for precipitation-related diagnostics. The correlation ranking shows a more scattered image, for the annual correlation as well as summer and winter correlations (see appendix Fig. A.712). Overall, as the reanalysis driven simulations with ALADIN53, RegCM4-2, WRF331F and ALARO-0 show the lowest skill compared to the other RCMs, we take them out of consideration to serve as ecosystem forcing.

Second, we evaluate the GCM downscalings for the period 1951-2005. The seasonal cycles of the temperature, precipitation, relative humidity and surface wind speed show a similar pattern as the reanalysis downscalings, with again a strong wet bias for precipitation in most models (see appendix Fig. A.714). The rankings show a mixed pattern for the different variables: there are no simulations which rank high for all considered variables (Fig. A.46). For precipitation, the simulations with CCLM4-8-17, RACMO22E have better relative skill compared to the other simulations, which is in line with the high ranking of these models in the reanalysis downscalings. Furthermore, it is remarkable that the simulations which show a high skill for precipitation, typically show lower skill for relative humidity and vice versa, e.g. CCLM4-8-17 driven by HadGEM2-ES (high ranking in precipitation, lowest in relative humidity) and REMO2009 driven by MPI-ESM-LR (high ranking in relative humidity and lower in precipitation). The three MPI-ESM-LR driven simulations appear to be better in reproducing the temperature climatology compared to the other simulations. For the climatological diagnostics, generally CCLM4-8-17 is scoring best for the precipitation-related diagnostics, whereas simulations with RCA4 are ranked the best for DTR (annual, summer and winter).

Based on the ranking of the GCM downscalings, the following simulations are considered potential candidates to serve as climate forcing: CCLM4-8-17 driven by CNRM-CM5, EC-EARTH and MPI-ESM-LR, HIRHAM5 driven by EC-EARTH and HadGEM2-ES, and RACMO22E driven by HadGEM2-ES (Figs. A.45,A.46 and A.47). Since precipitation biases strongly differ among RCMs (table A.1), and since precipitation is a critical variable for the ecosystem experiments (Van der Molen et al., 2011; Vicca et al., 2014; Estiarte

et al., 2016), we prioritize a minimum relative bias for precipitation over a lower bias for temperature, relative humidity and surface wind speed. The precipitation biases for the considered simulations are +150 mm year^{-1} for CCLM4-8-17 driven by CNRM-CM5, +8 mm year^{-1} for CCLM4-8-17 driven by EC-EARTH, +24 mm year^{-1} for CCLM4-8-17 driven by MPI-ESM-LR, +323 mm year^{-1} for HIRHAM5 driven by EC-EARTH, 101 mm year-1 for HIRHAM5 driven by HadGEM2-ES and 35.51 mm year^{-1} for RACMO22E driven by HadGEM2-ES. Based on this, the CCLM4-8-17 EC-EARTH driven simulations has the best chance to be chosen as forcing, followed by the CCLM4-8-17 MPI-ESM-LR and the RACMO22E HadGEM2-ES driven simulation.

Second criterion: Representativeness of multi-model mean in future projections

To verify the second requirement we look at anomalies from the mean signal of the four variables for the future period of the simulations under RCP 8.5. The EC-EARTH driven CCLM4-8-17 simulation is representative of the multi-model mean for all four variables (Fig. A.48), and even the median simulation for the mean temperature anomaly. For precipitation and relative humidity however, the CCLM4-8-17 EC-EARTH simulation show decreasing anomalies after 2050. underestimates the multi-model mean anomaly. The other selected simulations have a larger positive bias in precipitation for their GCM downscalings. A possible reason is that these simulations overestimate precipitation and simulate a more intensive hydrologic cycle, which also implies stronger changes in the future.

The remaining five simulations from step 1 (CCLM4-8-17 driven by MPI-ESM-LR, HIRHAM5 and RACMO22E driven by HadGEM2-ES) all systematically underestimate or overestimate other variables (Figs. A.715,A.716, A.717, A.718 and A.719). For instance, the mean temperature anomaly of CCLM4-8-17 driven by MPI-ESM-LR simulation (1.46 °C) is lower than the 10th percentile of all simulations (1.51 °C) and the temperature anomaly for CCLM4-8-17 driven by CNRM-CM5 is the 30th percentile (1.67 °C). HIRHAM5 driven by HadGEM2-ES overestimates relative humidity anomalies compared to the multi-model mean, with a mean value (1.26 %) around the 80th percentile. Finally, the HadGEM2-ES driven RACMO22E simulation overestimates relative humidity and temperature anomalies, up to the 90th percentile for temperature. Overall, we conclude that the EC-EARTH driven CCLM4-8-17 simulation is the most appropriate candidate for serving as climate forcing for the UHasselt Ecotron experiment.

Table A.1: Bias in annual precipitation (*P* bias) and rank based thereof (from 1-best to 18-worst) for the EURO-CORDEX GCM downscalings for the period 1951-2005 over Maastricht-Airport.

RCM	GCM	*P* bias (mm/year)	Rank
CCLM4-8-17	CNRM-CERFACS-CNRM-CM5	145	8
CCLM4-8-17	ICHEC-EC-EARTH	8	1
CCLM4-8-17	MOHC-HadGEM2-ES	-174	9
CCLM4-8-17	MPI-M-MPI-ESM-LR	24	2
ALADIN53	CNRM-CERFACS-CNRM-CM5	550	14
HIRHAM5	ICHEC-EC-EARTH	323	12
HIRHAM5	MOHC-HadGEM2-ES	101	6
HIRHAM5	NCC-NorESM1-M	571	16
WRF331F	IPSL-IPSL-CM5A-MR	726	18
RACMO22E	ICHEC-EC-EARTH	99	5
RACMO22E	MOHC-HadGEM2-ES	36	3
REMO2009	MPI-M-MPI-ESM-LR	225	10
ALARO-0	CNRM-CERFACS-CNRM-CM5	560	15
RCA4	CNRM-CERFACS-CNRM-CM5	319	11
RCA4	ICHEC-EC-EARTH	386	13
RCA4	IPSL-IPSL-CM5A-MR	691	17
RCA4	MOHC-HadGEM2-ES	111	7
RCA4	MPI-M-MPI-ESM-LR	70	4

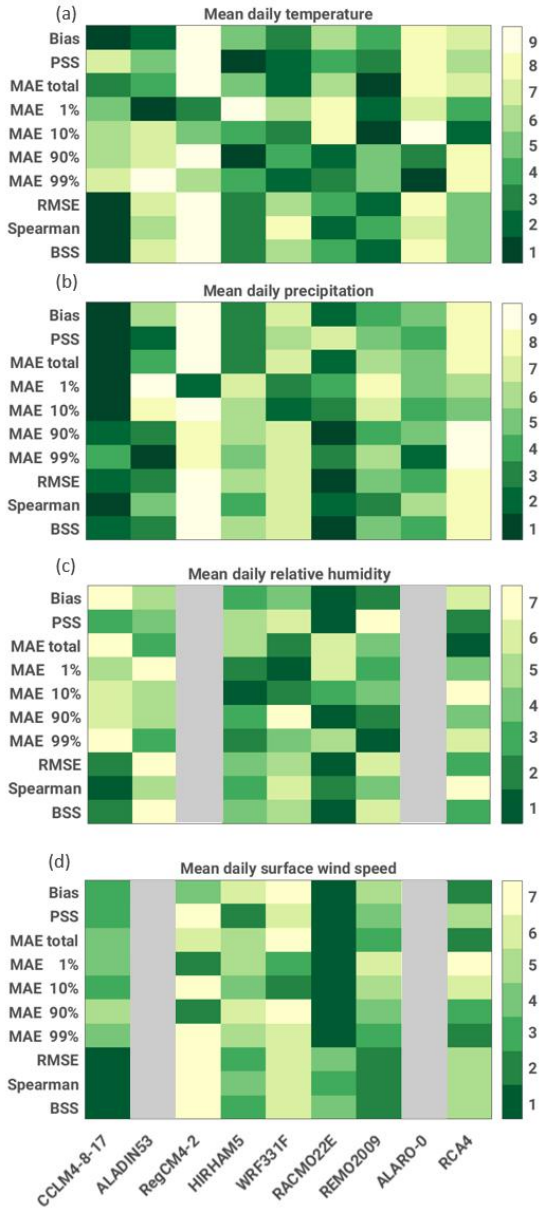

Figure A.45: **Ranking of the reanalysis downscalings** based on performance on temperature (a), precipitation (b), relative humidity (c) and surface wind speed (d) compared to observations from Maastricht. The metrics shown are the Bias, Perkins Skill Score (PSS), Mean Absolute Error (MAE) for the entire time series and the 1st, 10th, 90th and 99th percentiles, Root Mean Square Error (RMSE), Spearman rank correlation (Spearman) and Brier Skill Score (BSS). Rankings are from 1-best to 9-worst. Grey colors indicate that the variable is not available for the considered model.

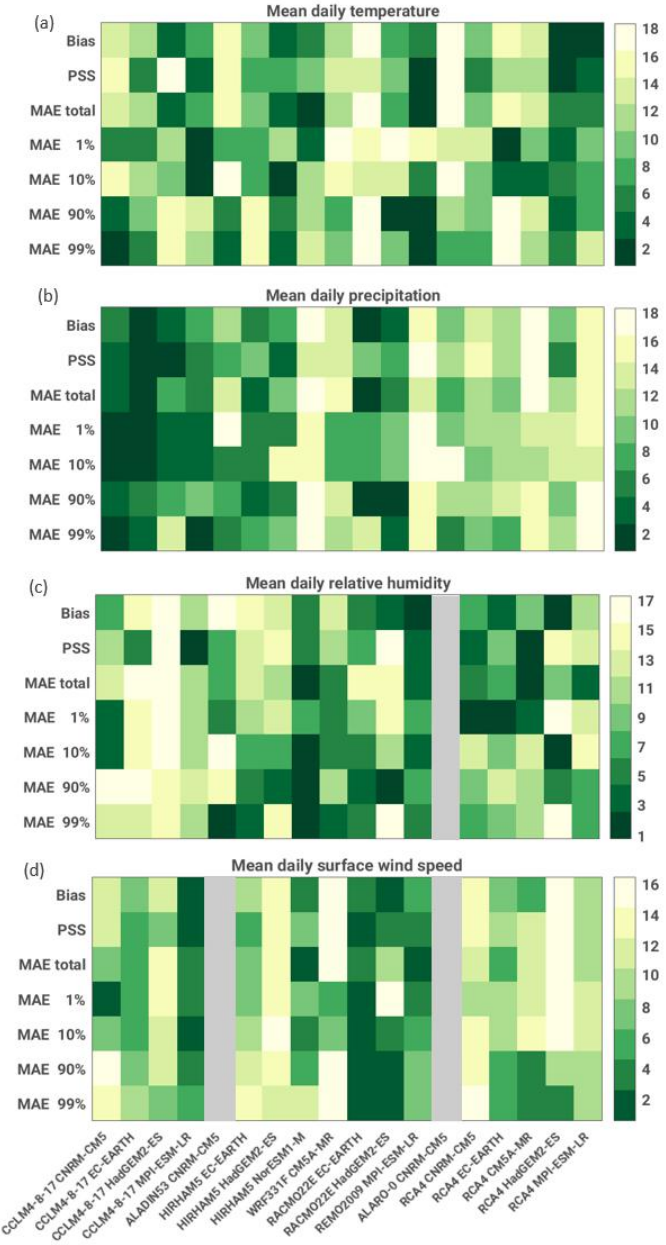

Figure A.46: **Ranking of the GCM downscalings** based on performance on temperature (a), precipitation (b), relative humidity (c) and surface wind speed (d) compared to observations from Maastricht. The metrics showed are the bias, Perkins Skill Score (PSS), Mean Absolute Error (MAE) for the total and 1st, 10th, 90th and 99th percentile. Rankings are from 1-best to 16, 17 or 18-worst for surface wind speed, relative humidity, precipitation and temperature, respectively. Grey colors indicate that the variable is not available for the considered model.

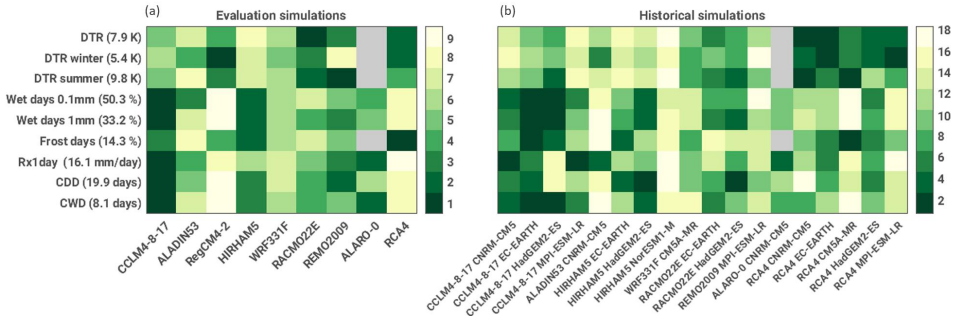

Figure A.47: **Ranking of the reanalysis (a) and GCM (b) downscalings for the historical period based on climatological diagnostics.** Diurnal temperature range (DTR) in summer (July-August) and winter (December-February), number of wet days defined as days with precipitation > 0.1 mm and precipitation > 1 mm, number of frost days defined as days with mean temperature < 273.15 K, Monthly maximum 1-day precipitation (Rx1day), consecutive dry days (CDD), the maximum length of a dry spell, and consecutive wet days (CWD), the maximum length of a wet spell. Next to the diagnostic name its value as observed in Maastricht-Airport is shown. Rankings are from 1-best to 9 or 18-worst for the reanalysis and GCM downscalings, respectively.

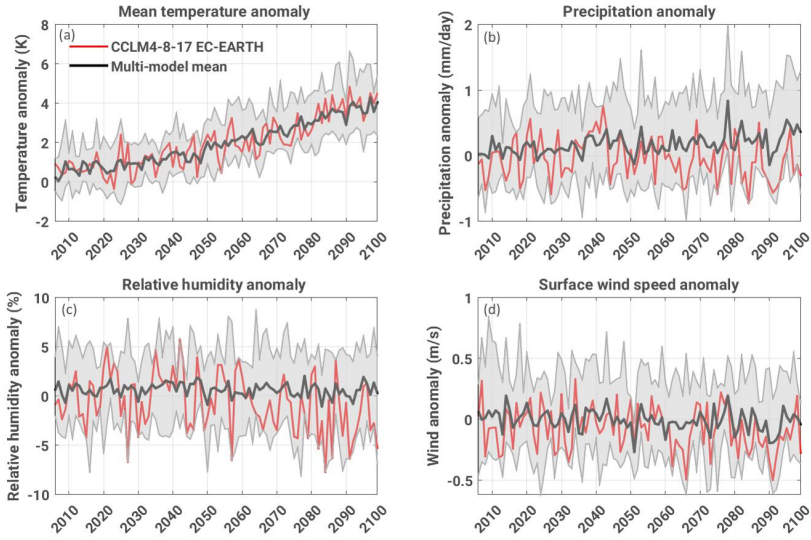

Figure A.48: **Anomalies for the CCLM4-8-17 EC-EARTH simulation following RCP 8.5** at the ecotron site for temperature (a), precipitation (b), relative humidity (c) and surface wind speed (d). The reference period is 1977 to 2006, the anomalies of the CLM4-8-17 EC-EARTH simulation are calculated compared to its own values in the reference period. In gray the envelope of all EURO-CORDEX RCP 8.5 simulations is showed.

A.4.2 Characterization of the selected meteorological forcing

Based on the selection criteria we single out the EC-EARTH (ensemble member r12i1p1) driven CCLM4-8-17 simulation as climate forcing for the UHasselt Ecotron experiment. The climatic conditions in the six units along the gradient represent an increasing signal of climate change. The overall trend of the local temperature anomaly compared to the reference period (0 °C) increases monotonically with the corresponding GMT anomalies (Fig. A.49a). No clear trends are visible for precipitation, relative humidity and surface wind speed anomalies, but very clear for the minimum and maximum temperature anomalies which are both increasing (Fig. A.49). The mean daily temperature is increasing at a similar rate compared to GMT anomaly, and minimum and maximum temperature show a larger increase (table A.2). None of the temperature indices show a linear increase, reflecting the difference between global and local climatic conditions and the influence of decadal internal variability. The ecotron unit representing a +4 °C world is the most extreme case, with increases of TXx of +6.30 °C and an increase of TNn with +10.21 °C (table A.2). The number of frost days decreases with about -76.2, while the number of summer days with a temperature above 25 °C increases with about 36.6 days. The annual growing season length is extended with 80 days on average, leaving only 59.4 days of the year not favourable for growth. The indices for precipitation show a less clear trend (table A.2). The total precipitation amount varies for the five units, without any trend and shows a substantial decadal variability in all seasons (see Fig. A.49) . $Rx1day$ has positive anomalies for the +1.5 °C, +2 °C and +3 °C units (+0.35 mm day^{-1} +1.92 mm day^{-1} and +2.34 mm day^{-1}, respectively). These +2 °C and +3 °C units also knows an increase in $R10mm$ (+3.2 and +3.6 days) compared to the other units. Finally, there is no clear trend in CWD, but there is an increase in CDD up to +11.8 days for the +4 °C unit. The +1.5 °C unit spans a drier time window, with an average CDD of +9.6 days. Figure A.49 further shows a systematic decrease of relative humidity during summer with increasing warming and a strong decadal variability of surface wind speed especially in winter.

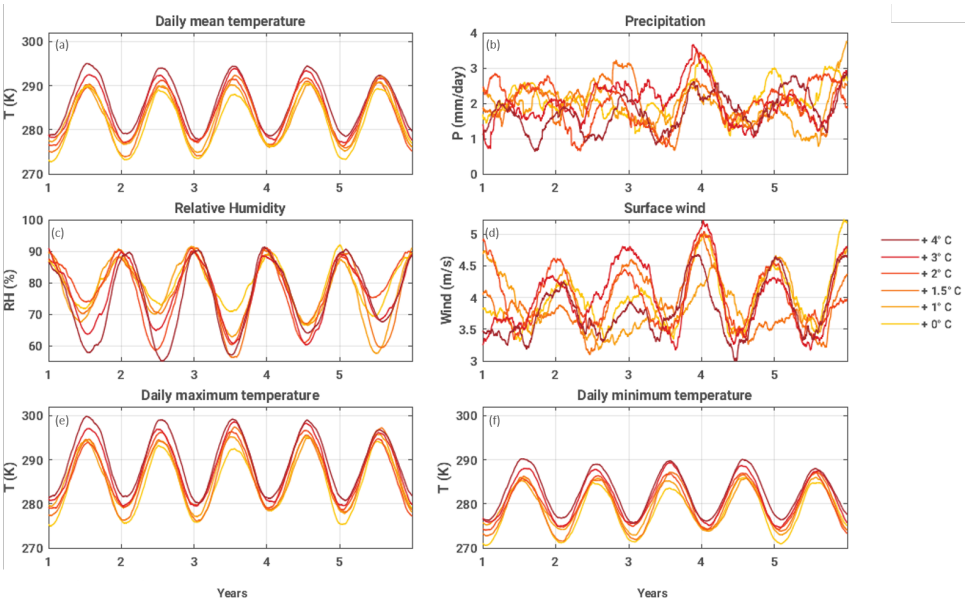

Figure A.49: **Annual cycles of the CCLM4-8-17 EC-EARTH ecotron unit forcing** for the +1 °C, +1.5 °C, +2 °C, +3 °C and +4 °C units compared to the 0 °C reference period. Curves were smoothed using Savitzky-Golay filtering (order = 2 frame = 301; Savitzky and Golay (1964)

Table A.2: **Extracted 5-year periods and temperature and precipitation indices based on ETCCDI for the CCLM4-8-17 EC-EARTH simulation at the ecotron location.** The 0 °C column gives the absolute reference values. The periods are calculated based on the 30-year averaged global mean temperature (GMT) anomaly calculated from EC-EARTH.

	0 °C *(ref value)* 1951 - 1955	+1 °C 2011 - 2015	+1.5 °C 2028 - 2032	+2 °C 2043 - 2047	+3 °C 2067 - 2071	+4 °C 2091 - 2095
ΔT [°C]	*8.17*	+1.13	+1.14	+1.81	+3.15	+4.49
ΔTXx [°C]	*30.98*	+0.82	+1.66	+1.34	+5.24	+6.30
ΔTNn [°C]	*-12.73*	+6.75	+3.34	+5.94	+8.27	+10.21
Δ Frost Days	*103*	-22	-14.8	-36.4	-59	-76.2
Δ Summer Days	*11.4*	+4	+12.2	+8.6	+26.2	+36.6
ΔGSL [days]	*225.6*	+9.6	+20	+33.6	+45.8	+80
$\Delta PRCPTOT$ [mm]	*771.09*	-81.32	-57.2	+25.12	-23.14	-136.05
$\Delta Rx1day$ [mm]	*14.38*	-0.2	+0.35	+1.92	+2.34	+0.5
$\Delta R10mm$ [days]	*14.6*	0	-1	+3.2	+3.6	-1.2
ΔCDD [days]	*17.2*	+2.4	+9.6	+1.6	+7.2	+11.8
ΔCWD [days]	*9.6*	-0.2	+1.2	+1.4	0	-1.8

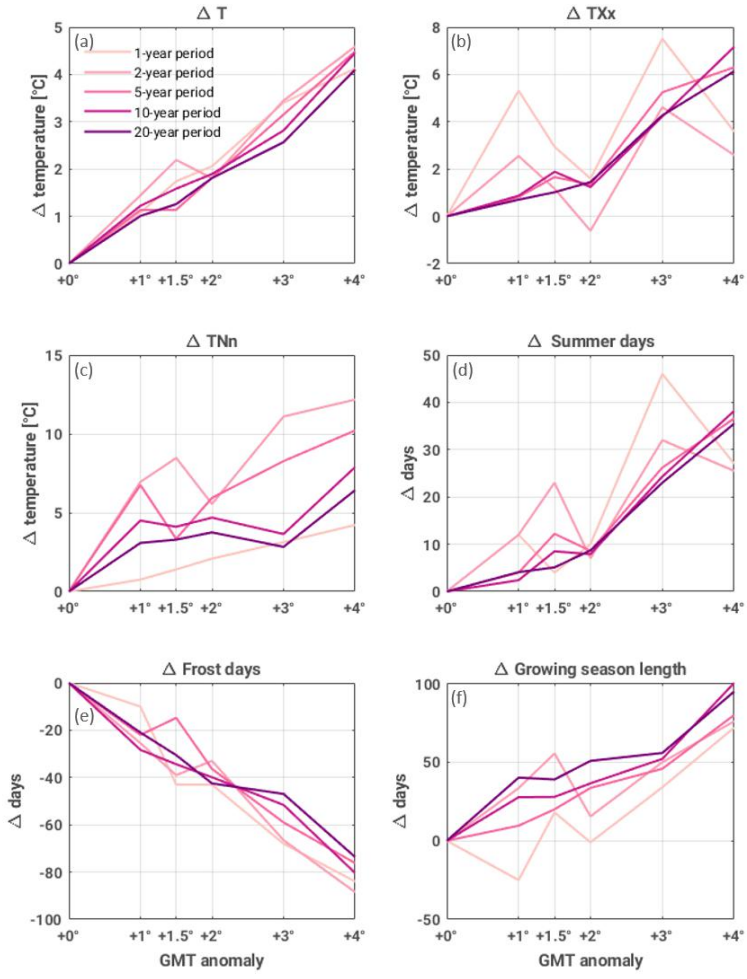

Figure A.410: **Annual anomalies per GMT anomaly for increasing time window lengths (ranging from a 1-year period to a 20-year period) of the CCLM4-8-17 EC-EARTH simulation following RCP 8.5** for temperature indices: mean temperature anomaly (ΔT; a), annual maximum temperature (ΔTXx; b), annual minimum temperature (ΔTNn; c); anomaly in annual number of summer days (d), frost days (e) and the anomaly in growing season length (f). Note the different y-axis scales.

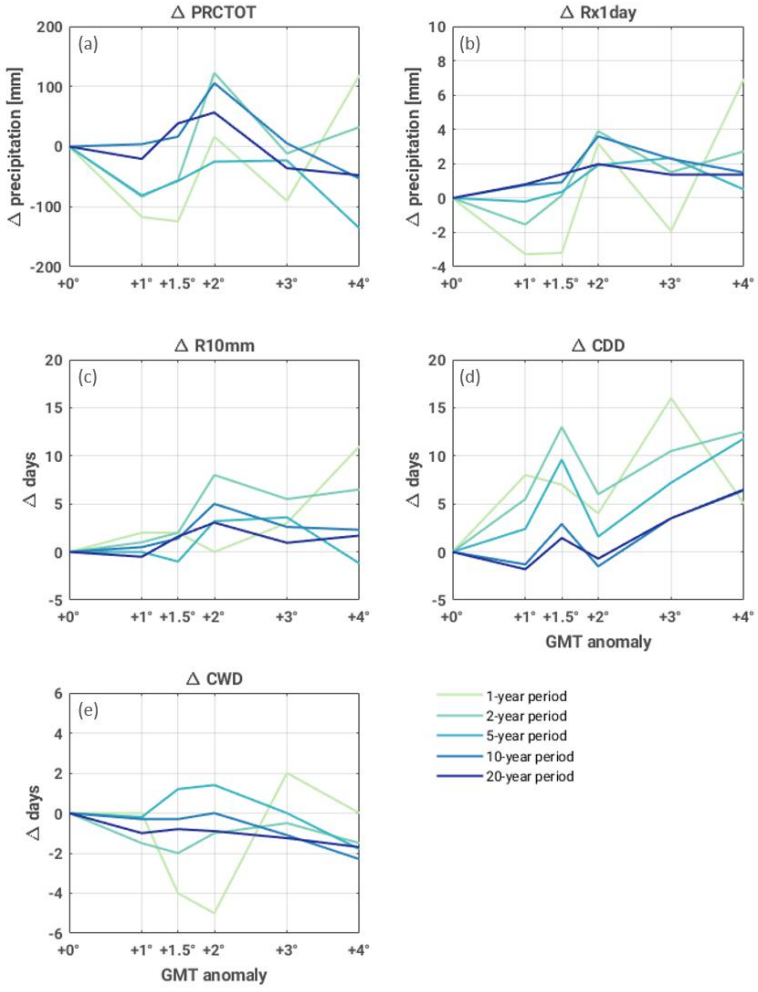

Figure A.411: Same as Fig. A.410, but now for precipitation indices: the annual accumulated precipitation anomaly ($\Delta PRCPTOT$; a), anomaly of monthly maximum 1-day precipitation ($\Delta Rx1day$; b), anomaly of annual number of days with more than 10 mm precipitation ($\Delta R10mm$; c), anomaly of annual maximum length of a dry spell (ΔCDD; d) and anomaly of maximum length of a wet spell (ΔCWD; e). Note the different y-axis scales.

A.5 Discussion

The presented methodology exhibit some challenges, which are addressed in the following section. We extract all climate variables from one grid cell of the RCM simulation to conserve a realistic, non smoothed signal. However, the extracted time series of the grid cell can differ a lot between different models and time periods, reflecting the natural climate variability. GCMs and RCMs provide robust signals when aggregated over a larger spatial area (Seneviratne et al., 2016; Fischer and Knutti, 2015). By taking the spatial mean, a more robust estimate of the mean climate is obtained, including robust signals of climate change. This explains the difference in local climate change signals (Fig. A.48, table A.2) and non-linearities compared to the GMT anomaly obtained by global averaging (Seneviratne et al., 2016). It is however necessary to use actual time series from a single grid cell to capture e.g. the extreme precipitation event occurring in the considered grid cell, but not in the neighbouring grid cells. The grid-cell values also reflect strong interannual to decadal variability which is of high relevance for a realistic forcing of the ecosystem.

Climate model simulations are often biased, which is mostly related to structural model deficiencies (Flato et al., 2013). Applying bias adjustment is a standard way to deal with biases (Gudmundsson et al., 2012; Vanderkelen et al., 2018b), but such methods face several challenges and need to be chosen carefully to not increase biases in the co-variability of variables (Zscheischler et al., 2019). In the proposed method we therefore directly use the 'raw' model output, as such preserving climate variability and the physically-consistent covariance of the different meteorological variables. In this way, the Ecotron experiment will study ecosystem responses to multi-variate drivers as compound controls. For instance, it will provide a unique opportunity to study the impact from realistic compound events (Zscheischler et al., 2018), e.g. events similar to the drought-heat event of 2018, which caused massive heather die-off both in the field and in the ecotrons, forced by conditions like they happened in the field.

The gradient for the different ecotron units does not follow a monotonic trend for some of the key indicators (Fig. A.49 and table A.2), due to the high local and inter-annual natural climate variability of the climate system. This issue could be alleviated by running the experiment for a longer period. Comparing different time frames, all extracted based on 30-year averaged GMT anomaly thresholds, shows that choosing longer time windows of 10 or 20 years leads to more clear monotonic trends (Figs. A.410 and A.411), which is more pronounced for temperature-derived indices than for precipitation-derived indices. For shorter time windows of 1 to 2 years, the inter-annual and local natural variability leads to larger variations in trend for the different GMT anomaly levels. Therefore, the experiment would have to run for a long period, but the experimental time frame is constrained by the experimental setup and possible renewal. As a compromise, here we use a 5-year experimental period. Ideally, the entire gradient should be replicated several times with different climate trajectories to average out the natural climate variability. This approach is however constrained by the high cost of the experimental set-up.

In the different ecotron units, we assume that the controlled variables (CO_2 and CH_4 concentration, temperature, precipitation, atmospheric humidity, wind, ...) are in equilibrium with the warming level, by extracting the 5-year period in which the GMT anomaly in the driving GCM is reached. While this is a reasonable assumption, several components in the climate system will not yet be in equilibrium with the GMT anomaly at the time of simulation (e.g. glaciers, ice sheets, sea level; Zekollari et al. (2019), Church et al. (2013). Therefore, we cannot rule out that changes in these slower components may still affect the meteorological conditions until these reach equilibrium too. For instance, a delayed melting of sea ice could alter the polar circulation and thereby affecting the mid-latitude circulation (Coumou et al., 2018), whereas ice sheet melting may affect oceanic pole-ward heat transport (Caesar et al., 2018). However, to select the time windows, we follow the same approach as the Transient Response to Cumulative Emissions (TRCE) as presented in the Intergovernmental Panel on Climate Change (IPCC) Fifth Assessment Report (IPCC 2013, 2013). This concept describes the warming per unit of carbon emissions, which largely follows a linear relationship independent of the emission scenario (Knutti and Rogelj, 2015).

The set-up of the UHasselt Ecotron experiment implies that the incoming shortwave radiation will follow current weather conditions and not the weather conditions as prescribed by the RCM forcing. It is thus possible to have, for instance, clear-sky conditions and associated high incoming shortwave radiation in the field, while in the ecotron unit a heavy precipitation event is simulated consistent with the RCM forcing. In this example, the system receives more incoming shortwave radiation than in the simulated climate. Likewise, the surface fluxes will be higher, but the resulting temperature and moisture is corrected within the ecotron unit by the controlling devices to fully follow the boundary layer conditions as they are prescribed by the RCM.

The UHasselt Ecotron experiment allows to investigate ecosystem responses to different levels of climate change. This allows to study subtle changes in ecosystem responses such as impacts of decreased frost frequency on plant mortality (Berendse et al., 1994) and the interactions between the occurrence of mild droughts and plant acclimation for longer droughts (Backhaus et al., 2014). Although climate variables are prescribed, ecosystem-climate feedbacks originating from interactions between the biosphere and atmosphere can by partially diagnosed. For instance, heatwave reinforcements by occurring droughts (Seneviratne et al., 2010; Zscheischler and Seneviratne, 2017) as well as soil moisture effects on precipitation events (Guillod et al., 2015) may be assessed by calculating imbalances in the energy budget.

A.6 Conclusions

Ecosystem experiments investigating climate change responses require a holistic, realistic climate forcing, reflecting not only the changes in the mean climate, but also representing physically consistent co-variance between climate drivers, natural variability, changes in extreme events. To this extent, we presented a new method for creating realistic climate forcing for manipulation experiments using a single Regional Climate Model (RCM) simulation, and subsequently applied it on the UHasselt Ecotron Experiment. To account for co-variances between variables and to fully capture the climate variability including extreme events, we selected an RCM simulation from the EURO-CORDEX ensemble based on the following criteria: (i) high skill in the local present-day climate and (ii) representative of local changes in the multi-model mean.

Based on a thorough evaluation of four key variables (temperature, precipitation, relative humidity and wind speed), we found that there is no single RCM-GCM combination outperforming all others for all considered variables and metrics. We made a selection of the six best performing simulations as potential candidates and verified whether they represent the multi-model mean for the considered variables. As precipitation is considered the most important variable in ecosystem experiments, and as most GCM downscalings have large bias for this variable, we use the precipitation bias as the decisive factor to single out the simulation which will serve as forcing: CCLM4-8-17 driven by EC-EARTH.

The units of the UHasselt Ecotron Experiment are forced with climate conditions along a Global Mean Temperature (GMT) anomaly gradient, representing conditions of a 0 °C (historical), +1 °C (present-day), +1.5 °C, +2 °C, +3 °C and +4 °C warmer world. Five-year time windows corresponding to these warming levels are defined based on when the 30-year averaged GMT anomaly of EC-EARTH, the driving GCM, crosses these temperature thresholds. Subsequently, the ecotron forcing is extracted from the 3-hourly RCM simulation according to the time windows.

Our new methodology provides realistic climate forcing, accounting for co-variances between climatic variables and their change in variability, well representing possible compound events. This is particularly interesting for controlled environment facilities, as their setup allows to realistically simulate future climate by controlling and measuring multiple parameters. Other controlled environment facilities could also benefit from the proposed methodology, depending on the posed research questions. The protocol for selecting a suitable regional climate simulation and extracting time series for the needed variables based on the time window defined by a global mean temperature threshold, provides a framework for different types of manipulation experiments aiming to investigate ecosystem responses to a realistic future climate change, even without a gradient approach.

Data and code availability

Reference station data of the European Climate Assessment and Dataset is publicly available at `https://www.ecad.eu/`. The greenhouse gas concentrations as prescribed by RCP 8.5 are available at `https://tntcat.iiasa.ac.at/RcpDb/`. Data from the Coordinated Regional Climate Downscaling Experiment (CORDEX) Africa framework is available at `http://cordex.org/data-access/esgf`. The scripts used in the analysis are available on github: `https://github.com/VUB-HYDR/2020_Vanderkelen_etal_IJBM`.

Acknowledgements

This research is supported by the Research Foundation Flanders (FWOTM920). Wim Thiery was supported by an ETH Zurich postdoctoral fellowship (Fel-45 15-1). The Uniscientia Foundation and the ETH Zurich Foundation are thanked for their support to this research. We are grateful to the World Climate Research Programme (WRCP) for initiating and coordinating the EURO-CORDEX initiative, to the modelling centres for making their downscaling results publicly available through ESGF. Computational resources and services were provided by the Shared ICT Services Centre funded by the Vrije Universiteit Brussel, the Flemish Supercomputer Center (VSC) and FWO. The authors thank the Flemish government (through Hercules stichting big infrastructure and the Fund for Scientific Research Flanders project G0H4117N), LSM (Limburg Sterk Merk, project 271) for providing funds to build the UHasselt Ecotron; Hasselt University for both funding and policy support (project BOF12BR01 and Methusalem project 08M03VGRJ); and the ecotron research committee for useful comments on the experimental design. We also thank RLKM (Regional Landscape Kempen and Maasland) for its collaboration and support.

A.7 Supplementary material

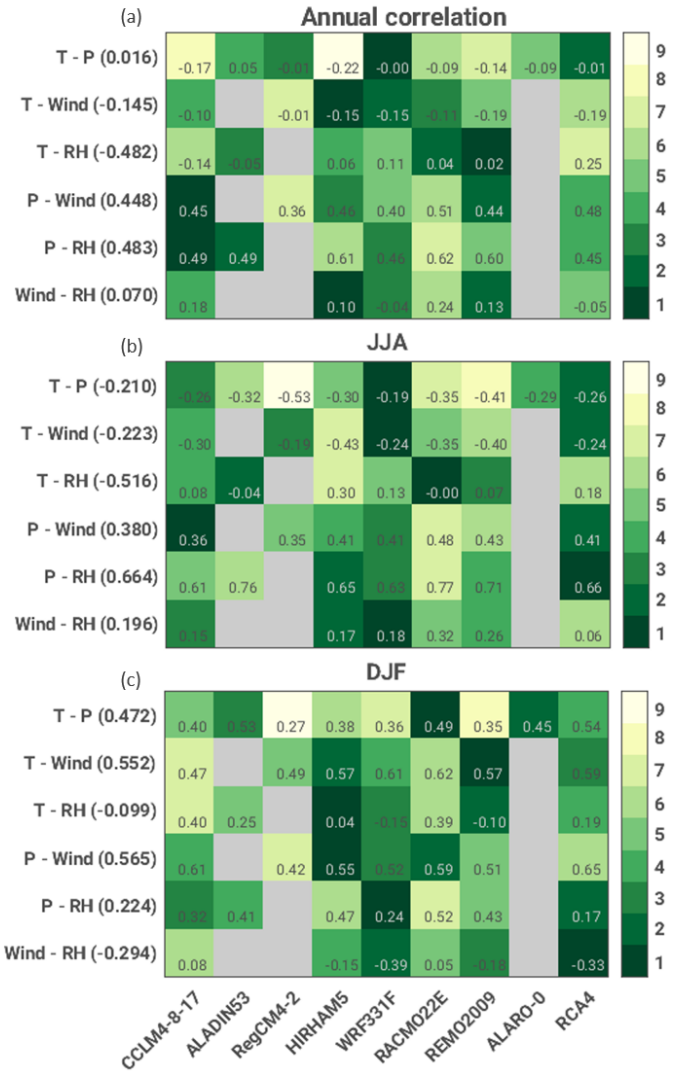

Figure A.712: Correlations for the reanalysis downscalings (1990-2008): Annual correlations (a), correlations in June, July and August (JJA; b) and correlations in December, January and February (DJF; c). T stands for temperature, P for precipitation and RH for relative humidity. The values in the y-axis labels are the observed correlations, and the other values correlations between the simulated variables. Rankings are from 1-best to 9-worst.

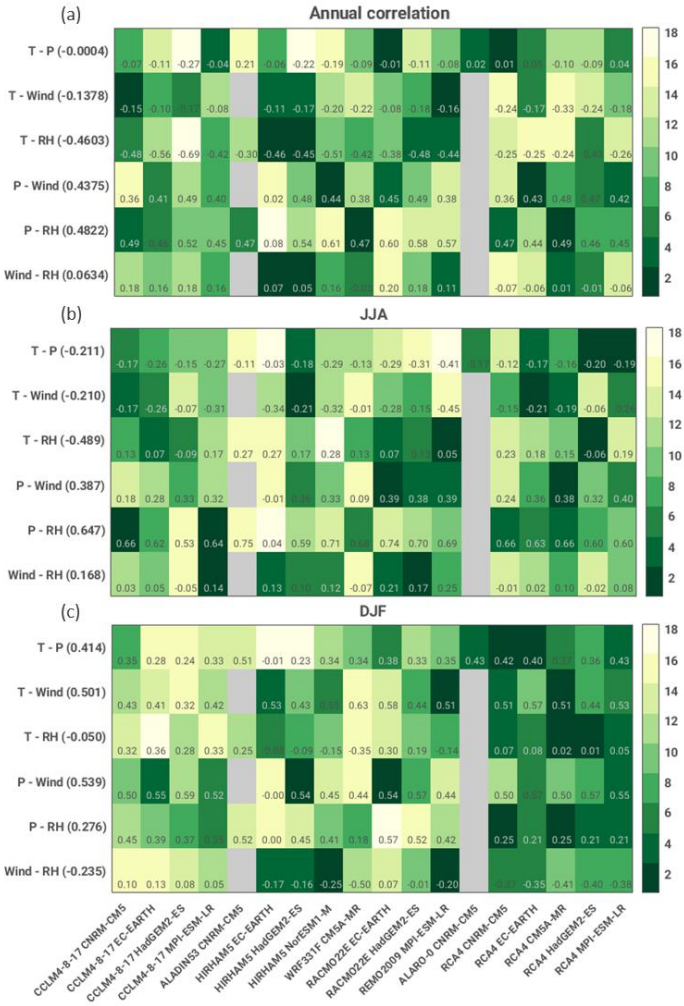

Figure A.713: Correlations for the GCM downscalings (1951-2005): Annual correlations (a), correlations in June, July and August (JJA; b) and correlations in December, January and February (DJF; c). T stands for temperature, P for precipitation and RH for relative humidity. The values in the y-axis labels are the observed correlations, and the other values correlations between the simulated variables. Rankings are from 1-best to 9-worst.

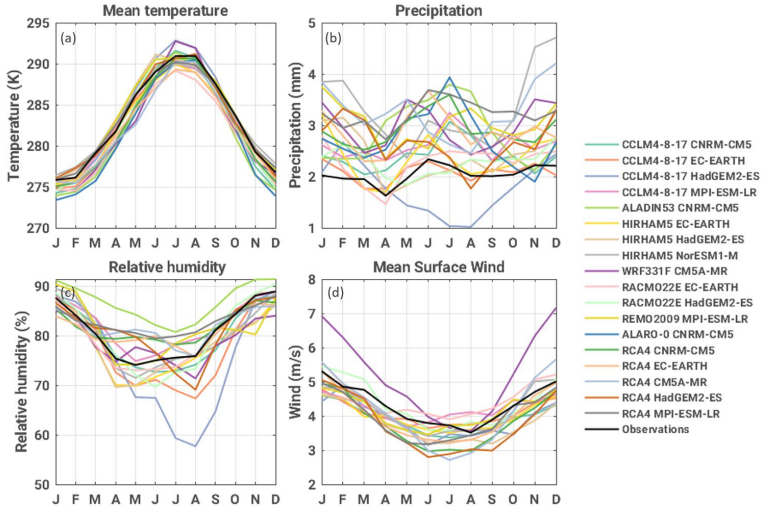

Figure A.714: **Seasonal cycle of the GCM downscalings** for mean temperature (a), precipitation (b), relative humidity (c) and mean surface wind speed (d).

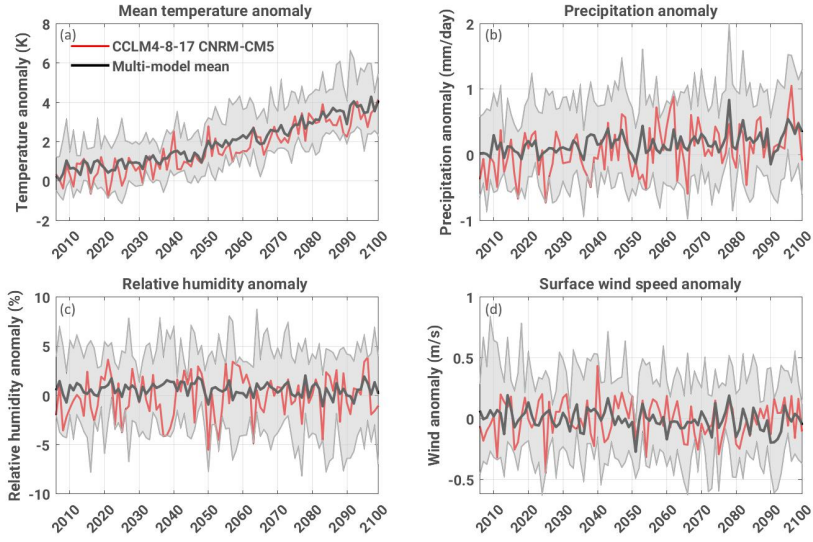

Figure A.715: Same as Fig. A.48, but now for CCLM4-8-17 CNRM-CM5.

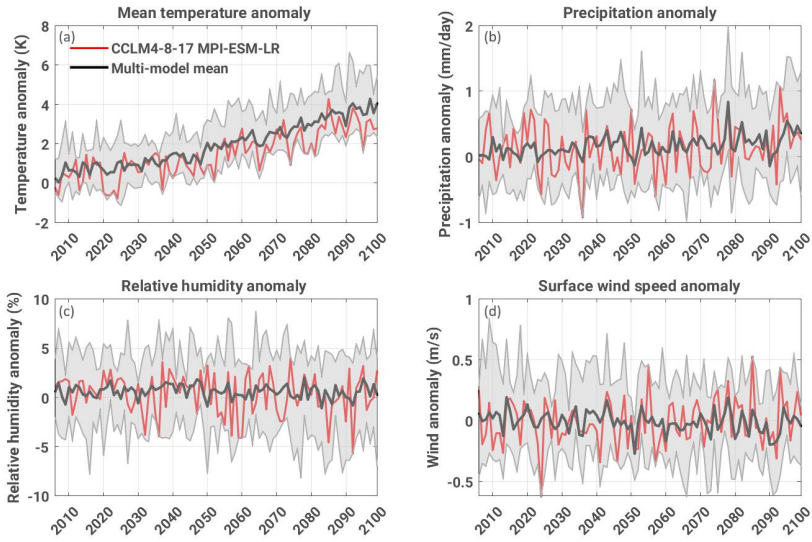

Figure A.716: Same as Fig. A.48, but now for CCLM4-8-17 MPI-ESM-LR.

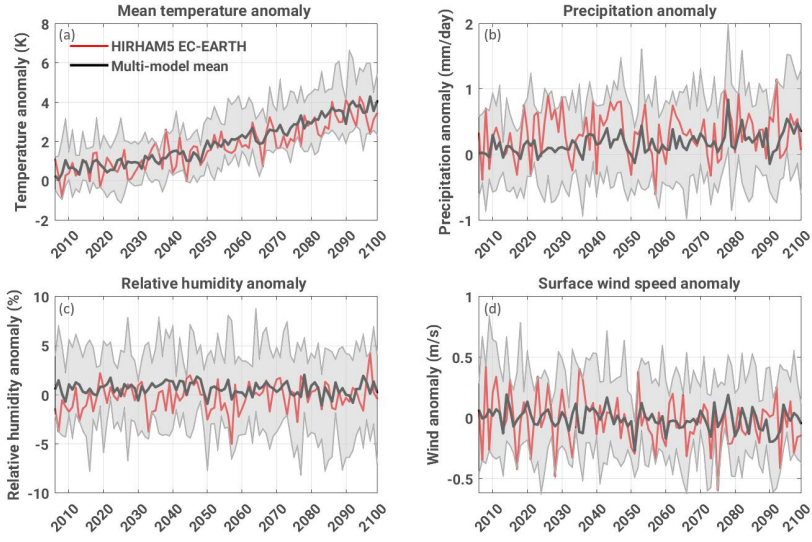

Figure A.717: Same as Fig. A.48, but now for HIRHAM5 EC-EARTH.

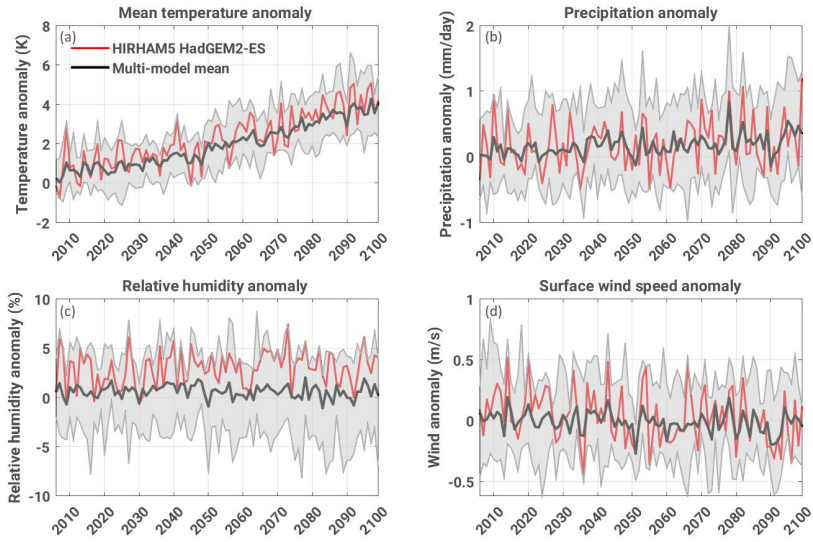

Figure A.718: Same as Fig. A.48, but now for HIRHAM5 HadGEM2-ES.

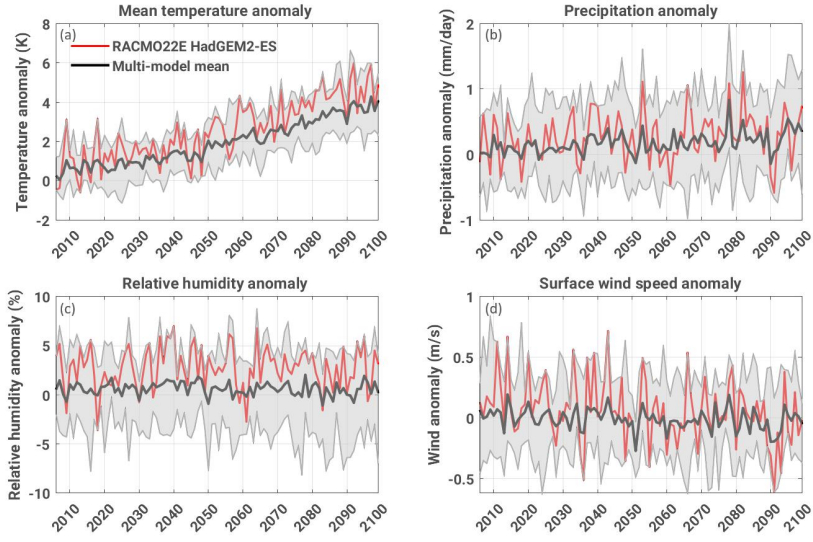

Figure A.719: Same as Fig. A.48, but now for RACMO22E HadGEM2-ES.

Bibliography

Abbott, B. W., Bishop, K., Zarnetske, J. P., Minaudo, C., Chapin, F. S., Krause, S., Hannah, D. M., Conner, L., Ellison, D., Godsey, S. E., Plont, S., Marçais, J., Kolbe, T., Huebner, A., Frei, R. J., Hampton, T., Gu, S., Buhman, M., Sara Sayedi, S., Ursache, O., Chapin, M., Henderson, K. D., and Pinay, G.: Human domination of the global water cycle absent from depictions and perceptions, Nature Geoscience, 12, 533–540, https://doi.org/10.1038/s41561-019-0374-y, 2019.

Adeyemi, K. O. and Asere, A. A.: a Review of the Energy Situation in Uganda, International Journal of Scientific and Research Publications, 4, 2250–3153, https://doi.org/10.1260/014459806779398811, 2014.

Adrian, R., O'reilly, C. M., Zagarese, H., Baines, S. B., Hessen, D. O., Keller, W., Livingstone, D. M., Sommaruga, R., Straile, D., Donk, E. V., Weyhenmeyer, G. A., Winder, M., and Muir, J.: Lakes as sentinels of climate change, Limnology and Oceanography, 54, 2283–2297, https://doi.org/https://doi.org/10.4319/lo.2009.54.6_part_2.2283, 2009.

Akkermans, T., Thiery, W., and Van Lipzig, N. P.: The Regional Climate Impact of a Realistic Future Deforestation Scenario in the Congo Basin, Journal of Climate, 27, 2714–2734, https://doi.org/10.1175/JCLI-D-13-00361.1, 2014.

Allen, G. H. and Pavelsky, T.: Global extent of rivers and streams, Science, 361, 585–588, https://doi.org/10.1126/science.aat063, 2018.

Ashouri, H., Hsu, K. L., Sorooshian, S., Braithwaite, D. K., Knapp, K. R., Cecil, L. D., Nelson, B. R., and Prat, O. P.: PERSIANN-CDR: Daily precipitation climate data record from multisatellite observations for hydrological and climate studies, Bulletin of the American Meteorological Society, 96, 69–83, https://doi.org/10.1175/BAMS-D-13-00068.1, 2015.

Awange, J. L., Ogalo, L., Bae, K. H., Were, P., Omondi, P., Omute, P., and Omullo, M.: Falling Lake Victoria water levels: Is climate a contributing factor?, Climatic Change, 89, 281–297, https://doi.org/10.1007/s10584-008-9409-x, 2007a.

Awange, J. L., Sharifi, M. A., Ogonda, G., Wickert, J., Grafarend, E. W., and Omulo, M. A.: The falling lake Victoria water level: GRACE, TRIMM and CHAMP satellite

analysis of the lake basin, Water Resources Management, 22, 775–796, https://doi.org/10.1007/s11269-007-9191-y, 2007b.

Backhaus, S., Kreyling, J., Grant, K., Beierkuhnlein, C., Walter, J., and Jentsch, A.: Recurrent Mild Drought Events Increase Resistance Toward Extreme Drought Stress, Ecosystems, 17, 1068–1081, https://doi.org/10.1007/s10021-014-9781-5, 2014.

Beltrami, H.: Earth's Long-Term Memory, Perspectives: Paleoclimae, 297, https://doi.org/10.1029/2001gl014310, 2002.

Berendse, F., Schmitz, M., and de Visser, W.: Experimental manipulation of succession in heathland ecosystems, Oecologia, 100, 38–44, https://doi.org/10.1007/BF00317128, 1994.

Biemans, H., Haddeland, I., Kabat, P., Ludwig, F., Hutjes, R. W. A., Heinke, J., Von Bloh, W., and Gerten, D.: Impact of reservoirs on river discharge and irrigation water supply during the 20th century, Water Resources Research, 47, 1–15, https://doi.org/10.1029/2009WR008929, 2011.

Bierkens, M. F. P.: Global hydrology 2015: State, trends, and directions, Water Resources Research, 51, 4923–4947, https://doi.org/10.1002/2015WR017173, 2015.

Bindoff, N. L., L Cheung, W. W., Kairo, J. G., Arístegui, J., Guinder, V. A., Hallberg, R., Hilmi Monaco, N., Jiao, N., saiful Karim, M., Levin, L., Acar, S., Jose Alava Ecuador, J., and Allison, E.: Changing Ocean, Marine Ecosystems, and Dependent Communities, in: IPCC Special Report on the Ocean and Crosphere in a Changing Climate, 2019.

Boé, J., Terray, L., Habets, F., and Martin, E.: Statistical and dynamical downscaling of the Seine basin climate for hydro-meteorological studies, International Journal of Climatology, 27, 1643–1655, https://doi.org/10.1002/joc.1602, 2007.

Bonan, G. B. and Doney, S. C.: Climate, ecosystems, and planetary futures: The challenge to predict life in Earth system models, Science, 359, https://doi.org/10.1126/science.aam8328, 2018.

Boulange, J., Hanasaki, N., Yamazaki, D., and Pokhrel, Y.: Role of dams in reducing global flood exposure under climate change, Nature Communications, 12, 417, https://doi.org/10.1038/s41467-020-20704-0, 2021.

Brier, G. W.: Verification of forecasts in terms of probability, Monthly Weather Review, 78, 1–3, 1950.

Brocca, L., Tarpanelli, A., Filippucci, P., Dorigo, W., Zaussinger, F., Gruber, A., and Fernández-Prieto, D.: How much water is used for irrigation? A new approach exploiting coarse resolution satellite soil moisture products, International Journal of Applied Earth Observation and Geoinformation, 73, 752–766, https://doi.org/10.1016/j.jag.2018.08.023, 2018.

Burek, P., Van Der Knijff, J., and De Roo, A.: LISFLOOD Distributed Water Balance and Flood Simulation Model: Revised User Manual, Tech. rep., Joint Research Center of the European Commission, Luxembourg, 2013.

Burek, P., Satoh, Y., Kahil, T., Tang, T., Greve, P., Smilovic, M., Guillaumot, L., Zhao, F., and Wada, Y.: Development of the Community Water Model (CWatM v1.04) - A high-resolution hydrological model for global and regional assessment of integrated water resources management, Geoscientific Model Development, 13, 3267–3298, https://doi.org/10.5194/gmd-13-3267-2020, 2020.

Busker, T., De Roo, A., Gelati, E., Schwatke, C., Adamovic, M., Bisselink, B., Pekel, J. F., and Cottam, A.: A global lake and reservoir volume analysis using a surface water dataset and satellite altimetry, Hydrology and Earth System Sciences, 23, 669–690, https://doi.org/10.5194/hess-23-669-2019, 2019.

Caesar, L., Rahmstorf, S., Robinson, A., Feulner, G., and Saba, V.: Observed fingerprint of a weakening Atlantic Ocean overturning circulation, Nature, 556, 191–196, https://doi.org/10.1038/s41586-018-0006-5, 2018.

Cannon, A. J.: Multivariate quantile mapping bias correction: an N-dimensional probability density function transform for climate model simulations of multiple variables, Climate Dynamics, 50, 31–49, https://doi.org/10.1007/s00382-017-3580-6, 2017.

Chao, B. F., Wu, Y. H., and Li, Y. S.: Impact of artificial reservoir water impoundment on global sea level, Science, 320, 212–214, https://doi.org/10.1126/science.1154580, 2008.

Chawanda, C. J., Arnold, J., Thiery, W., and van Griensven, A.: Mass balance calibration and reservoir representations for large-scale hydrological impact studies using SWAT+, Climatic Change, 163, 1307–1327, https://doi.org/10.1007/s10584-020-02924-x, 2020.

Cheng, L., Trenberth, K. E., Fasullo, J., Boyer, T., Abraham, J., and Zhu, J.: Improved estimates of ocean heat content from 1960 to 2015, Science Advances, 3, 1–10, https://doi.org/10.1126/sciadv.1601545, 2017.

Cheng, Y., Newman, A., Musselman, K. N., Swenson, S., Lawrence, D., Hamman, J., Dagon, K., and Kennedy, D.: Moving land models towards actionable science: A novel application of the Community Terrestrial Systems Model across Alaska and the Yukon River Basin, Water Resources Research, in review, https://doi.org/https://doi.org/10.1002/essoar.10510588.1, 2022.

Choulga, M., Kourzeneva, E., Zakharova, E., and Doganovsky, A.: Estimation of the mean depth of boreal lakes for use in numerical weather prediction and climate modelling, Tellus, Series A: Dynamic Meteorology and Oceanography, 66, https://doi.org/10.3402/tellusa.v66.21295, 2014.

Choulga, M., Kourzeneva, E., Balsamo, G., Boussetta, S., and Wedi, N.: Upgraded global mapping information for earth system modelling: An application to surface water depth

at the ECMWF, Hydrology and Earth System Sciences, 23, 4051–4076, https://doi.org/10.5194/hess-23-4051-2019, 2019.

Christensen, J. H., Boberg, F., Christensen, O. B., and Lucas-Picher, P.: On the need for bias correction of regional climate change projections of temperature and precipitation, Geophysical Research Letters, 35, 20 709, https://doi.org/10.1029/2008GL035694, 2008.

Church, J. A., Clark, P. U., Cazenave, A., Gregory, J. M., Jevrejeva, S., Levermann, M. A., Milne, G. A., Nerem, R. S., Nunn, P. D., Payne, A. J., Pfeffer, W. T., Stammer, D., and Unnikrishnan, A. S.: Sea Level Change, in: Climate Change 2013: The Physical Science Basis. Contribution of Working Group I to the Fifth Assessment Report of the Intergovernmental Panel on Climate Change, edited by Stocker, T. F., Qin, D., Plattner, G. K., Tignor, M., Allen, S. K., Boschung, J., Nauels, A., Xia, Y., Bex, V., and Midgley, P. M., pp. 1137–1216, Cambridge University Press, Cambridge, 2013.

Clark, M. P., Fan, Y., Lawrence, D. M., Adam, J. C., Bolster, D., Gochis, D. J., Hooper, R. P., Kumar, M., Leung, L. R., Mackay, D. S., Maxwell, R. M., Shen, C., Swenson, S. C., and Zeng, X.: Improving the representation of hydrologic processes in Earth System Models, Water Resources Research, 51, 5929–5956, https://doi.org/10.1002/2015WR017096, 2015.

Clobert, J., Chanzy, A., Galliard, J.-f. L., Chabbi, A., Greiveldinger, L., Caquet, T., Loreau, M., and Mougin, C.: How to Integrate Experimental Research Approaches in Ecological and Environmental Studies : AnaEE France as an Example, Frontiers in Ecology and Evolution, 6, 43, https://doi.org/10.3389/fevo.2018.00043, 2018.

Coerver, H. M., Rutten, M. M., and Van De Giesen, N. C.: Deduction of reservoir operating rules for application in global hydrological models, Hydrol. Earth Syst. Sci, 22, 831–851, https://doi.org/10.5194/hess-22-831-2018, 2018.

Collier, N., Hoffman, F. M., Lawrence, D. M., Keppel-Aleks, G., Koven, C. D., Riley, W. J., Mu, M., and Randerson, J. T.: The International Land Model Benchmarking (ILAMB) System: Design, Theory, and Implementation, Journal of Advances in Modeling Earth Systems, 10, 2731–2754, https://doi.org/10.1029/2018MS001354, 2018.

Compo, G. P., Whitaker, J. S., Sardeshmukh, P. D., Matsui, N., Allan, R. J., Yin, X., Gleason, B. E., Vose, R. S., Rutledge, G., Bessemoulin, P., BroNnimann, S., Brunet, M., Crouthamel, R. I., Grant, A. N., Groisman, P. Y., Jones, P. D., Kruk, M. C., Kruger, A. C., Marshall, G. J., Maugeri, M., Mok, H. Y., Nordli, O., Ross, T. F., Trigo, R. M., Wang, X. L., Woodruff, S. D., and Worley, S. J.: The Twentieth Century Reanalysis Project, https://doi.org/10.1002/qj.776, 2011.

Cooley, S. W., Ryan, J. C., and Smith, L. C.: Human alteration of global surface water storage variability, Nature, 591, 78–81, https://doi.org/10.1038/s41586-021-03262-3, 2021.

Coumou, D., Di Capua, G., Vavrus, S., Wang, L., and Wang, S.: The influence of Arctic amplification on mid-latitude summer circulation, https://doi.org/10.1038/s41467-018-05256-8, 2018.

Crétaux, J. F., Arsen, A., Calmant, S., Kouraev, A., Vuglinski, V., Bergé-Nguyen, M., Gennero, M. C., Nino, F., Abarca Del Rio, R., Cazenave, A., and Maisongrande, P.: SOLS: A lake database to monitor in the Near Real Time water level and storage variations from remote sensing data, Advances in Space Research, 47, 1497–1507, https://doi.org/10.1016/j.asr.2011.01.004, 2011.

Cuesta-Valero, F. J., García-García, A., Beltrami, H., and Smerdon, J. E.: First assessment of continental energy storage in CMIP5 simulations, Geophysical Research Letters, 43, 5326–5335, https://doi.org/10.1002/2016GL068496, 2016.

Curtis, P. S. and Wang, X.: A meta-analysis of elevated CO2 effects on woody plant mass, form, and physiology, Oecologia, 113, 299–313, https://doi.org/10.1007/s004420050381, 1998.

Dagon, K., Sanderson, B. M., Fisher, R. A., and Lawrence, D. M.: A machine learning approach to emulation and biophysical parameter estimation with the Community Land Model, version 5, Advances in Statistical Climatology, Meteorology and Oceanography, 6, 223–244, https://doi.org/10.5194/ascmo-6-223-2020, 2020.

Dai, A. and Trenberth, K. E.: Estimates of freshwater discharge from continents: Latitudinal and seasonal variations, Journal of Hydrometeorology, 3, 660–687, https://doi.org/10.1175/1525-7541(2002)003<0660:EOFDFC>2.0.CO;2, 2002.

Danabasoglu, G., Lamarque, J. F., Bacmeister, J., Bailey, D. A., DuVivier, A. K., Edwards, J., Emmons, L. K., Fasullo, J., Garcia, R., Gettelman, A., Hannay, C., Holland, M. M., Large, W. G., Lauritzen, P. H., Lawrence, D. M., Lenaerts, J. T., Lindsay, K., Lipscomb, W. H., Mills, M. J., Neale, R., Oleson, K. W., Otto-Bliesner, B., Phillips, A. S., Sacks, W., Tilmes, S., van Kampenhout, L., Vertenstein, M., Bertini, A., Dennis, J., Deser, C., Fischer, C., Fox-Kemper, B., Kay, J. E., Kinnison, D., Kushner, P. J., Larson, V. E., Long, M. C., Mickelson, S., Moore, J. K., Nienhouse, E., Polvani, L., Rasch, P. J., and Strand, W. G.: The Community Earth System Model Version 2 (CESM2), Journal of Advances in Modeling Earth Systems, 12, 1–35, https://doi.org/10.1029/2019MS001916, 2020.

Davin, E. L. and Seneviratne, S. I.: Role of land surface processes and diffuse/direct radiation partitioning in simulating the European climate, Biogeosciences, 9, 1695–1707, https://doi.org/10.5194/bg-9-1695-2012, 2012.

Davin, E. L., Maisonnave, E., and Seneviratne, S. I.: Is land surface processes representation a possible weak link in current Regional Climate Models?, Environmental Research Letters, 11, 74 027, https://doi.org/10.1088/1748-9326/11/7/074027, 2016.

De Boeck, H. J., Van De Velde, H., De Groote, T., and Nijs, I.: Ideas and perspectives: Heat stress: More than hot air, Biogeosciences, 13, 5821–5825, https://doi.org/10.5194/bg-13-5821-2016, 2016.

De Kauwe, M. G., Disney, M. I., Quaife, T., Lewis, P., and Williams, M.: An assessment of the MODIS collection 5 leaf area index product for a region of mixed coniferous forest, Remote Sensing of Environment, 115, 767–780, https://doi.org/10.1016/j.rse.2010.11.004, 2011.

De Vrese, P., Hagemann, S., and Claussen, M.: Asian irrigation, African rain: Remote impacts of irrigation, Geophysical Research Letters, 43, 3737–3745, https://doi.org/10.1002/2016GL068146, 2016.

de Vrese, P., Stacke, T., and Hagemann, S.: Exploring the biogeophysical limits of global food production under different climate change scenarios, Earth Syst. Dynam, 9, 393–412, https://doi.org/10.5194/esd-9-393-2018, 2018.

Deconinck, S.: Security as a threat to development: the geopolitics of water scarcity in the Nile River basin, Focus Paper, Royal High Insitute for Defence, Brussels-Belgium, 2009.

Degu, A. M., Hossain, F., Niyogi, D., Pielke, R., Shepherd, J. M., Voisin, N., and Chronis, T.: The influence of large dams on surrounding climate and precipitation patterns, Geophysical Research Letters, 38, 1–7, https://doi.org/10.1029/2010GL046482, 2011.

Deser, C., Knutti, R., Solomon, S., and Phillips, A. S.: Communication of the role of natural variability in future North American climate, Nature Climate Change, 2, 775–779, https://doi.org/10.1038/nclimate1562, 2012.

Devanand, A., Huang, M., Ashfaq, M., Barik, B., and Ghosh, S.: Choice of Irrigation Water Management Practice Affects Indian Summer Monsoon Rainfall and Its Extremes, Geophysical Research Letters, 46, 9126–9135, https://doi.org/10.1029/2019GL083875, 2019.

Devanand, A., Huang, M., Lawrence, D. M., Zarzycki, C. M., Feng, Z., Lawrence, P. J., Qian, Y., and Yang, Z.: Land Use and Land Cover Change Strongly Modulates Land-Atmosphere Coupling and Warm-Season Precipitation Over the Central United States in CESM2-VR, Journal of Advances in Modeling Earth Systems, 12, e2019MS001 925, https://doi.org/10.1029/2019MS001925, 2020.

Di Baldassarre, G., Elshamy, M., Van Griensven, A., Soliman, E., Kigobe, M., Ndomba, P., Mutemi, J., Mutua, F., Moges, S., Xuan, Y., Solomatine, D., and Uhlenbrook, S.: Future hydrology and climate in the River Nile basin: a review, Hydrological Sciences Journal, 56, 199–211, https://doi.org/10.1080/02626667.2011.557378, 2011.

Di Baldassarre, G., Martinez, F., Kalantari, Z., and Viglione, A.: Drought and flood in the Anthropocene: feedback mechanisms in reservoir operation, Earth Syst. Dynam, 8, 225–233, https://doi.org/10.5194/esd-8-225-2017, 2017.

Di Baldassarre, G., Wanders, N., AghaKouchak, A., Kuil, L., Rangecroft, S., Veldkamp, T. I. E., Garcia, M., van Oel, P. R., Breinl, K., and Van Loon, A. F.: Water shortages

worsened by reservoir effects, Nature Sustainability, 1, 617–622, https://doi.org/10.1038/s41893-018-0159-0, 2018.

Di Baldassarre, G., Mazzoleni, M., and Rusca, M.: The legacy of large dams in the United States, Ambio, 50, 1798–1808, https://doi.org/10.1007/s13280-021-01533-x, 2021.

Do, H. X., Gudmundsson, L., Leonard, M., and Westra, S.: The Global Streamflow Indices and Metadata Archive (GSIM)-Part 1: The production of a daily streamflow archive and metadata, Earth Syst. Sci. Data, 10, 765–785, https://doi.org/10.5194/essd-10-765-2018, 2018.

Docquier, D., Thiery, W., Lhermitte, S., and van Lipzig, N.: Multi-year wind dynamics around Lake Tanganyika, Climate Dynamics, 47, 3191–3202, https://doi.org/10.1007/s00382-016-3020-z, 2016.

Döll, P., Kaspar, F., and Lehner, B.: A global hydrological model for deriving water availability indicators: Model tuning and validation, Journal of Hydrology, 270, 105–134, https://doi.org/10.1016/S0022-1694(02)00283-4, 2003.

Döll, P., Fiedler, K., and Zhang, J.: Global-scale analysis of river flow alterations due to water withdrawals and reservoirs, Hydrology and Earth System Sciences, 13, 2413–2432, https://doi.org/10.5194/hess-13-2413-2009, 2009.

Droppers, B., Franssen, W. H. P., Van Vliet, M. T. H., Nijssen, B., and Ludwig, F.: Simulating human impacts on global water resources using VIC-5, Geosci. Model Dev, 13, 5029–5052, https://doi.org/10.5194/gmd-13-5029-2020, 2020.

Dutra, E., Stepanenko, V. M., Balsamo, G., Viterbo, P., Miranda, P. M., Mironov, D., and Schär, C.: An offline study of the impact of lakes on the performance of the ECMWF surface scheme, Boreal Environment Research, 15, 100–112, 2010.

Ehsani, N., Fekete, B. M., Vörösmarty, C. J., and Tessler, Z. D.: A neural network based general reservoir operation scheme, Stochastic Environmental Research and Risk Assessment, 30, 1151–1166, https://doi.org/10.1007/s00477-015-1147-9, 2016.

Endris, H. S., Omondi, P., Jain, S., Lennard, C., Hewitson, B., Chang'a, L., Awange, J. L., Dosio, A., Ketiem, P., Nikulin, G., Panitz, H. J., Büchner, M., Stordal, F., and Tazalika, L.: Assessment of the performance of CORDEX regional climate models in simulating East African rainfall, Journal of Climate, 26, 8453–8475, https://doi.org/10.1175/JCLI-D-12-00708.1, 2013.

Estiarte, M., Vicca, S., Peñuelas, J., Bahn, M., Beier, C., Emmett, B. A., Fay, P. A., Hanson, P. J., Hasibeder, R., Kigel, J., Kröel-Dulay, G., Larsen, K. S., Lellei-Kovács, E., Limousin, J. M., Ogaya, R., Ourcival, J. M., Reinsch, S., Sala, O. E., Schmidt, I. K., Sternberg, M., Tielbörger, K., Tietema, A., and Janssens, I. A.: Few multiyear precipitation-reduction experiments find a shift in the productivity-precipitation relationship, Global change biology, 22, 2570–2581, https://doi.org/10.1111/gcb.13269, 2016.

Eyring, V., Bony, S., Meehl, G. A., Senior, C. A., Stevens, B., Stouffer, R. J., and Taylor, K. E.: Overview of the Coupled Model Intercomparison Project Phase 6 (CMIP6) experimental design and organization, Geoscientific Model Development, 9, 1937–1958, https://doi.org/10.5194/gmd-9-1937-2016, 2016.

Farinotti, D., Round, V., Huss, M., Compagno, L., and Zekollari, H.: Large hydropower and water-storage potential in future glacier-free basins, Nature, 575, https://doi.org/10.1038/s41586-019-1740-z, 2019.

Felfelani, F., Lawrence, D. M., and Pokhrel, Y.: Representing Intercell Lateral Groundwater Flow and Aquifer Pumping in the Community Land Model, Water Resources Research, 57, e2020WR027 531, https://doi.org/10.1029/2020WR027531, 2020.

Felfelani, F., Lawrence, D. M., and Pokhrel, Y.: Representing Intercell Lateral Groundwater Flow and Aquifer Pumping in the Community Land Model, Water Resources Research, 57, https://doi.org/10.1029/2020WR027531, 2021.

Fischer, E. M. and Knutti, R.: Anthropogenic contribution to global occurrence of heavy-precipitation and high-temperature extremes, Nature Climate Change, 5, 560–564, https://doi.org/10.1038/nclimate2617, 2015.

Fischer, E. M., Sedláček, J., Hawkins, E., and Knutti, R.: Models agree on forced response pattern of precipitation and temperature extremes, Geophysical Research Letters, 41, 8554–8562, https://doi.org/10.1002/2014GL062018, 2014.

Flato, G., Marotzke, J., Abiodun, B., Braconnot, P., Chou, S. C., Collins, W., Cox, P., Driouech, F., Emori, S., Eyring, V., Forst, C., Gleckler, P., Guilyardi, E., Jakob, C., Kattsov, C., Reason, V., and Rummukainen, M.: Evaluation of Climate Models, in: Climate Change 2013: The Physical Science Basis. Contribution of Working Group I to the Fifth Assessment Report of the Intergovernmental Panel on Climate Change, edited by Stocker, T. F., Qin, D., Plattner, G.-K., Tignor, M., Allen, S. K., Boschung, J., Nauels, A., Xia, Y., Bex, V., and Midgley, P. M., pp. 741–866, Cambridge University Press, Cambridge, United Kingdom and New York, NY, USA, 2013.

Forster, P., Storelvmo, T., Armour, K., Collins, W., Dufresne, J. L., Frame, D., Lunt, D. J., Mauritsen, T., Palmer, M. D., Watanabe, M., Wild, M., and Zhang, H.: The Earth's Energy Budget, Climate Feedbacks, and Climate Sensitivity, in: Climate Change 2021: The Physical Science Basis. Contribution of Working Group I to the Sixth Assessment Report of the Intergovernmental Panel on Climate Change, edited by Masson-Delmotte, V., Zhai, P., Pirani, A., Connors, S. L., Péan, C., Berger, S., Caud, N., Chen, Y., Goldfarb, L., Gomis, M. I., Huang, M., Leitzell, K., Lonnoy, E., Matthews, J., Maycock, T. K., Waterfield, T., Yelekçi, O., R., Y., and Zhou, B., Cambridge University Press, in press edn., 2021.

Frederikse, T., Landerer, F., Caron, L., Adhikari, S., Parkes, D., Humphrey, V. W., Dangendorf, S., Hogarth, P., Zanna, L., Cheng, L., and Wu, Y. H.: The causes of sea-level rise since 1900, Nature, 584, 393–397, https://doi.org/10.1038/s41586-020-2591-3, 2020.

Friedrich, K., Grossman, R. L., Huntington, J., Blanken, P. D., Lenters, J., Holman, K. L. D., Gochis, D., Livneh, B., Prairie, J., Skeie, E., Healey, N. C., Dahm, K., Pearson, C., Finnessey, T., Hook, S. J., and Kowalski, T.: Reservoir evaporation in the Western United States, Bulletin of the American Meteorological Society, 99, 167–187, https://doi.org/10.1175/BAMS-D-15-00224.1, 2018.

Frieler, K., Lange, S., Piontek, F., Reyer, C. P. O., Schewe, J., Warszawski, L., Zhao, F., Chini, L., Denvil, S., Emanuel, K., Geiger, T., Halladay, K., Hurtt, G., Mengel, M., Murakami, D., Ostberg, S., Popp, A., Riva, R., Stevanovic, M., Suzuki, T., Volkholz, J., Burke, E., Ciais, P., Ebi, K., Eddy, T. D., Elliott, J., Galbraith, E., Gosling, S. N., Hattermann, F., Hickler, T., Hinkel, J., Hof, C., Huber, V., Jägermeyr, J., Krysanova, V., Marcé, R., Müller Schmied, H., Mouratiadou, I., Pierson, D., Tittensor, D. P., Vautard, R., van Vliet, M., Biber, M. F., Betts, R. A., Bodirsky, B. L., Deryng, D., Frolking, S., Jones, C. D., Lotze, H. K., Lotze-Campen, H., Sahajpal, R., Thonicke, K., Tian, H., and Yamagata, Y.: Assessing the impacts of 1.5 °C global warming - simulation protocol of the Inter-Sectoral Impact Model Intercomparison Project (ISIMIP2b), Geoscientific Model Development, 10, 4321–4345, https://doi.org/10.5194/gmd-10-4321-2017, 2017.

Gao, H., Birkett, C., and Lettenmaier, D. P.: Global monitoring of large reservoir storage from satellite remote sensing, Water Resources Research, 48, W09 504, https://doi.org/10.1029/2012WR012063, 2012.

Gettelman, A., Callaghan, P., Larson, V. E., Zarzycki, C. M., Bacmeister, J. T., Lauritzen, P. H., Bogenschutz, P. A., and Neale, R. B.: Regional Climate Simulations With the Community Earth System Model, Journal of Advances in Modeling Earth Systems, 10, 1245–1265, https://doi.org/10.1002/2017MS001227, 2018.

Gharari, S., Hrachowitz, M., Fenicia, F., and Savenije, H. H.: Hydrological landscape classification: Investigating the performance of HAND based landscape classifications in a central European meso-scale catchment, Hydrology and Earth System Sciences, 15, 3275–3291, https://doi.org/10.5194/hess-15-3275-2011, 2011.

Gharari, S., Vanderkelen, I., Tefs, A., Mizukami, N., Lawrence, D., and Clark, M. P.: A Flexible Multi-Scale Framework to Simulate Lakes 1 and Reservoirs in Earth System Models, Water Resources Research, in review, https://doi.org/10.1002/essoar.10510902.1, 2022.

Ghiggi, G., Humphrey, V., Seneviratne, S. I., and Gudmundsson, L.: GRUN: An observation-based global gridded runoff dataset from 1902 to 2014, Earth System Science Data, 11, 1655–1674, https://doi.org/10.5194/essd-11-1655-2019, 2019.

Ghiggi, G., Humphrey, V., Seneviratne, S. I., and Gudmundsson, L.: G-RUN ENSEMBLE: A Multi-Forcing Observation-Based Global Runoff Reanalysis, Water Resources Research, 57, e2020WR028 787, https://doi.org/10.1029/2020WR028787, 2021.

Gillespie, B. R., Desmet, S., Kay, P., Tillotson, M. R., and Brown, L. E.: A critical analysis of regulated river ecosystem responses to managed environmental flows from reservoirs, Freshwater Biology, 60, 410–425, https://doi.org/10.1111/fwb.12506, 2015.

Giorgi, F., Jones, C., and Asrar, G. R.: Addressing climate information needs at the regional level: The CORDEX framework, World Meteorological Organization Bulletin, 58, 175–183, 2009.

Gleeson, T., Cuthbert, M., Ferguson, G., and Perrone, D.: Annual Review of Earth and Planetary Sciences Global Groundwater Sustainability, Resources, and Systems in the Anthropocene, The Annual Review of Earth and Planetary Sciences is online at earth.annualreviews.org, 48, 431–63, https://doi.org/10.1146/annurev-earth-071719, 2020.

Golub, M., Thiery, W., Marcé, R., Pierson, D., Vanderkelen, I., Mercado, D., Iestyn Woolway, R., Grant, L., Jennings, E., Schewe, J., Zhao, F., Frieler, K., Mengel, M., Bogomolov, V. Y., Bouffard, D., Perroud, M., Piccolroaz, S., Raaman Vinnaa, L., Schmid, M., Shatwell, T., Stepanenko, V. M., Tan, Z., Yao, H., Adrian, R., Anneville, O., Arvola, L., Atkins, K., Boegman, L., Carey, C., Christianson, K., de Eyto, E., DeGasperi, C., Grechushnikova, M., Hejzlar, J., Joehnk, K., Jones, I. D., Laas, A., Mackay, E. B., Mammarella, I., Markensten, H., McBride, C., Özkundakci, D., Potes, M., Rinke, K., Robertson, D., Rusak, J., Salgado, R., van den Linden, L., Verburg, P., Ward, N. K., Wollrab, S., and Zdorovennova, G.: A framework for ensemble modelling of climate change impacts on lakes worldwide: the ISIMIP Lake Sector, Geoscientific Model Development Discussions, https://doi.org/10.5194/gmd-2021-433, 2022.

Goudsmit, G. H., Burchard, H., Peeters, F., and Wüest, A.: Application of k-e turbulence models to enclosed basins: The role of internal seiches, Journal of Geophysical Research C: Oceans, 107, 23–1, https://doi.org/10.1029/2001jc000954, 2002.

Grant, L., Vanderkelen, I., Gudmundsson, L., Tan, Z., Perroud, M., Stepanenko, V. M., Debolskiy, A. V., Droppers, B., Janssen, A. B., Woolway, R. I., Choulga, M., Balsamo, G., Kirillin, G., Schewe, J., Zhao, F., del Valle, I. V., Golub, M., Pierson, D., Marcé, R., Seneviratne, S. I., and Thiery, W.: Attribution of global lake systems change to anthropogenic forcing, Nature Geoscience, 14, 849–854, https://doi.org/10.1038/s41561-021-00833-x, 2021.

Greve, P., Orlowsky, B., Mueller, B., Sheffield, J., Reichstein, M., and Seneviratne, S. I.: Global assessment of trends in wetting and drying over land, Nature Geoscience, 7, 716–721, https://doi.org/10.1038/NGEO2247, 2014.

Greve, P., Gudmundsson, L., and Seneviratne, S. I.: Regional scaling of annual mean precipitation and water availability with global temperature change, Earth System Dynamics, 9, 227–240, https://doi.org/10.5194/esd-9-227-2018, 2018.

Griffin, K. L., Ross, P. D., Sims, D. A., Luo, Y., Seemann, J. R., Fox, C. A., and Ball, J. T.: EcoCELLs: Tools for mesocosm scale measurements of gas exchange, Plant, Cell and Environment, 19, 1210–1221, https://doi.org/10.1111/j.1365-3040.1996.tb00437.x, 1996.

Grill, G., Lehner, B., Thieme, M., Geenen, B., Tickner, D., Antonelli, F., Babu, S., Borrelli, P., Cheng, L., Crochetiere, H., Ehalt Macedo, H., Filgueiras, R., Goichot, M., Higgins, J., Hogan, Z., Lip, B., McClain, M. E., Meng, J., Mulligan, M., Nilsson, C., Olden, J. D., Opperman, J. J., Petry, P., Reidy Liermann, C., Sáenz, L., Salinas-Rodríguez, S., Schelle, P., Schmitt, R. J., Snider, J., Tan, F., Tockner, K., Valdujo, P. H., van Soesbergen, A., and Zarfl, C.: Mapping the world's free-flowing rivers, Nature, 569, 215–221, https://doi.org/10.1038/s41586-019-1111-9, 2019.

Grubert, E. A.: Water consumption from hydroelectricity in the United States, Advances in Water Resources, 96, 88–94, https://doi.org/10.1016/j.advwatres.2016.07.004, 2016.

Gudmundsson, L., Bremnes, J. B., Haugen, J. E., and Engen-Skaugen, T.: Technical Note: Downscaling RCM precipitation to the station scale using statistical transformations - A comparison of methods, Hydrology and Earth System Sciences, 16, 3383–3390, https://doi.org/10.5194/hess-16-3383-2012, 2012.

Gudmundsson, L., Do, H. X., Leonard, M., and Westra, S.: The Global Streamflow Indices and Metadata Archive (GSIM)-Part 2: Quality control, time-series indices and homogeneity assessment, Earth Syst. Sci. Data, 10, 787–804, https://doi.org/10.5194/essd-10-787-2018, 2018.

Gudmundsson, L., Leonard, M., Do, H. X., Westra, S., and Seneviratne, S. I.: Observed Trends in Global Indicators of Mean and Extreme Streamflow, Geophysical Research Letters, 46, 756–766, https://doi.org/10.1029/2018GL079725, 2019.

Gudmundsson, L., Boulange, J., Do, H. X., Gosling, S. N., Grillakis, M. G., Koutroulis, A. G., Leonard, M., Liu, J., Schmied, H. M., Papadimitriou, L., Pokhrel, Y., Seneviratne, S. I., Satoh, Y., Thiery, W., Westra, S., Zhang, X., and Zhao, F.: Globally observed trends in mean and extreme river flow attributed to climate change, Science, 371, 1159–1162, https://doi.org/10.1126/science.aba3996, 2021.

Guillod, B. P., Orlowsky, B., Miralles, D. G., Teuling, A. J., and Seneviratne, S. I.: Reconciling spatial and temporal soil moisture effects on afternoon rainfall, Nature Communications, 6, 6443, https://doi.org/10.1038/ncomms7443, 2015.

Gupta, H. V., Kling, H., Yilmaz, K. K., and Martinez, G. F.: Decomposition of the mean squared error and NSE performance criteria: Implications for improving hydrological modelling, Journal of Hydrology, 377, 80–91, https://doi.org/10.1016/j.jhydrol.2009.08.003, 2009.

Gutenson, J. L., Tavakoly, A. A., Wahl, M. D., and Follum, M. L.: Comparison of generalized non-data-driven lake and reservoir routing models for global-scale hydrologic forecasting of reservoir outflow at diurnal time steps, Hydrol. Earth Syst. Sci, 24, 2711–2729, https://doi.org/10.5194/hess-24-2711-2020, 2020.

Habel, M., Mechkin, K., Podgorska, K., Saunes, M., Babiński, Z., Chalov, S., Absalon, D., Podgórski, Z., and Obolewski, K.: Dam and reservoir removal projects: a mix of

social-ecological trends and cost-cutting attitudes, Scientific Reports, 10, https://doi.org/10.1038/s41598-020-76158-3, 2020.

Haddeland, I., Skaugen, T., and Lettenmaier, D. P.: Anthropogenic impacts on continental surface water fluxes, Geophysical Research Letters, 33, 2–5, https://doi.org/10.1029/2006GL026047, 2006.

Haddeland, I., Clark, D. B., Franssen, W., Ludwig, F., Voß, F., Arnell, N. W., Bertrand, N., Best, M., Folwell, S., Gerten, D., Gomes, S., Gosling, S. N., Hagemann, S., Hanasaki, N., Harding, R., Heinke, J., Kabat, P., Koirala, S., Oki, T., Polcher, J., Stacke, T., Viterbo, P., Weedon, G. P., and Yeh, P.: Multimodel Estimate of the Global Terrestrial Water Balance: Setup and First Results, Journal of Hydrometeorology, 12, 869–884, https://doi.org/10.1175/2011JHM1324.1, 2011.

Haddeland, I., Heinke, J., Biemans, H., Eisner, S., Flörke, M., Hanasaki, N., Konzmann, M., Ludwig, F., Masaki, Y., Schewe, J., Stacke, T., Tessler, Z. D., Wada, Y., and Wisser, D.: Global water resources affected by human interventions and climate change, Proceedings of the National Academy of Sciences, 111, 3251–3256, https://doi.org/10.1073/pnas.1222475110, 2014.

Hanasaki, N., Kanae, S., and Oki, T.: A reservoir operation scheme for global river routing models, Journal of Hydrology, 327, 22–41, https://doi.org/10.1016/j.jhydrol.2005.11.011, 2006.

Hanasaki, N., Kanae, S., Oki, T., Masuda, K., Motoya, K., Shirakawa, N., Shen, Y., and Tanaka, K.: An integrated model for the assessment of global water resources - Part 1: Model description and input meteorological forcing, Hydrology and Earth System Sciences, 12, 1007–1025, https://doi.org/10.5194/hess-12-1007-2008, 2008.

Hanasaki, N., Matsuda, H., Fujiwara, M., Hirabayashi, Y., Seto, S., Kanae, S., and Oki, T.: Toward hyper-resolution global hydrological models including human activities: application to Kyushu Island, Japan, Hydrology and Earth System Sciences Discussions, pp. 1–33, https://doi.org/10.5194/hess-2021-484, 2021.

Hassan, A. A. and Jin, S.: Lake level change and total water discharge in East Africa Rift Valley from satellite-based observations, Global and Planetary Change, 117, 79–90, https://doi.org/10.1016/j.gloplacha.2014.03.005, 2014.

Hauser, M., Thiery, W., and Isabelle Seneviratne, S.: Potential of global land water recycling to mitigate local temperature extremes, Earth System Dynamics, 10, 157–169, https://doi.org/10.5194/esd-10-157-2019, 2019.

Hawley, W. B., Hay, C. C., Mitrovica, J. X., and Kopp, R. E.: A Spatially Variable Time Series of Sea Level Change Due to Artificial Water Impoundment, Earth's Future, 8, e2020EF001 497, https://doi.org/10.1029/2020EF001497, 2020.

Heiskanen, J. J., Mammarella, I., Ojala, A., Stepanenko, V., Erkkilä, K. M., Miettinen, H., Sandström, H., Eugster, W., Leppäranta, M., Järvinen, H., Vesala, T., and Nordbo, A.: Effects of water clarity on lake stratification and lake-atmosphere heat exchange, Journal of Geophysical Research, 120, 7412–7428, https://doi.org/10.1002/2014JD022938, 2015.

Hernández-Díaz, L., Laprise, R., Laxmi, S., Martynov, A., Winger, K., and Dugas, B.: Climate simulation over CORDEX Africa domain using the fifth-generation Canadian Regional Climate Model (CRCM5), Clim Dyn, 40, 1415–1433, https://doi.org/10.1007/s00382-012-1387-z, 2012.

Hirsch, A. L., Wilhelm, M., Davin, E. L., Thiery, W., and Seneviratne, S. I.: Can climate-effective land management reduce regional warming?, Journal of Geophysical Research, 122, 2269–2288, https://doi.org/10.1002/2016JD026125, 2017.

Hirsch, A. L., Prestele, R., Davin, E. L., Seneviratne, S. I., Thiery, W., and Verburg, P. H.: Modelled biophysical impacts of conservation agriculture on local climates, Global Change Biology, 24, 4758–4774, https://doi.org/10.1111/gcb.14362, 2018.

Hossain, F., Jeyachandran, I., and Pielke, R.: Dam safety effects due to human alteration of extreme precipitation, Water Resources Research, 46, 1–7, https://doi.org/10.1029/2009WR007704, 2010.

Hossain, F., Degu, A. M., Yigzaw, W., Burian, S., Niyogi, D., Shepherd, J. M., and Pielke, R.: Climate feedback-based provisions for dam design, operations, and water management in the 21st century, Journal of Hydrologic Engineering, 17, 837–850, https://doi.org/10.1061/(ASCE)HE.1943-5584.0000541, 2012.

Hovenden, M. J., Newton, P. C. D., and Wills, K. E.: Seasonal not annual rainfall determines grassland biomass response to carbon dioxide, Nature, 511, 583–586, https://doi.org/10.1038/nature13281, 2014.

Huang, S.: 1851-2004 annual heat budget of the continental landmasses, Geophysical Research Letters, 33, L04 707, https://doi.org/10.1029/2005GL025300, 2006.

Hurrell, J. W., Hack, J. J., Shea, D., Caron, J. M., and Rosinski, J.: A new sea surface temperature and sea ice boundary dataset for the community atmosphere model, Journal of Climate, 21, 5145–5153, https://doi.org/10.1175/2008JCLI2292.1, 2008.

Hurtt, G. C., Chini, L., Sahajpal, R., Frolking, S., Bodirsky, B. L., Calvin, K., Doelman, J. C., Fisk, J., Fujimori, S., Klein Goldewijk, K., Hasegawa, T., Havlik, P., Heinimann, A., Humpenöder, F., Jungclaus, J., Kaplan, J. O., Kennedy, J., Krisztin, T., Lawrence, D., Lawrence, P., Ma, L., Mertz, O., Pongratz, J., Popp, A., Poulter, B., Riahi, K., Shevliakova, E., Stehfest, E., Thornton, P., Tubiello, F. N., Van Vuuren, D. P., and Zhang, X.: Harmonization of global land use change and management for the period 850-2100 (LUH2) for CMIP6, Geosci. Model Dev, 13, 5425–5464, https://doi.org/10.5194/gmd-13-5425-2020, 2020.

IPCC 2013: Summary for Policymakers, in: Climate Change 2013 - The Physical Science Basis, vol. 1542, pp. 1–30, Cambridge University Press, Cambridge, https://doi.org/10.1017/CBO9781107415324.004, 2013.

Iturbide, M., Gutiérrez, J. M., Alves, L. M., Bedia, J., Cerezo-Mota, R., Cimadevilla, E., Cofiño, A. S., Luca, A. D., Faria, S. H., Gorodetskaya, I. V., Hauser, M., Herrera, S., Hennessy, K., Hewitt, H. T., Jones, R. G., Krakovska, S., Manzanas, R., Martínez-Castro, D., Narisma, G. T., Nurhati, I. S., Pinto, I., Seneviratne, S. I., van den Hurk, B., and Vera, C. S.: An update of IPCC climate reference regions for subcontinental analysis of climate model data: definition and aggregated datasets, Earth System Science Data, 12, 2959–2970, https://doi.org/10.5194/essd-12-2959-2020, 2020.

Jacob, D., Petersen, J., Eggert, B., Alias, A., Christensen, O. B., Bouwer, L. M., Braun, A., Colette, A., Déqué, M., Georgievski, G., Georgopoulou, E., Gobiet, A., Menut, L., Nikulin, G., Haensler, A., Hempelmann, N., Jones, C., Keuler, K., Kovats, S., Kröner, N., Kotlarski, S., Kriegsmann, A., Martin, E., van Meijgaard, E., Moseley, C., Pfeifer, S., Preuschmann, S., Radermacher, C., Radtke, K., Rechid, D., Rounsevell, M., Samuelsson, P., Somot, S., Soussana, J. F., Teichmann, C., Valentini, R., Vautard, R., Weber, B., and Yiou, P.: EURO-CORDEX: New high-resolution climate change projections for European impact research, Regional Environmental Change, 14, 563–578, https://doi.org/10.1007/s10113-013-0499-2, 2014.

Jägermeyr, J., Gerten, D., Heinke, J., Schaphoff, S., Kummu, M., and Lucht, W.: Water savings potentials of irrigation systems: Global simulation of processes and linkages, Hydrology and Earth System Sciences, 19, 3073–3091, https://doi.org/10.5194/hess-19-3073-2015, 2015.

Johnson, M. S., Matthews, E., Bastviken, D., Deemer, B., Du, J., and Genovese, V.: Spatiotemporal Methane Emission From Global Reservoirs, Journal of Geophysical Research: Biogeosciences, 126, e2021JG006 305, https://doi.org/10.1029/2021JG006305, 2021.

Jung, M., Reichstein, M., Ciais, P., Seneviratne, S. I., Sheffield, J., Goulden, M. L., Bonan, G., Cescatti, A., Chen, J., De Jeu, R., Dolman, A. J., Eugster, W., Gerten, D., Gianelle, D., Gobron, N., Heinke, J., Kimball, J., Law, B. E., Montagnani, L., Mu, Q., Mueller, B., Oleson, K., Papale, D., Richardson, A. D., Roupsard, O., Running, S., Tomelleri, E., Viovy, N., Weber, U., Williams, C., Wood, E., Zaehle, S., and Zhang, K.: Recent decline in the global land evapotranspiration trend due to limited moisture supply, Nature, 467, 951–954, https://doi.org/10.1038/nature09396, 2010.

Kardol, P., De Long, J. R., and Sundgvist, M. K.: Crossing the threshold: the power of multi-level experiments in identifying global change responses, New Phytologist, 196, 323–326, 2012.

Karlowsky, S., Augusti, A., Ingrisch, J., Hasibeder, R., Lange, M., Lavorel, S., Bahn, M., and Gleixner, G.: Land use in mountain grasslands alters drought response and recovery

of carbon allocation and plant-microbial interactions, Journal of Ecology, 106, 1230–1243, https://doi.org/10.1111/1365-2745.12910, 2018.

Kato, S., Loeb, N. G., Rose, F. G., Doelling, D. R., Rutan, D. A., Caldwell, T. E., Yu, L., and Weller, R. A.: Surface irradiances consistent with CERES-derived top-of-atmosphere shortwave and longwave irradiances, Journal of Climate, 26, 2719–2740, https://doi.org/10.1175/JCLI-D-12-00436.1, 2013.

Kennedy, D., Swenson, S., Oleson, K. W., Lawrence, D. M., Fisher, R., Lola da Costa, A. C., and Gentine, P.: Implementing Plant Hydraulics in the Community Land Model, Version 5, Journal of Advances in Modeling Earth Systems, 11, 485–513, https://doi.org/10.1029/2018MS001500, 2019.

Kent, C., Chadwick, R., and Rowell, D. P.: Understanding uncertainties in future projections of seasonal tropical precipitation, Journal of Climate, 28, 4390–4413, https://doi.org/10.1175/JCLI-D-14-00613.1, 2015.

Keuler, K., Radtke, K., Kotlarski, S., and Lüthi, D.: Regional climate change over Europe in COSMO-CLM: Influence of emission scenario and driving global model, Meteorologische Zeitschrift, 25, 121–136, https://doi.org/10.1127/metz/2016/0662, 2016.

Khazaei, B., Read, L. K., Casali, M., Sampson, K. M., and Yates, D. N.: GLOBathy, the global lakes bathymetry dataset, Scientific Data, 9, 36, https://doi.org/10.1038/s41597-022-01132-9, 2022.

Kim, J., Waliser, D. E., Mattmann, C. A., Goodale, C. E., Hart, A. F., Zimdars, P. A., Crichton, D. J., Jones, C., Nikulin, G., Hewitson, B., Jack, C., Lennard, C., and Favre, A.: Evaluation of the CORDEX-Africa multi-RCM hindcast: Systematic model errors, Climate Dynamics, 42, 1189–1202, https://doi.org/10.1007/s00382-013-1751-7, 2014.

Kite, G. W.: Recent changes in level of lake victoria, Hydrological Sciences Bulletin, 26, 233–243, https://doi.org/10.1080/02626668109490883, 1981.

Kizza, M. and Mugume, S.: The Impact of a Potential Dam Break on the Hydro Electric Power Generation: Case of: Owen Falls Dam Break Simulation, Uganda, in: International Conference on Advances in Engineering and Technology, edited by Mwakali, J. A. and Taban-Wani, G., pp. 711–722, Entebbe, Uganda, 2006.

Klein Tank, A. M. G., Wijngaard, J. B., Können, G. P., Böhm, R., Demarée, G., Gocheva, A., Mileta, M., Pashiardis, S., Hejkrlik, L., Kern-Hansen, C., Heino, R., Bessemoulin, P., Müller-Westermeier, G., Tzanakou, M., Szalai, S., Pálsdóttir, T., Fitzgerald, D., Rubin, S., Capaldo, M., Maugeri, M., Leitass, A., Bukantis, A., Aberfeld, R., Van Engelen, A. F. V., Forland, E., Mietus, M., Coelho, F., Mares, C., Razuvaev, V., Nieplova, E., Cegnar, T., Antonio López, J., Dahlström, B., Moberg, A., Kirchhofer, W., Ceylan, A., Pachaliuk, O., Alexander, L. V., and Petrovic, P.: Daily dataset of 20th-century surface air temperature and precipitation series for the European Climate Assessment, International Journal of Climatology, 22, 1441–1453, https://doi.org/10.1002/joc.773, 2002.

Knapp, A. K., Carroll, C. J. W., Griffin-Nolan, R. J., Slette, I. J., Chaves, F. A., Baur, L. E., Felton, A. J., Gray, J. E., Hoffman, A. M., Lemoine, N. P., Mao, W., Post, A. K., and Smith, M. D.: A reality check for climate change experiments: Do they reflect the real world?, Ecology, 99, 2145–2151, https://doi.org/10.1002/ecy.2474, 2018.

Knoben, W. J., Freer, J. E., and Woods, R. A.: Technical note: Inherent benchmark or not? Comparing Nash-Sutcliffe and Kling-Gupta efficiency scores, Hydrology and Earth System Sciences, 23, 4323–4331, https://doi.org/10.5194/hess-23-4323-2019, 2019.

Knutti, R. and Rogelj, J.: The legacy of our CO2 emissions: a clash of scientific facts, politics and ethics, Climatic Change, 133, 361–373, https://doi.org/10.1007/s10584-015-1340-3, 2015.

Koch, H., Liersch, S., and Hattermann, F. F.: Integrating water resources management in eco-hydrological modelling, Water Science and Technology, 67, 1525–1533, https://doi.org/10.2166/wst.2013.022, 2013.

Kondolf, G. M., Rubin, Z. K., and Minear, J. T.: Dams on the Mekong: Cumulative sediment starvation, Water Resources Research, 50, 5158–5169, https://doi.org/10.1002/2013WR014651, 2014.

König-Langlo, G., Sieger, R., Schmithüsen, H., Bücker, A., Richte, F., and Dutton, E. G.: Baseline Surface Radiation Network (BSRN) Update of the Technical Plan for BSRN Data Management, World Meteorological Organization, p. 30, 2013.

Korell, L., Auge, H., Chase, J. M., Harpole, S., and Knight, T. M.: We need more realistic climate change experiments for understanding ecosystems of the future, Global Change Biology, 00, 1–3, https://doi.org/10.1111/gcb.14797, 2019.

Kotlarski, S., Keuler, K., Christensen, O. B., Colette, A., Déqué, M., Gobiet, A., Goergen, K., Jacob, D., Lüthi, D., Van Meijgaard, E., Nikulin, G., Schär, C., Teichmann, C., Vautard, R., Warrach-Sagi, K., and Wulfmeyer, V.: Regional climate modeling on European scales: A joint standard evaluation of the EURO-CORDEX RCM ensemble, Geoscientific Model Development, 7, 1297–1333, https://doi.org/10.5194/gmd-7-1297-2014, 2014.

Kourzeneva, E.: External data for lake parameterization in numerical weather prediction and climate modeling, Boreal Environment Research, 15, 165–177, https://doi.org/10.3402/tellusa.v64i0.15640, 2010.

Kraemer, B. M., Pilla, R. M., Woolway, R. I., Anneville, O., Ban, S., Colom-Montero, W., Devlin, S. P., Dokulil, M. T., Gaiser, E. E., Hambright, K. D., Hessen, D. O., Higgins, S. N., Jöhnk, K. D., Keller, W., Knoll, L. B., Leavitt, P. R., Lepori, F., Luger, M. S., Maberly, S. C., Müller-Navarra, D. C., Paterson, A. M., Pierson, D. C., Richardson, D. C., Rogora, M., Rusak, J. A., Sadro, S., Salmaso, N., Schmid, M., Silow, E. A., Sommaruga, R., Stelzer, J. A., Straile, D., Thiery, W., Timofeyev, M. A., Verburg, P., Weyhenmeyer, G. A., and Adrian, R.: Climate change drives widespread shifts in lake

thermal habitat, Nature Climate Change, 11, 521–529, https://doi.org/10.1038/s41558-021-01060-3, 2021.

Kreyling, J., Schweiger, A. H., Bahn, M., Ineson, P., Migliavacca, M., Morel-Journel, T., Christiansen, J. R., Schtickzelle, N., and Larsen, K. S.: To replicate, or not to replicate – that is the question: how to tackle nonlinear responses in ecological experiments, Ecology Letters, 21, 1629–1638, https://doi.org/10.1111/ele.13134, 2018.

Kull, D.: Connections Between Recent Water Level Drops in Lake Victoria, Dam Operations and Drought, 2006.

Lake Victoria Basin Commission: Special Report on the Declining of Water Levels of Lake Victoria, East African Community Secretariat, pp. 1–15, 2006.

Lange, S.: Bias correction of surface downwelling longwave and shortwave radiation for the EWEMBI dataset, Earth Syst. Dynam, 9, 627–645, https://doi.org/10.5194/esd-9-627-2018, 2018.

Lange, S., Volkholz, J., Geiger, T., Zhao, F., Vega, I., Veldkamp, T., Reyer, C. P., Warszawski, L., Huber, V., Jägermeyr, J., Schewe, J., Bresch, D. N., Büchner, M., Chang, J., Ciais, P., Dury, M., Emanuel, K., Folberth, C., Gerten, D., Gosling, S. N., Grillakis, M., Hanasaki, N., Henrot, A. J., Hickler, T., Honda, Y., Ito, A., Khabarov, N., Koutroulis, A., Liu, W., Müller, C., Nishina, K., Ostberg, S., Müller Schmied, H., Seneviratne, S. I., Stacke, T., Steinkamp, J., Thiery, W., Wada, Y., Willner, S., Yang, H., Yoshikawa, M., Yue, C., and Frieler, K.: Projecting Exposure to Extreme Climate Impact Events Across Six Event Categories and Three Spatial Scales, Earth's Future, 8, https://doi.org/10.1029/2020EF001616, 2020.

Lasslop, G., Reichstein, M., Papale, D., Richardson, A., Arneth, A., Barr, A., Stoy, P., and Wohlfahrt, G.: Separation of net ecosystem exchange into assimilation and respiration using a light response curve approach: Critical issues and global evaluation, Global Change Biology, 16, 187–208, https://doi.org/10.1111/j.1365-2486.2009.02041.x, 2010.

Lawrence, D. M., Fisher, R. A., Koven, C. D., Oleson, K. W., Swenson, S. C., Bonan, G., Collier, N., Ghimire, B., van Kampenhout, L., Kennedy, D., Kluzek, E., Lawrence, P. J., Li, F., Li, H., Lombardozzi, D., Riley, W. J., Sacks, W. J., Shi, M., Vertenstein, M., Wieder, W. R., Xu, C., Ali, A. A., Badger, A. M., Bisht, G., van den Broeke, M., Brunke, M. A., Burns, S. P., Buzan, J., Clark, M., Craig, A., Dahlin, K., Drewniak, B., Fisher, J. B., Flanner, M., Fox, A. M., Gentine, P., Hoffman, F., Keppel-Aleks, G., Knox, R., Kumar, S., Lenaerts, J., Leung, L. R., Lipscomb, W. H., Lu, Y., Pandey, A., Pelletier, J. D., Perket, J., Randerson, J. T., Ricciuto, D. M., Sanderson, B. M., Slater, A., Subin, Z. M., Tang, J., Thomas, R. Q., Val Martin, M., and Zeng, X.: The Community Land Model Version 5: Description of New Features, Benchmarking, and Impact of Forcing Uncertainty, Journal of Advances in Modeling Earth Systems, 11, 4245–4287, https://doi.org/10.1029/2018MS001583, 2019a.

Lawrence, D. M., Fisher, R. A., Koven, C. D., Oleson, K. W., Swenson, S. C., Bonan, G., Collier, N., Ghimire, B., van Kampenhout, L., Kennedy, D., Kluzek, E., Lawrence, P. J., Li, F., Li, H., Lombardozzi, D., Riley, W. J., Sacks, W. J., Shi, M., Vertenstein, M., Wieder, W. R., Xu, C., Ali, A. A., Badger, A. M., Bisht, G., van den Broeke, M., Brunke, M. A., Burns, S. P., Buzan, J., Clark, M., Craig, A., Dahlin, K., Drewniak, B., Fisher, J. B., Flanner, M., Fox, A. M., Gentine, P., Hoffman, F., Keppel-Aleks, G., Knox, R., Kumar, S., Lenaerts, J., Leung, L. R., Lipscomb, W. H., Lu, Y., Pandey, A., Pelletier, J. D., Perket, J., Randerson, J. T., Ricciuto, D. M., Sanderson, B. M., Slater, A., Subin, Z. M., Tang, J., Thomas, R. Q., Val Martin, M., and Zeng, X.: The Community Land Model Version 5: Description of New Features, Benchmarking, and Impact of Forcing Uncertainty, Journal of Advances in Modeling Earth Systems, 11, 4245–4287, https://doi.org/10.1029/2018MS001583, 2019b.

Lawston, P. M., Santanello, J. A., and Kumar, S. V.: Irrigation Signals Detected From SMAP Soil Moisture Retrievals, Geophysical Research Letters, 44, 11,860–11,867, https://doi.org/10.1002/2017GL075733, 2017.

Lawton, J. H.: The Ecotron: a controlled environmental facility for the investigation of population and ecosystem processes, Philosophical Transactions - Royal Society of London, B, 341, 181–194, https://doi.org/10.1098/rstb.1993.0102, 1993.

Lawton, J. H.: The ecotron facility at silwood park: The value of "Big Bottle" experiments, Ecology, 77, 665–669, https://doi.org/10.2307/2265488, 1996.

Leguy, G., Lipscomb, W., and Sacks, W.: CESM land ice documentation and user guide, Tech. rep., National Center for Atmospheric Research, 2018.

Lehner, B., Liermann, C. R., Revenga, C., Vörömsmarty, C., Fekete, B., Crouzet, P., Döll, P., Endejan, M., Frenken, K., Magome, J., Nilsson, C., Robertson, J. C., Rödel, R., Sindorf, N., and Wisser, D.: High-resolution mapping of the world's reservoirs and dams for sustainable river-flow management, Frontiers in Ecology and the Environment, 9, 494–502, https://doi.org/10.1890/100125, 2011.

Lejeune, Q., Davin, E. L., Guillod, B. P., and Seneviratne, S. I.: Influence of Amazonian deforestation on the future evolution of regional surface fluxes, circulation, surface temperature and precipitation, Climate Dynamics, 44, 2769–2786, https://doi.org/10.1007/s00382-014-2203-8, 2015.

Leng, G., Huang, M., Tang, Q., and Leung, L. R.: A modeling study of irrigation effects on global surface water and groundwater resources under a changing climate, Journal of Advances in Modeling Earth Systems, 7, 1285–1304, https://doi.org/10.1002/2015MS000437, 2015.

Li, H., Wigmosta, M. S., Wu, H., Huang, M., Ke, Y., Coleman, A. M., and Leung, L. R.: A physically based runoff routing model for land surface and earth system models, Journal of Hydrometeorology, 14, 808–828, https://doi.org/10.1175/JHM-D-12-015.1, 2013.

Li, Y., Gao, H., Zhao, G., and Tseng, K. H.: A high-resolution bathymetry dataset for global reservoirs using multi-source satellite imagery and altimetry, Remote Sensing of Environment, 244, 111 831, https://doi.org/10.1016/j.rse.2020.111831, 2020.

Lin, D., Xia, J., and Wan, S.: Climate warming and biomass accumulation of terrestrial plants: A meta-analysis, New Phytologist, 188, 187–198, https://doi.org/10.1111/j.1469-8137.2010.03347.x, 2010.

Lombardozzi, D. L., Lu, Y., Lawrence, P. J., Lawrence, D. M., Swenson, S., Oleson, K. W., Wieder, W. R., and Ainsworth, E. A.: Simulating Agriculture in the Community Land Model Version 5, Journal of Geophysical Research: Biogeosciences, 125, https://doi.org/10.1029/2019JG005529, 2020.

Lorenz, R., Pitman, A. J., and Sisson, S. A.: Does Amazonian deforestation cause global effects; Can we be sure?, Journal of Geophysical Research, 121, 5567–5584, https://doi.org/10.1002/2015JD024357, 2016.

Luyssaert, S., Jammet, M., Stoy, P. C., Estel, S., Pongratz, J., Ceschia, E., Churkina, G., Don, A., Erb, K., Ferlicoq, M., Gielen, B., Grünwald, T., Houghton, R. A., Klumpp, K., Knohl, A., Kolb, T., Kuemmerle, T., Laurila, T., Lohila, A., Loustau, D., McGrath, M. J., Meyfroidt, P., Moors, E. J., Naudts, K., Novick, K., Otto, J., Pilegaard, K., Pio, C. A., Rambal, S., Rebmann, C., Ryder, J., Suyker, A. E., Varlagin, A., Wattenbach, M., and Dolman, A. J.: Land management and land-cover change have impacts of similar magnitude on surface temperature, Nature Climate Change, 4, 389–393, https://doi.org/10.1038/nclimate2196, 2014.

Lyon, B. and Dewitt, D. G.: A recent and abrupt decline in the East African long rains, Geophysical Research Letters, 39, 1–5, https://doi.org/10.1029/2011GL050337, 2012.

Maraun, D., Wetterhall, F., Ireson, A. M., Chandler, R. E., Kendon, E. J., Widmann, M., Brienen, S., Rust, H. W., Sauter, T., Themel, M., Venema, V. K., Chun, K. P., Goodess, C. M., Jones, R. G., Onof, C., Vrac, M., and Thiele-Eich, I.: Precipitation downscaling under climate change: Recent developments to bridge the gap between dynamical models and the end user, Reviews of Geophysics, 48, 2009RG000 314, https://doi.org/10.1029/2009RG000314, 2010.

Maraun, D., Shepherd, T. G., Widmann, M., Zappa, G., Walton, D., Gutiérrez, J. M., Hagemann, S., Richter, I., Soares, P. M., Hall, A., and Mearns, L. O.: Towards process-informed bias correction of climate change simulations, Nature Climate Change, 7, 764–773, https://doi.org/10.1038/nclimate3418, 2017.

Martynov, A., Laprise, R., Sushama, L., Winger, K., Šeparović, L., and Dugas, B.: Reanalysis-driven climate simulation over CORDEX North America domain using the Canadian Regional Climate Model, version 5: Model performance evaluation, Climate Dynamics, 41, 2973–3005, https://doi.org/10.1007/s00382-013-1778-9, 2012.

Masaki, Y., Hanasaki, N., Biemans, H., Schmied, H. M., Tang, Q., Wada, Y., Gosling, S. N., Takahashi, K., and Hijioka, Y.: Intercomparison of global river discharge simulations focusing on dam operation - Multiple models analysis in two case-study river basins, Missouri-Mississippi and Green-Colorado, Environmental Research Letters, 12, 055 002, https://doi.org/10.1088/1748-9326/aa57a8, 2017.

Massari, C., Modanesi, S., Dari, J., Gruber, A., De Lannoy, G. J., Girotto, M., Quintana-Seguí, P., Le Page, M., Jarlan, L., Zribi, M., Ouaadi, N., Vreugdenhil, M., Zappa, L., Dorigo, W., Wagner, W., Brombacher, J., Pelgrum, H., Jaquot, P., Freeman, V., Volden, E., Prieto, D. F., Tarpanelli, A., Barbetta, S., and Brocca, L.: A review of irrigation information retrievals from space and their utility for users, https://doi.org/10.3390/rs13204112, 2021.

Masson-Delmotte, V. P., Zhai, A., Pirani, S., Connors, C., Péan, S., Berger, N., Caud, Y., Chen, L., Goldfarb, M., Gomis, M., Huang, K., Leitzell, E., Lonnoy, J., Matthews, T., Maycock, T., Waterfield, O., Yelekçi, R., (eds.), Y., and Zhou, B.: IPCC, 2021: Climate Change 2021: The Physical Science Basis. Contribution of Working Group I to the Sixth Assessment Report of the Intergovernmental Panel on Climate Change, Tech. rep., Cambridge University Press., 2021.

Mayaux, P., Massart, M., Cutsem, C. V., Cabral, a., Nonguierma, a., Diallo, O., Pretorius, C., Thompson, M., Cherlet, M., Defourny, P., Vasconcelos, M., Gregorio, a. D., Grandi, G. D., and Belward, a.: A land cover map of Africa. Carte de l'occupation du sol de l'Afrique, EUR 20665 EN, URL `http://www.tiger.esa.int/TrainingCds/cd{_}03/content{_}2/sez{_}1{_}2/documents/D2L1{_}5{_}GLC2000{_}africa3.pdf`, 2003.

Meehl, G. A., Goddard, L., Boer, G., Burgman, R., Branstator, G., Cassou, C., Corti, S., Danabasoglu, G., Doblas-Reyes, F., Hawkins, E., Karspeck, A., Kimoto, M., Kumar, A., Matei, D., Mignot, J., Msadek, R., Navarra, A., Pohlmann, H., Rienecker, M., Rosati, T., Schneider, E., Smith, D., Sutton, R., Teng, H., Van Oldenborgh, G. J., Vecchi, G., and Yeager, S.: Decadal climate prediction an update from the trenches, Bulletin of the American Meteorological Society, 95, 243–267, https://doi.org/10.1175/BAMS-D-12-00241.1, 2014.

Meigh, J. R., Mckenzie, A. A., and Sene, K. J.: A Grid-Based Approach to Water Scarcity Estimates for Eastern and Southern Africa, Water Resources Management, 13, 85–115, 1999.

Messager, M. L., Lehner, B., Grill, G., Nedeva, I., and Schmitt, O.: Estimating the volume and age of water stored in global lakes using a geo-statistical approach, Nature Communications, 7, 13 603, https://doi.org/10.1038/ncomms13603, 2016.

Miralles, D. G., Holmes, T. R. H., De Jeu, R. A. M., Gash, J. H., Meesters, A. G. C. A., and Dolman, A. J.: Global land-surface evaporation estimated from satellite-based observations, Hydrology and Earth System Sciences, 15, 453–469, https://doi.org/10.5194/hess-15-453-2011, 2011.

Mishra, V., Ambika, A. K., Asoka, A., Aadhar, S., Buzan, J., Kumar, R., and Huber, M.: Moist heat stress extremes in India enhanced by irrigation, Nature Geoscience, https://doi.org/10.1038/s41561-020-00650-8, 2020.

Mizukami, N., Clark, M. P., Sampson, K., Nijssen, B., Mao, Y., McMillan, H., Viger, R. J., Markstrom, S. L., Hay, L. E., Woods, R., Arnold, J. R., and Brekke, L. D.: MizuRoute version 1: A river network routing tool for a continental domain water resources applications, Geoscientific Model Development, 9, 2223–2228, https://doi.org/10.5194/gmd-9-2223-2016, 2016.

Mizukami, N., Clark, M. P., Gharari, S., Kluzek, E., Pan, M., Lin, P., Beck, H. E., and Yamazaki, D.: A Vector-Based River Routing Model for Earth System Models: Parallelization and Global Applications, Journal of Advances in Modeling Earth Systems, 13, e2020MS002 434, https://doi.org/10.1029/2020MS002434, 2021.

Moon, H., Guillod, B. P., Gudmundsson, L., and Seneviratne, S. I.: Soil Moisture Effects on Afternoon Precipitation Occurrence in Current Climate Models, Geophysical Research Letters, 46, 1861–1869, https://doi.org/10.1029/2018GL080879, 2019.

Müller Schmied, H., Adam, L., Eisner, S., Fink, G., Florke, M., Kim, H., Oki, T., Theodor Portmann, F., Reinecke, R., Riedel, C., Song, Q., Zhang, J., and Doll, P.: Variations of global and continental water balance components as impacted by climate forcing uncertainty and human water use, Hydrology and Earth System Sciences, 20, 2877–2898, https://doi.org/10.5194/hess-20-2877-2016, 2016.

Mulligan, M., van Soesbergen, A., and Sáenz, L.: GOODD, a global dataset of more than 38,000 georeferenced dams, Scientific Data, 7, 31, https://doi.org/10.1038/s41597-020-0362-5, 2020.

Mulligan, M., Lehner, B., Zarfl, C., Thieme, M., Beames, P., van Soesbergen, A., Higgins, J., Januchowski-Hartley, S. R., Brauman, K. A., De Felice, L., Wen, Q., Garcia de Leaniz, C., Belletti, B., Mandle, L., Yang, X., Wang, J., and Mazany-Wright, N.: Global Dam Watch: curated data and tools for management and decision making, Environmental Research: Infrastructure and Sustainability, 1, 033 003, https://doi.org/10.1088/2634-4505/ac333a, 2021.

Murphy, A. H.: A New Vector Partition of the Probability Score, Journal of Applied Meteorology, 12, 595–600, 1973.

Nazemi, A. and Wheater, H. S.: On inclusion of water resource management in Earth system models -Part 1: Problem definition and representation of water demand, Hydrology and Earth System Sciences, 19, 33–61, https://doi.org/10.5194/hess-19-33-2015, 2015a.

Nazemi, A. and Wheater, H. S.: On inclusion of water resource management in Earth system models Part 2: Representation of water supply and allocation and opportunities for improved modeling, Hydrology and Earth System Sciences, 19, 63–90, https://doi.org/10.5194/hess-19-63-2015, 2015b.

NEH4: Hydrologic Soil-Cover Complexes, in: National Engineering Handbook Part 630 Hydrology, chap. Chapter 9, p. 14, United States Department of Agriculture (USDA) - Natural Resources Conservation Service (NRCS), 2004.

Nicholson, S.: A review of climate dynamics and climate variability in Eastern Africa, Springer, Dordrecht, 1996.

Nicholson, S. E.: An analysis of recent rainfall conditions in eastern Africa, International Journal of Climatology, 36, 526–532, https://doi.org/10.1002/joc.4358, 2016.

Nicholson, S. E.: Climate and climatic variability of rainfall over eastern Africa, Reviews of Geophysics, 55, 590–635, https://doi.org/10.1002/2016RG000544, 2017.

Nikulin, G., Jones, C., Giorgi, F., Asrar, G., Büchner, M., Cerezo-Mota, R., Christensen, O. B., Déqué, M., Fernandez, J., Hänsler, A., van Meijgaard, E., Samuelsson, P., Sylla, M. B., and Sushama, L.: Precipitation climatology in an ensemble of CORDEX-Africa regional climate simulations, Journal of Climate, 25, 6057–6078, https://doi.org/10.1175/JCLI-D-11-00375.1, 2012.

Nilsson, C., Reidy, C. A., Dynesius, M., and Revenga, C.: Fragmentation and flow regulation of the world's large river systems, Science, 308, 405–408, https://doi.org/10.1126/science.1107887, 2005.

Nobre, A. D., Cuartas, L. A., Hodnett, M., Rennó, C. D., Rodrigues, G., Silveira, A., Waterloo, M., and Saleska, S.: Height Above the Nearest Drainage - a hydrologically relevant new terrain model, Journal of Hydrology, 404, 13–29, https://doi.org/10.1016/j.jhydrol.2011.03.051, 2011.

O'Connor, J. E., Duda, J. J., and Grant, G. E.: 1000 dams down and counting: Dam removals are reconnecting rivers in the United States, Science, 348, 496–497, https://doi.org/10.1126/science.aaa9204, 2015.

Oki, T. and Kanae, S.: Global hydrological cycles and world water resources, Science, 313, 1068–1072, https://doi.org/10.1126/science.1128845, 2006.

Oleson, K. W., Lead, D. M. L., Bonan, G. B., Drewniak, B., Huang, M., Koven, C. D., Levis, S., Li, F., Riley, W. J., Subin, Z. M., Swenson, S. C., Thornton, P. E., Bozbiyik, A., Fisher, R., Heald, C. L., Kluzek, E., Lamarque, J.-F., Lawrence, P. J., Leung, L. R., Lipscomb, W., Muszala, S., Ricciuto, D. M., Sacks, W., Sun, Y., Tang, J., and Yang, Z.-L.: Technical Description of version 4.5 of the Community Land Model (CLM) Coordinating Lead Authors, Tech. rep., NCAR/TN-503+STR, https://doi.org/10.5065/D6RR1W7M, 2013.

O'Reilly, C. M., Sharma, S., Gray, D. K., Hampton, S. E., Read, J. S., Rowley, R. J., Schneider, P., Lenters, J. D., McIntyre, P. B., Kraemer, B. M., Weyhenmeyer, G. A., Straile, D., Dong, B., Adrian, R., Allan, M. G., Anneville, O., Arvola, L., Austin, J., Bailey, J. L., Baron, J. S., Brookes, J. D., De Eyto, E., Dokulil, M. T., Hamilton, D. P., Havens, K.,

Hetherington, A. L., Higgins, S. N., Hook, S., Izmest'Eva, L. R., Joehnk, K. D., Kangur, K., Kasprzak, P., Kumagai, M., Kuusisto, E., Leshkevich, G., Livingstone, D. M., MacIntyre, S., May, L., Melack, J. M., Mueller-Navarra, D. C., Naumenko, M., Noges, P., Noges, T., North, R. P., Plisnier, P. D., Rigosi, A., Rimmer, A., Rogora, M., Rudstam, L. G., Rusak, J. A., Salmaso, N., Samal, N. R., Schindler, D. E., Schladow, S. G., Schmid, M., Schmidt, S. R., Silow, E., Soylu, M. E., Teubner, K., Verburg, P., Voutilainen, A., Watkinson, A., Williamson, C. E., and Zhang, G.: Rapid and highly variable warming of lake surface waters around the globe, Geophysical Research Letters, 42, 10 773–10 781, https://doi.org/10.1002/2015GL066235, 2015.

Orlowsky, B. and Seneviratne, S. I.: Elusive drought: Uncertainty in observed trends and short-and long-term CMIP5 projections, Hydrology and Earth System Sciences, 17, 1765–1781, https://doi.org/10.5194/hess-17-1765-2013, 2013.

Otieno, V. O. and Anyah, R. O.: CMIP5 simulated climate conditions of the Greater Horn of Africa (GHA). Part II: Projected climate, Climate Dynamics, 41, 2099–2113, https://doi.org/10.1007/s00382-013-1694-z, 2013.

Panofsky, H. and Brier, G. W.: Some Apllications of Statistics to Meteorology, The Pennsylvania State University Press, Philadelphia, 1968.

Pekel, J. F., Cottam, A., Gorelick, N., and Belward, A. S.: High-resolution mapping of global surface water and its long-term changes, Nature, 540, 418–422, https://doi.org/10.1038/nature20584, 2016a.

Pekel, J. F., Cottam, A., Gorelick, N., and Belward, A. S.: High-resolution mapping of global surface water and its long-term changes, Nature, 540, 418–422, https://doi.org/10.1038/nature20584, 2016b.

Perkins, S. E. and Fischer, E. M.: The usefulness of different realizations for the model evaluation of regional trends in heat waves, Geophysical Research Letters, 40, 5793–5797, https://doi.org/10.1002/2013GL057833, 2013.

Perkins, S. E., Pitman, A. J., Holbrook, N. J., and McAneney, J.: Evaluation of the AR4 climate models' simulated daily maximum temperature, minimum temperature, and precipitation over Australia using probability density functions, Journal of Climate, 20, 4356–4376, https://doi.org/10.1175/JCLI4253.1, 2007.

Philip, S., Kew, S. F., van Oldenborgh, G. J., Otto, F., O'Keefe, S., Haustein, K., King, A., Zegeye, A., Eshetu, Z., Hailemariam, K., Singh, R., Jjemba, E., Funk, C., Cullen, H., Philip, S., Kew, S. F., van Oldenborgh, G. J., Otto, F., O'Keefe, S., Haustein, K., King, A., Zegeye, A., Eshetu, Z., Hailemariam, K., Singh, R., Jjemba, E., Funk, C., and Cullen, H.: Attribution analysis of the Ethiopian drought of 2015, Journal of Climate, 31, 2465–2486, https://doi.org/10.1175/JCLI-D-17-0274.1, 2017.

Piper, B. S., Plinston, D. T., and Sutcliffe, J. V.: The water balance of lake victoria, Hydrological Sciences Journal, 31, 25–37, https://doi.org/10.1080/02626668609491025, 1986.

Pokhrel, Y., Hanasaki, N., Koirala, S., Cho, J., Yeh, P. J.-F., Kim, H., Kanae, S., and Oki, T.: Incorporating Anthropogenic Water Regulation Modules into a Land Surface Model, Journal of Hydrometeorology, 13, 255–269, https://doi.org/10.1175/JHM-D-11-013.1.

Pokhrel, Y., Koirala, S., Yeh, P. J.-F., Hanasaki, N., Longuevvergne, L., Kanae, S., and Oki, T.: Incorporation of groundwater pumping in a global Land Surface Model with the representation of human impacts, Water Resources Research, 51, 78–96, https://doi.org/10.1002/2014WR015602, 2015.

Pokhrel, Y., Hanasaki, N., Wada, Y., and Kim, H.: Recent progresses in incorporating human land-water management into global land surface models toward their integration into Earth system models, Wiley Interdisciplinary Reviews: Water, 3, 548–574, https://doi.org/10.1002/wat2.1150, 2016.

Pokhrel, Y., Felfelani, F., Shin, S., Yamada, T. J., and Satoh, Y.: Modeling large-scale human alteration of land surface hydrology and climate, Geoscience Letters, 4, 13, https://doi.org/10.1186/s40562-017-0076-5, 2017.

Pokhrel, Y., Shin, S., Lin, Z., Yamazaki, D., and Qi, J.: Potential Disruption of Flood Dynamics in the Lower Mekong River Basin Due to Upstream Flow Regulation, Scientific Reports, 8, 17 767, https://doi.org/10.1038/s41598-018-35823-4, 2018.

Pokhrel, Y., Felfelani, F., Satoh, Y., Boulange, J., Burek, P., Gädeke, A., Gerten, D., Gosling, S. N., Grillakis, M., Gudmundsson, L., Hanasaki, N., Kim, H., Koutroulis, A., Liu, J., Papadimitriou, L., Schewe, J., Müller Schmied, H., Stacke, T., Telteu, C. E., Thiery, W., Veldkamp, T., Zhao, F., and Wada, Y.: Global terrestrial water storage and drought severity under climate change, Nature Climate Change, 11, 226–233, https://doi.org/10.1038/s41558-020-00972-w, 2021.

Pokhrel, Y. N., Hanasaki, N., Yeh, P. J., Yamada, T. J., Kanae, S., and Oki, T.: Model estimates of sea-level change due to anthropogenic impacts on terrestrial water storage, Nature Geoscience, 5, 389–392, https://doi.org/10.1038/ngeo1476, 2012.

Potes, M., Costa, M. J., and Salgado, R.: Satellite remote sensing of water turbidity in Alqueva reservoir and implications on lake modelling, Hydrology and Earth System Sciences, 16, 1623–1633, https://doi.org/10.5194/hess-16-1623-2012, 2012.

Punzet, M., Voß, F., Voß, A., Kynast, E., and Bärlund, I.: A global approach to assess the potential impact of climate change on stream water temperatures and related in-stream first-order decay rates, Journal of Hydrometeorology, 13, 1052–1065, https://doi.org/10.1175/JHM-D-11-0138.1, 2012.

Rajczak, J. and Schär, C.: Projections of Future Precipitation Extremes Over Europe: A Multimodel Assessment of Climate Simulations, Journal of Geophysical Research: Atmospheres, 122, 10,710–773,800, https://doi.org/10.1002/2017JD027176, 2017.

Rhein, M., Rintoul, S. R., Aoki, S., Campos, E., Chambers, D., Feely, R. A., Gulev, S., Johnson, G. C., Josey, S. A., Kostianoy, A., Mauritzen, C., Roemmich, D., Talley, L. D., and Wang, F.: Observations: Ocean, in: Climate Change 2013 - The Physical Science Basis. Contribution of Working Group I to the Fifth Assessment Report of the Intergovernmental Panel on Climate Change [Stocker, T.F., D. Qin, G.-K. Plattner, M. Tignor, S.K. Allen, J. Boschung, A. Nauels, Y. Xia, pp. 465–570, Cambridge University Press, Cambridge, United Kingdom and New York, NY, USA, https://doi.org/10.1017/CBO9781107415324.015, 2013.

Riahi, K., Rao, S., Krey, V., Cho, C., Chirkov, V., Fischer, G., Kindermann, G., Nakicenovic, N., and Rafaj, P.: RCP 8.5-A scenario of comparatively high greenhouse gas emissions, Climatic Change, 109, 33–57, https://doi.org/10.1007/s10584-011-0149-y, 2011.

Rineau, F., Malina, R., Beenaerts, N., Arnauts, N., Bardgett, R. D., Berg, M. P., Boerema, A., Bruckers, L., Clerinx, J., Davin, E. L., De Boeck, H. J., De Dobbelaer, T., Dondini, M., De Laender, F., Ellers, J., Franken, O., Gilbert, L., Gudmundsson, L., Janssens, I. A., Johnson, D., Lizin, S., Longdoz, B., Meire, P., Meremans, D., Milbau, A., Moretti, M., Nijs, I., Nobel, A., Pop, I. S., Puetz, T., Reyns, W., Roy, J., Schuetz, J., Seneviratne, S. I., Smith, P., Solmi, F., Staes, J., Thiery, W., Thijs, S., Vanderkelen, I., Van Landuyt, W., Verbruggen, E., Witters, N., Zscheischler, J., and Vangronsveld, J.: Supplementary materials: Towards more predictive and interdisciplinary climate change ecosystem experiments, Nature Climate Change, 9, 809–816, https://doi.org/10.1038/s41558-019-0609-3, 2019.

Rockström, J., W. Steffen, K. Noone, Å. Persson, F. S. Chapin, E. F. Lambin, T. M. Lenton, M. Scheffer, C. Folke, H. J. Schellnhuber, B. Nykvist, C. A. de Wit, T. Hughes, S. van der Leeuw, H. Rodhe, S. Sörlin, P. K. Snyder, R. Costanza, U. Svedin, M. Falkenmark, L. Karlberg, R. W. Corell, V. J. Fabry, J. Hansen, B. Walker, D. Liverman, K. Richardson, P. Crutzen, and J. A. Foley: A safe operation space for humanity, Nature, 461, 472–475, https://doi.org/10.1038/461472a, 2009.

Rodell, M., Famiglietti, J. S., Wiese, D. N., Reager, J. T., Beaudoing, H. K., Landerer, F. W., and Lo, M. H.: Emerging trends in global freshwater availability, Nature, 557, 651–659, https://doi.org/10.1038/s41586-018-0123-1, 2018.

Rowell, D. P., Booth, B. B. B., Nicholson, S. E., and Good, P.: Reconciling past and future rainfall trends over East Africa, Journal of Climate, 28, 9768–9788, https://doi.org/10.1175/JCLI-D-15-0140.1, 2015.

Roy, J., Picon-Cochard, C., Augusti, A., Benot, M.-L., Thiery, L., Darsonville, O., Landais, D., Piel, C., Defossez, M., Devidal, S., Escape, C., Ravel, O., Fromin, N., Volaire, F., Milcu, A., Bahn, M., and Soussana, J.-F.: Elevated CO2 maintains grassland net carbon uptake under a future heat and drought extreme, Proceedings of the National Academy of Sciences, 113, 6224–6229, https://doi.org/10.1073/pnas.1524527113, 2016.

Rustad, L. E., Campbell, J. L., Marion, G. M., Norby, R. J., Mitchell, M. J., Hartley, A. E., Cornelissen, J. H. C., and Gurevitch, J.: A meta-analysis of the response of soil respiration, net nitrogen mineralization, and aboveground plant growth to experimental ecosystem warning, Oecologia, 126, 543–562, https://doi.org/10.1007/s004420000544, 2001.

Ryken, N., Vanmaercke, M., Wanyama, J., Isabirye, M., Vanonckelen, S., Deckers, J., and Poesen, J.: Impact of papyrus wetland encroachment on spatial and temporal variabilities of stream flow and sediment export from wet tropical catchments, Science of the Total Environment, 511, 756–766, https://doi.org/10.1016/j.scitotenv.2014.12.048, 2014.

Sacks, W. J., Cook, B. I., Buenning, N., Levis, S., and Helkowski, J. H.: Effects of global irrigation on the near-surface climate, Climate Dynamics, 33, 159–175, https://doi.org/10.1007/s00382-008-0445-z, 2008.

Sacks, W. J., Deryng, D., Foley, J. A., and Ramankutty, N.: Crop planting dates: An analysis of global patterns, Global Ecology and Biogeography, 19, 607–620, https://doi.org/10.1111/j.1466-8238.2010.00551.x, 2010.

Samuelsson, P., Kourzeneva, E., and Mironov, D.: The impact of lakes on the European climate as simulated by a regional climate model, Boreal Environment Research, 15, 113–129, 2010.

Samuelsson, P., Gollvik, S., Jansson, C., Kupiainen, M., Kourzeneva, E., and Berg, W. J. V. D.: The surface processes of the Rossby Centre regional atmospheric climate model (RCA4), Meteorologi, 157, 2013.

Savitzky, A. and Golay, M. J.: Smoothing and Differentiation of Data by Simplified Least Squares Procedures, Analytical Chemistry, 36, 1627–1639, https://doi.org/10.1021/ac60214a047, 1964.

Schewe, J., Heinke, J., Gerten, D., Haddeland, I., Arnell, N. W., Clark, D. B., Dankers, R., Eisner, S., Fekete, B. M., Colón-González, F. J., Gosling, S. N., Kim, H., Liu, X., Masaki, Y., Portmann, F. T., Satoh, Y., Stacke, T., Tang, Q., Wada, Y., Wisser, D., Albrecht, T., Frieler, K., Piontek, F., Warszawski, L., and Kabat, P.: Multimodel assessment of water scarcity under climate change, Proceedings of the National Academy of Sciences of the United States of America, 111, 3245–3250, https://doi.org/10.1073/pnas.1222460110, 2014.

Schneider, P. and Hook, S. J.: Space observations of inland water bodies show rapid surface warming since 1985, Geophysical Research Letters, 37, L22 405, https://doi.org/10.1029/2010GL045059, 2010.

Schwatke, C., Dettmering, D., Bosch, W., and Seitz, F.: DAHITI - An innovative approach for estimating water level time series over inland waters using multi-mission satellite altimetry, Hydrology and Earth System Sciences, 19, 4345–4364, https://doi.org/10.5194/hess-19-4345-2015, 2015.

Semazzi, F. H. M.: Enhancing Safety of Navigation and Efficient Exploitation of Natural Resources over Lake Victoria and Its Basin by Strengthening Meteorological Services on the Lake, p. 104, 2011.

Sene, K. J.: Theoretical estimates for the influence of Lake Victoria on flows in the upper White Nile, Hydrological Sciences Journal, 45, 125–145, https://doi.org/10.1080/02626660009492310, 2000.

Sene, K. J. and Plinston, D. T.: A review and update of the hydrology of lake victoria in east africa, Hydrological Sciences Journal, 39, 47–63, https://doi.org/10.1080/02626669409492719, 1994.

Seneviratne, S. I., Corti, T., Davin, E. L., Hirschi, M., Jaeger, E. B., Lehner, I., Orlowsky, B., and Teuling, A. J.: Investigating soil moisture-climate interactions in a changing climate: A review, Earth-Science Reviews, 99, 125–161, https://doi.org/10.1016/j.earscirev.2010.02.004, 2010.

Seneviratne, S. I., Donat, M. G., Pitman, A. J., Knutti, R., and Wilby, R. L.: Allowable CO2 emissions based on regional and impact-related climate targets, https://doi.org/10.1038/nature16542, 2016.

Shin, S., Pokhrel, Y., and Miguez-Macho, G.: High-Resolution Modeling of Reservoir Release and Storage Dynamics at the Continental Scale, Water Resources Research, 55, 787–810, https://doi.org/10.1029/2018WR023025, 2019.

Shin, S., Pokhrel, Y., Yamazaki, D., Huang, X., Torbick, N., Qi, J., Pattanakiat, S., Ngo-Duc, T., and Nguyen, T. D.: High Resolution Modeling of River-Floodplain-Reservoir Inundation Dynamics in the Mekong River Basin, Water Resources Research, 56, https://doi.org/10.1029/2019WR026449, 2020.

Shugar, D. H., Burr, A., Haritashya, U. K., Kargel, J. S., Watson, C. S., Kennedy, M. C., Bevington, A. R., Betts, R. A., Harrison, S., and Strattman, K.: Rapid worldwide growth of glacial lakes since 1990, Nature Climate Change, 10, 939–945, https://doi.org/10.1038/s41558-020-0855-4, 2020.

Sillmann, J., Kharin, V. V., Zwiers, F. W., Zhang, X., and Bronaugh, D.: Climate extremes indices in the CMIP5 multimodel ensemble: Part 2. Future climate projections, Journal of Geophysical Research: Atmospheres, 118, 2473–2493, https://doi.org/10.1002/jgrd.50188, 2013.

Smith, K. A. and Semazzi, F. H. M.: The Role of the Dominant Modes of Precipitation Variability over Eastern Africa in Modulating the Hydrology of Lake Victoria, Advances in Meteorology, 2014, 1–11, https://doi.org/10.1155/2014/516762, 2014.

Sood, A. and Smakhtin, V.: Global hydrological models: a review, Hydrological Sciences Journal, 60, 549–565, https://doi.org/10.1080/02626667.2014.950580, 2015.

Souverijns, N., Thiery, W., Demuzere, M., and Lipzig, N. P. M. V.: Drivers of future changes in East African precipitation Drivers of future changes in East African precipitation, Environ. Res. Lett, 11, 114 011, 2016.

Stackhouse, P. W. J., Gupta, S. K., Cox, S. J., Mikovitz, J. C., T., Z., and Hinkelman, L. M.: The NASA/GEWEX surface radiation budget release 3.0: 24.5-year dataset, GEWEX News, 21, 10–12, 2011.

Stepanenko, V. M., Martynov, A., Jöhnk, K. D., Subin, Z. M., Perroud, M., Fang, X., Beyrich, F., Mironov, D., and Goyette, S.: A one-dimensional model intercomparison study of thermal regime of a shallow, turbid midlatitude lake, Geoscientific Model Development, 6, 1337–1352, https://doi.org/10.5194/gmd-6-1337-2013, 2013.

Sterl, S., Vanderkelen, I., Chawanda, C. J., Russo, D., Brecha, R. J., van Griensven, A., van Lipzig, N. P., and Thiery, W.: Smart renewable electricity portfolios in West Africa, Nature Sustainability, 3, 710–719, https://doi.org/10.1038/s41893-020-0539-0, 2020.

Sterl, S., Devillers, A., Chawanda, C. J., van Griensven, A., Thiery, W., and Russo, D.: A spatiotemporal atlas of hydropower in Africa for energy modelling purposes, Open Research Europe, 1, 29, https://doi.org/10.12688/openreseurope.13392.1, 2021a.

Sterl, S., Fadly, D., Liersch, S., Koch, H., and Thiery, W.: Linking solar and wind power in eastern Africa with operation of the Grand Ethiopian Renaissance Dam, Nature Energy, 6, 407–418, https://doi.org/10.1038/s41560-021-00799-5, 2021b.

Sterling, S. M., Ducharne, A., and Polcher, J.: The impact of global land-cover change on the terrestrial water cycle, Nature Climate Change, 3, 385–390, https://doi.org/10.1038/nclimate1690, 2013.

Stewart, R. I. A., Dossena, M., Bohan, D. A., Jeppesen, E., Kordas, R. L., Ledger, M. E., Meerhoff, M., Moss, B., Mulder, C., Shurin, J. B., Suttle, B., Thompson, R., Trimmer, M., and Woodward, G.: Mesocosm Experiments as a Tool for Ecological Climate-Change Research, Advances in Ecological Research, 48, 71–181, https://doi.org/10.1016/B978-0-12-417199-2.00002-1, 2013.

Steyaert, J. C., Condon, L. E., W.D. Turner, S., and Voisin, N.: ResOpsUS, a dataset of historical reservoir operations in the contiguous United States, Scientific Data, 9, 34, https://doi.org/10.1038/s41597-022-01134-7, 2022.

Strachan, I. B., Tremblay, A., Pelletier, L., Tardif, S., Turpin, C., and Nugent, K. A.: Does the creation of a boreal hydroelectric reservoir result in a net change in evaporation?, Journal of Hydrology, 540, 886–899, https://doi.org/10.1016/j.jhydrol.2016.06.067, 2016.

Subin, Z. M., Murphy, L. N., Li, F., Bonfils, C., and Riley, W. J.: Boreal lakes moderate seasonal and diurnal temperature variation and perturb atmospheric circulation: Analyses in the Community Earth System Model 1 (CESM1), Tellus, Series A: Dynamic Meteorology and Oceanography, 64, https://doi.org/10.3402/tellusa.v64i0.15639, 2012a.

Subin, Z. M., Riley, W. J., and Mironov, D.: An improved lake model for climate simulations: Model structure, evaluation, and sensitivity analyses in CESM1, Journal of Advances in Modeling Earth Systems, 4, 1–27, https://doi.org/10.1029/2011MS000072, 2012b.

Subin, Z. M., Riley, W. J., and Mironov, D.: An improved lake model for climate simulations: Model structure, evaluation, and sensitivity analyses in CESM1, Journal of Advances in Modeling Earth Systems, 4, 1–27, https://doi.org/10.1029/2011MS000072, 2012c.

Sutcliffe, J. V. and Parks, Y. P.: The Hydrology of the Nile, IAHS Special Publication, 5, 192, 1999.

Sutcliffe, J. V. and Petersen, G.: Lake Victoria: derivation of a corrected natural water level series / Lac Victoria: dÃ©rivation d'une sÃ©rie naturelle corrigÃ©e des niveaux d'eau, Hydrological Sciences Journal, 52, 1316–1321, https://doi.org/10.1623/hysj.52.6.1316, 2007.

Swenson, S. and Wahr, J.: Post-processing removal of correlated errors in GRACE data, Geophysical Research Letters, 33, L08 402, https://doi.org/10.1029/2005GL025285, 2006.

Swenson, S. and Wahr, J.: Monitoring the water balance of Lake Victoria, East Africa, from space, Journal of Hydrology, 370, 163–176, https://doi.org/10.1016/j.jhydrol.2009.03.008, 2009.

Swenson, S. C. and Lawrence, D. M.: A new fractional snow-covered area parameterization for the Community Land Model and its effect on the surface energy balance, Journal of Geophysical Research Atmospheres, 117, D21 107, https://doi.org/10.1029/2012JD018178, 2012.

Swenson, S. C. and Lawrence, D. M.: A GRACE-based assessment of interannual groundwater dynamics in the Community Land Model, Water Resources Research, 51, 8817–8833, https://doi.org/10.1002/2015WR017582, 2015.

Swenson, S. C., Clark, M., Fan, Y., Lawrence, D. M., and Perket, J.: Representing Intrahillslope Lateral Subsurface Flow in the Community Land Model, Journal of Advances in Modeling Earth Systems, 11, 4044–4065, https://doi.org/10.1029/2019MS001833, 2019.

Tan, Z., Zhuang, Q., and Anthony, K. W.: Modeling methane emissions from arctic lakes: Model development and site-level study, Journal of Advances in Modeling Earth Systems, 7, 459–483, https://doi.org/10.1002/2014MS000344, 2015.

Tate, E., Sutcliffe, J., Conway, D., and Farquharson, F.: Water balance of Lake Victoria: update to 2000 and climate change modelling to 2100, Hydrological Sciences Journal, 49, 563–574, https://doi.org/10.1623/hysj.49.4.563.54422, 2004.

Taye, M. T., Ntegeka, V., Ogiramoi, N. P., and Willems, P.: Assessment of climate change impact on hydrological extremes in two source regions of the Nile River Basin, Hydrology and Earth System Sciences, 15, 209–222, https://doi.org/10.5194/hess-15-209-2011, 2011.

Telteu, C. E., Müller Schmied, H., Thiery, W., Leng, G., Burek, P., Liu, X., Boulange, J. E. S., Andersen, L. S., Grillakis, M., Gosling, S. N., Satoh, Y., Rakovec, O., Stacke, T., Chang, J., Wanders, N., Shah, H. L., Trautmann, T., Mao, G., Hanasaki, N., Koutroulis, A., Pokhrel, Y., Samaniego, L., Wada, Y., Mishra, V., Liu, J., Döll, P., Zhao, F., Gädeke, A., Rabin, S. S., and Herz, F.: Understanding each other's models An introduction and a standard representation of 16 global water models to support intercomparison, improvement, and communication, Geoscientific Model Development, 14, 3843–3878, https://doi.org/10.5194/gmd-14-3843-2021, 2021.

Terrer, C., Vicca, S., Stocker, B. D., Hungate, B. A., Phillips, R. P., Reich, P. B., Finzi, A. C., and Prentice, I. C.: Ecosystem responses to elevated CO2 governed by plant–soil interactions and the cost of nitrogen acquisition, https://doi.org/10.1111/nph.14872, 2018.

Teutschbein, C. and Seibert, J.: Is bias correction of regional climate model (RCM) simulations possible for non-stationary conditions, Hydrology and Earth System Sciences, 17, 5061–5077, https://doi.org/10.5194/hess-17-5061-2013, 2013.

Themeßl, M. J., Gobiet, A., and Leuprecht, A.: Empirical-statistical downscaling and error correction of daily precipitation from regional climate models, International Journal of Climatology, 31, 1530–1544, https://doi.org/10.1002/joc.2168, 2011.

Themeßl, M. J., Gobiet, A., and Heinrich, G.: Empirical-statistical downscaling and error correction of regional climate models and its impact on the climate change signal, Climatic Change, 112, 449–468, https://doi.org/10.1007/s10584-011-0224-4, 2012.

Thiery, W., Martynov, A., Darchambeau, F., Descy, J.-P., Plisnier, P.-D., Sushama, L., and Van Lipzig, N. P. M.: Understanding the performance of the FLake model over two African Great Lakes, Geosci. Model Dev, 7, 317–337, https://doi.org/10.5194/gmd-7-317-2014, 2014a.

Thiery, W., Martynov, A., Darchambeau, F., Descy, J.-P., Plisnier, P.-D., Sushama, L., and Van Lipzig, N. P. M.: Understanding the performance of the FLake model over two African Great Lakes, Geosci. Model Dev, 7, 317–337, https://doi.org/10.5194/gmd-7-317-2014, 2014b.

Thiery, W., Stepanenko, V. M., Fang, X., Jöhnk, K. D., Zhongshun, L., Martynov, A., Perroud, M., Subin, Z. M., Darchambeau, F., Mironov, D., and Van Lipzig, N. P. M.: LakeMIP Kivu: evaluating the representation of a large, deep tropical lake by a set of one-dimensional lake models, Tellus A, 66, 21 390, https://doi.org/10.3402/tellusa.v66.21390, 2014c.

Thiery, W., Davin, E. L., Panitz, H.-J., Demuzere, M., Lhermitte, S., and van Lipzig, N.: The Impact of the African Great Lakes on the Regional Climate, Journal of Climate, 28, 4061–4085, https://doi.org/10.1175/JCLI-D-14-00565.1, 2015.

Thiery, W., Davin, E. L., Seneviratne, S. I., Bedka, K., Lhermitte, S., and Van Lipzig, N. P.: Hazardous thunderstorm intensification over Lake Victoria, Nature Communications, 7, 12 786, https://doi.org/10.1038/ncomms12786, 2016.

Thiery, W., Davin, E. L., Lawrence, D. M., Hirsch, A. L., Hauser, M., and Seneviratne, S. I.: Present-day irrigation mitigates heat extremes, Journal of Geophysical Research, 122, 1403–1422, https://doi.org/10.1002/2016JD025740, 2017.

Thiery, W., Visser, A. J., Fischer, E. M., Hauser, M., Hirsch, A. L., Lawrence, D. M., Lejeune, Q., Davin, E. L., and Seneviratne, S. I.: Warming of hot extremes alleviated by expanding irrigation, Nature Communications, 11, 290, https://doi.org/10.1038/s41467-019-14075-4, 2020.

Thiery, W., Lange, S., Rogelj, J., Schleussner, C. F., Gudmundsson, L., Seneviratne, S. I., Andrijevic, M., Frieler, K., Emanuel, K., Geiger, T., Bresch, D. N., Zhao, F., Willner, S. N., Büchner, M., Volkholz, J., Bauer, N., Chang, J., Ciais, P., Dury, M., François, L., Grillakis, M., Gosling, S. N., Hanasaki, N., Hickler, T., Huber, V., Ito, A., Jägermeyr, J., Khabarov, N., Koutroulis, A., Liu, W., Lutz, W., Mengel, M., Müller, C., Ostberg, S., Reyer, C. P., Stacke, T., and Wada, Y.: Intergenerational inequities in exposure to climate extremes, Science, 374, 158–160, https://doi.org/10.1126/science.abi7339, 2021.

Thompson, R. M., Beardall, J., Beringer, J., Grace, M., and Sardina, P.: Means and extremes: Building variability into community-level climate change experiments, Ecology Letters, 16, 799–806, https://doi.org/10.1111/ele.12095, 2013.

Tierney, J. E., Russell, J. M., and Huang, Y.: A molecular perspective on Late Quaternary climate and vegetation change in the Lake Tanganyika basin, East Africa, Quaternary Science Reviews, 29, 787–800, https://doi.org/10.1016/j.quascirev.2009.11.030, 2010.

Trenberth, K. E.: An imperative for climate change planning: tracking Earth's global energy, https://doi.org/10.1016/j.cosust.2009.06.001, 2009.

Turner, S. W., Xu, W., and Voisin, N.: Inferred inflow forecast horizons guiding reservoir release decisions across the United States, Hydrology and Earth System Sciences, 24, 1275–1291, https://doi.org/10.5194/hess-24-1275-2020, 2020.

Turner, S. W., Steyaert, J. C., Condon, L., and Voisin, N.: Water storage and release policies for all large reservoirs of conterminous United States, Journal of Hydrology, 603, 126 843, https://doi.org/10.1016/j.jhydrol.2021.126843, 2021.

Van Beek, L. P., Wada, Y., and Bierkens, M. F.: Global monthly water stress: 1. Water balance and water availability, Water Resources Research, 47, W07 517, https://doi.org/10.1029/2010WR009791, 2011.

Van de Walle, J., Thiery, W., Brousse, O., Souverijns, N., Demuzere, M., and van Lipzig, N. P. M.: A convection-permitting model for the Lake Victoria Basin: Evaluation and insight into the mesoscale versus synoptic atmospheric dynamics., Climate Dynamics, 1, 3, https://doi.org/10.1007/s00382-019-05088-2, 2019.

Van der Molen, M. K., Dolman, A. J., Ciais, P., Eglin, T., Gobron, N., Law, B. E., Meir, P., Peters, W., Phillips, O. L., Reichstein, M., Chen, T., Dekker, S. C., Doubková, M., Friedl, M. A., Jung, M., van den Hurk, B. J., de Jeu, R. A., Kruijt, B., Ohta, T., Rebel, K. T., Plummer, S., Seneviratne, S. I., Sitch, S., Teuling, A. J., van der Werf, G. R., and Wang, G.: Drought and ecosystem carbon cycling, Agricultural and Forest Meteorology, 151, 765–773, https://doi.org/10.1016/j.agrformet.2011.01.018, 2011.

van Vliet, M. T., van Beek, L. P., Eisner, S., Flörke, M., Wada, Y., and Bierkens, M. F.: Multi-model assessment of global hydropower and cooling water discharge potential under climate change, Global Environmental Change, 40, 156–170, https://doi.org/10.1016/j.gloenvcha.2016.07.007, 2016.

van Vuuren, D. P., Edmonds, J., Kainuma, M., Riahi, K., Thomson, A., Hibbard, K., Hurtt, G. C., Kram, T., Krey, V., Lamarque, J. F., Masui, T., Meinshausen, M., Nakicenovic, N., Smith, S. J., and Rose, S. K.: The representative concentration pathways: An overview, Climatic Change, 109, 5–31, https://doi.org/10.1007/s10584-011-0148-z, 2011.

Vanderkelen, I., Van Lipzig, N. P., and Thiery, W.: Modelling the water balance of Lake Victoria (East Africa)-Part 1: Observational analysis, Hydrology and Earth System Sciences, 22, 5509–5525, https://doi.org/10.5194/hess-22-5509-2018, 2018a.

Vanderkelen, I., Van Lipzig, N. P., and Thiery, W.: Modelling the water balance of Lake Victoria (East Africa)-Part 2: Future projections, Hydrology and Earth System Sciences, 22, 5527–5549, https://doi.org/10.5194/hess-22-5527-2018, 2018b.

Vanderkelen, I., van Lipzig, N. P., Lawrence, D. M., Droppers, B., Golub, M., Gosling, S. N., Janssen, A. B., Marcé, R., Schmied, H. M., Perroud, M., Pierson, D., Pokhrel, Y., Satoh, Y., Schewe, J., Seneviratne, S. I., Stepanenko, V. M., Tan, Z., Woolway, R. I., and Thiery, W.: Global Heat Uptake by Inland Waters, Geophysical Research Letters, 47, e2020GL087 867, https://doi.org/10.1029/2020GL087867, 2020a.

Vanderkelen, I., Zscheischler, J., Gudmundsson, L., Keuler, K., Rineau, F., Beenaerts, N., Vangronsveld, J., Vicca, S., and Thiery, W.: A novel method for assessing climate change impacts in ecotron experiments, International Journal of Biometeorology, 64, 1709–1727, https://doi.org/10.1007/s00484-020-01951-8, 2020b.

Vanderkelen, I., van Lipzig, N. P., Sacks, W. J., Lawrence, D. M., Clark, M. P., Mizukami, N., Pokhrel, Y., and Thiery, W.: Simulating the Impact of Global Reservoir Expansion on the Present-Day Climate, Journal of Geophysical Research: Atmospheres, 126, e2020JD034 485, https://doi.org/10.1029/2020JD034485, 2021.

Veldkamp, T. I., Wada, Y., Aerts, J. C., Döll, P., Gosling, S. N., Liu, J., Masaki, Y., Oki, T., Ostberg, S., Pokhrel, Y., Satoh, Y., Kim, H., and Ward, P. J.: Water scarcity hotspots travel downstream due to human interventions in the 20th and 21st century, Nature Communications, 8, 15 697, https://doi.org/10.1038/ncomms15697, 2017.

Verdin, K.: Hydrologic Derivatives for Modeling and Applications (HDMA) database: U.S. Geological Survey data release, https://doi.org/https://doi.org/10.5066/F7S180ZP, 2017.

Vicca, S., Bahn, M., Estiarte, M., Van Loon, E. E., Vargas, R., Alberti, G., Ambus, P., Arain, M. A., Beier, C., Bentley, L. P., Borken, W., Buchmann, N., Collins, S. L., De Dato, G., Dukes, J. S., Escolar, C., Fay, P., Guidolotti, G., Hanson, P. J., Kahmen, A., Kröel-Dulay, G., Ladreiter-Knauss, T., Larsen, K. S., Lellei-Kovacs, E., Lebrija-Trejos, E., Maestre, F. T., Marhan, S., Marshall, M., Meir, P., Miao, Y., Muhr, J., Niklaus, P. A., Ogaya, R., Peñuelas, J., Poll, C., Rustad, L. E., Savage, K., Schindlbacher, A., Schmidt, I. K., Smith, A. R., Sotta, E. D., Suseela, V., Tietema, A., Van Gestel, N., Van Straaten, O., Wan, S., Weber, U., and Janssens, I. A.: Can current moisture responses predict soil CO2 efflux under altered precipitation regimes? A synthesis of manipulation experiments, Biogeosciences, 11, 2991–3013, https://doi.org/10.5194/bg-11-2991-2014, 2014.

Voisin, N., Li, H., Ward, D., Huang, M., Wigmosta, M., and Leung, L. R.: On an improved sub-regional water resources management representation for integration into earth system models, Hydrology and Earth System Sciences, 17, 3605–3622, https://doi.org/10.5194/hess-17-3605-2013, 2013a.

Voisin, N., Liu, L., Hejazi, M., Tesfa, T., Li, H., Huang, M., Liu, Y., and Leung, L. R.: One-Way coupling of an integrated assessment model and a water resources model: Evaluation and implications of future changes over the US Midwest, Hydrology and Earth System Sciences, 17, 4555–4575, https://doi.org/10.5194/hess-17-4555-2013, 2013b.

Von Schuckmann, K., Cheng, L., Palmer, M. D., Hansen, J., Tassone, C., Aich, V., Adusumilli, S., Beltrami, H., Boyer, T., Cuesta-Valero, F. J., Desbruyères, D., Domingues, C., García-García, A., Gentine, P., Gilson, J., Gorfer, M., Haimberger, L., Ishii, M., Johnson, G. C., Killick, R., King, B. A., Kirchengast, G., Kolodziejczyk, N., Lyman, J., Marzeion, B., Mayer, M., Monier, M., Monselesan, P., Purkey, S., Roemmich, D., Schweiger, A., Seneviratne, S. I., Shepherd, A., Slater, D. A., Steiner, A. K., Straneo, F., Timmermans, M.-L., and Wijffels, S. E.: Heat stored in the Earth system: where does the energy go?, Earth Syst. Sci. Data, 12, 2013–2041, https://doi.org/10.5194/essd-12-2013-2020, 2020.

Vörösmarty, C. J. and Sahagian, D.: Evidence for global-scale human impacts on the terrestrial water cycle, BioScience, 50, 753–765, 2000.

Vörösmarty, C. J., McIntyre, P. B., Gessner, M. O., Dudgeon, D., Prusevich, A., Green, P., Glidden, S., Bunn, S. E., Sullivan, C. A., Liermann, C. R., and Davies, P. M.: Global threats to human water security and river biodiversity, Nature, 467, 555–561, https://doi.org/10.1038/nature09440, 2010.

Vrac, M. and Friederichs, P.: Multivariate-intervariable, spatial, and temporal-bias correction, Journal of Climate, 28, 218–237, https://doi.org/10.1175/JCLI-D-14-00059.1, 2015.

Wada, Y., Wisser, D., and Bierkens, M. F. P.: Global modeling of withdrawal, allocation and consumptive use of surface water and groundwater resources, Earth System Dynamics, 5, 15–40, https://doi.org/10.5194/esd-5-15-2014, 2014.

Wada, Y., Bierkens, M. F. P., De Roo, A., Dirmeyer, P. A., Famiglietti, J. S., Hanasaki, N., Konar, M., Liu, J., and Schmied, H. M.: Human–water interface in hydrological modelling: current status and future directions, Hydrol. Earth Syst. Sci, 21, 4169–4193, https://doi.org/10.5194/hess-21-4169-2017, 2017.

Wanders, N. and Wada, Y.: Human and climate impacts on the 21st century hydrological drought, Journal of Hydrology, 526, 208–220, https://doi.org/10.1016/j.jhydrol.2014.10.047, 2015.

Wanders, N., van Vliet, M. T. H., Wada, Y., Bierkens, M. F. P., and van Beek, L. P.: High-Resolution Global Water Temperature Modeling, Water Resources Research, 55, 2760–2778, https://doi.org/10.1029/2018WR023250, 2019.

Wang, J., Walter, B., Yao, F., Song, C., Ding, M., Maroof, A., Zhu, J., Fan, C., Xin, A., McAlister, J., Sikder, S., Sheng, Y., Allen, G., Crétaux, J.-F., and Wada, Y.: GeoDAR: Georeferenced global dam and reservoir dataset for bridging attributes and geolocations, Earth System Science Data Discussions, pp. 1–52, https://doi.org/10.5194/essd-2021-58, 2021.

Wild, M.: Global dimming and brightening: A review, Journal of Geophysical Research Atmospheres, 114, https://doi.org/10.1029/2008JD011470, 2009.

Wilks, D. S.: On "field significance" and the false discovery rate, Journal of Applied Meteorology and Climatology, 45, 1181–1189, https://doi.org/10.1175/JAM2404.1, 2006.

Williams, K., Chamberlain, J., Buontempo, C., and Bain, C.: Regional climate model performance in the Lake Victoria basin, Climate Dynamics, 44, 1699–1713, https://doi.org/10.1007/s00382-014-2201-x, 2015.

Winemiller, K. O., McIntyre, P. B., Castello, L., Fluet-Chouinard, E., Giarrizzo, T., Nam, S., Baird, I. G., Darwall, W., Lujan, N. K., Harrison, I., Stiassny, M. L., Silvano, R. A., Fitzgerald, D. B., Pelicice, F. M., Agostinho, A. A., Gomes, L. C., Albert, J. S., Baran, E., Petrere, M., Zarfl, C., Mulligan, M., Sullivan, J. P., Arantes, C. C., Sousa, L. M., Koning, A. A., Hoeinghaus, D. J., Sabaj, M., Lundberg, J. G., Armbruster, J., Thieme, M. L., Petry, P., Zuanon, J., Torrente Vilara, G., Snoeks, J., Ou, C., Rainboth, W., Pavanelli, C. S., Akama, A., Van Soesbergen, A., and Sáenz, L.: Balancing hydropower and biodiversity in the Amazon, Congo, and Mekong, Science, 351, 128–129, https://doi.org/10.1126/science.aac7082, 2016.

Wisser, D., Fekete, B. M., Vörösmarty, C. J., and Schumann, A. H.: Reconstructing 20th century global hydrography: A contribution to the Global Terrestrial Network-Hydrology (GTN-H), Hydrology and Earth System Sciences, 14, 1–24, https://doi.org/10.5194/hess-14-1-2010, 2010.

WMO: Hydrometeorological survey of the catchments of lakes Victoria, Kyoga and Mobutu Sese Seko, Tech. rep., Geneva, 1981.

Wohlfahrt, G., Tomelleri, E., and Hammerle, A.: The albedo–climate penalty of hydropower reservoirs, Nature Energy, 6, 372–377, https://doi.org/10.1038/s41560-021-00784-y, 2021.

Woldemichael, A. T., Hossain, F., Pielke, R., and Beltrán-Przekurat, A.: Understanding the impact of dam-triggered land use/land cover change on the modification of extreme precipitation, Water Resources Research, 48, W09 547, https://doi.org/10.1029/2011WR011684, 2012.

Wood, A. W., Leung, L. R., Sridhar, V., and Lettenmaier, D. P.: Hydrologic implications of dynamical and statistical approaches to downscaling climate model outputs, Climatic Change, 62, 189–216, https://doi.org/10.1023/B:CLIM.0000013685.99609.9e, 2004.

Woolway, R. I. and Merchant, C. J.: Worldwide alteration of lake mixing regimes in response to climate change, Nature Geoscience, 12, 271–276, https://doi.org/10.1038/s41561-019-0322-x, 2019.

Woolway, R. I., Kraemer, B. M., Lenters, J. D., Merchant, C. J., O'Reilly, C. M., and Sharma, S.: Global lake responses to climate change, Nature Reviews Earth & Environment, 1, 388–403, https://doi.org/10.1038/s43017-020-0067-5, 2020.

Woolway, R. I., Sharma, S., Weyhenmeyer, G. A., Debolskiy, A., Golub, M., Mercado-Bettín, D., Perroud, M., Stepanenko, V., Tan, Z., Grant, L., Ladwig, R., Mesman, J., Moore, T. N., Shatwell, T., Vanderkelen, I., Austin, J. A., DeGasperi, C. L., Dokulil, M., La Fuente, S., Mackay, E. B., Schladow, S. G., Watanabe, S., Marcé, R., Pierson, D. C., Thiery, W., and Jennings, E.: Phenological shifts in lake stratification under climate change, Nature Communications, 12, 2318, https://doi.org/10.1038/s41467-021-22657-4, 2021.

Wu, Z., Dijkstra, P., Koch, G. W., Peñuelas, J., and Hungate, B. A.: Responses of terrestrial ecosystems to temperature and precipitation change: A meta-analysis of experimental manipulation, Global Change Biology, 17, 927–942, https://doi.org/10.1111/j.1365-2486.2010.02302.x, 2011.

Yamazaki, D., Ikeshima, D., Sosa, J., Bates, P. D., Allen, G. H., and Pavelsky, T. M.: MERIT Hydro: A High-Resolution Global Hydrography Map Based on Latest Topography Dataset, Water Resources Research, 55, 5053–5073, https://doi.org/10.1029/2019WR024873, 2019.

Yang, W., Seager, R., Cane, M. A., Lyon, B., Yang, W., Seager, R., Cane, M. A., and Lyon, B.: The Annual Cycle of East African Precipitation, Journal of Climate, 28, 2385–2404, https://doi.org/10.1175/JCLI-D-14-00484.1, 2015.

Yao, Y., Vanderkelen, I., Lombardozzi, D., Swenson, S., Lawrence, D., Jägermeyr, J., Grant, L., and Thiery, W.: Implementation and evaluation of irrigation techniques in the Community Land Model, Journal of Advances in Modeling Earth Systems, In review, 2022.

Yassin, F., Razavi, S., Elshamy, M., Davison, B., Sapriza-Azuri, G., and Wheater, H.: Representation and improved parameterization of reservoir operation in hydrological and land-surface models, Hydrology and Earth System Sciences, 23, 3735–3764, https://doi.org/10.5194/hess-23-3735-2019, 2019.

Yigzaw, W.: Leveraging Precipitation Modification around Large Reservoirs in Orographic Environments for Water Resources Management, Journal of Civil & Environmental Engineering, 4, 1000 161, https://doi.org/10.4172/2165-784x.1000161, 2014.

Yigzaw, W., Li, H. Y., Demissie, Y., Hejazi, M. I., Leung, L. R., Voisin, N., and Payn, R.: A New Global Storage-Area-Depth Data Set for Modeling Reservoirs in Land Surface and Earth System Models, Water Resources Research, 54, 10,372–10,386, https://doi.org/10.1029/2017WR022040, 2018.

Yin, X. and Nicholson, S. E.: The water balance of Lake Victoria, Hydrological Sciences Journal, 43, 789–811, https://doi.org/10.1080/02626669809492173, 1998.

Yokohata, T., Kinoshita, T., Sakurai, G., Pokhrel, Y., Ito, A., Okada, M., Satoh, Y., Kato, E., Nitta, T., Fujimori, S., Felfelani, F., Masaki, Y., Iizumi, T., Nishimori, M., Hanasaki, N., Takahashi, K., Yamagata, Y., and Emori, S.: MIROC-INTEG-LAND version 1: a global biogeochemical land surface model with human water management, crop growth, and land-use change, Geoscientific Model Development, 13, 4713–4747, https://doi.org/10.5194/gmd-13-4713-2020, 2020.

Yue, K., Fornara, D. A., Yang, W., Peng, Y., Peng, C., Liu, Z., and Wu, F.: Influence of multiple global change drivers on terrestrial carbon storage: additive effects are common, Ecology Letters, 20, 663–672, https://doi.org/10.1111/ele.12767, 2017.

Zajac, Z., Revilla-Romero, B., Salamon, P., Burek, P., Hirpa, F., and Beck, H.: The impact of lake and reservoir parameterization on global streamflow simulation, Journal of Hydrology, 548, 552–568, https://doi.org/10.1016/j.jhydrol.2017.03.022, 2017.

Zarfl, C., Lumsdon, A. E., Berlekamp, J., Tydecks, L., and Tockner, K.: A global boom in hydropower dam construction, Aquatic Sciences, 77, 161–170, https://doi.org/10.1007/s00027-014-0377-0, 2014.

Zaussinger, F., Dorigo, W., Gruber, A., Tarpanelli, A., Filippucci, P., and Brocca, L.: Estimating irrigation water use over the contiguous United States by combining satellite

and reanalysis soil moisture data, Hydrology and Earth System Sciences, 23, 897–923, https://doi.org/10.5194/hess-23-897-2019, 2019.

Zekollari, H., Huss, M., and Farinotti, D.: Modelling the future evolution of glaciers in the European Alps under the EURO-CORDEX RCM ensemble, Cryosphere, 13, 1125–1146, https://doi.org/10.5194/tc-13-1125-2019, 2019.

Zhang, X., Zwiers, F. W., and Hegerl, G.: The influences of data precision on the calculation of temperature percentile indices, International Journal of Climatology, 29, 321–327, https://doi.org/10.1002/joc.1738, 2009.

Zhang, X., Alexander, L., Hegerl, G. C., Jones, P., Tank, A. K., Peterson, T. C., Trewin, B., and Zwiers, F. W.: Indices for monitoring changes in extremes based on daily temperature and precipitation data, Wiley Interdisciplinary Reviews: Climate Change, 2, 851–870, https://doi.org/10.1002/wcc.147, 2011.

Zhao, G., Gao, H., Naz, B. S., Kao, S. C., and Voisin, N.: Integrating a reservoir regulation scheme into a spatially distributed hydrological model, Advances in Water Resources, 98, 16–31, https://doi.org/10.1016/j.advwatres.2016.10.014, 2016.

Zhou, T., Nijssen, B., Gao, H., and Lettenmaier, D. P.: The Contribution of Reservoirs to Global Land Surface Water Storage Variations, American Meteorological Society, 17, 309–325, https://doi.org/https://doi.org/10.1175/JHM-D-15-0002.1, 2016.

Zhou, T., Leung, L. R., Leng, G., Voisin, N., Li, H. Y., Craig, A. P., Tesfa, T., and Mao, Y.: Global Irrigation Characteristics and Effects Simulated by Fully Coupled Land Surface, River, and Water Management Models in E3SM, Journal of Advances in Modeling Earth Systems, 12, e2020MS002 069, https://doi.org/10.1029/2020MS002069, 2020.

Zhou, W., Wang, L., Li, D., and Leung, L. R.: Spatial pattern of lake evaporation increases under global warming linked to regional hydroclimate change, Communications Earth & Environment, 2, 255, https://doi.org/10.1038/s43247-021-00327-z, 2021.

Zscheischler, J. and Seneviratne, S. I.: Dependence of drivers affects risks associated with compound events, Science Advances, 3, e1700 263, https://doi.org/10.1126/sciadv.1700263, 2017.

Zscheischler, J., Westra, S., Van Den Hurk, B. J., Seneviratne, S. I., Ward, P. J., Pitman, A., Aghakouchak, A., Bresch, D. N., Leonard, M., Wahl, T., and Zhang, X.: Future climate risk from compound events, Nature Climate Change, 8, 469–477, https://doi.org/10.1038/s41558-018-0156-3, 2018.

Zscheischler, J., Fischer, E. M., and Lange, S.: The effect of univariate bias adjustment on multivariate hazard estimates, Earth System Dynamics, 10, 31–43, https://doi.org/10.5194/esd-10-31-2019, 2019.

List of Outputs

Peer reviewed articles in scientific journals - as first author

Vanderkelen I., Gharari S., Mizukami N., Clark M., Lawrence D. M., Swenson S., Pokhrel Y., Hanasaki N., van Griensven A., Thiery W. (2022) Evaluating a reservoir parametrisation in the vector-based global routing model mizuRoute (v2.0.1) for Earth System Model coupling. Geoscientific Model Development, 15, 4163-4192.

Vanderkelen, I., Lipzig, N. P. M., Sacks, W. J., Lawrence, D. M., Clark, M. P., Mizukami, N., Pokhrel, Y., Thiery, W. (2021). Simulating the Impact of Global Reservoir Expansion on the Present-Day Climate. Journal of Geophysical Research: Atmospheres, 126(16), e2020JD034485.

Vanderkelen I., van Lipzig N.P.M., Lawrence D. M., Droppers B., Gosling S. N., Janssen A. B. G., Marcé R., Müller-Schmied H., Perroud M., Pierson D., Pokhrel Y., Satoh Y., Schewe J., Seneviratne S. I., Stepanenko V. M., Tan Z., Woolway R. I., Thiery W. (2020) Global heat uptake by inland waters. Geographical Research Letters, 47(12), e2020GL087867.

Vanderkelen I., Zscheischler J., Gudmundsson L. Keuler K., Rineau F., Beenaerts N., Vangronsveld J., Vicca S., Thiery W. (2020) A new method for assessing climate impacts in ecotron experiments. International Journal of Biometeorology, 64, 1709–1727.

Vanderkelen, I., van Lipzig, N.P.M., Thiery, W. (2018) Modelling the water balance of Lake Victoria (East Africa) - Part 1: Observational analysis. Hydrology and Earth System Sciences, 22, 5509-5525 (HESS highlight article).

Vanderkelen, I., van Lipzig, N.P.M., Thiery, W. (2018) Modelling the water balance of Lake Victoria (East Africa) - Part 2: Future projections. Hydrology and Earth System Sciences, 22, 5527-5549 (HESS highlight article).

Peer reviewed articles in scientific journals - as contributing author

Publications in preparation and submitted for review are listed in grey.

Cuesta-Valero F J., Beltrami H., Burke E., García-García A., MacDougall A., Peng J., von Schuckmann K., Seneviratne S. I., Smith N., Thiery W., **Vanderkelen I.**, Wu T. Continental Heat Storage: Contributions from the Ground, Inland Waters, and Permafrost Thawing. In preparation for Earth System Dynamics.

Gharari S., **Vanderkelen I.,** Tefs A., Mizukami N., Stadnyk T. A., Lawrence D., Clark, M. P. (2022) A flexible and unifying framework for lake and reservoir water balance modeling in Earth system modelling. Water Resources Research, in review.

Yao Y., **Vanderkelen I.,** Lombardozzi D., Swenson S., Lawrence D., Jägermeyr J., Grant L., Thiery W. (2022). Implementation and evaluation of irrigation techniques in the Community Land Model, Journal of Advances in Modeling Earth Systems, in review.

De Hertog S., Haverman F., **Vanderkelen I.,** Guo S., Manola I., Luo F., Coumo D., Davin E. L., Duveiller G., Lejeune Q., Pongratz J., Schleussner C. F., Seneviratne S. I., Thiery W. (2022). Comparing Earth System Models under drastic land cover and land management changes for their effects on biogeophysics. Earth System Dynamics Discussions, in review.

Golub, M., Thiery, W., Marcé, R., Pierson, D., **Vanderkelen, I.**, Mercado, D., Woolway, R. I., Grant, L., Jennings, E., Schewe, J., Zhao, F., Frieler, K., Mengel, M. et al. (2022). A framework for ensemble modelling of climate change impacts on lakes worldwide: the ISIMIP Lake Sector, Geoscientific Model Development, in press.

Nakulopa F., **Vanderkelen I.**, Van de Walle J., Tabari H., Jacobs L., Dewitte O., van Lipzig N. P. M., Thiery W. (2022). Evaluation of high-resolution precipitation products over the Mountains of the Moon (Uganda). International Journal of Hydrometeorology, 23(5), 747-768.

Grant L., **Vanderkelen I.**, Gudmundsson L., Tan Z., Perroud M., Stepanenko V. M., Debolskiy A., Droppers B., Janssen A. B. G., Woolway I. R., Schmid M., Schewe J., Zhao F., Golub M., Pierson D., Marcé R., Seneviratne S. I., Kirillin G., Thiery W. (2021). Attribution of worldwide lake systems change to anthropogenic forcing. Nature Geoscience, 14, 849–854.

Woolway, R. I., Sharma, S., Weyhenmeyer, G. A., Debolskiy, A., Golub, M., Mercado-Bettín, D., Perroud, M., Stepanenko, V., Tan, Z., Grant, L., Ladwig, R., Mesman, J., Moore, T. N., Shatwell, T., **Vanderkelen, I.**, Austin, J. A., DeGasperi, C. L., Dokulil, M., La Fuente S., Mackay, E. B., Schladow, S. G., Watanabe, S., Marcé, R., Pierson, D. C., Thiery, W., Jennings, E. (2021). Phenological shifts in lake stratification under climate change. Nature Communications, 12(1), 2318.

Sterl, S., **Vanderkelen, I.**, Chawanda, C. J., Russo, D., Brecha, R., van Griensven, A., van Lipzig, N. P. M., Thiery, W. (2020) Smart renewable electricity portfolios in West Africa. Nature Sustainability 3, 710–719.

Rineau F., Malina R., Beenaerts N., ... , Thiery W., Thijs S., **Vanderkelen I.**, Van Landuyt W., Verbruggen E., Witters N., Zscheischler J., Vangronsveld J. (2019) Towards more predictive and interdisciplinary climate change ecosystem experiments. Nature Climate Change, 9(11), 809–816.

Reports

Hassler, B., Lauer, A., Reimuth, A., Müller, B., Davin, E., Hirschi, M., Coll, J., Grant, L., Thiery, W., **Vanderkelen, I.** (2021). Thematic Assessment Report on Task 7.3: Earth Energy Balance, Copernicus Climate Change Service report, 36 p.

Presentations at conferences and workshops

CESM Annual Workshop, June 2022. Changing storage: towards dams and reservoirs representation in Earth System Models. (online presentation in plenary)

EGU General Assembly, Vienna, May 2022. Evaluating a reservoir parametrization in a vector-based global routing model for Earth System Model coupling. (oral presentation)

ISIMIP and PROCLIAS workshop, Potsdam, May 2022. Quantifying lifetime water scarcity with ISIMIP 3b. (poster)

Land Model & Biogeochemistry Working Group Winter Meeting, February 2022. Evaluating a reservoir parametrization in a vector-based global routing model for Earth System Model coupling. (online presentation)

AGU General Assembly, December 2021. Implementation and evaluation of a reservoir parametrization in a vector-based global routing model for Earth System Model coupling. (online presentation)

VUB PhD day: Sustainable Development Goals, 27th of May 2021. The impact of global reservoir expansion on the present-day climate. (oral presentation)

EGU General Assembly, April 2021. The impact of global reservoir expansion on the present-day climate. (virtual PICO presentation)

Land Model Working Group Winter Meeting, February 2021. The impact of global reservoir expansion on the present-day climate. (online presentation – Andrew Slater award for best graduate student presentation).

AGU General Assembly, December 2020. The impact of global reservoir expansion on the present-day climate. (online presentation)

International Environmental Modelling and Software Society Conference, Brussels, July 2020. Global heat uptake of inland waters. (online presentation)

International Environmental Modelling and Software Society Conference, Brussels, July 2020. Implementing the role of reservoirs in the CTSM land surface model. (online presentation)

Cross-sectoral ISIMIP online workshop 2020, June 2020. Global heat uptake of inland waters. (online presentation)

EGU General Assembly, May 2020. Global heat uptake of inland waters. (online display)

6th Workshop on Parameterization of Lakes in Numerical Weather Prediction and Climate Modelling, Toulouse, October 2019. Implementing reservoirs in CLM5: Accounting for reservoir construction in the 20th century. (oral presentation)

EGU General Assembly, Vienna, April 2019. Ecosystem response to climate variability and change: the Ecotron Experiment. (poster)

Land Model Working Group Winter Meeting, Boulder, February 2019. The impacts of Reservoirs on the Climate: Towards representing Reservoirs in CLM5. (oral presentation)

Swiss Climate Summerschool 2018, Grindelwald, August 2018. Ecosystem response to climate variability and change: the Ecotron Experiment. (poster)

Flemish Supercomputer Users day, May 2018. Generating climate forcing for the Ecotron experiment using HPC. (poster – 3rd place best poster prize)

EGU General Assembly, Vienna, April 2018. Projecting the future levels of Lake Victoria. (oral presentation)

The Disaster Risk Reduction workshop, Kampala, Uganda, 6th of February 2018. Modelling the present and future levels of Lake Victoria. (oral presentation)

The 7th Belgian Geography day, Liège, Belgium, 17th of November 2017. Projecting the future levels of Lake Victoria. (oral presentation)

EGU General Assembly, Vienna, April 2017. Reconstructing the lake levels of Lake Victoria. (poster)

Awards and recognitions

CESM Graduate Student Award, for graduate students that made significant contributions to CESM or used CESM in innovative ways, awarded at the CESM Annual workshop, June 2022

Regional Finalist of the Green Impact International Special Awards 2022, category Sustainability Hero

Andrew Slater Award for Best Graduate Student presentation at the 2021 Land Model Working Group annual meeting at the National Center for Atmospheric Research, Boulder

Prize Ernest Dubois awarded by the King Baudouin Foundation in 2020 for doctoral research on the theme of water and its availability in Belgium or throughout the world

Travel grant for attending EGU General Assembly 2018 in Vienna, awarded by VUB NSE Doctoral School

Third best poster prize at Flemish Supercomputer Centre User Day 2018 in Brussels

EGU Highlight Article award for Vanderkelen et al. (2018a, Hydrol. Earth Syst. Sci.).

EGU Highlight Article award for Vanderkelen et al. (2018b, Hydrol. Earth Syst. Sci.)

Humans are an integral component of the terrestrial water cycle, both through direct water management and anthropogenic climate change. Damming rivers creates reservoirs, which alters river flows and stores additional water on land. To investigate the interactions of reservoirs with their surrounding environment and the atmosphere, holistic frameworks like Earth System models (ESMs) are necessary. However, ESMs typically do not include reservoirs in their river and land models. The aim of this doctoral thesis is to improve our understanding of reservoirs in the Earth system.

A case study on the future water level projections for Lake Victoria shows the importance of both climate change and dam management, and serves as a stepping stone to investigate those interactions at the global scale. Next, the amount of heat taken up by inland waters is quantified for the first time, and the role of reservoirs to store and redistribute heat in a warming world is highlighted. In the last two contributions, the representation of reservoirs in the Community Earth System Model is advanced by including historical lake expansion through reservoir construction in its land component, the Community Land Model, and flow regulation through dam management in the river routing model mizuRoute.

These developments improve the representation of the terrestrial water cycle in ESMs by including a key component of human water management. This enables investigating future water availability for food, fiber, and energy in a changing climate.